



The  
University  
Of  
Sheffield.

# Controls upon the location and size of glacial overdeepenings

March 2015

Overdeepening is an important glaciological and geomorphological process that has the potential to influence the response of ice masses to climatic changes. We have examined several hundred glacial overdeepenings proximal to/ within Labrador, Canada, to investigate the controls upon overdeepening location and size. Our analyses show that overdeepening appears to correlate strongly with glacial confluence and, importantly, the correlation is strongest where confluence-geometry indicates the speed up of ice-flow. Further, we find that the magnitude of ice-flow speed up correlates with overdeepening depth only for confluences situated in or near major geological fault-zones. Our findings therefore support the hypothesis that overdeepening can be initiated by an increase in ice velocity. Further, we conclude that overdeepening is most efficacious where fractured bedrock enables efficient quarrying.

Christopher  
Thomas  
Lloyd

### Acknowledgements

With thanks to my supervisors, Prof. Chris Clark and Dr. Darrel Swift, for advice and guidance. Also, special thanks to my family.

This work was funded by a University of Sheffield fees bursary. Additional thanks to the British Society for Geomorphology, and the University of Sheffield (Learned Society Fund), for the provision of grants to assist conference attendance.

## Table of Contents

1	Introduction .....	- 1 -
2	Literature Review .....	- 9 -
2.1	Possible controls upon overdeepening location and size .....	- 9 -
2.2	Processes of overdeepening initiation and development .....	- 10 -
2.3	Numerical, theoretical, and empirical research of relevance to the study of overdeepening .....	- 12 -
2.4	The over-simplicity of current numerical models of glacial landscape evolution ..	- 19 -
2.5	Review summary .....	- 21 -
2.6	Palaeoglaciology .....	- 23 -
2.7	Development of a typology of overdeepenings .....	- 25 -
2.7.1	Pure (glacial) controls upon overdeepening location and size .....	- 25 -
2.7.2	External (topographical and geological) controls upon overdeepening location and size	- 29 -
2.7.3	Interaction of controls .....	- 35 -
2.7.4	Developing testable hypotheses to examine controls upon overdeepening location and size .....	- 37 -
2.8	The Study Region: Labrador .....	- 42 -
3	Research Design .....	- 45 -
3.1	Objectives .....	- 48 -
4	Research Method .....	- 50 -
4.1	Selecting DEMs and datasets for use in investigation .....	- 50 -
4.1.1	DEMs and datasets used in Labrador (regional) investigation .....	- 50 -
4.1.2	Additional dataset to test reproducibility of Labradorian results for a supplementary (Swiss) study region .....	- 52 -
4.1.3	DEMs and datasets used in global investigation, within LGM limit (World map of potential overdeepenings) .....	- 52 -
4.1.4	DEM and dataset accuracy .....	- 54 -
4.2	Identifying overdeepenings (Objective 1) .....	- 61 -
4.2.1	Study region extent(s) .....	- 62 -
4.2.2	Identifying sinks, and projection of data .....	- 64 -
4.2.3	Removal of small artefacts/errors from sink data (thresholding) .....	- 66 -
4.2.4	Defining overdeepenings that contain lakes, within sink data .....	- 67 -
4.2.5	Defining topographically low lying overdeepenings, within sink data (filtering; applied to regional study only) .....	- 70 -
4.2.6	Defining overdeepenings, within sink data (further thresholding; applied to global study only) .....	- 73 -
4.3	Identifying glacial valley confluences (for regional study) (Objective 2) .....	- 74 -
4.3.1	Confluence identification, criteria, and certainty .....	- 74 -

4.3.2	Defining confluence extent (perimeter) .....	- 87 -
4.3.3	Defining the internal geometry of confluences .....	- 91 -
4.3.4	Defining confluence extent (up-tributary valley).....	- 98 -
4.3.5	Defining confluence extent (down-trunk valley) .....	- 103 -
4.3.6	Defining further 'liberal' down-trunk terminations.....	- 106 -
4.4	Sensitivity testing in order to justify parameter choices .....	- 108 -
4.4.1	Dataset visualisation parameters .....	- 108 -
4.4.2	Overdeepening parameters .....	- 108 -
4.4.3	Confluence parameters (regional study) .....	- 113 -
4.5	Investigating ice velocity hypotheses (1 & 2); Assessing the co-location of glacial confluence and overdeepenings, for Labrador study region (Objective 3).....	- 123 -
4.5.1	Evaluating the strength of the co-location relationship between glacial confluence and overdeepenings.....	- 123 -
4.5.2	Measuring valley cross-sectional area change through glacial confluences (Objective 4).....	- 126 -
4.5.3	Evaluating the influence of confluence cross-sectional area change upon overdeepening location (Objective 5).....	- 127 -
4.5.4	Evaluating the influence of confluence cross-sectional area change upon overdeepening size (Objective 6).....	- 130 -
4.6	Investigating bedrock erosion hypotheses (3 & 4); Assessing the co-location of geological zones and glacial confluence, for Labrador study region (Objective 7) .....	- 136 -
4.6.1	Evaluating the strength of the co-location relationship between geological zones and glacial confluence.....	- 136 -
4.6.2	Assessing the co-location of geological zones and overdeepenings (Objective 8) -	141 -
4.6.3	Assessing the co-location of glacial confluence and overdeepenings, per each geological zone (Objective 9).....	- 141 -
4.6.4	Assessing the co-location of geological zones and glacial confluence co-located with overdeepenings (Objective 10).....	- 142 -
4.6.5	Evaluating the influence of confluence bedrock mass strength upon overdeepening location (Objective 11) .....	- 142 -
4.6.6	Evaluating the influence of confluence bedrock mass strength upon overdeepening size (Objective 12) .....	- 143 -
4.7	Testing reproducibility: A supplementary (Swiss) study region (Objective 13)....	- 145 -
4.7.1	Defining structural fault zone extent, within structural geology zone .....	- 145 -
4.8	Identifying probable overdeepenings within limits of the LGM, globally (Objective 14) -	147 -
5	Results.....	- 148 -
5.1	Sensitivity testing in order to justify parameter choices .....	- 148 -
5.1.1	To what extent does the working definition of confluence affect confluence speed-up ratio? (regional study).....	- 148 -
5.2	Qualitative analysis of the Labrador study region .....	- 153 -

5.3	Investigating ice velocity hypotheses (1&2) for Labrador study region .....	- 154 -
5.3.1	Evaluating the strength of the co-location relationship between glacial confluence and overdeepenings.....	- 155 -
5.3.2	Co-location of individual confluences with overdeepenings.....	- 159 -
5.3.3	Co-location of individual overdeepenings with confluence .....	- 160 -
5.3.4	Investigating ice velocity hypothesis (1): Evaluating the influence of confluence cross-sectional area change upon overdeepening location .....	- 160 -
5.3.5	Investigating ice velocity hypothesis (2): Evaluating the influence of confluence cross-sectional area change upon overdeepening size .....	- 164 -
5.4	Investigating bedrock erosion hypotheses (3&4) for Labrador study region .....	- 167 -
5.4.1	Evaluating the strength of the co-location relationship between specific geological types and glacial confluence.....	- 167 -
5.4.2	Evaluating the strength of the co-location relationship between geological zones and overdeepenings.....	- 170 -
5.4.3	Evaluating the strength of the relationship between glacial confluence and overdeepenings, within the structural geology zone .....	- 172 -
5.4.4	Evaluating the strength of the relationship between the structural geology zone and glacial confluence (for confluences with overdeepenings) .....	- 174 -
5.4.5	Investigating bedrock erosion hypothesis (3): Evaluating the influence of confluence bedrock mass strength change upon overdeepenings within the structural geology zone .....	- 176 -
5.4.6	Investigating bedrock erosion hypothesis (4): Evaluating the influence of confluence bedrock mass strength change upon overdeepening size within the structural geology zone .....	- 182 -
5.5	Testing reproducibility: A supplementary (Swiss) study region .....	- 186 -
5.5.1	Investigating bedrock erosion hypothesis (4): Evaluating the influence of confluence bedrock mass strength change upon overdeepening size.....	- 186 -
5.6	World map of overdeepenings .....	- 189 -
6	Discussion.....	- 198 -
6.1	Sensitivity testing of operator variability in confluence definition.....	- 200 -
6.2	Confluence allometry.....	- 200 -
6.3	The development of Labradorian topography: The influence of topographical and glacial controls upon geology .....	- 204 -
6.4	Glacial buzz-saw: Accounting for the difference between valley overdeepening depth in the Labradorian compared to the Swiss structural zone.....	- 205 -
7	Conclusions .....	- 208 -
7.1	Outcomes of analyses.....	- 208 -
7.2	Future Research .....	- 211 -
	References .....	- 214 -
	Appendix .....	- 235 -
8	The internal geometry of confluences: Discussion.....	- 235 -
8.1	Defining the absolute tributary-trunk valley boundary (ADTT).....	- 235 -

8.2	Applying the ADTT method: Problems.....	- 237 -
8.2.1	The DTT method: A solution .....	- 237 -

### List of figures

Figure 1.	Comparison of fluvial and glacial valley longitudinal profiles.....	- 2 -
Figure 2.	A terminal overdeepening. ....	- 3 -
Figure 3.	DEMs and valley profiles showing overdeepened basins, inc. surface ice velocity map. 4 -	
Figure 4.	Fjords; longitudinal profile, and bathymetry. ....	- 5 -
Figure 5.	Longitudinal profile and plan map of Storglaciaren Glacier, Northern Sweden.....	- 6 -
Figure 6.	Schematic of an overdeepening. Water and sediment filled overdeepenings.....	- 7 -
Figure 7.	Output from the Tomkin (2009) model, showing glacial overdeepening.....	- 13 -
Figure 8.	Schematic profile and plan of pure overdeepening(s), inc. process diagram (ice velocity).....	- 26 -
Figure 9.	Schematic profile and plan of pure overdeepening(s), inc. process diagram (meltwater abundance). ....	- 28 -
Figure 10.	Schematic plans of topographical overdeepenings, inc. process diagram (valley CSA change).....	- 30 -
Figure 11.	Schematic plan of topographical overdeepenings, inc. process diagram (valley-floor perturbations).....	- 32 -
Figure 12.	Schematic plan of geological overdeepenings, inc. process diagram (bedrock mass strength change). ....	- 34 -
Figure 13.	Schematic plan of several valley glaciers, summarising the various potential types of overdeepening. ....	- 36 -
Figure 14.	Schematic plan of topographical/geological overdeepening, inc. process diagram (change in valley CSA & bedrock mass strength, simplified). ....	- 41 -
Figure 15.	The study region (Labrador, Canada and surrounding region).....	- 43 -
Figure 16.	The north-east coast of the Labrador province of Canada.....	- 46 -
Figure 17.	US NASA SRTM coverage map. ....	- 51 -
Figure 18.	The main elements of the workflow for overdeepening identification and definition.- 63 -	
Figure 19.	Defining overdeepenings that contain lakes, within sink data (for Labrador study region, and for world map). ....	- 69 -
Figure 20.	Defining topographically low lying overdeepenings, within sink data (filtering; for Labrador study region only).....	- 71 -
Figure 21.	Defining topographically low lying overdeepenings, elevation threshold (Labrador study only).....	- 73 -
Figure 22.	The study region (Labrador, Canada and surrounding region).....	- 75 -
Figure 23.	The main elements of the workflow for confluence identification and definition..- 76 -	
Figure 24.	Schematic plan of an idealised confluence.....	- 79 -
Figure 25.	Schematic plans of confluences: Tributary-Trunk angle.....	- 80 -
Figure 26.	Schematic plans of confluences: Major and minor tributaries.....	- 81 -
Figure 27.	Schematic plans of confluences: Hanging valley & stepping valley.....	- 82 -
Figure 28.	Example of hanging valley.....	- 83 -
Figure 29.	Example of stepped valley. ....	- 84 -
Figure 30.	Schematic plan of ice flow direction within a valley system. ....	- 85 -
Figure 31.	Poorly defined confluences: Glacial erosion.....	- 86 -
Figure 32.	Defining confluence extent (perimeter). ....	- 88 -

Figure 33. Dealing with 'interrupted' confluence perimeters.....	- 89 -
Figure 34. Validity of confluence perimeter, in the context of the surrounding valley network. .	- 90 -
Figure 35. Defining the down-tributary termination (DTT). .....	- 91 -
Figure 36. Defining the trending direction of tributary valley-sides in order to define valley axis. ....	- 93 -
Figure 37. Dealing with change in the trending direction of tributary valley-sides about the position of the DTT on one tributary flank. ....	- 94 -
Figure 38. Identifying the trending direction of tributary valley-sides where irregular. ....	- 95 -
Figure 39. Maintaining realistic internal confluence geometry.....	- 97 -
Figure 40. Defining the up-tributary termination (UTT). .....	- 99 -
Figure 41. Surface ice velocity vectors for the Lambert Glacier, Antarctica.....	- 100 -
Figure 42. Dealing with problems that arise where UTT is not well contained by topography... -	101 -
Figure 43. Dealing with the scenario where the up-tributary end of a confluence occurs close to the DTT.....	- 102 -
Figure 44. Defining the down-trunk termination. ....	- 104 -
Figure 45. Defining the trending direction of trunk valley-sides in order to define valley axis.....	- 105 -
Figure 46. Defining 'conservative' and 'liberal' down-trunk terminations.....	- 106 -
Figure 47. Dealing with problems that arise where the liberal perimeter is not well contained by topography.....	- 107 -
Figure 48. The frequency distribution of elevation values for the Labrador study region... -	110 -
Figure 49. Considering the sensitivity of overdeepened area to variation of the elevation threshold.....	- 111 -
Figure 50. Schematic plans of confluences: Tributary-Trunk angle.....	- 113 -
Figure 51. Example of a hanging valley.....	- 114 -
Figure 52. Testing the sensitivity of confluence speed-up ratio to change in (lateral) confluence extent. ....	- 116 -
Figure 53. Considering the optimal relief threshold, with which to test the sensitivity of confluence speed-up ratio to change in (lateral) confluence extent. ....	- 117 -
Figure 54. Testing the sensitivity of confluence speed-up ratio to change in down-tributary termination (DTT) position and tributary valley axis orientation. ....	- 118 -
Figure 55. Considering optimal angle thresholds, with which to test the sensitivity of confluence speed-up ratio to change in down-tributary termination (DTT) position and tributary valley axis orientation.....	- 120 -
Figure 56. Considering operator variability in the location of the down-trunk termination. -	122 -
Figure 57. Assessing co-location of glacial confluence and overdeepenings using a GIS.....	- 123 -
Figure 58. Defining the precise extent of the Labrador study region.....	- 124 -
Figure 59. Quality control of the confluence/overdeepening datasets. ....	- 129 -
Figure 60. Dealing with ice flow direction reversal in confluences. ....	- 130 -
Figure 61. Further quality control of the confluence/overdeepening datasets: Overdeepening scale, low certainty. ....	- 132 -
Figure 62. Further quality control of the confluence/overdeepening datasets: Overdeepening scale, low certainty, other indicators.....	- 133 -
Figure 63. Further quality control of the confluence/overdeepening datasets: Overdeepening scale, moderate certainty. ....	- 134 -
Figure 64. Further quality control of the confluence/overdeepening datasets: Overdeepening scale, high certainty. ....	- 135 -
Figure 65. The study region (Labrador, Canada and surrounding region), with the geological zones for the province of Labrador (modified from Wardle, et al., 1997) superimposed. ..	- 137 -
Figure 66. Defining structural fault zone extent.....	- 140 -

Figure 67. The Swiss study region.....	- 145 -
Figure 68. Defining structural fault zone extent (Swiss study region).....	- 146 -
Figure 69. Sensitivity testing. Map of confluence case study locations. ....	- 149 -
Figure 70. Results of testing the sensitivity of confluence ratio to change in the working definition of confluence (extent and internal geometry), sorted in order of performance, showing each case study and the range of each corresponding ratio value.....	- 151 -
Figure 71. Confluence case studies 3 and 9, demonstrating excellent and poor outcomes (respectively) to testing of the sensitivity of confluence ratio to change in the working definition of confluence (extent and internal geometry). ....	- 152 -
Figure 72. Evaluating the strength of the area co-location relationship between glacial confluence and overdeepenings.....	- 156 -
Figure 73. The frequency distribution of confluence 'speed up' ratio, for confluences with and without overdeepenings.....	- 162 -
Figure 74. A summary graph of frequency distribution of confluence 'speed up' ratio. ....	- 163 -
Figure 75. Relationship between confluence CSA ratio and the maximum depth of overdeepenings, after some quality control.....	- 165 -
Figure 76. Relationship between confluence CSA ratio and the maximum depth of overdeepenings, after further quality control.....	- 166 -
Figure 77. A comparison of the expected 'random' and the actual observed percentage of total confluence area that is co-located with geological zones, within the Labrador study region. ....	- 169 -
Figure 78. A comparison of the expected 'random' and the actual observed percentage of total overdeepened area, that is co-located with geological zones. ....	- 171 -
Figure 79. A comparison of the expected 'random' and the actual observed percentage of total overdeepened area that is estimated to be co-located with glacial confluence within the (expanded) structural geology zone. ....	- 173 -
Figure 80. A comparison of the expected 'random' and the actual observed percentage of total glacial confluence area that is co-located with the structural geology zone (for confluences with overdeepenings). ....	- 174 -
Figure 81. The frequency distribution of confluence 'speed up' ratio, for confluences with and without overdeepenings, within and outwith the structural geology zone.....	- 178 -
Figure 82. The frequency distribution of confluence 'speed up' ratio for confluences with overdeepenings, within and outwith the structural zone. ....	- 179 -
Figure 83. Relationship between confluence CSA ratio and the maximum depth of co-located overdeepenings, outwith the structural geology zone.....	- 183 -
Figure 84. Relationship between confluence CSA ratio and the maximum depth of co-located overdeepenings, within the structural geology zone. ....	- 185 -
Figure 85. Relationship between confluence CSA ratio and the maximum depth of co-located overdeepenings, within the structural geology zone, Swiss study region.....	- 187 -
Figure 86a-h. Topographical depressions within the limits of the Last Glacial Maximum (LGM), emphasising localities of likely glacial overdeepening. ....	- 190 -
Figure 87. A summary graph of frequency distribution of confluence 'speed up' ratio. ....	- 202 -
Figure A1. Defining the absolute tributary-trunk valley boundary (ADTT).....	- 236 -
Figure A2. Applying the ADTT method, problems. ....	- 238 -

List of Tables

Table 1. Reviewed numerical models which simulate overdeepenings, and the controls and feedbacks included within each model. ....	- 22 -
Table 2. Predicted overdeepening controls and characteristics, which could be examined in future studies. ....	- 35 -
Table 3. Methods with which potential hypotheses of controls upon overdeepening location and size could be tested in future studies. ....	- 38 -
Table 4. Results of testing the sensitivity of confluence ratio to change in the working definition of confluence (extent and internal geometry), sorted in order of performance. ....	- 150 -
Table 5. Summary statistics for the Labrador study region. ....	- 154 -
Table 6. Summary statistics showing the area co-location relationship between glacial confluence and overdeepenings, for subsets of overdeepenings within the Labrador study region. ....	- 155 -
Table 7. The chi-squared test of independence for the relationship between confluence and overdeepening, within the Labrador study region. ....	- 158 -
Table 8. Summary statistics showing the co-location of individual confluences with overdeepenings, for subsets of overdeepenings within the Labrador study region. ....	- 159 -
Table 9. Summary statistics showing the co-location of individual overdeepenings with confluence, for subsets of overdeepenings within the Labrador study region. ....	- 160 -
Table 10. Summary statistics showing the number, percentage, and average ratio values of confluences demonstrating ice velocity speed up (i.e. a ratio > 1), for subsets of confluences within the Labrador study region. ....	- 161 -
Table 11. Summary statistics for the geological study of the Labrador region. ....	- 167 -
Table 12. Summary statistics showing the area co-location relationship between geological zones and glacial confluence within the Labrador study region. ....	- 168 -
Table 13. The chi-squared test of independence for the relationship between structural zone and confluence, within the Labrador study region. ....	- 169 -
Table 14. Summary statistics showing the area co-location relationship between geological zones and overdeepenings within the Labrador study region. ....	- 170 -
Table 15. The chi-squared test of independence for the relationship between structural zone and overdeepening, within the Labrador study region. ....	- 171 -
Table 16. Summary statistics showing the estimated area co-location relationship between glacial confluence and overdeepenings, within the (expanded) structural geology zone. ..	- 173 -
Table 17. Summary statistics showing the area co-location relationship between glacial confluence and the structural geology zone, for confluences with overdeepenings. ....	- 174 -
Table 18. The chi-squared test of independence for the relationship between structural zone and confluence (for only confluences that contain overdeepenings), within the Labrador study region. ....	- 175 -
Table 19. Summary statistics showing the number, percentage, and average ratio values of confluences demonstrating ice velocity speed up (i.e. a ratio > 1), for subsets of confluences co-located with overdeepenings within the Labrador study region. ....	- 177 -
Table 20. Summary statistics showing the number of individual confluences in the geological study region that occur within each geological zone, and that are co-located with overdeepenings in each zone. ....	- 180 -
Table 21. Summary statistics showing the number and percentage of individual confluences in the geological study region that occur in the structural zone and that are co-located with overdeepenings in the structural zone. ....	- 181 -
Table 22. Statistics, for subsets of confluences within the Labrador study region. ....	- 182 -
Table 23. Summary statistics for the world map of potential overdeepenings. ....	- 189 -
Table 24. Statistics, for subsets of confluences within the Labrador study region (reproduction of table 22). ....	- 203 -

## 1 Introduction

*This chapter offers a fundamental overview of the glacial landform that is commonly referred to as an overdeepening, and summarises why the phenomenon is of interest in both a theoretical and an applied sense. For context, the nature of fluvial graded and glacial valley longitudinal profiles are discussed and compared. Reasons for differences between the two profiles are examined. The typical location of overdeepenings within the glacial landscape, basic overdeepening characteristics, and likely processes of overdeepening formation are briefly outlined. Real-world examples of overdeepenings are presented. The rationale for the research project is explained.*

Overdeepenings are glacial landforms that are created by glacial erosion of the bedrock underlying a glacier, to form a closed-basin (Gannett, 1898; Penck, 1900). Overdeepenings occur where glaciers erode below the pre-existing fluvial valley graded profile (figure 1a) (Sugden & John, 1976).

Fluvial valley longitudinal profiles naturally tend towards a graded profile, and will never erode below it. This is because rivers concentrate erosion upon upstream steeper slopes, but lose sediment transport capacity (and therefore deposit sediment) upon downstream gentler slopes (Gilbert, 1877; Mackin, 1948). An idealised fluvial valley graded profile can be approximated to a concave-up parabolic curve (figure 1a), with the gentlest part of the profile occurring where the river approaches base level (which is usually the ocean). The idealised fluvial valley graded profile is rarely achieved in real world scenarios because transient abrupt changes in gradient of slope (knick points), within the profile, usually arise (figure 1b) over geological time scales (e.g. Stange, et al. (2013)). Causes of such changes include (but are not limited to) resistant geology and/or topographic obstructions (e.g. landslides or perhaps ice, acting as a dam), which potentially result in waterfalls and/or lakes. These imperfections in the profile are temporary, because a river will focus erosion and deposition in order to allow the profile to approach (i.e. re-)grade. Terrestrial fluvial valley longitudinal profiles tend towards a graded profile over a time scale of thousands to millions of years (e.g. Stange, et al. (2013)).

In contrast, in glacial environments erosion and sediment transport are limited by the slope of the ice surface, which drives ice (and water) flow. Thus, ice can erode deep basins (figure 1c) provided that ice mass supply is sufficient to maintain a positive ice surface profile, and provided that the bed of the basin remains shallow enough that sub-glacial meltwater cannot pond and so the overlying ice mass can flow. If the bed of the basin steepens excessively the

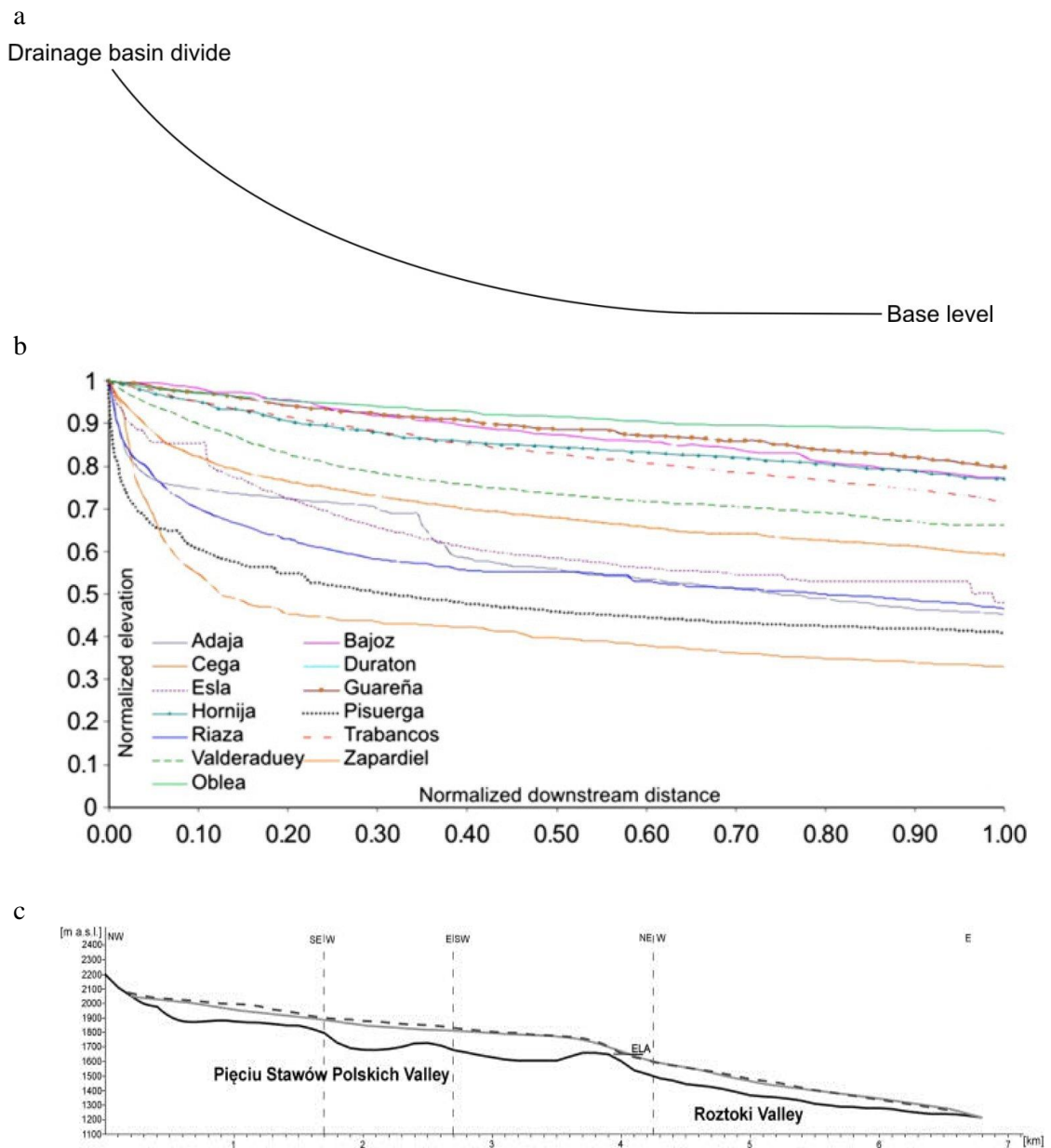


Figure 1. Comparison of fluvial and glacial valley longitudinal profiles.

(a) An idealised fluvial valley graded longitudinal profile. (b) Real-world fluvial valley longitudinal profiles for rivers within the Cenozoic Duero basin, north-western Iberia, Spain (Antón, et al., 2012). Valleys within this region have never been glaciated. It can be noted that each profile is simple concave, with no depressions apparent within. Knick points are visible at positions along many of the longitudinal profiles, evidence of re-grading due to change in base level. (c) Glacial valley longitudinal profile of the Pieciu Stawów Polskich/Roztoki Valley and the Roztoki glacier, high Tatra Mountains, Western Carpathians. Solid light-grey and dashed dark-grey lines respectively show a manually reconstructed and a modelled profile of the post-last glacial maximum (LGM) palaeo-glacier (Makos, et al., 2013). Overdeepening is evident at several positions along the glaciated valley longitudinal profile, where the glacier has eroded below the former fluvial graded profile (not shown). The occurrence of many overdeepenings along almost the full length of the glacial valley longitudinal profile is a likely consequence of change in glacier extent over time and the influence of localised non-glacial controls upon overdeepening location and size.

result will be that meltwater will pond and the ice mass will float, with the consequence that the ice mass will be unable to erode the bed. Glacial environments are not limited by a base level in the same way as their fluvial counterparts, other than by one indirectly imposed by the size of the parent landmass and by the equilibrium line altitude (ELA) of the glacier (Sugden & John, 1976; Linton, 1963). Terrestrial glacial valley longitudinal profiles (figure 1c) develop over a time scale of thousands to tens of thousands of years (depending upon the length of glacial occupancy, whether the glacier is warm or cold based, and the influence of localised non-glacial controls, etc.). The time scale for development of a glacial valley longitudinal profile is often quicker than the time it takes for fluvial valley longitudinal profiles to reach grade. This is because glacial erosion is more efficient relative to fluvial erosion (Anderson, et al., 2006).

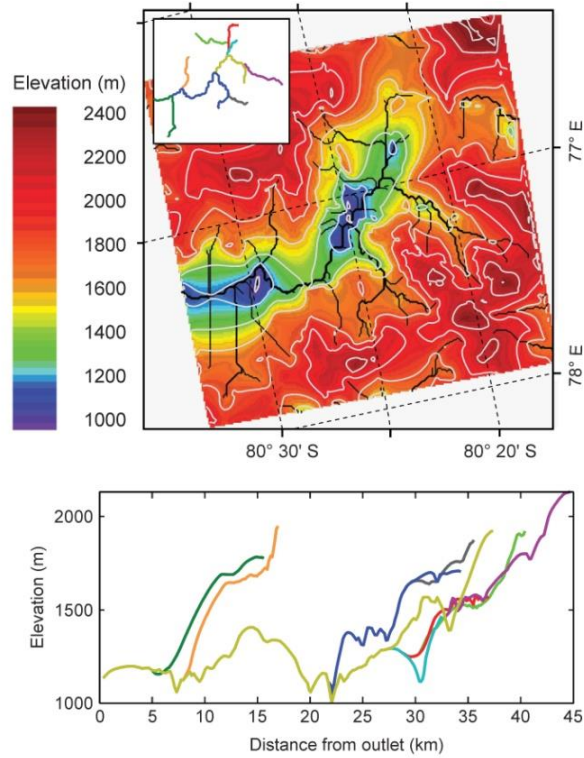
As a consequence of the controls upon glacial erosion and sediment transport, glacial landscapes are littered with abrupt jumps in topography (e.g. steps, hanging valleys) and isolated depressions (e.g. overdeepenings, figure 2). Overdeepenings are common features of glacial and/or formerly glaciated landscapes and are typically found in glacial troughs and cirques (Sugden & John, 1976; Linton, 1963) (figures 3-5). They are thought to develop by glacial erosive processes (primarily by quarrying, but also by abrasion and by glacial meltwater erosion) acting upon a particular locality, usually governed by an ice erosion feedback (Hooke, 1991; Alley, et al., 2003). The pre-existing valley geometry (topography) and geology are thought to be a significant control upon overdeepening development (Glasser, 1995; MacGregor, et al., 2000; Preusser, et al., 2010).



**Figure 2. A terminal overdeepening.**

**A terminal (i.e. situated at down-glacier end of glacier) overdeepening, partially exposed by glacier retreat; the overdeepening is partly confined by an arcuate moraine (glacial debris) ridge (Bagley Icefield, Alaska) (image: Don McCully). Modified from Cook and Swift, 2012.**

a



b

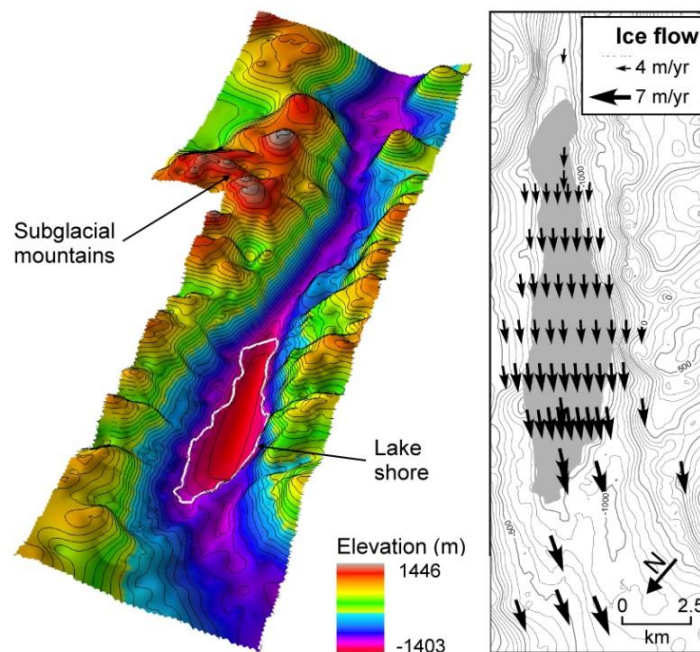


**Figure 3. DEMs and valley profiles showing overdeepened basins, inc. surface ice velocity map.**

(a) Contoured digital elevation model (DEM) of bed topography (upper panel) in the Gamburtsev Mountains, Antarctica, showing classic alpine topography with overdeepened basins occupying a pre-glacial fluvial valley network; profiles along major valley-axes (inset, upper panel) reveal the depth and extent of overdeepening (lower panel) (modified by Cook & Swift, 2012, with permission from Bo et al., 2009), ranging upto several hundred metres depth, and from hundreds of metres to several kilometres in extent. (b) Contoured map (left) and DEM (right) of bed topography, showing the glaciated-valley context of the overdeepened basin occupied by Ellsworth sub-glacial lake, Antarctica; map also shows surface ice velocities (contours are 100 m intervals; figures provided by Neil Ross) (Ross, et al., 2011). Modified from Cook & Swift, 2012.

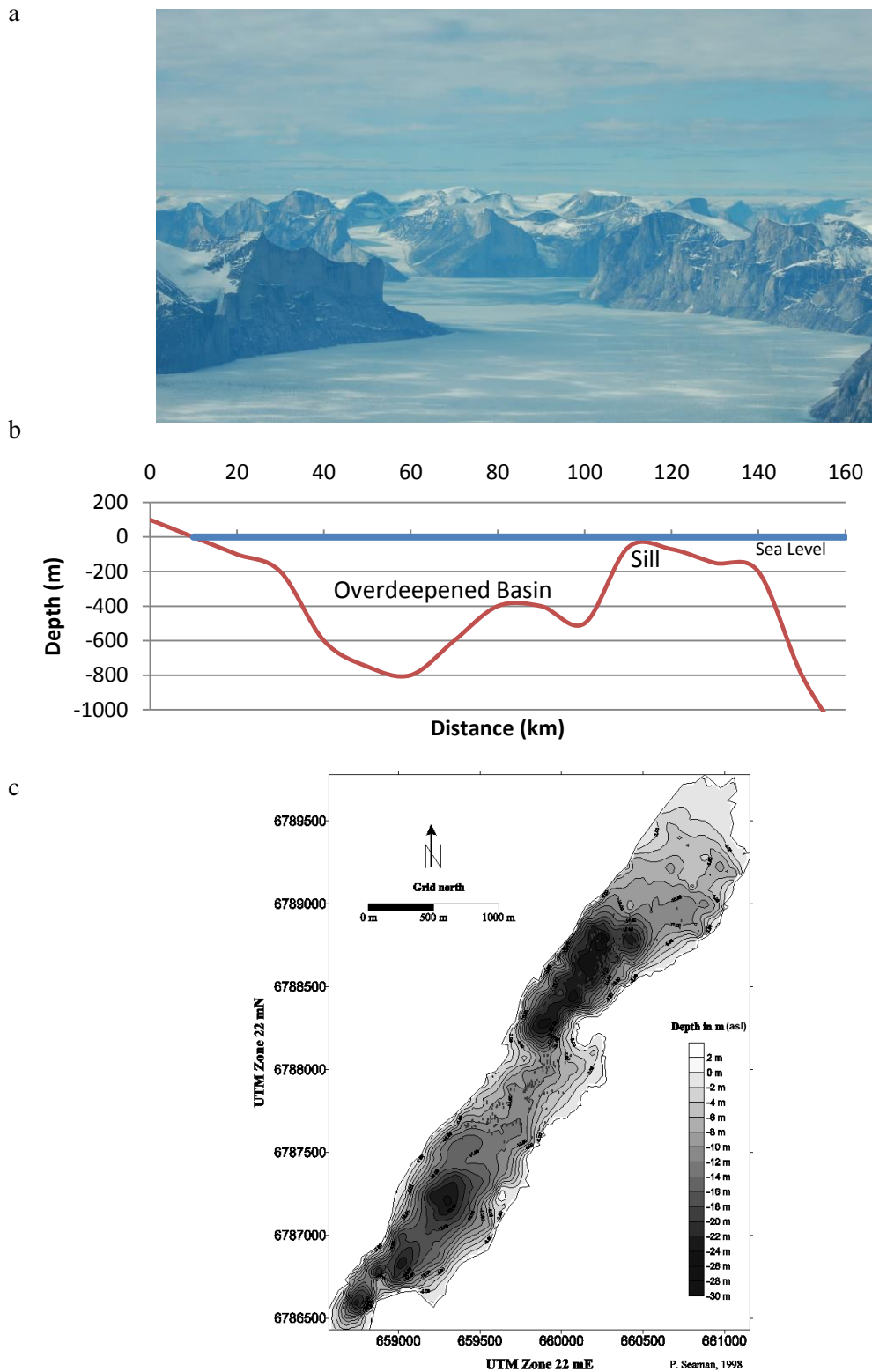


Figure 4. Fjords; longitudinal profile, and bathymetry.

(a) Sam Ford Fjord, Baffin Island, Nunavut, northern Canada. The fjord is overdeepened to 800 m depth (image: Stefan Plazier). (b) Longitudinal profile of Sam Ford Fjord, Baffin Island, Nunavut, northern Canada, showing the overdeepening within the fjord (based upon data from Kessler et al., 2008). (c) The bathymetry of the Ikka Fjord, southwest Greenland, as mapped by side scan sonar. The survey has detected several overdeepenings of up to 30 m depth, as indicated by the darkest coloured closed contours (modified from Seaman, 1998).

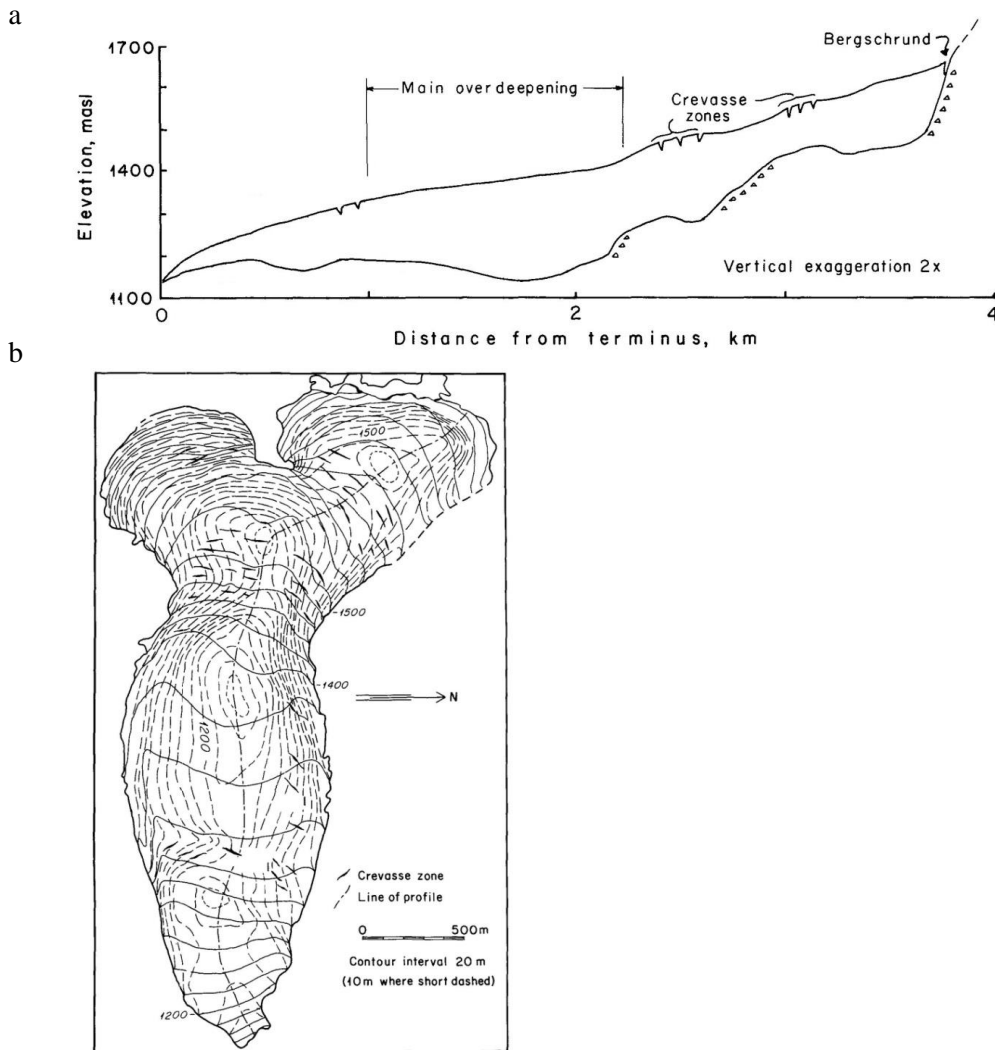


Figure 5. Longitudinal profile and plan map of Storglaciaren Glacier, Northern Sweden.

(a) A longitudinal profile of Storglaciaren, a small glacier in northern Sweden, showing the relationship between locations of water-input (i.e. crevasse zones and bergschrund) and presumed sites of bedrock quarrying (triangles). Four overdeepenings are clearly visible, each situated immediately down-glacier of locations of water-input and presumed sites of quarrying. (b) Plan map of Storglaciaren, showing surface and bed topography, and the line of the longitudinal profile. Bed topography from Eriksson (1990). Modified from Hooke (1991).

An important defining characteristic of an overdeepening is the presence of an adverse slope (Linton, 1963) (figure 6a). Overdeepenings, and any associated adverse slope, may be difficult to identify in the field because of the large size of the phenomenon relative to the observer, and because of possible infill by water (figure 6b) and sediment (figure 6c). Typically, overdeepenings occur on a scale of hundreds of square metres to many square kilometres in the horizontal plane (i.e. length, width), and on a scale of tens to hundreds of metres in the vertical plane (i.e. depth) (Hooke, 1991; Seaman, 1998; Kessler, et al., 2008; Ross, et al., 2011; Cook & Swift, 2012; Makos, et al., 2013), although no work has yet been undertaken to quantify these metrics.

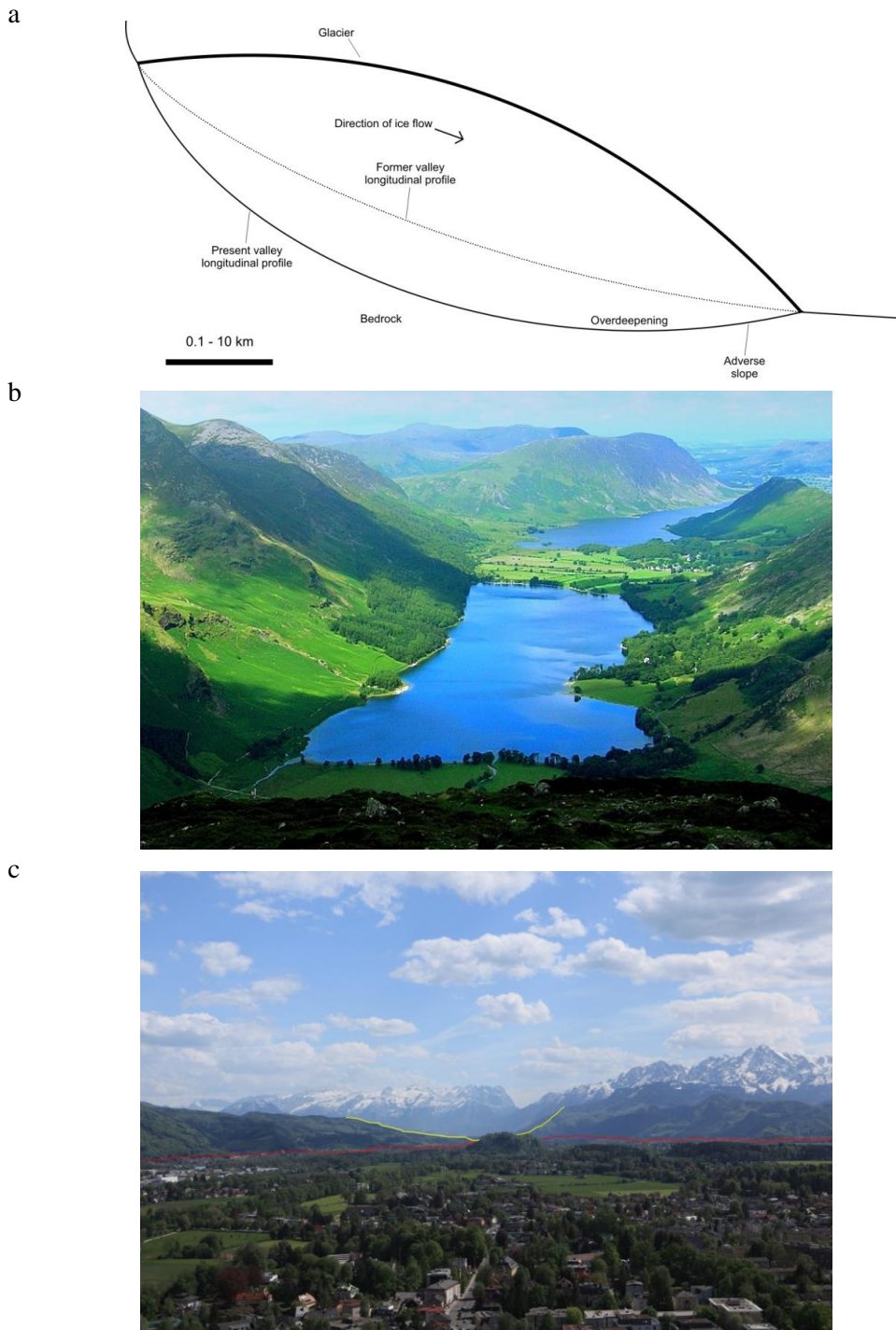


Figure 6. Schematic of an overdeepening. Water and sediment filled overdeepenings.

(a) A schematic longitudinal profile of a glacier-scale overdeepening. An important defining characteristic of all overdeepenings is the presence of an adverse slope at the down-glacier end. (b) A trunk-valley overdeepening bisected by post-glacial alluvial deposition and otherwise infilled by water (Buttermere Lake and Crummock Water, UK) (image: Rob Larkamb). From Cook and Swift, 2012. (c) The Salzburg Basin, Austria. The basin is of tectonic origin, glacially overdeepened by the Salzach Glacier to approximately 200 m depth (an example of a terminal overdeepening), prior to the Last Glacial Maximum. The overdeepened basin was subsequently a pro-glacial lake, which later became infilled with sediment. The view looks south, upstream. The U-shaped glacial valley, carved by the Salzach Glacier at the Last Glacial Maximum, is visible (yellow), and the limit of the sediment infill (foreground) of the basin is also clearly apparent (red).

Overdeepening is of interest because it is an important glaciological and geomorphological process that is thought to be a major control upon glacial landscape development, and which has the potential to influence the response of ice masses (i.e. morphology, dynamics, retreat rate, stability) to change in the global climate system. The study of the location and size of overdeepenings is crucial in enabling us to make process inferences that will aid development of a broader understanding of the relationships and feedbacks within glacial systems, and of landscape evolution (Cook & Swift, 2012). Additionally, overdeepenings are of interest in an applied sense. The phenomenon is quite commonly investigated in geotechnical engineering studies (Taylor & Wilson, 1997), and has also been considered in geohazard assessment analyses (Frey, et al., 2010). Some studies have investigated the use of overdeepenings as aquifers (Cormier, et al., 1998; Schneider & Rybach, 1999), for hydropower generation (Linsbauer, et al., 2012; Malyutkin & Molokov, 1985), or as potential locations for storage/disposal of nuclear waste (Sykes, et al., 2009; Talbot, 1999).

Despite their significance, outlined above, a systematic study of overdeepenings has yet to be undertaken. It has not been possible to establish whether different types of overdeepening exist (i.e. in different locations, occurring at different scales); or to develop a deeper understanding of the processes of overdeepening initiation and development, and the primary controls that are in operation. This research aims to contribute towards closing this gap in current knowledge utilising GIS tools and digital elevation models (DEMs). Overdeepening location and size are investigated within a study region and the potential controls on initiation and development are evaluated with a view to enhancing process understanding by empirical means. Research outcomes on the metrics of overdeepenings or process insights may help refine numerical models of glacial erosion and landscape evolution in the future. Locations of possible overdeepening are also investigated systematically at global scale, as an aid to future study.

In the first instance, literature is examined to demonstrate the extent of current understanding of overdeepening processes and of the landform. Afterwards, a novel typology of overdeepenings is developed based around their primary control. Testable hypotheses and project objectives are then developed to examine some controls upon overdeepening location and size. The methodology is subsequently discussed, concerning the DEMs and datasets used and how overdeepenings and other landforms (relevant to the study) are identified and defined; and how hypotheses are tested. Results are then evaluated and discussed.

## 2 Literature Review

*This chapter provides an appraisal of core theory pertaining to glacial overdeepening, as well as elucidation regarding a selection of important numerical models and theoretical and empirical studies of relevance to the study of overdeepening. Palaeoglaciology is explored, as a method to investigate past and contemporary processes. A typology of overdeepening is established, according to overdeepening controls and characteristics suggested by the literature. The interaction of controls is considered, before potentially testable hypotheses of controls are appraised. The geographical region to be studied is discussed.*

The general concept of the glacial overdeepening is traceable to the pioneering work of Henry Gannett (1898) and Albrecht Penck (1900). However, a widely agreed definition of the term has always been missing. For much of the 20<sup>th</sup> century, overdeepenings have typically only been mentioned in relevant research either obliquely or in passing. Studies which have directly mentioned and discussed overdeepenings in any detail have usually provided only an observational and/or morphometric description of the phenomenon, with little or no emphasis upon analysis of glacial processes and systems. Such studies were undertaken prior to the quantitative revolution in geomorphology, which occurred during the 1970s. Subsequent numerical models of glacial landscape evolution, and theoretical/ empirical studies of glacial erosion and the glacial landscape, have slowly developed process understanding to the point where processes that are possible controls upon overdeepening (and other glacial landform) location and size are being explored. Such development (presumably linked to improvements in computing technology) appears to have accelerated significantly within the last few years, hinting that our knowledge of glacial systems may be about to enter an exciting period of potentially rapid advancement.

### 2.1 Possible controls upon overdeepening location and size

It has been suggested that a variety of controls may be responsible for the location and size of glacial overdeepenings. From reviewing the wider literature I propose that overdeepenings can be simply categorised (by their context or primary control). Such overdeepening types, suggested in the literature, include: *cirque* (formed near the head of a glacier, during early glacier development, e.g. Antarctic examples (Aniya & Welch, 1981)), *equilibrium line altitude* (formed at the altitude of maximum glacier ice velocity, as the glacier reaches maturity, e.g. Alaskan examples (Hallet, et al., 1996)), *terminus* (formed near the glacier terminus, where meltwater is abundant, e.g. Kviarjokull, southeast Iceland example (Spedding & Evans, 2002)), *confluence* (formed at the confluence of two glaciers, where ice velocity increases due to

effective decrease in channel cross-sectional area, e.g. Yosemite Valley, USA example (MacGregor, et al., 2000)), *valley-floor perturbation* (formed immediately downstream of topographic steps or hanging valleys, due to focusing of meltwater, as discussed for Alpine examples (Bakker, 1965)), and *geological* (formed in lithological or structural zones of particular weakness, where glacial quarrying is most effective, e.g. Alpine examples (Preusser, et al., 2010)). Linton (1963), in his review of various field evidence of glacial landforms, asserts that overdeepenings are not an exceptional but a usual feature of glacial troughs.

## 2.2 Processes of overdeepening initiation and development

The work of Hooke is possibly the most significant modern contribution to research regarding glacial overdeepening. Hooke (1991) explains that glaciers erode by the processes of quarrying and abrasion, as well as by sub-glacial meltwater erosion. In the case of overdeepenings, quarrying is thought to be the dominant process. Hooke argues that a positive feedback operates, which amplifies perturbations in the longitudinal profile of the glacier valley. Crevassing, over a minor convexity in the bed, localises water input (and hence erosion), thus amplifying the convexity, and resulting in the creation or enhancement of the overdeepening (Hooke, 1991). The steepness of the adverse bed slope of an overdeepening may be limited by the ability of water to flow along the bed. This should result in an accumulated layer of till. This layer will increase in thickness until the down-glacier mass transfer, by deformation within the layer, equals sediment production by erosion. Such a sediment layer would protect the bed throughout the down-glacier reaches of an overdeepening, thus concentrating erosion at its head. It is postulated that this is why overdeepenings exist, and why their longitudinal profiles are characteristically asymmetrical, with the deepest point at their up-glacier ends (Hooke, 1991).

Alley, et al. (2003), propose that hydraulic erosion (or at least sediment evacuation by water) also controls overdeepening location and size. A debris layer protects the bed surface, where there is insufficient meltwater to evacuate it. However, as meltwater moves down-glacier, hydraulic erosion and/ or evacuation of products of glacial meltwater intensifies, removing the protective debris layer, and focusing glacial erosion, as it does so. Alley, et al. (2003), suggest that the supercooling of sub-glacial meltwater may then set up a negative (stabilising) feedback process that limits erosion and bed steepening, thus maintaining the profile of the overdeepening.

There is uncertainty regarding the equivalence of the processes of initiation and development of cirques versus those of other types of overdeepenings. This is because of the relative difference

in scale and location, and because the origin of cirques is contested. Cirque overdeepenings occur at the glacier head (prior to the advance of a full valley glacier), where ice velocity and meltwater abundance is thought significant (Sugden & John, 1976). However, erosion of cirques at the head of mountain glaciers is difficult to explain (Mindrescu & Evans, 2014). Cirques are not investigated further in this study because they represent a different form of overdeepening; the focus here is upon overdeepenings that occur at valley-scale, under the influence of controls associated with mature valley glaciers. Such overdeepenings are not likely to develop very far up-glacier from the ELA because a glacier cannot easily erode bedrock or flush out debris very far up-glacier from the ELA due to low ice velocity and lack of meltwater (Sugden & John, 1976). The processes of overdeepening initiation and development at valley-scale, and the relationship of such processes with potential controls, are elaborated upon in section 2.7.

Turnbull & Davies (2006) put forward an alternative origin for cirques, by rock avalanche instead of by glacial erosion. Evans (2006) summarises the conventional view that rotational flow in steep glaciers (Lewis, 1960) compensates for low ice discharge and velocity, and glacial quarrying at the base of the headwall is aided by water pressure fluctuations (Hooke, 1991), as discussed by Mindrescu & Evans (2014). However, as argued by Brown & Ward (1996), whilst the conventional and well-entrenched (e.g. Davis, 1954; Sugden & John, 1976) 'top down' model of glacier growth may be appropriate for upland areas that are reglaciated, a 'bottom up' model may be more applicable to steeply dissected upland terrain experiencing initial glaciation. Brown & Ward (1996) assert that the 'top down' model is where upslope nival hollows develop into cirques, and small glaciers then later extend downslope. The 'bottom up' model is where valley floor nival hollows develop into overdeepenings, experiencing more accumulation and less ablation than cirques (due to location and form), even after the relative difference in landform scale has been accounted for. In the 'bottom up' (initial glaciation) case, considerable thicknesses of snow and ice may develop in stream valleys, with glaciers enlarging up-valley as well as down-valley (Brown & Ward, 1996), until an equilibrium steady-state valley glacier is established. This view has implications for how valley enlargement takes place, and may overcome some of the difficulties involved in the assumed transition from nivation hollow to valley glacier (Brown & Ward, 1996).

### 2.3 Numerical, theoretical, and empirical research of relevance to the study of overdeepening

Numerical models of glacial landscape evolution can model overdeepenings (e.g. Oerlemans, 1984; MacGregor, et al., 2009; Egholm, et al., 2012b). Such models use mathematical formula (in the form of computer code) to simulate the behaviour of ice and consequent landscape change. In such models, landscape change is a response to erosion by ice and to associated physical processes. The greater the number of *relevant* physical processes (sometimes termed forcings) included in a model, the more complex and computationally expensive the model will become, but the more accurately the model should be able to simulate the real world (provided that the formula representing a given physical process is correct). Further, models will become significantly more complex and computationally expensive as they increase in dimensionality and scale, but again should produce a more accurate simulation of the real world as long as processes are accurately represented.

As with all types of model, numerical models are intended to improve our understanding of processes within a system. They can be used purely to this end or to predict what may happen within a system in the future, perhaps if certain variables change (e.g. to investigate climate change). Numerical models are often simplifications of the real world, and are not necessarily as accurate as analytical ones (Hooke, 2005). Simplifications are made in order to lower computational expense and so allow models to run efficiently, or simply because real world physical parameters are ill-defined or unknown. Some model parameters can be estimated from what is known in the real world (model calibration). Models often vary in the way they discretise the real world. For these reasons different models can produce different results based on the same input, and so comparison of the output from different models is important in order to optimally interpret (and assess weaknesses in) a given model, as discussed by Hooke (2005). Further, it is important that output from numerical models are validated against empirical observations (Hooke, 2005), thus allowing us to see whether a model is representing the real world effectively. Computer modelling of ice sheet dynamics began in the 1970s, with the shallow ice approximation (SIA) model (Hutter, 1983) being the most sophisticated from this early phase. It is later evolutions of this model (as well as other more complex models devised subsequently) that have since been utilised to examine valley glaciers in increasing detail. We now discuss some of these models, where relevant to the study of overdeepening.

Oerlemans (1984) is widely acknowledged to have developed the first surface process model to incorporate glacial erosion, thus enabling the recreation of the (glacial valley scale) overdeepenings that result from glacial erosion, and illustrating the importance of the ELA upon the erosion pattern (Tomkin, 2009). A glacier-scale numerical model, developed by Tomkin

(2009), employs glacial sliding-dependent erosion to qualitatively reproduce glacial morphologies for the Southern Alps of New Zealand. The simulation illustrates how models of surface processes can produce overdeepenings (at glacial valley scale, located at and below the location of the long-term ELA), as well as other geomorphic features, that are similar to those actually observed in the region. The model is of shallow ice approximation (SIA) type, which builds upon earlier work in that it is fully two-dimensional and employs first order forcing on mountain evolution. These forcings include tectonic uplift, isostasy, and hillslope and fluvial processes. A climate-dependent model of ice dynamics is employed to determine ice coverage and ice flux (Tomkin, 2009). Output from the model (figure 7) shows glacial overdeepening, and subsequent development of the graded fluvial profile for the principal river which later drains to the west of the basin divide, within the simulation. The diversity of glacial landforms produced by the model indicates that use of the model may be extended to cases beyond those discussed within the paper (with the consequence of potentially reproducing overdeepenings for other glacial scenarios and locations). To test the erosion model more fully, Tomkin (2009) indicates that future work should compare glacial erosion predicted by the model with that observed in the field.

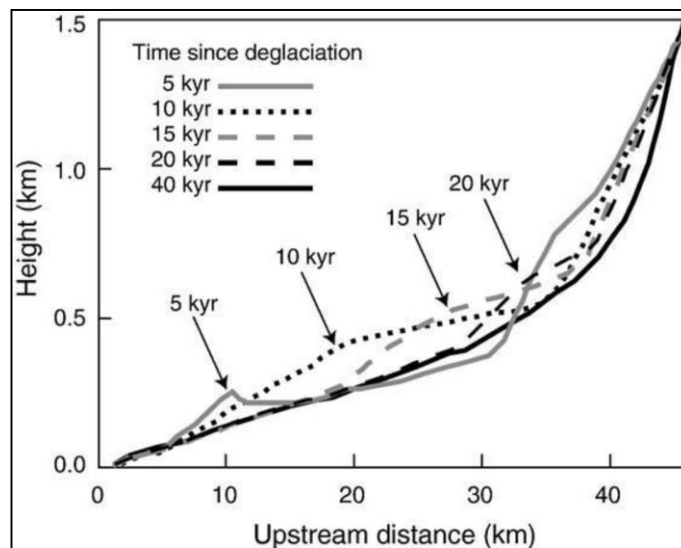


Figure 7. Output from the Tomkin (2009) model, showing glacial overdeepening.

Output shows glacial overdeepening, and subsequent development of the graded fluvial profile for the principal river which later drains to the west of the basin divide, within the Southern Alps simulation. The arrows point to the evolution of the glacially constructed convexity, which migrates upstream over time. It takes 40 kyrs for the smooth concave shape associated with steady-state river profiles to develop (Tomkin, 2009). The glacial overdeepening, observed in the modelled profile at 5 kyrs, is eradicated by fluvial erosion before 10 kyrs.

At a much larger scale, an ice-sheet model (GLIMMER) has been utilised by Jamieson, et al. (2008), to examine the evolution of landscapes under ice-sheets over long time scales (1280x1280 km matrix, over  $10^5$  to  $10^7$  years), in hypothetical situations. GLIMMER is a fully coupled thermo-mechanical 3-dimensional ice-sheet model with an SIA-based sliding component (scaled to yield erosion), which succeeds in generating overdeepenings (at glacial valley scale, located at the location of the long-term ELA). Output from the model suggests that valley overdeepening may be influential in stabilising the thermal regime of ice-sheets because as existing valleys are overdeepened they are more likely to become the permanent locations of warm-based ice (Jamieson, et al., 2008).

MacGregor, et al. (2009), develop a 'higher-order' model of the evolution of (glacier-scale) valley longitudinal profiles, which considers horizontal stress gradients within the ice (and thus allows more accurate simulation of ice flow on much smaller length scales). Output from the simulation successfully reproduces both cirque (located at the glacier head) and glacial valley scale overdeepenings (located below the location of the long-term ELA). MacGregor, et al. (2009), develop an earlier model (MacGregor, et al., 2000) by considering meltwater, quarrying and sediment transport processes, as well as isostasy, in addition to ice erosion and climate. Further, hillslope and headwall-specific processes are considered, such as added mass balance to the glacier head from blowing or avalanching snow, and associated geomorphic processes such as temporal variability in water inputs (discussed by Hooke (1991)) and increased clast concentration at the bed that could enhance erosion near the glacier head. MacGregor, et al. (2009), assert that a simple erosion model cannot predict the glacial landscape effectively, and that it is critical to ensure that headwall processes are considered in current and future models, in the light of previous (oversimplified) model results (such as those from the MacGregor, et al. (2000) study), which have not accurately developed cirque forms. The MacGregor, et al. (2009), modelled simulations only develop cirque overdeepenings under conditions where temperature is constant. The application of more realistic variable temperature scenarios (i.e. the glacial–interglacial cycles that characterise the late Quaternary) yield no such phenomena. Glacial valley scale overdeepenings do form under variable climate scenarios, but they are less well developed than their counterparts formed under steady temperature conditions. MacGregor, et al. (2009), emphasize that treatment of sub-glacial erosion within output of the model remains significantly oversimplified, ignoring important processes such as supercooling and rotational sliding within overdeepenings. MacGregor, et al. (2009), state that current knowledge of how these processes operate on the spatial scales involved in such models is limited. MacGregor, et al. (2009), assert that the interactions between long-term glacial erosion, lithospheric uplift, and climate may be important under more realistic climate variability (than is presented by the model), and that such interactions will be explored in future modelling work. MacGregor, et al. (2009), also argue that overdeepenings observed in the output of the model

are likely to be enhanced in nature as a result of initial geological conditions (i.e. joint spacing, variable rock hardness) and positive erosional feedbacks, such as enhanced water flow and variability in water pressure near crevasses across bedrock steps, as discussed by Hooke (1991). Models are not yet sophisticated enough to simulate such feedbacks accurately.

Herman, et al. (2011), incorporate simple sub-glacial hydrology into an ice-cap erosion model. The model is otherwise similar to that of Herman & Braun (2008), being based upon a SIA-based sliding rule, being of high spatial resolution, tested over a  $10^3$  to  $10^5$  year time scale, with a matrix at the scale of an orogen, and incorporating mountain evolution (tectonic uplift, isostasy), hillslope and fluvial processes. The results of the study indicate that sub-glacial hydrology is profoundly important to the temporal and spatial patterns of sub-glacial erosion, and suggest that the distribution of erosion is bimodal, with a peak at the ELA, and another peak at lower altitudes within the ablation area, where water due to melting abounds (Herman, et al., 2011). The model produces glacial valley scale overdeepenings, supporting the empirical evidence that large overdeepenings are generated at these erosional positions beneath glaciers.

Durst Stucki, et al. (2010), imply that a partial or complete decoupling between sub-glacial ice and meltwater erosion can occur (Herman, et al., 2011), in their theoretical and empirical investigation (a stratigraphic/ geomorphological reconstruction) of sub-glacial tunnel valleys of the Alpine foreland, Bern, Switzerland. The reconstruction is derived from empirical borehole evidence (Durst Stucki, et al., 2010). Durst Stucki, et al. (2012), go further, by using a simple hydrological model paired with geomorphological and seismic field observations (for the Lammschlucht inner gorge of the northern foothills of the central Alps), and postulate that a substantial contribution of the sub-glacial erosion mechanism (as per Herman, et al. (2011)) for observed overdeepenings could be related to the erosional effect of sub-glacial meltwater alone, resulting in the deepening of inner gorges (and the ultimate creation of overdeepenings) by either continuous meltwater flow or outburst flood. The concept of partial or complete decoupling between sub-glacial ice and meltwater erosion could have important implications as to how investigation of sub-glacial landform initiation and development might be approached in the future. Durst Stucki, et al. (2012), also discuss the influence of the underlying lithology upon the topography of the valley, outlining how mechanical contrasts of the bedrock constrain ice flow, which in turn has implications for hydraulic potential (which is associated with quarrying efficiency) beneath the glacier.

Other modelling, theoretical, and empirical research suggests that investigation of glacial overdeepenings is best focused upon glacial valley networks, and that glacial valley confluence may be significant in the initiation and development of overdeepenings. The numerical ice-sheet model employed by Glasser (1995) examines the effect of topography upon ice-sheet erosion, for a former Scottish ice-sheet (late Weichselian), and concludes that zones of intense ice-sheet erosion are concentrated in areas where basal melting is found to be highest and where basal topography favours convergence of flow. This implies that general glacial landscape evolution (including the development of landforms such as overdeepened troughs and scoured bedrock) is governed to a great extent by the exploitation of the pre-glacial topography, via a positive erosional feedback mechanism (Glasser, 1995), a point also highlighted by Swift, et al. (2008), in their discussion of the East Greenland (overdeepened) fjord system. Within the East Greenland fjord system, glacial erosion appears to have been confined mainly to the modification of the pre-glacial valley system, the pattern of which indicates that lithological strength is also a potentially important control on fjord morphology and fast ice flow (Swift, et al., 2005; Stroeven & Swift, 2008). Alley, et al. (2003), describe convergent flow as favouring erosion and transport, accelerating local deepening of the glacier bed, and allowing formation and steepening of the down-glacier side of overdeepenings. It has been suggested that a simple decrease in valley width can function as a means for focusing erosion (and therefore creating overdeepenings), by increasing ice discharge per unit width (e.g. MacGregor, et al., 2000; Anderson, et al., 2006), as can the addition of tributary glacier ice in confluences (e.g. MacGregor, et al., 2000; Amundson and Iverson, 2006) (MacGregor, et al., 2009). As described previously, Herman and Braun (2008) employ a numerical ice-cap model to assess the role of ice erosion upon landscape evolution. The model is tested using a case study of the Southern Alps of New Zealand. Output from the model shows small-scale topographic steering, and suggests that ice convergence can cause overdeepening to occur within valleys. Kessler, et al. (2008), use a two dimensional ice-sheet model to simulate the incision of fjords through a coastal mountain range. They show that topographic steering of ice, and erosion proportional to ice discharge, are sufficient to form (overdeepened) fjords, without the usually stated requirement of there being a contrasting thermal regime between valley and interfluvium (Sugden, 1978). Holtedahl (1967) discusses the (overdeepened) depth conditions in the Hardangerfjord and Sognefjord of Norway, and concludes that such conditions are largely the result of changes in glacial erosion, the effect of which varies according to the thickness of the glaciers, being greatest in the inner parts where confluence takes place, and least in the outer areas where diffluence occurs.

MacGregor, et al. (2000), use a numerical model of glacial erosion to explore the development of the longitudinal profiles of glacial valleys, including glacial valley scale overdeepenings, under variable climate conditions. They test the importance of tributaries in setting the pattern of glacial erosion. The model focuses on sub-glacial landform development, using a conservative rule set with minimal feedbacks which might otherwise enhance or focus erosion (pro-glacial fluvial processes, though important in glacial valley geomorphology, are also ignored) (MacGregor, et al., 2000). Output from the model shows that persistent high-relief overdeepenings are most commonly generated in simulations where tributary glaciers are incorporated into the model (i.e. where ice is focused at confluences), and that shallower overdeepenings also occur at the glacier terminus. Meltwater, quarrying, and sediment transport processes (which might be important in developing small-scale valley-floor roughness, e.g. the crevasse-water feedback of Hooke, 1991), and positive feedbacks (which might steepen headwalls) are not incorporated into the model (MacGregor, et al., 2000). Consequently model output is rather simple.

Haynes (1968) analyses cirque overdeepenings located in northern Scotland, and suggests that bedrock structure may influence overdeepening geometry/ size. She matches observed cirque longitudinal profiles to logarithmic (k) curves and describes how apparent similarities between the cirque morphometries are commonplace (being a consequence of the general effect of glacial erosive processes associated with ice flow, and being common to all cirques), but that differences between the cirque morphometries are extraordinary (being clearly related to variation in underlying rock structure). Haynes laments the fact that rock structure and erosional processes are not more often considered together, a reality that is still somewhat the case today, at least with regard to the study of overdeepenings. Krizek, et al. (2012), develop the (k curve) methodology established by Haynes (1968), using field data from the Bohemian Massif (Czech Rep. borders), focusing specifically upon analysis of degree of cirque overdeepening, rather than analysis of overall cirque morphometry. The resulting classification of the analysed overdeepenings (according to k-value) supports the findings of Haynes (1968), that bedrock structure may influence overdeepening geometry/ size. Krizek, et al. (2012), find that classified overdeepenings are deemed to correspond well with regional geological divisions, as well as with regional variations in the intensity and development of mountain glaciation. The overdeepenings also correspond well with classifications derived from analysis of other morphometric characteristics for cirques in the region.

Seguinot (2008) presents results of a numerical model of glacial erosion, based upon flow modelling using the SIA, combined with a bed separation calculation, and a calculation to estimate glacial quarrying by sub-critical crack growth, in conjunction with empirical observations of geology and geomorphology for the Erdalen region of western Norway. The model output and empirical observations suggest that small-scale (within valley) overdeepenings (such as those within the Erdalen region) are mainly the expression of bedrock resistance variations and ice flux pattern of a glacier. Quarrying, as modelled by the study, mainly contributes to valley headwall steepening, although it is reported that the quarrying model could be improved by better modelling of valley glacier hydraulics, snow and ice adhesion on steep slopes, and climatic variations. Seguinot (2008) states that the glacier sliding law used in the model requires better quantification (via water pressure measurements), and further suggests that change in valley width and the presence of tributary junctions are important factors in enhancing glacial erosion, which should be investigated further.

## 2.4 The over-simplicity of current numerical models of glacial landscape evolution

Numerical models of ice mass erosion are currently too simplistic. They are not comprehensive enough in their inclusion of controls and feedbacks, to allow confidence in model outcomes regarding the generation (or not) of overdeepenings (and of other glacial landforms). As discussed in section 2.3, modern numerical models of ice mass erosion build upon the basic shallow ice approximation (SIA) type of model. SIA models neglect longitudinal and transverse stress gradients (among other parameters) and consequently fail to capture the full effects of rugged topography and related feedbacks, between erosion by glacial sliding and the extent and style of glaciation (Egholm, et al., 2011). Egholm, et al. (2011), present a depth integrated ice-sheet model (integrated second order shallow ice approximation (iSOSIA)), which takes into account the 'higher order' effects (from horizontal stress gradients within the ice) related to steep and rugged bed topography whilst still providing the computational efficiency needed for three dimensional simulations of glaciation and landscape evolution in response to, for example, long term climate variations. The iSOSIA model demonstrates the potential complexity and sophistication of modern numerical models of ice dynamics.

Egholm, et al. (2012a), compare SIA and iSOSIA model output, and demonstrate how gradients in horizontal stress play a primary role in scaling the bed shear stress of glaciers. They demonstrate how higher order ice dynamics influence the feedback between glacial sliding and erosion in models, thereby providing important stabilization mechanisms that prevent runaway effects associated with the steepening of longitudinal profiles and the formation of overdeepenings (Egholm, et al., 2012a). In contrast, SIA-based models can incise and steepen the landscape without sensing the stabilizing effect of the horizontal stress gradients (Egholm, et al., 2012a). Consequently SIA-based models may develop overdeepenings where there should be none, or exaggerate the magnitude of the phenomenon. Higher order ice dynamics are therefore particularly important for models of long-term glacial landscape evolution, because the relevance of the higher order effects generally increase with time as erosion accumulates (Egholm, et al., 2012a). However, the iSOSIA modelling approach of Egholm, et al. (2012a), only addresses isolated feedbacks associated with ice dynamics, in simplified settings (Egholm, et al., 2012a). A number of other processes associated with glacial erosion, such as meltwater modulated quarrying (Cohen, et al., 2006), the confluence of glaciers at tributary junctions (MacGregor, et al., 2000), and the formation of ice crevasses (Hooke, 1991) are known to provide other important feedback mechanisms, which lead to the formation of glacial overdeepenings and topographic steps (Egholm, et al., 2012a). Such processes are not included in the Egholm, et al. (2012a) model.

Egholm, et al. (2012b), build upon the iSOSIA modelling approach of Egholm, et al. (2011; 2012a), to achieve a more unifying model (in terms of process and feedback inclusion) than has been realised in other studies. Processes incorporated in the model include en-glacial and sub-glacial meltwater and sediment transport, and quarrying (all simulated with greater complexity than has previously been possible), as well as fluvial and hillslope related erosion processes, bedrock mass strength change, the effect of climate, and tectonic uplift. Output from the model shows that addition of glacial hydrology to the iSOSIA modelling approach creates small-scale (within valley) overdeepenings within the terminus zone. Generally, sub-glacial sediment coverage and limited transport prevent the formation of large overdeepenings, although small (cirque) overdeepenings form high in the catchment near glacial valley headwalls. However, the modelling of more efficient sub-glacial sediment deformation leads to the development of numerous small-scale (within valley) overdeepenings. Simulating change in bedrock mass strength is enough to provoke the formation of a glacial valley scale overdeepening in the terminus zone (Egholm, et al., 2012b), which is enlarged significantly by meltwater modulated quarrying. Although the Egholm, et al. (2012a; 2012b) model implementations account for higher order effects and utilise a real-world topographic scenario, the processes and feedbacks associated with confluence (and subsequent potential overdeepening development) are not explored. The modelled scenario is a simple trunk valley with associated minor tributaries (i.e. tributaries that are not well proportioned relative to their counterpart tributary, when potential confluence with the trunk valley is considered), and as such does not include an example of confluence as defined in this investigation (i.e. where tributaries are well proportioned relative to each other), and as modelled elsewhere (MacGregor, et al., 2000; Herman & Braun, 2008; Kessler, et al., 2008). Minor tributaries commonly develop hanging valleys. This is observed consistently in the model output of Egholm, et al. (2012a; 2012b). Many process and feedback simplifications remain in the Egholm, et al. (2012b) model, but the flexibility of interaction between various components of the model allow the comparison of model predictions with observations of overdeepening morphology (from theoretical and empirical studies) on a much more systematic level than has previously been possible (Egholm, et al., 2012b). The processes and feedbacks associated with confluence should be explored in future implementations of this model. Application of the model to further real-world topographic scenarios in the future may perhaps help identify the governing processes behind overdeepening initiation and development.

## 2.5 Review summary

As this review of recent research demonstrates, it is clear that there are many potential controls which could drive the initiation and development of overdeepenings (as well as that of other glacial landforms) within the glacial system, the relationships and feedbacks within which are not fully understood. Table 1 summarises the reviewed models which simulate overdeepenings, and which controls and feedbacks are included within each model. Reviewed research suggests that the location and size of overdeepenings is not controlled solely by glacial processes (i.e. by ice velocity and meltwater abundance), but is also strongly influenced by external topographical (i.e. confluence and valley-floor perturbation) and geological (i.e. bedrock mass strength) components. It is clear that numerical models of ice mass erosion are currently not yet sophisticated enough (in their inclusion of controls and feedbacks) to generate overdeepenings with sufficient certainty, and therefore cannot yet be relied upon to accurately explain the controls upon overdeepening location and size, and the significance of the phenomenon within the wider glacial system (although this situation does seem to be rapidly improving). The full coupling of the flow of ice, water and sediment (and other processes) within numerical models of ice mass erosion is important in this regard; as is the inclusion of higher order ice dynamics in order that a realistic stabilising feedback mechanism (as seen in nature) may be incorporated into models to prevent (model induced) runaway effects associated with the steepening of longitudinal profiles and the formation of overdeepenings (Egholm, et al., 2012a). Further, the more frequent application of models to real-world topographic scenarios is required, both in order to make predictions, and to refine models. It is important that a particular type of overdeepening predicted by a given model is realistic (i.e. situated in the expected location, at correct size and scale, and with the correct frequency) when compared to a similar type of overdeepening, observed in nature. If the predicted overdeepening is not plausible then there may be some problem or over-simplification within the model.

It is apparent that far greater research is required in order to appreciate the significance of overdeepenings (within the glacial system), and to appreciate consequent implications for other glacial and landscape processes (Cook & Swift, 2012). Outcomes from development and testing of hypotheses relating to the aforementioned controls will help to explore and resolve the unknowns, and will help to improve numerical models.

Numerical model (Reference)	Controls & feedbacks included in model	Overdeepening simulation
<b>Oerlemans (1984)</b>	Ice flow, thermal regime, climate, isostasy	At equilibrium line altitude (ELA); at glacial valley scale
<b>Tomkin (2009)</b>	Velocity based ice flow, thermal regime, climate, mountain evolution (tectonic uplift, isostasy), hillslope processes, fluvial processes	At and below ELA; at glacial valley scale
<b>Jamieson, et al. (2008)</b>	Velocity based ice flow, thermal regime, climate, isostasy	At ELA; at glacial valley scale
<b>MacGregor, et al. (2000)</b>	Velocity based ice flow, thermal regime, climate	At valley confluences and below the ELA; at up to glacial valley scale
<b>MacGregor, et al. (2009)</b>	Velocity based ice flow, thermal regime, climate, isostasy, en-glacial and sub-glacial meltwater, sub-glacial sediment transport, quarrying, hillslope processes, headwall specific processes	At glacier head and below the ELA; at cirque and glacial valley scale
<b>Herman &amp; Braun (2008)</b>	Velocity based ice flow, thermal regime, climate, mountain evolution (tectonic uplift, isostasy), hillslope processes, fluvial processes	At valley confluences and within glacial valleys; at up to glacial valley scale
<b>Herman, et al. (2011)</b>	Velocity based ice flow, thermal regime, climate, mountain evolution (tectonic uplift, isostasy), hillslope processes, fluvial processes, sub-glacial meltwater	At and below ELA; at glacial valley scale
<b>Kessler, et al. (2008)</b>	Velocity based ice flow, climate, isostasy	At valley confluences and within glacial valleys (fjords); at up to glacial valley scale
<b>Egholm, et al (2012b)</b>	Velocity based ice flow (inc. accounting for horizontal stress gradients within ice), thermal regime, climate, tectonic uplift, hillslope processes, fluvial processes, en-glacial and sub-glacial meltwater, en-glacial and sub-glacial sediment transport, quarrying, bedrock mass strength change	At glacier head, within glacial valleys, where there is a change in bedrock mass strength, and at glacier terminus; at cirque, localised (within valley) and glacial valley scales

**Table 1. Reviewed numerical models which simulate overdeepenings, and the controls and feedbacks included within each model.**

## 2.6 Palaeoglaciology

Palaeoglaciology deals with glaciation cycles of the Quaternary ice age. It combines the dynamics of present day ice sheets and glaciers deduced from glaciology, with the history of former ice sheets and glaciers deduced from glacial geology (Fastook & Hughes, 2013). Palaeoglaciology allows the reconstruction of ancient ice sheets and glaciers, for the purpose of investigating past and contemporary glacial processes. The spatial analysis of glacial landforms is essential to such reconstruction. Glacial landforms are the clues in the landscape from which the dimensions, geometry, dynamics and history of former ice sheets and glaciers can be reconstructed (Glasser & Bennett, 2004).

Glacial landforms can be caused by either erosional or depositional processes. There is limited literature discussing the processes and landforms of glacial erosion, especially when compared to that discussing glacial deposition. This is partly because detailed palaeoenvironmental information is commonly preserved within depositional landforms, which are more easily dated both by absolute and relative means (Lowe & Walker, 1997). Depositional landforms have therefore been widely used in palaeoglaciology, especially in the glacial inversion models that have been developed for continental-scale palaeo-ice sheets (Glasser & Bennett, 2004). Numerical modelling has traditionally largely separated ice sheet/ glacier dynamics (and associated atmospheric, oceanic and climate change dynamics) from the underlying glacial geology (Fastook & Hughes, 2013). This simplification may have been due to the computational expense of potential calculations, and/ or perhaps because real world physical parameters were ill-defined or unknown. Modern studies are now beginning to (re)unify these disciplines (e.g. Fastook & Hughes, 2013). However, in part because of this legacy separation (and in part because of a lack of empirical study) glacial erosional landforms have been much less widely utilised in palaeoglaciology. Consequently there is a lack of understanding as to how such landforms reflect former glaciological parameters. As discussed by Glasser & Bennett (2004), reconstructions of former ice dynamics from glacial erosional landforms remain rare. Such landforms are as yet only considered in terms of former glaciological parameters such as basal thermal regime (Sugden, 1977), and in reconstructions of the vertical extent of former ice masses (Dahl, et al., 1996).

Much literature supports the view that the relationship between glacial erosional processes/ landforms and former ice sheets/ glaciers is important. Given our lack of understanding of these relationships, it is clear that further research should be undertaken. Oerlemans (1984) asserts that glacial erosion can modify the bed of an ice sheet and therefore alter large-scale ice dynamics and mass balance, over the timescale of a glacial cycle. Glasser & Bennett (2004) remark that sub-glacial erosion plays a crucial role in providing the sediment that underlies

many of the Earth's large ice masses (Boulton, 1996; Alley, et al., 1997; Clark & Pollard, 1998), and comment that glacial erosion is important in determining sediment yields in fluvial (Warburton & Beecroft, 1993) and fjordal settings (Elverhoi, et al., 1998); in long-term landscape evolution (Meigs & Sauber, 2000); and in relief production (Whipple, et al., 1999; Tomkin & Braun, 2002). Glasser & Bennett (2004) further state that landforms of glacial erosion are used as palaeo-environmental indicators of glacial climates in the geological record (e.g. Spenceley, 2001).

Glacial erosional landforms have rarely been used in palaeoglaciology because erosional forms have a higher preservation potential through multiple glacial cycles than depositional landforms and consequently developing relative chronologies for suites or assemblages of erosional landforms is often complex (Rudberg, 1997). For most erosional landforms only approximate chronologies may be identified (Rudberg, 1992; 1994; 1997). Glasser & Bennett (2004) remark that the absolute ages of glacial erosional landforms are poorly constrained (due to lack of dateable material), and that the age of specific landforms has usually been inferred from their relationship with other features for which age estimates are available. Recent advances in exposure-age dating techniques (e.g. cosmogenic isotope dating) make it possible to obtain absolute age estimates for bare rock surfaces in glaciated areas (Brook, et al., 1996), for dating erratic boulders (Jackson, et al., 1997), and for estimating glacial erosion rates (Davis, et al., 1999); thus providing the means to establish glacial chronologies for erosional landforms for the purpose of palaeoglaciological investigations (Glasser & Bennett, 2004).

Glacial troughs (and the overdeepenings contained within) are considered to be palimpsest landforms that have developed over many glaciations (Bronge, 1996). A landscape is said to be palimpsest where (for example) it experiences significant areal scouring and selective linear erosion (by warm based ice), and/or experiences successive phases of valley glacier, ice cap, and ice sheet erosion to form a composite erosional landscape (Sugden & John, 1976; Sugden, 1978). In such circumstances, some glacial landforms may be obliterated or appear very poorly defined within the landscape. Often, only the most recent ice flow directions are recorded by erosional surface features, and so it is conceivable that the processes operating during deglaciation are those that leave the strongest imprint on the landscape (Glasser & Bennett, 2004). Improved dating control may improve estimates of the age and rates of glacial processes, and so help provide better interpretation of glacial palimpsest landscapes (Glasser & Bennett, 2004).

This study will focus on the spatial analysis of glacial landforms formed by erosional processes, and will explore the initiation and development of one such landform (overdeepenings) by controls associated with former glaciers, thus enhancing understanding of the processes

involved. The study is empirical, utilising GIS and digital elevation models of topography. The study does not explore exposure-age data, or utilise numerical modelling, because of the scope of available resources. However, research outcomes will help refine numerical models of glacial erosion and landscape evolution, and may aid the reconstruction of ancient ice sheets and glaciers, in future studies.

## **2.7 Development of a typology of overdeepenings**

To construct a framework for further investigation of overdeepenings, I develop a typology of overdeepening according to their controls and characteristics. ‘Pure’ types of overdeepenings are initiated and (their size subsequently) developed only by fundamentally glacial controls. ‘Topographical’ and ‘geological’ types of overdeepenings are initiated and (their size subsequently) developed first and foremost by non-glacial, external, controls. Potential hypotheses to be tested in future studies should examine all such potential controls upon overdeepening location and size. Such controls have been considered further, during the initial stages of this investigation and are discussed in the following sections of this chapter. Predicted overdeepening controls and characteristics are summarised in Table 2.

### **2.7.1 Pure (glacial) controls upon overdeepening location and size**

The most fundamental control upon the location and size of (pure) overdeepenings is that of variation in ice velocity. As ice-mass erosional potential at the glacier-scale is presumed to scale with ice velocity (Sugden & John, 1976), it is expected that overdeepenings will occur in zones of a glacier where ice velocity is maximised. For a steady-state glacier, this zone should occur directly beneath the ELA (e.g. Hallet, et al., 1996; Oerlemans, 1984; Herman, et al., 2011) (figure 8a, 8b). The ELA of a glacier is the position at which the accumulating mass of ice or snow, up-glacier, balances the ablating mass that is taken away by melting and calving, down-glacier. This position on the glacier is therefore the location of maximum ice flux (i.e. the position of maximum movement of ice mass down-glacier), where the ice velocity is consequently greatest (figure 8c) (Sugden & John, 1976).

If ice velocity were the primary control upon overdeepening location and size, the phenomenon would be expected to occur in a clear regional pattern, as a ring of overdeepenings surrounding a mountain chain, each located at the ELA for each glacier (Sugden & John, 1976). Overdeepenings of this type would be of a magnitude comparable to the scale of the overlying glacier.

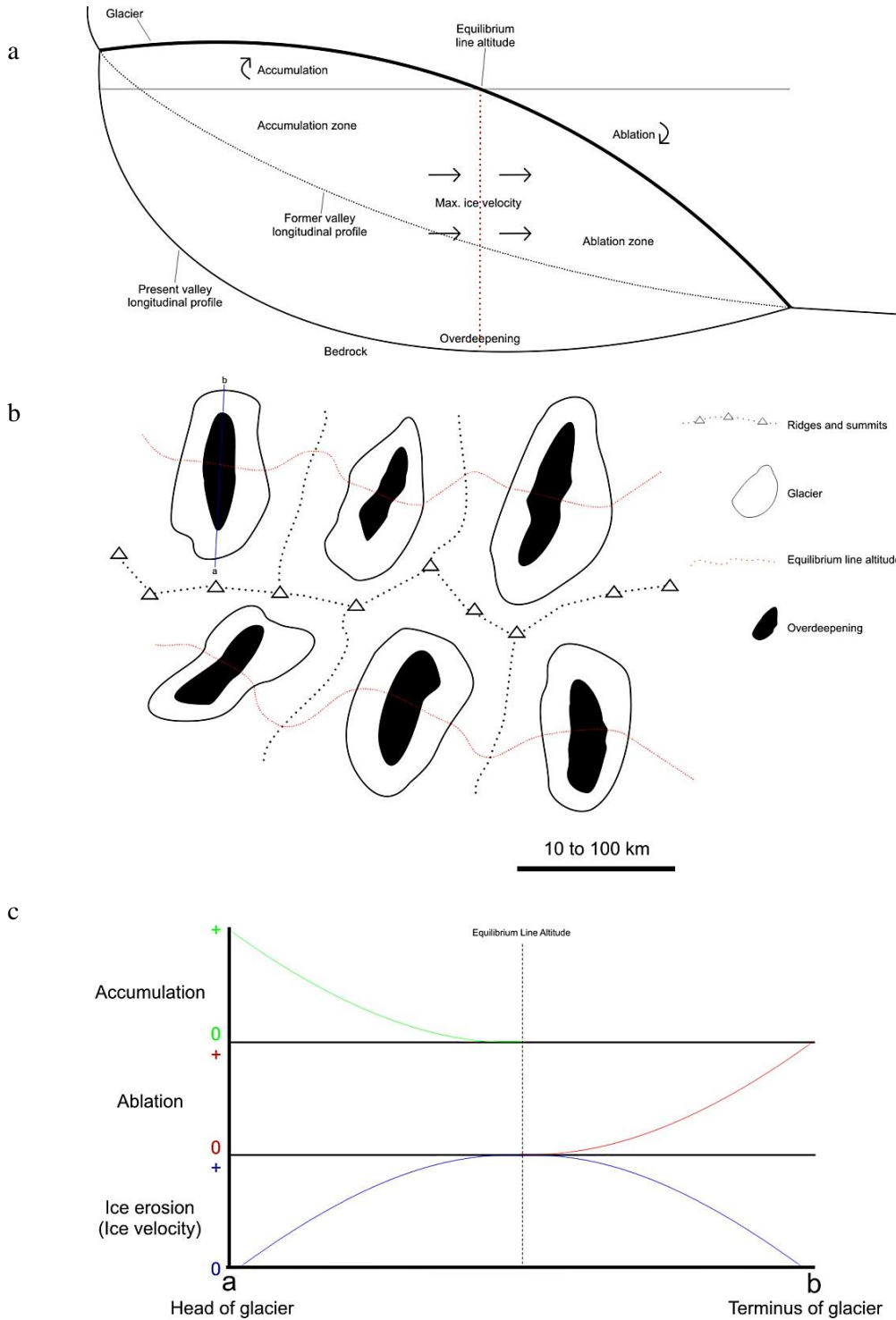


Figure 8. Schematic profile and plan of pure overdeepening(s), inc. process diagram (ice velocity).

(a) Schematic profile of a pure overdeepening, driven by variations in ice velocity. Erosional potential of a glacier scales with velocity, which is at its greatest beneath the equilibrium line altitude (ELA) (Sugden & John, 1976), creating a glacier-scale overdeepening. (b) Schematic plan of multiple valleys, each occupied by a glacier, each containing a glacier-scale overdeepening centred about the ELA. (c) Process diagram for the production of a pure overdeepening, driven by variations in ice velocity. The location of maximum ice flux (maximum movement of mass down-glacier) is located at the ELA, where the accumulating mass of ice or snow, up-glacier, balances the ablating mass that is taken away by melting and calving, down-glacier (Sugden & John, 1976). This is where the ice velocity is greatest, and so consequently where the greatest erosional potential is located.

The other fundamental control upon the location and size of (pure) overdeepenings is that of variation in meltwater abundance. As sub-glacial meltwater plays a critical role in erosion (Hooke, 1991; Sugden & John, 1976; Herman, et al., 2011) it is expected that maximum potential erosion (and therefore the potential for overdeepening), at glacier-scale, will occur in zones where meltwater is most abundant (e.g. Spedding & Evans, 2002). Meltwater abundance increases down-glacier from the ELA (due to increasing ablation). Therefore, for a glacier in steady-state, the zone of maximum erosion (by meltwater) should occur down-glacier from the ELA (figure 9a, 9b).

It is expected that overdeepenings will form where meltwater is abundant enough to be efficient at flushing away the debris, generated by up-glacier erosion, which would otherwise protect the bed from further denudation (figure 9c). This efficiency will allow direct erosion of the bed by meltwater (concentrating erosion at the overdeepening head, some distance up-glacier from the glacier terminus). An abundance of meltwater will act to further lubricate ice movement (i.e. increase ice velocity) over the substrate, thus further enhancing erosion (Alley, et al., 2003).

If meltwater abundance were the primary control upon overdeepening location and size, the phenomenon would be expected to occur in a clear regional pattern, as a ring of overdeepenings surrounding a mountain chain, each positioned down-glacier of the ELA for each glacier. Overdeepening form would be such that the location of maximum overdeepening depth would be situated somewhere down-glacier of the ELA (i.e. where actual ice erosion is greatest) (Hooke, 1991; Alley, et al., 2003). Each overdeepening of this type would be of a magnitude that scales with the respective overlying glacier.

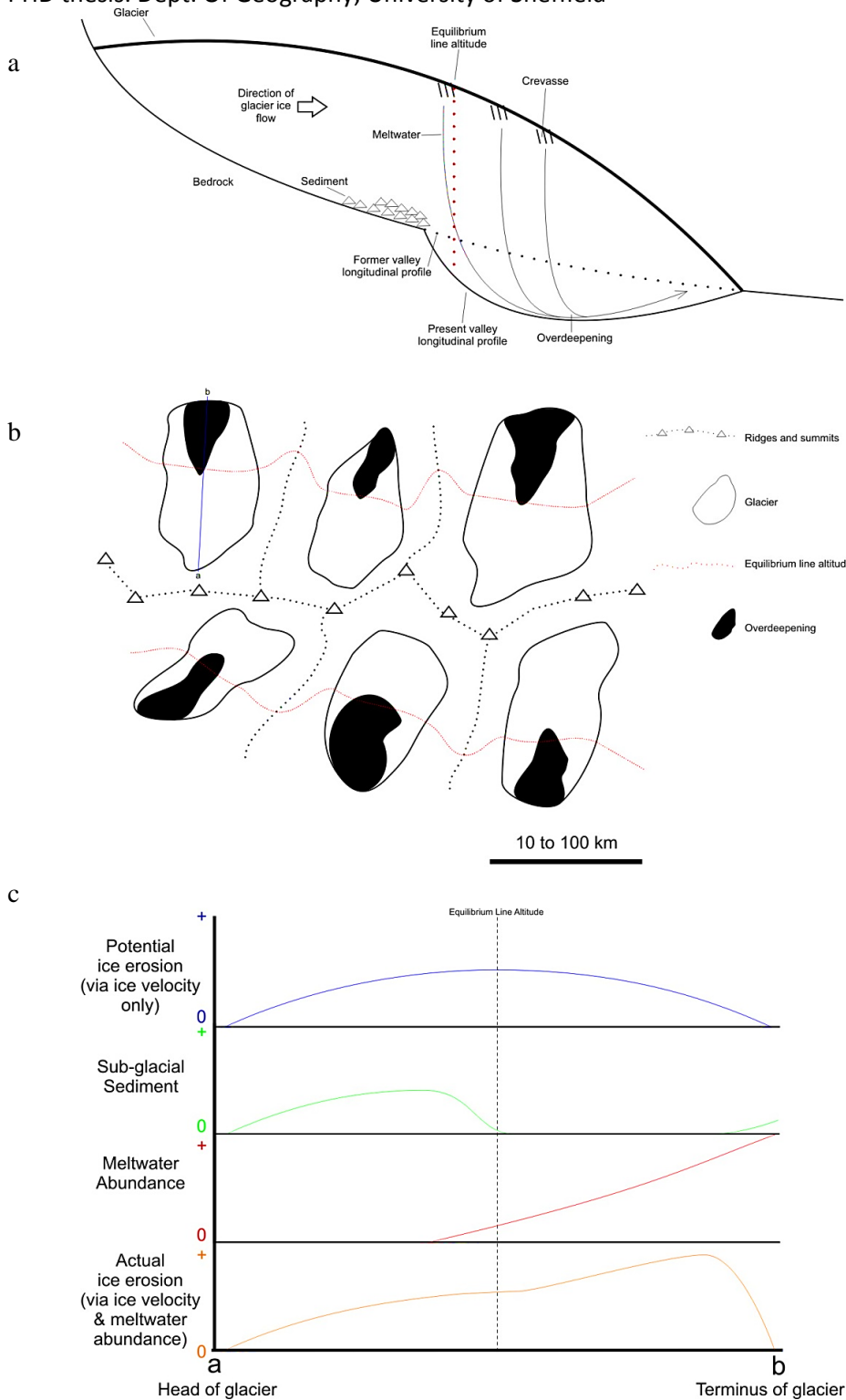


Figure 9. Schematic profile and plan of pure overdeepening(s), inc. process diagram (meltwater abundance).

(a) Schematic profile of a pure overdeepening driven by variations in meltwater abundance. Erosional potential of a glacier scales with the availability of basal meltwater (Hooke, 1991; Sugden & John, 1976; Herman, et al., 2011), down-glacier of the ELA, creating a glacier-scale overdeepening at this position. (b) Schematic plan of multiple valleys, each occupied by a glacier, each containing a glacier-scale overdeepening located down-glacier of the ELA. (c) Process diagram for the production of a pure overdeepening, driven by variations in meltwater abundance. The greatest erosional potential is located where meltwater is abundant enough to be efficient at flushing away the debris, generated by up-glacier erosion, which would otherwise protect the bed from further denudation (Alley, et al., 2003).

### 2.7.2 External (topographical and geological) controls upon overdeepening location and size

Other controls upon the location and size of overdeepenings are either topographical or geological. A major topographical control is via valley cross-sectional area (CSA) change, influencing ice velocity within. As with any other flowing media, where ice encounters a decrease in channel CSA along its course (e.g. a valley or channel constriction) there must be a localised flow acceleration (or ice 'speed up') for continuity reasons, and a corresponding increase in erosion (figure 10a). It can therefore be reasoned that potential glacial erosion should scale nearly inversely with valley CSA (figure 10b).

Valley confluences are possibly the most easily identifiable exemplar of valley CSA decrease within landscapes (figure 10c). Within glacial valley confluences, it can be reasoned that glacial erosion works to balance the sum of tributary channel CSAs with trunk channel CSA (i.e. confluence allometry may naturally reach an equilibrium steady-state in which ice speed up will no longer occur). However, from visual analysis of landscapes I suggest that valley confluences seldom reach this state over glacial timescales (most probably because the process is self-limiting). As a result, an effective decrease in channel CSA is typically observed through glacial valley confluences as tributaries merge into the trunk. It is therefore expected that valley confluences will be areas of localised ice speed up and maximum local glacial erosion (Glasser, 1995; Kessler, et al., 2008), and that overdeepenings will develop as a consequence of this (Alley, et al., 2003; Herman & Braun, 2008; Kessler, et al., 2008; Holtedahl, 1967; MacGregor, et al., 2000). The effective decrease in channel CSA observed through most valley confluences is thought to be a first order control upon ice velocity speed up within glacial valley confluences. Additionally however, it can be reasoned that ice flow will become less impeded by bed and lateral drag (i.e. frictional forces), where tributary channels merge within a confluence, because ice will have less contact area with valley floor and sides (i.e. ice will have a decreased wetted perimeter) within the trunk channel. Such decrease in frictional forces is thought to be a second order control upon ice velocity speed up within glacial valley confluences.

If glacial valley CSA change were the primary control upon overdeepening location and size, the phenomenon would be identified in strong association with confluence. Such associations would typically be localised in scale, relative to the magnitude of the overlying glacier. Overdeepenings of this type would be of a magnitude that scales with the respective valley confluence with which each is associated.

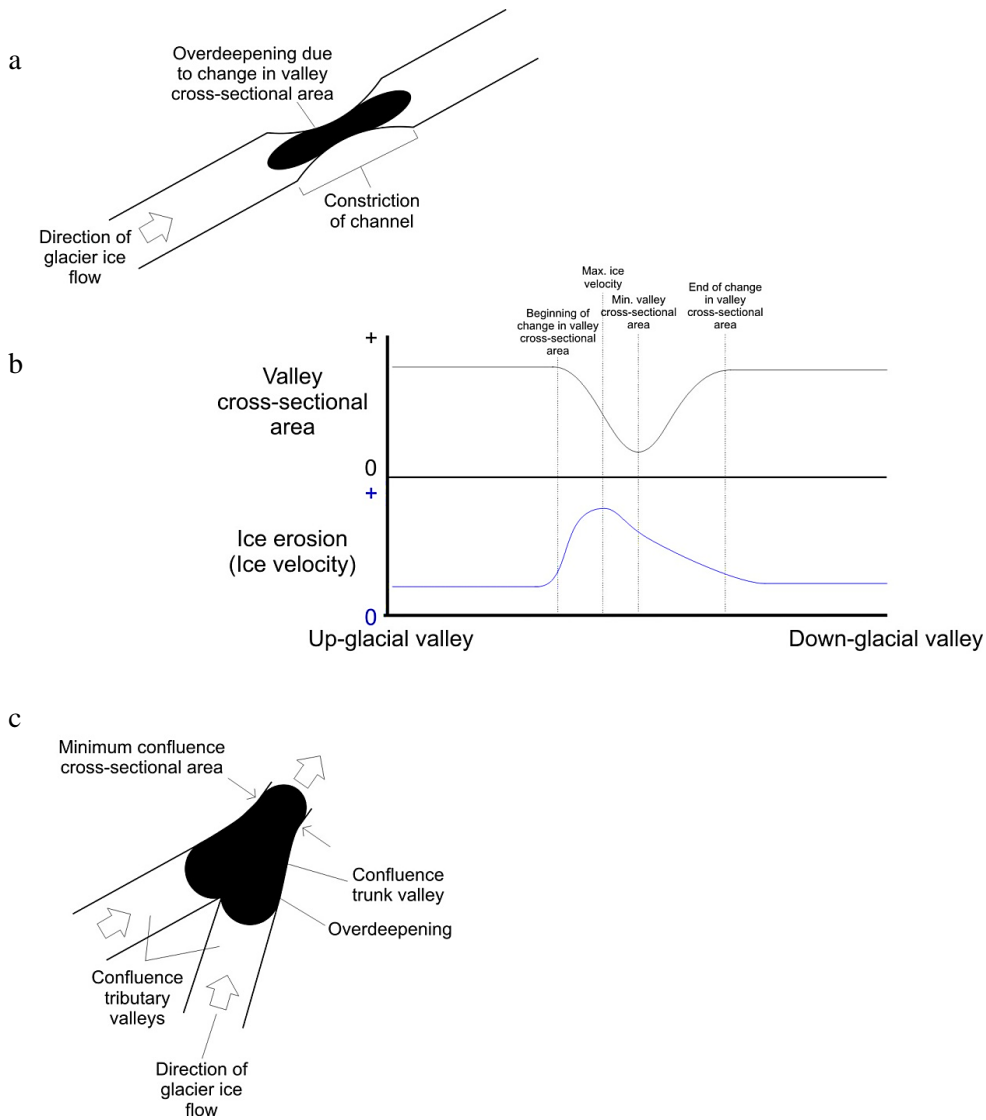


**Figure 10. Schematic plans of topographical overdeepenings, inc. process diagram (valley CSA change).**

(a) Schematic plan of a valley channel constriction. It can be reasoned that the narrower part of the valley (smaller cross-sectional area (CSA)) will experience faster glacier ice flow (and hence more erosion), than the wider part of the valley, thus producing an overdeepening. (b) Process diagram for the production of a simple topographical overdeepening (i.e. within a valley channel constriction), driven by change in glacial valley CSA. Where ice encounters a decrease in channel CSA along its course there must be a localised increase in ice velocity, and a corresponding increase in erosion. Therefore it is predicted that potential glacial erosion will scale nearly inversely with valley CSA. Maximum ice velocity will occur up-glacial of the location of minimum CSA within the valley channel constriction, for flow continuity reasons (i.e. localised flow acceleration (or ice ‘speed up’) must occur up-glacial of the effective channel constriction). The speculated position of maximum ice velocity is supported by empirical observations for glacial valley confluences (which are possibly the most easily identifiable exemplar of valley CSA decrease within landscapes). The empirical observations suggest that a zone of ice velocity increase occurs up-glacial of the location of minimum CSA, within confluences, at the junction of glacial tributary lateral moraines, where they join to form a medial moraine (Gudmundsson, et al., 1997). (c) Schematic plan of a valley confluence. Valley confluences demonstrate an effective decrease in channel CSA (see text). It is therefore expected that valley confluences will be areas of localised ice velocity speed up and maximum local glacial erosion (Glasser, 1995; Kessler, et al., 2008). As a consequence, it is expected that overdeepenings will occur within confluences (Alley, et al., 2003; Herman & Braun, 2008; Kessler, et al., 2008; Holtedahl, 1967; MacGregor, et al., 2000).

It is expected that this type of overdeepening would be positioned about the location of minimum CSA within a valley confluence. Empirical observations suggest that a zone of ice velocity increase occurs within glacial valley confluences, at the junction of glacial tributary lateral moraines, where they join to form a medial moraine (Gudmundsson, et al., 1997). The form of this type of overdeepening is therefore expected to be such that maximum overdeepening depth would be situated immediately down-glacier of this position within the valley confluence (i.e. where ice erosion is greatest). This form is also anticipated, because it can be reasoned that peak flow acceleration (or ice 'speed up') would occur up-glacier of the location of minimum CSA within the valley confluence, for flow continuity reasons.

Another topographical control upon the location and size of overdeepenings is via abrupt change in glacial valley longitudinal profile (i.e. valley-floor perturbations such as steps or hanging valleys) causing ice crevassing and consequent localised sub-glacial focusing of meltwater. As it can be reasoned that particularly competent (strong) bedrock will be able to withstand glacial erosion, it can be supposed that valley-floor perturbations within the competent bedrock may survive a glacial episode. Where this is the case, it is expected that valley-floor perturbations will concentrate subsequent glacial erosion, producing overdeepenings (e.g. Bakker, 1965).

It is expected that a valley-floor perturbation (created by prior tectonic/fluviol activity, and/or by glacial processes active during an earlier glacial period) will accentuate glacial erosion (Hooke, 1991). Ice crevassing (brittle deformation) will occur where sub-glacial topography steepens sufficiently (i.e. at the valley-floor perturbation) that the ice cannot elastically deform adequately to accommodate the change in bed slope gradient. This will focus meltwater at the bed (i.e. the crevasse will provide a conduit for surface waters; figure 11a) and result in a positive feedback ice erosion mechanism (i.e. slope gradient/ crevasse/ meltwater/ ice velocity) as an overdeepening develops (Hooke, 1991; Alley, et al., 2003) (figure 11b).

If abrupt change in glacial valley longitudinal profile were the primary control upon overdeepening location and size, overdeepenings would be identified in strong association with valley-floor perturbations. Such associations would be localised in scale, relative to the magnitude of the overlying glacier. An overdeepening of this type would be of a size comparable to the scale of the valley-floor perturbation with which it was associated. It is expected that this type of overdeepening would be positioned immediately down-glacier from the valley-floor perturbation (Hooke, 1991; Alley, et al., 2003).

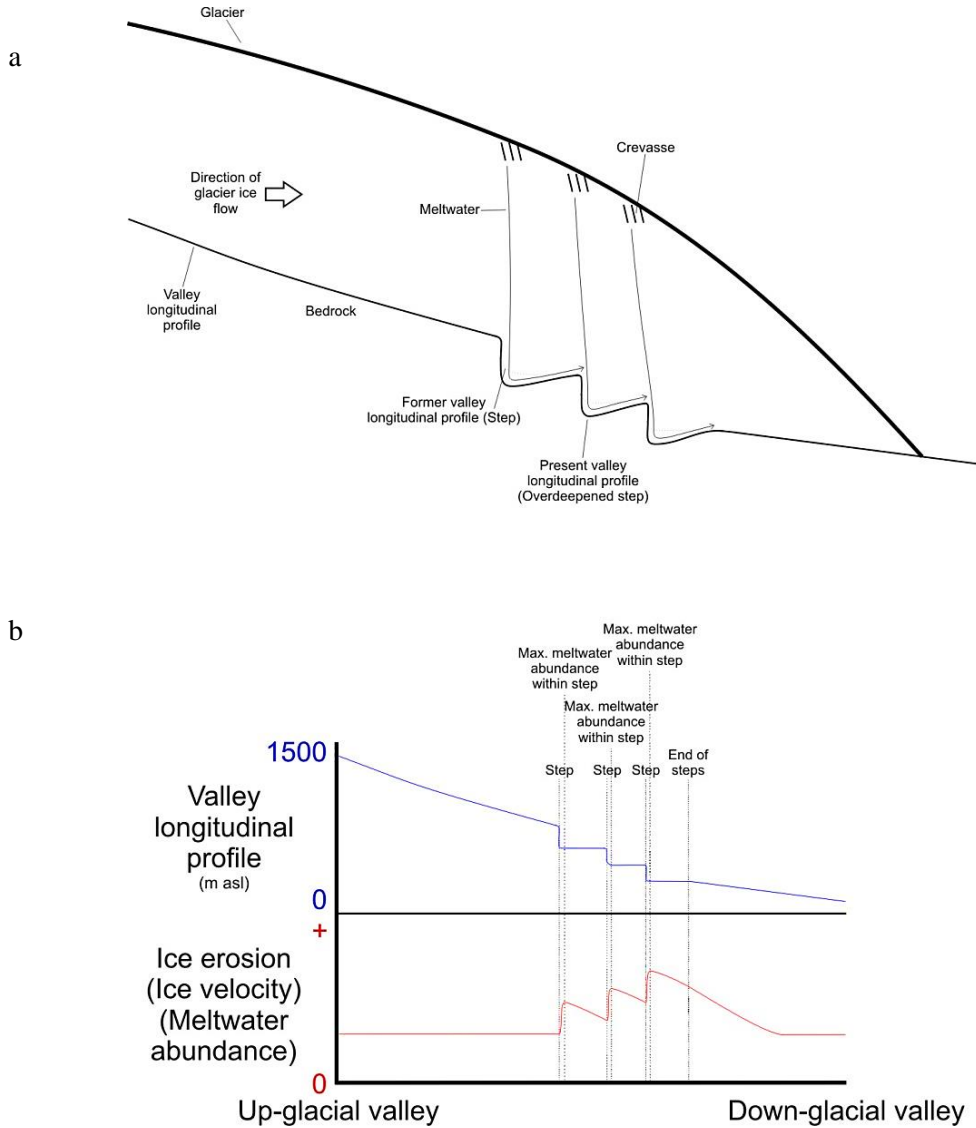


Figure 11. Schematic plan of topographical overdeepenings, inc. process diagram (valley-floor perturbations).

(a) Schematic profile of a series of valley steps (i.e. valley-floor perturbations). It is expected that each valley step will concentrate glacial meltwater, thus increasing glacial erosion and producing an overdeepening within each step (Hooke, 1991). (b). Process diagram for the production of topographical (valley-floor perturbation type) overdeepenings, driven by abrupt change in glacial valley longitudinal profile. Meltwater abundance will increase where ice crevassing focuses meltwater into a step (also increasing ice velocity in the process), increasing glacial erosion within each step and producing overdeepenings (Hooke, 1991; Alley, et al., 2003).

Geological control upon overdeepenings may occur where there is a change in bedrock mass strength. As it can be reasoned that zones of less competent (weaker) bedrock will be more easily eroded by a glacier than zones of bedrock that are more competent, it is expected that overdeepenings will be more common within less competent lithologies. Similarly, it is expected that zones of structural weakness (i.e. a fault or shear zone), within otherwise homogenous bedrock units, will erode more easily than similar lithologies which lack a zone of structural weakness; and that, again, overdeepenings will be more likely to occur within structurally weakened zones (MacGregor, et al., 2009; Haynes, 1968; Seguinot, 2008).

Glacial processes (i.e. those of quarrying and abrasion) will be more effective at eroding within structural fault zones and/or lithological zones of weak mass strength, where bedrock is blockier (i.e. where bedrock is jointed, loosened and/or faulted or sheared; figure 12a) (Hallet, 1996). Within structural fault zones and/or lithological zones of weak mass strength, the quarrying process will exploit the weakness (by fast glacier sliding, low basal pressures, and the focusing of meltwater (Hallet, 1996; Hooke, 1991) (figure 12b). This will result in increased glacial erosion within weak zones (relative to that experienced within more competent lithologies), and subsequent development of overdeepenings (e.g. Preusser, et al., 2010). Within such weaker zones, it can be reasoned that the quarrying process will provide a greater quantity of entrained basal ice debris within the glacier sole, than is the case within more competent lithologies, creating a positive feedback which will contribute further towards bedrock erosion (i.e. by providing the tools necessary for increased abrasion).

If change in bedrock mass strength were the primary control upon overdeepening location and size, it is expected that overdeepening would be identified in strong association with structural fault zones and/or lithological zones of weak mass strength (zones classified as igneous, metamorphic, sedimentary and structural, in broadly decreasing order of competency). Such associations may occur on a variety of scales (i.e. overdeepenings of varying size may be observed, at up to glacial valley scale), depending upon the relative size of the weak rock zone and the ice mass. Overdeepening form would be such that the location of maximum overdeepening depth would be situated at the local position of maximum ice velocity & meltwater abundance (i.e. quarrying), where ice erosion is greatest, within these zones (Hallet, 1996; Hooke, 1991).

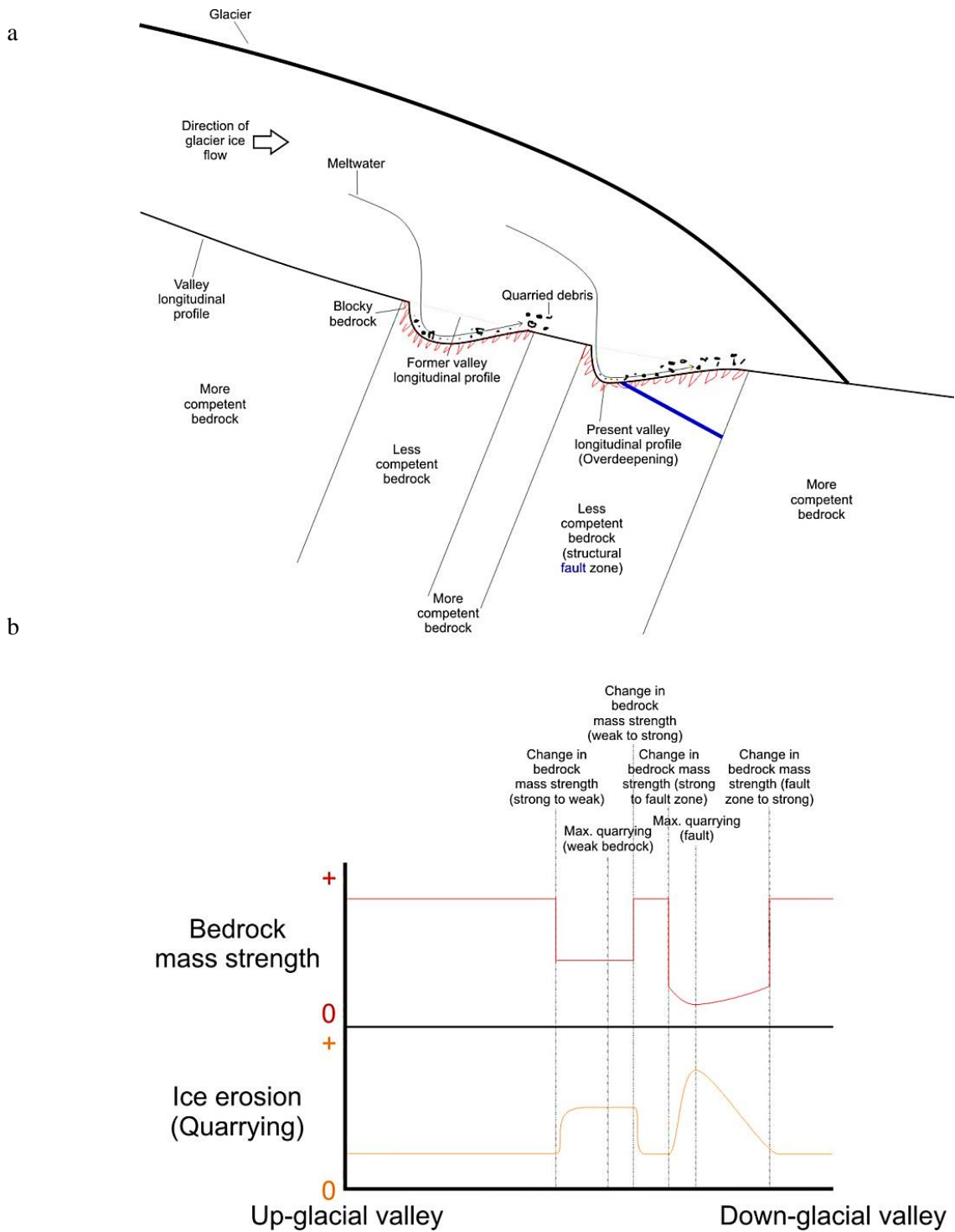


Figure 12. Schematic plan of geological overdeepenings, inc. process diagram (bedrock mass strength change).

(a). Schematic profile of various lithologies and a structural fault zone, denoting change in bedrock mass strength. It is expected that structural fault zones and/or lithological zones of weak mass strength will concentrate glacial meltwater and increase ice velocity (i.e. quarrying), thus increasing glacial erosion and producing overdeepenings (MacGregor, et al., 2009; Haynes, 1968; Seguinot, 2008). (b). Process diagram for the production of geological overdeepenings, driven by change in rock mass strength. Decrease in bedrock competency will accentuate glacial erosion. Where bedrock is jointed, loosened and/or faulted or sheared, the quarrying process will exploit the increasingly blocky bedrock (by fast glacier sliding, low basal pressures, and the focusing of meltwater (Hallet, 1996; Hooke, 1991)), increasing glacial erosion and producing overdeepenings.

Control	Location of overdeepening	Location of maximum overdeepening depth	Predicted spatial pattern of overdeepenings	Scale of overdeepening
<b>1. Pure - ice velocity</b>	At equilibrium line altitude (ELA)	Beneath ELA	Regional pattern about mountain chain	At glacial valley scale
<b>2. Pure - meltwater abundance</b>	Down-glacier of ELA	Towards glacier terminus	Regional pattern about mountain chain	At glacial valley scale
<b>3. Topographical - valley cross-sectional area change (CSA), influencing ice velocity</b>	Within glacial confluence, at location of minimum valley CSA	Up-glacier of location of minimum valley CSA	No regional pattern. Local associations between confluences and overdeepenings	Within valley, mainly localised
<b>4. Topographical - abrupt change in glacial valley longitudinal profile, influencing meltwater abundance</b>	Immediately down-glacier of valley-floor perturbation (e.g. step)	Immediately down-glacier of headwall of valley-floor perturbation (e.g. step)	No regional pattern. Local associations between valley-floor perturbations and overdeepenings	Within valley, localised
<b>5. Geological - bedrock mass strength change, influencing ice velocity and meltwater abundance</b>	Within weak lithology or structural fault zone	At local position of maximum quarrying	No regional pattern. Local associations between weak lithologies/ structural fault zones and overdeepenings	Within valley, localised; up to glacial valley scale

Table 2. Predicted overdeepening controls and characteristics, which could be examined in future studies.

### 2.7.3 Interaction of controls

It is reasonable to expect that pure (i.e. fundamentally glacial) controls upon overdeepening location and size will create simple (regional, ice-cap scale) patterns of overdeepenings, with each overdeepening occurring at glacial valley scale (see section 2.2.1, figures 8 and 9). Other (i.e. external) controls are expected to create additional complexity to these patterns; with overdeepenings most commonly occurring at much more localised scales (see section 2.2.2, figures 10-12). Whilst at glacial valley scale it is likely that ice velocity and meltwater abundance will control overdeepening location and size, from visual analysis of landscapes I suggest that at more localised scales topographical features (such as valley confluences and valley-floor perturbations) are significant external controls upon ice velocity and meltwater

abundance, consequently similarly controlling overdeepening location and size. It is therefore important that such topographical features are investigated further. In the same way, it is visually apparent from analysis of landscapes that, at a variety of scales, geology (i.e. bedrock lithology and/or geological structure) is a significant external control upon erodibility, again potentially controlling overdeepening location and size.

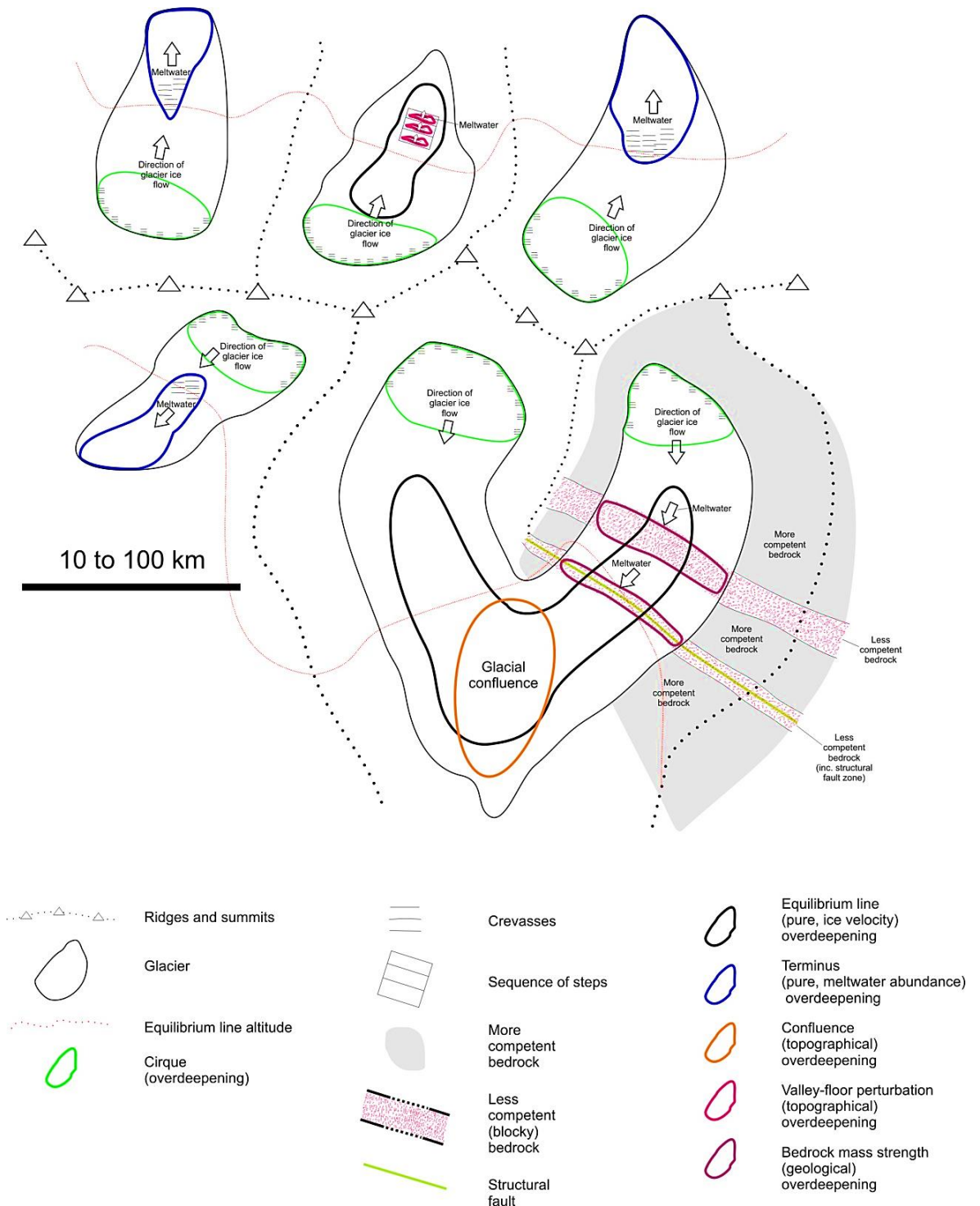


Figure 13. Schematic plan of several valley glaciers, summarising the various potential types of overdeepening.

Each predicted type of overdeepening (as detailed previously), is presented schematically in figure 13. The pure, ice velocity, control is considered to be primarily responsible for initial cirque formation and subsequent development of an overdeepening at the ELA, which is predicted to occur as a valley glacier develops (Sugden & John, 1976; Oerlemans, 1984). It is reasonable to suppose that controls upon overdeepening location and size may compound or simplify to produce not only the various types of overdeepening expressed previously, but also significant variation in the general morphology of the glacially eroded landscape, at a variety of scales.

#### **2.7.4 Developing testable hypotheses to examine controls upon overdeepening location and size**

Given the generalisations and ideas about overdeepening locations and controls, previously described in this chapter, I now explore the extent to which some testable hypotheses could be developed with regard to controls upon overdeepening location and size (summarised in Table 3).

It will be quite difficult to test for pure controls (i.e. ice velocity and meltwater abundance) upon overdeepening location and size. A predicted positive outcome of testing would be that a regional, ice-cap scale spatial pattern of overdeepenings should be observed in the landscape (i.e. a ring of overdeepenings should surround a mountain chain, either at the former estimated steady-state ELA or near the terminus). This pattern should be easy to observe if it is present, using digital elevation models (DEMs). However, identifying the former equilibrium line and terminus position for any given glacier is problematic, especially given the fact that glacial erosion is slow in relation to the speed of ice dynamics and climate change. For many past ice-sheets/ glaciers it can be presumed that there is a position of the former equilibrium line and glacier terminus that has been more stable than other positions. Such positions can be determined using radio-isotope analyses of glacial moraines (Fabel, et al., 2006). Unfortunately, data on glacial extents is almost always very limited in coverage. Where radio-isotope data are not available, alternative methodology is needed. The up-valley limit of lateral moraines can offer an estimate of steady-state palaeo-ELA for a former glacier, since no lateral moraines form in the accumulation area (Porter, 2001). However, although lateral moraine features are sometimes visually identifiable in DEMs (by the use of a GIS surface curvature algorithm), they are subtle landforms which are often difficult to detect, and which can be easily erased by post-glacial geomorphological processes. Similarly, the down-valley limit of terminal moraines can offer an estimate of steady-state palaeo-terminus position for a former glacier, using the same method, but problems similarly remain in terms of moraine identification. So whilst it

Control	Location of over-deepening	Predicted spatial pattern of overdeepenings	Scale of over-deepening	Method of testing	Method viability
<b>1. Pure - ice velocity</b>	At equilibrium line altitude (ELA)	Regional pattern about mountain chain	At glacial valley scale	Overdeepening locations evaluated against equilibrium line position (using radio-isotope data and DEMs)	Moderate (availability and coverage of data restricted)
<b>2. Pure - meltwater abundance</b>	Down-glacier of ELA	Regional pattern about mountain chain	At glacial valley scale	Overdeepening locations evaluated against terminus position (using radio-isotope data and DEMs)	Moderate (availability and coverage of data restricted)
<b>3. Topographical - valley cross-sectional area change (CSA), influencing ice velocity</b>	Within glacial confluence, at location of minimum valley CSA	No regional pattern. Local associations between confluences and overdeepenings	Within valley, mainly localised	Overdeepening locations evaluated against confluence location (using DEMs). Valley cross-sectional area change measured.	Excellent
<b>4. Topographical - abrupt change in glacial valley longitudinal profile, influencing meltwater abundance</b>	Immediately down-glacier of valley-floor perturbation (e.g. step)	No regional pattern. Local associations between valley-floor perturbations and overdeepenings	Within valley, localised	Overdeepening locations evaluated against valley-floor perturbation locations (using DEMs)	Quite poor (only viable where testable, see text)
<b>5. Geological - bedrock mass strength change, influencing ice velocity and meltwater abundance</b>	Within weak lithology or structural fault zone	No regional pattern. Local associations between weak lithologies/ structural fault zones and overdeepenings	Within valley, localised; up to glacial valley scale	Overdeepening locations evaluated against lithological/ structural zones (using geological data and DEMs)	Moderate (availability and coverage of data restricted)

Table 3. Methods with which potential hypotheses of controls upon overdeepening location and size could be tested in future studies.

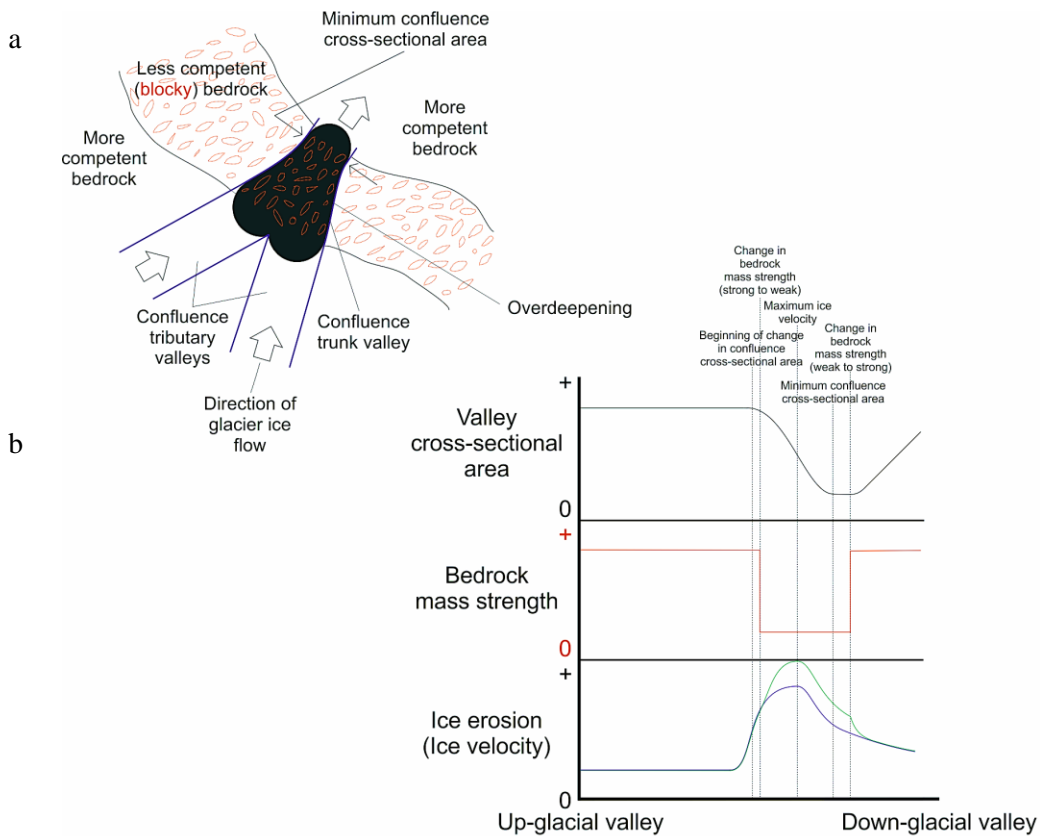
seems reasonable that pure (ice velocity and meltwater) overdeepenings could occur in well defined regional patterns, it is probably quite difficult to compare predicted verses observed overdeepening locations, because to make these predictions we would need much better control on changes in ice mass extent through time.

It is quite easy to test the influence of glacial valley confluence CSA change upon overdeepening location and size. Localised associations (i.e. at less than glacial valley scale) should be apparent between overdeepenings and valley confluences observed in the landscape (identified from visual inspection of DEMs (elevation values), and by use of DEM slope maps and DEM contours). Glacial valley confluence can be deemed to influence overdeepening location if confluence and overdeepenings are spatially coincident to a significantly greater degree than that predicted by random chance, within a given study region. In order to have some confidence in the causality of this influence, confluence tributary and trunk valley CSAs can be calculated using GIS and spreadsheet software. This allows comparison of ice velocity speed up (expressed as a ratio value), for groupings of confluences containing and not containing overdeepenings. The influence of confluence CSA change upon overdeepening size can then be examined by consideration of the relationship between confluence ice velocity speed up and overdeepening metrics (e.g. overdeepening depth, area, etc).

It will be difficult to examine the influence of abrupt change in valley longitudinal profile upon overdeepening location and size. For a positive outcome, testing should reveal localised associations (i.e. at less than glacial valley scale) between overdeepenings and valley-floor perturbations observed in the landscape (identified from visual inspection of DEMs, and by use of DEM slope maps and DEM contours), which should be spatially coincident to a significantly greater degree than that predicted by random chance, within a given study region. Whilst it is reasonable to expect that this type of overdeepening will occur in nature, it is difficult to test because the pre-existing topography is rarely known (i.e. a straight forward analysis of valley-floor perturbation and overdeepening co-location cannot contribute towards establishing the causality of any relationship that is found). It may be possible to test this control fully, for valleys where examples of overdeepened valley-floor perturbations occur, but only where neighbouring valleys also have the same lithology (perhaps, similarly, containing valley-floor perturbations), and where the neighbouring valleys show no evidence of previous glaciation. These neighbouring valleys effectively represent the pre-glacial topography of the valley under test. Such a methodology will provide evidence to support or oppose the causality of any valley-floor perturbation-overdeepening co-location relationship that is found, although the sample size (of testable valley-floor perturbations) may be small unless a very large study area can be analysed.

It is quite difficult to test the influence of bedrock mass strength change upon overdeepening location and size. Testing should reveal regional to local (i.e. ice-cap to significantly less than glacial valley) scale associations between overdeepenings observed in the landscape and lithologies/ structural zones observed as being of relatively weak bedrock mass strength (identified using digital geological maps). Bedrock mass strength can be deemed to influence overdeepening location if specific bedrock types/ structural zones and overdeepenings are spatially coincident to a significantly greater degree than that predicted by random chance, within a given study region. However, to have some certainty regarding the causality of any co-location relationships found between geological zones and overdeepenings, and to determine the further influence of geological zones upon overdeepening size, additional data concerning bedrock erosion (quarrying) rate for relevant study regions is required. Availability and coverage of such data is inadequate, and extensive field and/or lab work may therefore be required in order to pursue testing. Availability and coverage of geological maps is also a significant difficulty in the investigation of this control. Should the necessary data be obtained, the causality of relationships found between geological zones and overdeepenings can be assessed by comparison of bedrock quarrying rate, for groupings of overdeepenings situated within and outwith each geological zone for which a co-location relationship with overdeepenings is indicated. The influence of bedrock mass strength upon overdeepening size can subsequently be examined by consideration of the relationship between bedrock quarrying rate and overdeepening metrics within each relevant geological zone.

After consideration of the potential controls upon overdeepening location and size, it is clear that certain hypotheses will be more viable to test than others, within the context and scope of this investigation. This conclusion has been reached due to the complexity of certain methodologies and the lack of availability of necessary data in some cases. A hypothesis to test the influence of confluence valley CSA change is quite easy to test in the first instance. A simplified hypothesis to test the influence of bedrock mass strength change is also testable. Such a hypothesis can provide useful outcomes regarding control upon overdeepening location and size when amended to examine the influence of bedrock mass strength upon ice velocity speed up (alone), within glacial valley confluence (i.e. as a zone of influence) within geological zones (rather than within whole geological zones) within the study region. Simplification of the test is necessary due to lack of data concerning quarrying rate, and also due to the fact that available ice velocity speed up data are very location specific (i.e. within confluences). It is reasonable to consider the influence of bedrock mass strength upon ice velocity alone, as ice velocity has the potential to enhance erosion independently, irrespective of the involvement of other processes (such as meltwater erosion and quarrying) and the feedbacks between them. The consideration of ice velocity speed up alone is convenient, as it is possible to derive this data from confluences investigated in the confluence valley CSA change hypothesis. Comprehensively



Change in ice erosion rate driven solely by change in valley cross-sectional area  
 Change in ice erosion rate additionally driven by change in bedrock mass strength

Figure 14. Schematic plan of topographical/geological overdeepening, inc. process diagram (change in valley CSA & bedrock mass strength, simplified).

(a) Schematic plan of a valley confluence, occurring across several lithologies of different bedrock mass strength (the weakest is either a lithology, or a structural fault zone). The narrower part of the valley confluence (i.e. the trunk, smaller CSA) will experience faster glacier ice flow (and hence more erosion), than the wider part of the valley confluence (i.e. the sum of the tributaries, larger CSA) (Glasser, 1995; Kessler, et al., 2008), thus producing an overdeepening (Alley, et al., 2003; Herman & Braun, 2008; Kessler, et al., 2008; Holtedahl, 1967; MacGregor, et al., 2000). It is expected that structural and/or lithological zones of weak mass strength will further increase ice velocity, thus further increasing glacial erosion (Hallet, 1996; Hooke, 1991), and producing (or modifying the size of) an overdeepening (MacGregor, et al., 2009; Haynes, 1968; Seguinot, 2008). (b) Process diagram for the production of an overdeepening controlled by change in both confluence valley CSA and bedrock mass strength. Where ice encounters a valley confluence (i.e. an effective decrease in CSA) along its course there must be a localised increase in ice velocity, and a corresponding increase in erosion (Glasser, 1995; Kessler, et al., 2008). Therefore it is predicted that potential glacial erosion will scale nearly inversely with valley CSA, resulting in the production of an overdeepening. Maximum ice velocity will occur up-glacial of the location of minimum CSA within the valley confluence, for flow continuity reasons (see figure 10 and related text). Additionally, it is predicted that a decrease in bedrock competency will accentuate glacial erosion by increased ice velocity within a confluence. Glacial processes will be more effective at eroding within structural and/or lithological zones of weak mass strength, because bedrock is blockier (i.e. bedrock is jointed, loosened and/or faulted or sheared). Within weak zones the quarrying process (of which ice velocity is one component) is likely to exploit the increasingly blocky bedrock (by fast glacier sliding, low basal pressures, and the focusing of meltwater), increasing glacial erosion (Hallet, 1996; Hooke, 1991) and producing (or modifying the size of) an overdeepening.

positive outcomes to such tests, for a particular geological zone, will strongly suggest that bedrock mass strength is a control upon overdeepening location and size within the whole of the geological zone in question (rather than simply within confluences). This may then be investigated further in future studies.

The simplified test to examine the influence of bedrock mass strength upon overdeepening location and size within confluences should initially reveal up to regional scale associations between confluence observed in the study region, overdeepenings observed in the study region, and lithologies/ structural zones (identified using digital geological maps). Bedrock mass strength may influence overdeepening location if specific bedrock types/ structural zones and overdeepenings are spatially coincident to a significantly greater degree than that predicted by random chance, within a given study region. Subsequently, the test focuses upon the localised associations (i.e. at up to glacial valley scale) between geological zones and overdeepenings specifically within confluences (figure 14a). This is in order that the causality of any co-location relationships found between geological zones and overdeepenings can be assessed by comparison of ice velocity speed up, for groupings of confluences with overdeepenings, within and outwith each geological zone for which a co-location relationship is indicated. The influence of bedrock mass strength upon overdeepening size can subsequently be examined by consideration of the relationship between ice velocity speed up and overdeepening metrics within each relevant geological zone. The process diagram for the production of an overdeepening controlled by both confluence valley CSA change and bedrock mass strength change is shown in figure 14b.

## 2.8 The Study Region: Labrador

The geographical area that has been selected to be investigated in this study is the Labrador province of Canada, and some surrounding topography and bathymetry. The precise boundaries of the study region are defined later, because proper definition of the study region can only happen once the extent of confluence occurrence is known (see section 4.5.1.1). The geographical area has been selected in the light of its history of extensive glaciation during the Quaternary and because of the varied geology of the region, which has much structural faulting owing to its location and antiquity. Another important reason for selection of this study region is because of DEM/ dataset availability, with particular regard to geological data.

The study region (figure 15) is loosely defined by the edge of the continental shelf within the bathymetry, to the east. The northern limit is defined by the highest surveyed latitude for the

topographic data used (60° north). The western and southern limits are such so as to allow a generous perimeter around the political border of the Labrador province, within neighbouring Quebec and Ungava Bay. This definition of the study region facilitates the analysis of overdeepenings which are likely to form part of the fjords into the Labrador Sea (to the east) or Ungava Bay (to the west), or which may occur on the western side of the Torngat Mountains (and/or straddle the border between Labrador and Quebec provinces).

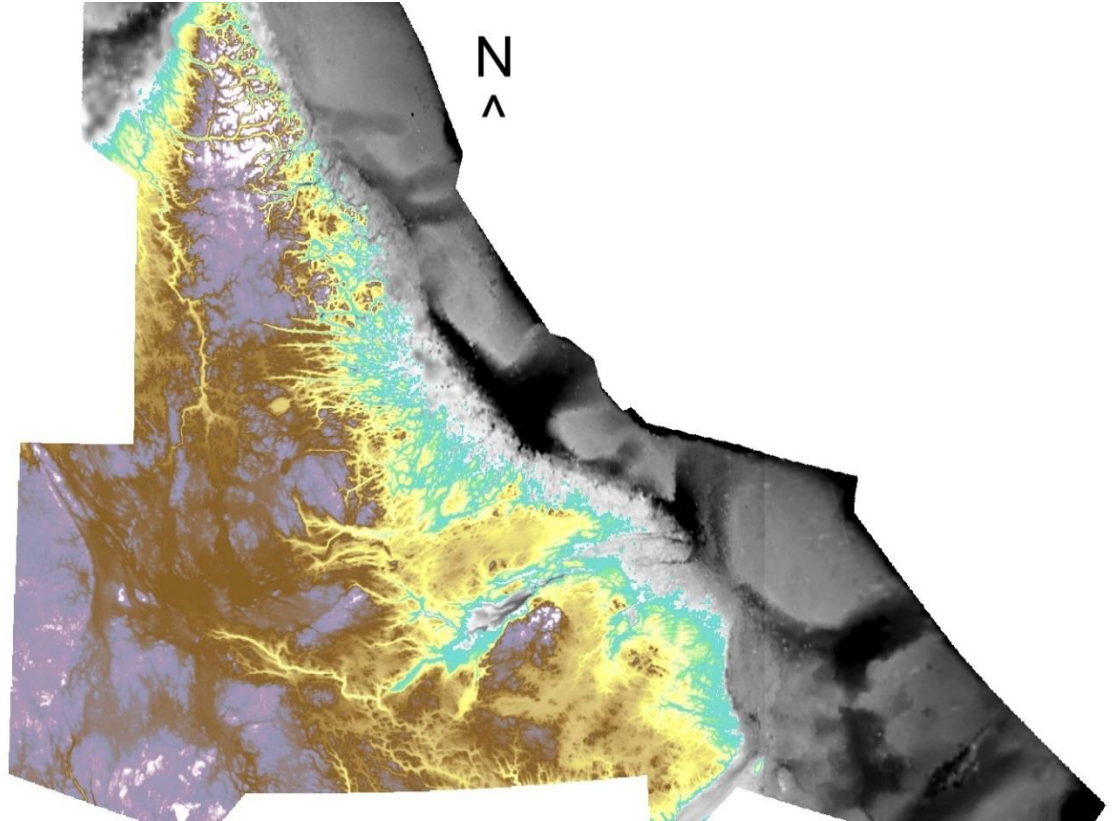


**Figure 15. The study region (Labrador, Canada and surrounding region).**

SRTM3 land topography data (ll coord 52.0, -67.8 DD) are shown in ESRI ArcGIS 'elevation' colour scale. Scale ranges from sea level (turquoise) to ~1600 m a.s.l (white). GEBCO bathymetry data are shown in greyscale. Scale ranges from sea level (white/grey) to ~ -1700 m depth (black).

Much of Labrador has evidence for at least two phases of ice movement within the Quaternary. These are probably related to shifting Late Wisconsinan dispersal centres (Batterson, 1990). During the Late Wisconsin (the last glacial period) the Laurentide Ice Sheet reached maximum extent (in the study region) 15.5 cal. ka BP (Occhietti, et al., 2011), when it advanced to occupy the continental shelf region offshore of the east coast of Labrador, in the Labrador Sea. Towards the Labradorian east coast, ice movement was topographically controlled during the late glacial stages (Batterson, 1990). There is strong evidence for east flowing valley glaciers post-dating northeast-flowing ice on surrounding highlands (Batterson, 1990; Batterson & Liverman, 2011; Winsborrow, et al., 2004).

Bedrock within the study region is part of the ancient Canadian Shield (Laurentian Craton). The Torngat mountain range (the main orogenic belt within the region) was formed during the Torngat Orogeny over 1.7 Ga ago (St-Onge, et al., 2009), and has since been extensively denuded, including by numerous (ice sheet scale) glaciations (Occhietti, et al., 2011; Staiger, et al., 2005). The region has complex (mostly igneous and metamorphic) geology, with significant structural faulting (Davenport, et al., 1999; Wardle, et al., 1997) due to the extensive and complicated geological history of the region (St-Onge, et al., 2009). In the northern part, structural faulting is largely east-west, and north-west to south-east trending within the Torngat orogenic belt (the northern mountains), and proximal to the North Atlantic (Nain) Craton (to the east) and the South-eastern Churchill Province (to the west) (Wardle, et al., 1997). Here, structural faulting is mainly the result of continental collision and crustal amalgamation between a north-eastern composite continent (consisting of the North American Craton and Torngat orogenic belt) and the south-western (North American) Superior Craton (2.3 to 1.8 Ga ago) (St-Onge, et al., 2009), sutured by a southwards projecting promontory of the Archaean Rae Province (i.e. the South-eastern Churchill Province) (Wardle & Van Kranendonk, 1996). In the southern part of the study region, structural faulting is largely north-west to south-east, with some south-west to north-east trending (Wardle, et al., 1997) within the (younger) Grenville Province. Here, structural faulting is mainly the result of over 800 Ma of diverse tectonic activity at the margin of pre-Labradorian Laurentia (i.e. cratonic compression and amalgamation, basin extension, arc accretion, and plutonism) before crustal stability was achieved (1.3-1.0 Ga ago) (Gower, 1996).

### 3 Research Design

*This chapter summarises the research problem, and discusses the research design. The aims, hypotheses, and anticipated outcomes of the investigation are stated. The overarching methodology that is used to investigate the hypotheses is summarised, and the objectives of the study are defined.*

As a consequence of the lack of systematic study of glacial overdeepenings, it has not yet been possible to establish whether different types of overdeepening exist; say at characteristic positions beneath a glacier, each at a characteristic scale, and each produced by a different primary control. Nor has it been possible to investigate specific types of the phenomenon in order to improve our understanding regarding the processes of overdeepening initiation and development. This research aims to contribute towards closing this gap in current knowledge.

In this empirical investigation we use GIS tools and various digital elevation models (DEMs) and datasets to systematically study several hundred glacial overdeepenings proximal to/ within the Labrador province of Canada (figure 15; example overdeepening from the region, figure 16). The GIS tools used are ArcGIS and Microsoft Excel computer software. Key DEMs and datasets are SRTM3 (ESRI sourced) topography data (ESRI Inc./ US NASA, 2006), GEBCO topography and bathymetry data (GEBCO, 2009a), a digital geological map of Labrador (Wardle, et al., 1997), BEDMAP (British Antarctic Survey (BAS), 2000) and NSIDC (US National Snow & Ice Data Center (NSIDC), 2005) topography data. Other datasets are also utilised. Datasets and their application are described in full in section 4.1.

In addition to developing a method for deriving basic metrics of overdeepenings, the main aim of the investigation is to exploit inferred ice velocity changes within glacial valley confluences to gain insight into controls upon overdeepening location and size. The investigation will focus specifically upon the influence of:

1. Glacial valley cross-sectional area (CSA) change within confluences (a topographical control)
2. Bedrock mass strength change within confluences (a geological control)

Such aims will improve our understanding of the overdeepening processes at work. A further outcome from the investigation will be the provision of systematic data (i.e. a series of maps) pertaining to topographical depressions within the limits of the Last Glacial Maximum (LGM),

emphasising localities of likely glacial overdeepening. Such data may be useful in future investigations of overdeepening, and might also be applied in the testing of numerical models of glacial erosion and landscape evolution.



**Figure 16. The north-east coast of the Labrador province of Canada.**

An overdeepened fjord (centre) can be seen, as well as out-lying islands (image: Stefan Plazier).

In order to fulfil the main aim of the investigation, the following hypotheses are explored:

- 1. Overdeepenings will be preferentially located at glacial valley confluence, because this is where ice velocity speed up (due to change in valley CSA) should occur*
- 2. Overdeepening size will be larger in confluences where there is greater ice velocity speed up (due to change in valley CSA), because this is where ice erosion should be greatest*
- 3. Overdeepenings will more frequently occur in confluences with weaker bedrock, because of the greater potential for erosion and removal of material (due to change in bedrock mass strength)*
- 4. Overdeepening size will be larger in confluences with weaker bedrock, because of the greater potential for erosion and removal of material (due to change in bedrock mass strength)*

In order to advance process understanding, in this study a GIS based methodology is developed to identify and define confluences and overdeepenings. An assessment is then made of the strength of the co-location relationship between confluence and overdeepenings, within the Labrador study region. This is in order to establish whether further investigation of the relationship is warranted. Confluence valley cross-sectional area (CSA) is measured. This allows the first and second hypotheses to be addressed. Subsequently, the strength of co-location relationships between geological (i.e. igneous, metamorphic, sedimentary and structural) zones (of assumed differing bedrock mass strength) and confluence and overdeepenings is assessed, to see whether further study is warranted. This allows the third and fourth hypotheses to be addressed.

Identical methodology is selectively applied to a smaller group of confluences and overdeepenings within the Swiss Alps as an exploratory exercise, in order to determine whether some of the outcomes from analyses for the Labrador study region are replicated elsewhere. The Swiss study region has been selected in the light of its history of extensive glaciation during the Quaternary (Champagnac, et al., 2007; Buoncristiani & Campy, 2011); and because of its similar (orogenic) geology to that of Labrador, with much structural faulting (Swiss Federal Office of Topography (SwissTopo), 2010). A further reason for selection of the Swiss study region has been because of DEM/ dataset availability, with particular regard to geological data. Maps of probable overdeepenings within the limits of the Last Glacial Maximum (LGM), at global scale, are also produced.

### 3.1 Objectives

For Labrador study region:

1. To develop and employ methodology to identify and define overdeepenings and overdeepening metrics (e.g. overdeepening depth, area, etc) in DEMs
2. To develop and employ methodology to identify and define glacial valley confluences in DEMs

*To investigate hypotheses 1 and 2:*

3. To assess the co-location of confluence and overdeepenings, and evaluate the strength of the co-location relationship, to establish whether further investigation is warranted
4. To measure valley CSA change through each glacial confluence (expressed as a ratio value, indicative of ice velocity speed up)
5. To evaluate the influence of confluence CSA change upon overdeepening location, via comparison of ice velocity speed up, for groupings of confluences containing and not containing overdeepenings
6. To evaluate the influence of confluence CSA change upon overdeepening size, via analysis of ice velocity speed up correlation with overdeepening metrics

*To investigate hypotheses 3 and 4:*

7. To assess the co-location of geological (i.e. igneous, metamorphic, sedimentary and structural) zones (of assumed differing bedrock mass strength) and confluence, and evaluate the strength of co-location relationships, to establish whether further investigation is warranted
8. To assess the co-location of geological zones and overdeepenings, and evaluate the strength of co-location relationships, to establish whether further investigation is warranted
9. To assess the co-location of glacial confluence and overdeepenings, for geological zones, and evaluate the strength of co-location relationships
10. To assess the co-location of geological zones and glacial confluence (co-located with overdeepenings), and evaluate the strength of co-location relationships

11. To evaluate the influence of confluence bedrock mass strength upon overdeepening location, via comparison of ice velocity speed up, for groupings of confluences containing overdeepenings within and outwith each geological zone
12. To evaluate the influence of confluence bedrock mass strength upon overdeepening size, via analysis of ice velocity speed up correlation with overdeepening metrics within each geological zone

For elsewhere:

13. To *selectively* apply identical methodology (i.e. objectives 1-12) to a smaller group of confluences and overdeepenings within the Swiss Alps, in order to determine whether some of the outcomes from analyses for the Labrador study region are replicated elsewhere
14. A further objective of the study is to identify probable overdeepenings within the limits of the Last Glacial Maximum (LGM), at global scale, in order to produce systematic data for future studies

## **4 Research Method**

*This chapter describes the methodologies employed during this investigation. The DEMs and datasets that are made use of in analyses are discussed. DEM and dataset accuracy is assessed. Relevant methodologies are considered for each of the study areas investigated, both regional (Labrador, Swiss) and global (within the limits of the LGM). The techniques that have been developed to identify and define overdeepenings and confluences are presented. The methods utilized to subsequently explore the hypotheses are discussed. Further, consideration is given to the potential sensitivity of research outcomes to parameter choices made in overdeepening and confluence definition. Methods to test sensitivity are devised.*

### **4.1 Selecting DEMs and datasets for use in investigation**

The DEMs and other datasets used in this investigation have been selected for suitability in the task of overdeepening identification. Suitability (at relevant scale) has been assessed in terms of spatial resolution, error (consistent and minimal) and coverage area. The DEMs and datasets are freely available.

#### **4.1.1 DEMs and datasets used in Labrador (regional) investigation**

1. ESRI supplied US NASA Seamless Shuttle Radar Topography Mission (SRTM) "Finished" (void filled) research grade (version 2) 3 Arc Second land topography data (SRTM3). Coverage is of approximately 80 % of the land surface of the Earth (latitudes 60° north to 56° south), at ~90 m horizontal resolution and 1m vertical resolution (ESRI Inc./ US NASA, 2006). See figure 17.

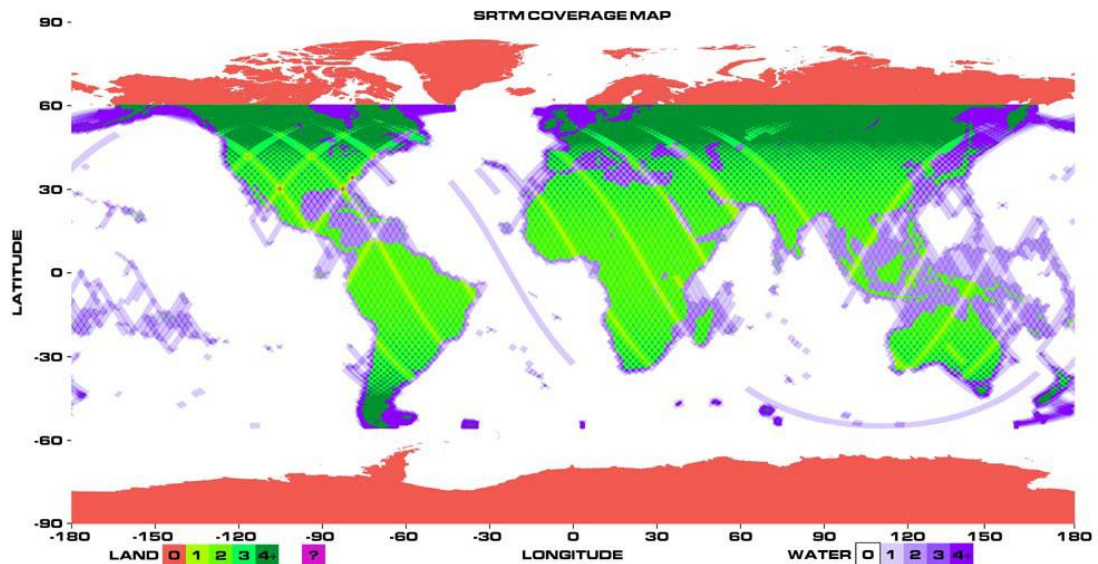


Figure 17. US NASA SRTM coverage map.

The colours of the swaths indicate the number of times the area was imaged by SRTM, over land, key at lower left; over water, key at lower right. Areas in red were not mapped. SRTM, a topography mission, mostly acquired data over land - although small amounts of data were collected over water for calibration purposes (US NASA, 2012).

2. ESRI supplied 'inland water bodies' polygon shapefile dataset – derived from SRTM data, US Geological Survey (USGS) Landsat 5 data supplemented with medium-scale maps and charts, and the Digital Chart of the World (DCW, 1:1,000,000 scale) (ESRI Inc./ US NASA, 2006; ESRI/ US Geological Survey, 2006; ESRI Inc., 2007a)
  
3. General Bathymetric Chart of the Oceans (GEBCO) bathymetry data (version 20091120) (GEBCO, 2009a). Data has 30 Arc Second grid spacing (~900 m nominal horizontal resolution, 1 m vertical resolution). The dataset is a continuous digital terrain model for ocean floor and land topography, of which only the bathymetric data are utilised in this investigation (alternative land topography datasets offer superior resolution with regard to the study area in question). The bathymetric data consists of a database of over 290 million shallow ship-track soundings (from various sources), with interpolation between soundings guided by satellite-derived gravity data (GEBCO, 2009b; Smith & Sandwell, 1997). The gravity data are based on the Smith and Sandwell global topographical grid for latitudes 80° north to 81° south (version 11.1, September 2008). Within the Smith and Sandwell global topographical grid, the predicted depths are based on version v16.1 of the Smith and Sandwell gravity anomaly from GeoSat and ERS-1 satellite altimetry, created March 2007 (GEBCO, 2009b; Sandwell & Smith, 1997).

4. Geological map of Labrador; 1:1,000,000 scale, polygon shapefile dataset (Wardle, et al., 1997). The dataset is based on the Geoscience database, built up by the Department of Mines and Energy, Geological Survey, Government of Newfoundland and Labrador, Canada, for the Labrador region. The overdeepening investigation utilises the bedrock geology part of the database; specifically components: geological units, geological contacts, geological faults and shear zones (Davenport, et al., 1999).

#### **4.1.2 Additional dataset to test reproducibility of Labradorian results for a supplementary (Swiss) study region**

5. Geological Map of Switzerland; 1:500,000 scale, polygon shapefile dataset (version 1.2) (Swiss Federal Office of Topography (SwissTopo), 2010). The dataset has coverage of all of Switzerland and adjoining parts of neighbouring countries. It presents an overview of the distribution of the bedrock geology occurring in Switzerland (Swiss Federal Office of Topography (SwissTopo), 2010) as well as details of geological faults, and shear zones.

#### **4.1.3 DEMs and datasets used in global investigation, within LGM limit (World map of potential overdeepenings)**

6. General Bathymetric Chart of the Oceans (GEBCO) dataset (version 20091120). For reasons of consistency of spatial resolution, superior (near global) coverage, and less intensive computer processing (of large global dataset), the land topography data of the GEBCO dataset has been used in the world map analysis, rather than the SRTM3 data utilised in the Labrador investigation. The GEBCO land topography data are based on 1 km averages of data derived from (version 2) of the 30 Arc Second (~900 m horizontal resolution and 1 m vertical resolution) SRTM30 dataset (GEBCO, 2009b), which has identical coverage to that of the SRTM3 dataset (detailed previously), being based on the same source data. For coverage areas where SRTM30 topographical data are not available (i.e. high latitudes), GTOPO30 data are used; which is a composite of several source datasets at 30 Arc Second grid spacing (~900 m nominal horizontal resolution, 1 m vertical resolution) (US Geological Survey, 1997).
7. For the land mass (and surrounding continental shelf) of Antarctica, bed elevation (and bathymetry) data are taken from the BEDMAP DEM (5 km nominal horizontal resolution, 1 m vertical resolution), which is sourced from a consortium of terrestrial radar and seismic soundings, most of which have been undertaken since 1980 (British Antarctic Survey (BAS), 2000).

8. For the land mass of Greenland, bed elevation data are taken from the NSIDC Greenland 5 km DEM (5 km nominal horizontal resolution, 1 m vertical resolution), which is sourced from a combination of ERS-1 and Geosat satellite radar altimetry data, Airborne Topographic Mapper (ATM) data, and photogrammetric digital height data. Ice thickness data are based on approximately 700,000 data points collected in the 1990s from a University of Kansas airborne ice penetrating radar (IPR) survey. Nearly 30,000 data points were collected in the 1970s from a Technical University of Denmark (TUD) airborne echo sounder (US National Snow & Ice Data Center (NSIDC), 2005; Bamber, et al., 2001b; Layberry & Bamber, 2001).
  
9. Last glacial maximum (LGM) global limit(s) polygon shapefile dataset (Ehlers, et al., 2011a). These shapefiles are a synthesis of current understanding of last glacial maximum ice limits (Ehlers, et al., 2011b).

#### 4.1.4 DEM and dataset accuracy

##### 4.1.4.1 SRTM

Both the SRTM3 and the SRTM30 datasets are based on the same US NASA source data, downsampled to 90 m and 900 m grid spacing respectively. The source data are 1 Arc Second (30 m) resolution. The accuracy of the data is discussed in Rabus, et al. (2003). More detailed analysis is found in Rodríguez, et al. (2005). There is less than or equal to 12.6 m absolute horizontal circular error for 90 % of the data, and less than or equal to 9 m absolute vertical linear error for 90 % of the data, globally (Rodríguez, et al., 2005). Relative horizontal circular error is less than 15 m, globally (Rodríguez, et al., 2005), and relative vertical linear error is  $\leq 9.8$  m, globally. For the Labrador study region, used in this investigation, absolute vertical linear error is  $\leq 5$  m for  $>90$  % of the data (Rodríguez, et al., 2005). For the Swiss study region, absolute vertical linear error is  $<10$  m for  $>90$  % of the data (Rodríguez, et al., 2005). The greatest errors in the global SRTM data are associated with steep terrain (i.e. Himalaya, Andes), and very smooth sandy surfaces (i.e. Sahara Desert), of which the former is particularly relevant to this investigation.

It should be noted that a limitation of the original SRTM survey is that the radar is unable to sense the land surface beneath vegetation canopies, radar waves being influenced by the vegetation height, structure, and density. However, the radar often penetrates significantly into the vegetation canopy. Schemes for correction for this vegetation bias have been proposed, but the issue remains a subject for research. As a consequence of this issue, elevation measurements in vegetated areas should be assumed to be from near the top of the canopies (Farr, et al., 2007). The issue is probably irrelevant to vertical height accuracy in the regions investigated in this study, given the lack of vegetation cover in formerly glaciated polar desert and tundra regions. Even in taiga (boreal forest) regions, this error will be negligible for the purposes of investigating overdeepenings, given the nature of an overdeepening as an erosional landform (i.e. an overdeepening is unlikely to become forested unless completely infilled by sediment). Furthermore, differences between land surface and vegetation canopy elevation measurements are likely to be inconsequential at the scale of all but the smallest overdeepenings, and will certainly be so at the scale of the larger overdeepenings considered in the preparation of global scale maps.

#### **4.1.4.2 GTOPO30**

Precise horizontal positional accuracy figures were unavailable for the GTOPO30 dataset. This is due to the composite nature of the GTOPO data (further compounded by the composite nature of some of those sources). The 30 Arc Second grid spacing is appropriate for the resolution and accuracy of most of the (better resolution) DEM's that make up the GTOPO dataset (US Geological Survey, 1997), and is certainly appropriate for nearly all of the GTOPO data used in this investigation (i.e. those areas within the LGM limit, but outside of SRTM30 coverage). Much of the GTOPO data that has been utilised in this investigation is Digital Terrain Elevation Data (DTED, 3 Arc Second resolution), which has a  $\leq 50$  m absolute horizontal circular error at 90 % confidence (US Defense Mapping Agency, 1996). However, for some very high latitude locations (i.e. parts of the Arctic Canada land topography), the actual horizontal accuracy of the source data may be insufficient to best utilise the (nominal) 900 m grid spacing (used in the GEBCO land topography dataset). The absolute horizontal circular accuracy of the lowest accuracy source to be used (DCW 1:1,000,000 scale, also known as VMap Level 0), for these locations, is typically 2,040 m error at 90 % confidence, according to the performance specification, although error could increase to as much as 4,270 m in some regions, dependent upon source data (US Defense Mapping Agency, 1992). Despite this, the findings of empirical studies which have examined respective vertical accuracies (see below) indicate that actual absolute horizontal circular error within the DCW is significantly better than that stated in the dataset specification (US Geological Survey, 1997).

The absolute vertical linear error at the 90 % confidence level, for GTOPO30 data, is typically at or better than 30 m (RMSE of 18 m), although (again) for some very high latitude locations (i.e. parts of Arctic Canada) this accuracy could decrease to approximately 160 m absolute vertical linear error at the 90 % confidence level (DCW, RMSE of 97 m) (US Geological Survey, 1997; US Defense Mapping Agency, 1995a; US Defense Mapping Agency, 1995c), although this is significantly better than the specified performance of 610 m (US Defense Mapping Agency, 1992). Spot height accuracy is around 30 m in the worst case (e.g. DCW) (Shortridge & Goodchild, 1999; US Defense Mapping Agency, 1995a; US Defense Mapping Agency, 1995c).

#### **4.1.4.3 General Bathymetric Chart of the Oceans (GEBCO) bathymetry data (version 20091120)**

Less than 10 % of global bathymetry has been mapped. As a consequence, any gridded dataset of bathymetry requires much interpolation and interpretation, and is consequently highly variable in quality. For this reason the 30 Arc Second grid spacing of the global bathymetry data

is, in effect, quite arbitrary. The grid spacing does not indicate that the source data are of consistent 900 m resolution.

The GEBCO dataset uses contour intervals of 500 m depth, with 200 m and 100 m contours in shallow zones only where justified. Although significant quantities of bathymetry data contoured at intervals of 200 m and 100 m have been incorporated into GEBCO bathymetry, the standard 500 m contours comprise the bulk of the current contour dataset. Contour style and character is unique, reflecting the interpretative skill and experience of each of the GEBCO contributors/ gridders (GEBCO, 2003). Literature suggests that plotting the grid depths as a histogram reveals numerous peaks, each of which occur at a multiple of 500 m. These peaks correspond to the 500 m contour interval of the input digitized contour data. It is understood that this terracing effect is a well-known problem of constructing grids from contours (GEBCO, 2003). Compared to total-coverage, high-resolution multi-beam bathymetric surveys it is unjustifiable to plot the GEBCO global grid at a fine contour interval of 10 m or 20 m except in very rare cases (where contours of this interval size were used as input) (GEBCO, 2003).

Attempting to assess GEBCO grid quality is difficult, owing to the composite nature of the dataset and the inconsistency in methods used to produce it. Some measure of the quality of the contouring is perhaps more useful than a numerical quality statistic determined from the grid depths. However, the subjective and interpretative nature of the contouring makes even assessment of this difficult (GEBCO, 2003). The contributor/ gridded of the GEBCO data for the Labrador coastal bathymetry is unknown, as is the accuracy of this region of the dataset. As a guide to typical depth survey accuracy, it is the case that multibeam swath sonar and hydrographic surveys undertaken prior to 1998 will have a vertical accuracy of 0.3 m for depths of less than 30 m, and a vertical accuracy of 1 % of depth for depths of greater than 30 m (GEBCO, IHO and IOC, 2014). Coastal areas in and around the fjords and bays of Labrador are likely to have some of the better bathymetry within the dataset, owing to comparatively dense survey coverage relative to many open water locations, and because of fjordal areas being typically well constrained by surrounding land topography.

#### **4.1.4.4 BEDMAP DEM**

Accuracy varies across the composite bedrock DEM according to the distribution of the original source data and the procedure used in its construction. The absolute positional horizontal accuracy of the bedrock DEM generally varies between 100 m and 300 m although this figure can be as much as 10 km in some inland areas (i.e. the inland plateau). The absolute vertical accuracy of the grounded ice-sheet model is between 150 m and 300 m in most areas. The vertical accuracy of the bedrock DEM is between 50 m and 500 m (Lythe, et al., 2001).

Probably the most important sources of error within the BEDMAP dataset are those derived from inaccuracies in the navigation systems. A wide range of navigation methods have been used to fix the ice thickness data sets, including astronomical fixes, dead reckoning, inertial avionics, doppler avionics and global positioning systems (GPS). Positional uncertainty in these methods range from several metres for differential GPS, to several kilometres for the inertial and dead reckoning navigation systems. The other principal error source is the precision to which the actual ice thickness observations are determined. Documented precision of the observations in the database ranges from 10 m to 180 m (British Antarctic Survey (BAS), 2000).

#### **4.1.4.5 NSIDC Greenland DEM**

The bedrock elevation DEM is interpolated to 5 km grid resolution. However, the true horizontal spatial resolution varies according to slope and surface characteristics. An earlier version of the DEM (using identical source data) was gridded with a horizontal spatial resolution of 1 km. Analysis of this DEM confirmed horizontal accuracy ranging from 20 m to 200 m over bare rock areas, depending on the source data. Further analysis showed that the DEM has a slope dependent accuracy ranging from -1.04 m ( $\pm 1.98$  m) to -0.06 m ( $\pm 14.33$  m) over the ice-sheet for a slope range of 0.0-1.0°. Mean accuracy over the whole ice-sheet is -0.33 m ( $\pm 6.97$  m) (Bamber, et al., 2001a). Horizontal resolution of the ice thickness grid (used to calculate the bedrock elevation DEM) is between 5 km and 50 km, and vertical accuracy is between 10 m and 100 m, depending on flight line coverage. Typical radar-sounding surveys have an inherent uncertainty of about 15 m for ice depth measurements (Bogorodsky, et al., 1985) (US National Snow & Ice Data Center (NSIDC), 2005).

Errors in satellite radar altimetry data come from several sources including geographically correlated orbit errors, errors in slope correction procedures, and non-uniform spatial sampling (Bamber, et al., 2001a). Uncertainties in airborne radar sounding relate to the magnitude of the refractive indices of solid ice, uncertainty in the profile of refractive index in the firn, signal contamination by thermal noise in the equipment, insufficient clarity of the oscilloscope signal, and imperfect signal definition on the recording medium. Large errors in ice thickness measurements can result if pulses reflected from ice inhomogeneities are mistaken for bottom echoes (Bogorodsky, et al., 1985) (US National Snow & Ice Data Center (NSIDC), 2005).

#### ***4.1.4.6 ESRI supplied dataset of 'inland water bodies'***

The inland water body dataset is based on the SRTM Water Body dataset (SWBD), produced by the US National Geospatial-Intelligence Agency (NGA) from the US NASA SRTM (version 2) source data, and (for the polar areas, not covered by SRTM) based on the Digital Chart of the World (DCW, VMap Level 0) dataset (ESRI Inc., 2007b).

As a consequence of the resolution/ scale, and accuracy, of the source data, accuracy of the water body dataset varies significantly. For SRTM coverage area (i.e. Labrador study region), source data are 1 Arc Second resolution. Water bodies are depicted as they appeared in February 2000 (at the time of the SRTM flight). USGS Landsat 5 data and medium-scale maps and charts have been used as supplemental data sources, generally as supporting evidence for water identified in the SRTM data. However, Landsat 5 data was collected a decade earlier than the Shuttle mission, and other map sources are also significantly older than the SRTM data. As a consequence, in many instances there are significant temporal and further seasonal differences between the depiction of water in the ancillary sources and the actual extent of water bodies as seen in February 2000. In rare cases, where SRTM data are missing or unusable, the ancillary sources have been used to delineate water bodies (US National Geospatial-Intelligence Agency (NGA), 2005). The accuracy specification for SWBD is as for SRTM data, as previously discussed (US National Geospatial-Intelligence Agency (NGA), 2003). For polar areas, not covered by SRTM data, source data are far more variable in quality. The accuracy specification for these data is as previously discussed for the DCW/VMap Level 0 dataset (US Defense Mapping Agency, 1992; US Defense Mapping Agency, 1995a).

#### ***4.1.4.7 Last glacial maximum (LGM) global limit(s) polygon shapefile dataset (Ehlers, et al., 2011a)***

The base maps used as the basis for the LGM shapefile dataset are primarily the SRTM and DCW (VMAP0) datasets, as well as the higher resolution successor to the DCW (VMAP1, 1:250,000 scale) and OpenStreetMap data (OSM, a 'volunteered geographical information' project, with detailed but limited global coverage, initiated in 2004) (Ehlers, et al., 2011b).

The base maps for the latest edition (2011) of the LGM ice limit shapefile are of larger scale than was the case for the last edition (2004). Accuracy of information contained in the maps has increased by a factor of 16. The last edition of the shapefile was based entirely on the DCW (Ehlers, et al., 2011b), with accuracy limits in line with the DCW specification (US Defense Mapping Agency, 1992; US Defense Mapping Agency, 1995a). The accuracy of the base maps used in the current version of the LGM shapefile dataset is as previously discussed with regard to the respective dataset specifications (Rodríguez, et al., 2005; Farr, et al., 2007; US Defense

Mapping Agency, 1992; US Defense Mapping Agency, 1995a). The accuracy specifications for those extra base maps that have not yet been discussed are:

#### 4.1.4.7.1 VMAP1

The performance specification for VMAP1 indicates an absolute horizontal circular error of 125 m to 500 m for 90 % of the data (dependent upon class of data). Absolute vertical linear error is 0.5 m to 2 m for 90 % of the data (dependent upon class of data) (US Defense Mapping Agency, 1995b).

#### 4.1.4.7.2 OpenStreetMap

When analysing 'volunteered geographical information' (i.e. OpenStreetMap), the issue of assessing spatial data quality (i.e. accuracy, as previously defined and discussed for other datasets) is a clear challenge. The manner in which OpenStreetMap data are contributed does not comply with standard spatial data quality assurance procedures (Haklay, et al., 2010). However, the data does hold an intrinsic quality assurance measure through the analysis of the number of contributors who have worked on a given spatial unit. The assumption that as the number of contributors increases so does the quality of the data, is known as 'Linus' Law'. Recent studies show that this rule applies, with regard to positional accuracy, for the OpenStreetMap dataset (Haklay, et al., 2010) and that, as a consequence, OpenStreetMap dataset quality for a given location is comparable with the most accurate of the other datasets discussed here, provided that OpenStreetMap coverage is considered satisfactory for that location.

The SRTM, VMAP1 and OSM information can be regarded as accurate at a scale of 1:250,000. However, The DCW (and GTOPO30 data) is only true at 1:1,000,000 scale (Ehlers, et al., 2011b).

The positional accuracy of the ice limit margin within the LGM shapefile dataset is affected not simply by base map resolution and accuracy alone. There is an additional intrinsic error which, whilst not likely to commonly be the limiting factor in terms of overall dataset accuracy, concerns the confidence with which the interpretation of ice limit position for any given field site/ area may be regarded. The error is linked to the number of studies that have been undertaken, concerning ice limit position, for any given field site/ area (i.e. the application of Linus's Law, see above definition), irrespective of the quality of any individual study. It then follows that there is additional uncertainty regarding the position of the interpreted (interpolated) ice limit margin between each field site/ area. For some locations, and relative to

some base maps that have been used in the creation of the dataset, this additional error is more likely to be the limiting factor in terms of overall dataset accuracy, rather than base map resolution and accuracy.

#### ***4.1.4.8 Geological map of Labrador; 1:1,000,000 scale, polygon shapefile dataset (Wardle, et al., 1997)***

The geological information that is contained within the dataset is compiled from published and unpublished sources (at various scales) located within the Geoscience database of the Department of Mines and Energy, Geological Survey, Government of Newfoundland and Labrador, Canada, with additional contributions of information and advice from personnel of the Geological Survey of Canada (Wardle, et al., 1997). The geological map adheres to good map accuracy standards. The use of a 1:1,000,000 scale reflects the limitations in scale/resolution, accuracy and coverage of the relevant source documents/datasets, for which specific accuracy information is not available. The accuracy of the geological map is comparable with the DCW and GTOPO30 datasets that are also used in this investigation.

#### ***4.1.4.9 Geological Map of Switzerland; 1:500,000 scale, polygon shapefile dataset (version 1.2) (Swiss Federal Office of Topography (SwissTopo), 2010)***

The dataset is primarily based on the detailed geological map sheets of the Geological Atlas of Switzerland, at the scale of 1:25,000. Where this information is not available the dataset is based on a compilation of special maps and map originals of different scales, provided by the Swiss Geological Survey or various universities as well as by individual cantons. The quality of this additional data does not necessarily match the quality of the data derived from the 1:25,000 map sheets, varying in scale from 1:25,000 to 1:100,000 (Swiss Federal Office of Topography (SwissTopo), 2011; Swiss Federal Office of Topography (SwissTopo), 2012). The geological map adheres to good map accuracy standards, although accuracy information for source data is not available. All source data are of significantly larger scale than the dataset (and therefore assumed greater accuracy). The positional accuracy of the geological map falls somewhere between that of the SRTM dataset and the DCW, being more comparable with that of the SRTM dataset.

## 4.2 Identifying overdeepenings (Objective 1)

In order to investigate all hypotheses within this study, overdeepenings must first be identified and defined within relevant DEMs. Where a glaciated (or formerly glaciated) environment is represented by a DEM, local minima (i.e. sinks or depressions) within the DEM will likely represent empty or partially (water or sediment) filled overdeepenings. The analysis of relevant datasets (for Labrador study region: SRTM3 land topography (ESRI Inc./ US NASA, 2006), GEBCO bathymetry (GEBCO, 2009a); for world map: GEBCO land topography dataset(s) (GEBCO, 2009a), NSIDC Greenland bed topography dataset (US National Snow & Ice Data Center (NSIDC), 2005), BEDMAP Antarctica bed topography and bathymetry dataset (British Antarctic Survey (BAS), 2000), and other bathymetry (GEBCO, 2009a); for Swiss study region: SRTM3 land topography (ESRI Inc./ US NASA, 2006)), allows identification of these sinks. Processing and display of datasets and corresponding sink data are undertaken using ESRI ArcGIS 9.3.1 GIS software. The main elements of the workflow for overdeepening identification and definition are summarised in figure 18.

It is not always possible to identify a filled overdeepening (i.e. an overdeepening filled entirely by either water or sediment, up to its pour point) within a DEM (e.g. SRTM3), due to the limitations of the survey instrumentation. Entirely water filled overdeepenings (i.e. lakes) are sometimes undetectable (depending upon the extent and type of radar backscatter from the lake water surface), and entirely sediment filled overdeepenings are always undetectable (being obscured). It is therefore unlikely that every overdeepening will be detected within any given study region, after analysis of the relevant DEM(s). Despite this, it is safe to assume that the majority of overdeepenings will be detected, as most will be only partially filled to some extent (by either water or sediment), and some may be entirely empty.

Within formerly glaciated regions, where a natural lake occurs, it is safe to assume that the lake occupies an overdeepening and is therefore an entirely water filled/ partially water filled example of the phenomenon. However, clearly, less certainty (of being an overdeepening) can be attached to water filled depressions in the landscape (i.e. it is possible that a lake is formed by some other glacial process, e.g. that the lake is dammed by moraine deposition) than can be attached to non-water filled depressions. The investigation considers the location and size of lakes (via use of the inland water bodies dataset), as well as the location and size of empty/ partially sediment filled overdeepenings; for the Labrador study region, the Swiss study region, and at global scale (i.e. for the world map).

The analysis of further datasets, such as lake bathymetric data (i.e. DEMs, or hard copy bathymetric maps), might increase certainty as to whether some lakes are examples of entirely

water filled/ partially water filled overdeepenings or not. Similarly, geological drift maps and geophysical datasets might be useful in examining specific entirely sediment filled/ partially sediment filled overdeepenings. However, on the whole, such datasets are not readily (or freely) available, and typically lack coverage. Such analysis is therefore outside of the scope of this study, which instead utilises contiguous topographic and bathymetric DEMs to examine all detectable overdeepenings within two study regions, and at global scale.

#### 4.2.1 Study region extent(s)

Hypothesis testing is undertaken via analysis of the Labrador study region. In the initial stages of the investigation (i.e. when initially identifying sinks/ potential overdeepenings and, later, when identifying and defining confluences), the extent of the Labrador study region is loosely defined by the edge of the continental shelf within the bathymetry (GEBCO DEMs), to the east. The northern limit of the study region is defined by the highest latitude at which SRTM data has been collected during surveying (i.e. latitude 60° north). The western and southern limits of the study region are such as to allow a generous perimeter around the political border of the Labrador province, within neighbouring Quebec and Ungava Bay. This definition of the study region facilitates the analysis of overdeepenings which may form part of the fjords into the Labrador Sea (to the east) or Ungava Bay (to the west), or which may straddle the political border between Labrador and Quebec (and/or which may occur on the western side of the Torngat Mountains). The precise extent of the study region is defined later in the investigation (section 4.5.1.1), when area calculations are required in order to evaluate the strength of co-location relationships for various hypotheses (see objectives).

The supplementary Swiss study focuses on the Swiss Alps - examined in the later stages of the investigation as an exploratory exercise in order to determine whether some of the outcomes from analyses for the Labrador study region are replicable elsewhere. The region examined also includes areas of France and Italy but, for reasons of brevity, in this investigation is referred to as the Swiss study region. The study region is approximately 300 x 150 km in size (SRTM3 data).

The world map may be useful in future investigations of overdeepening, and might also be applied in the testing of numerical models of glacial erosion and landscape evolution. The maps provide systematic global data regarding topographical depressions within the limits of the Last Glacial Maximum (LGM), emphasising localities of likely glacial overdeepening.

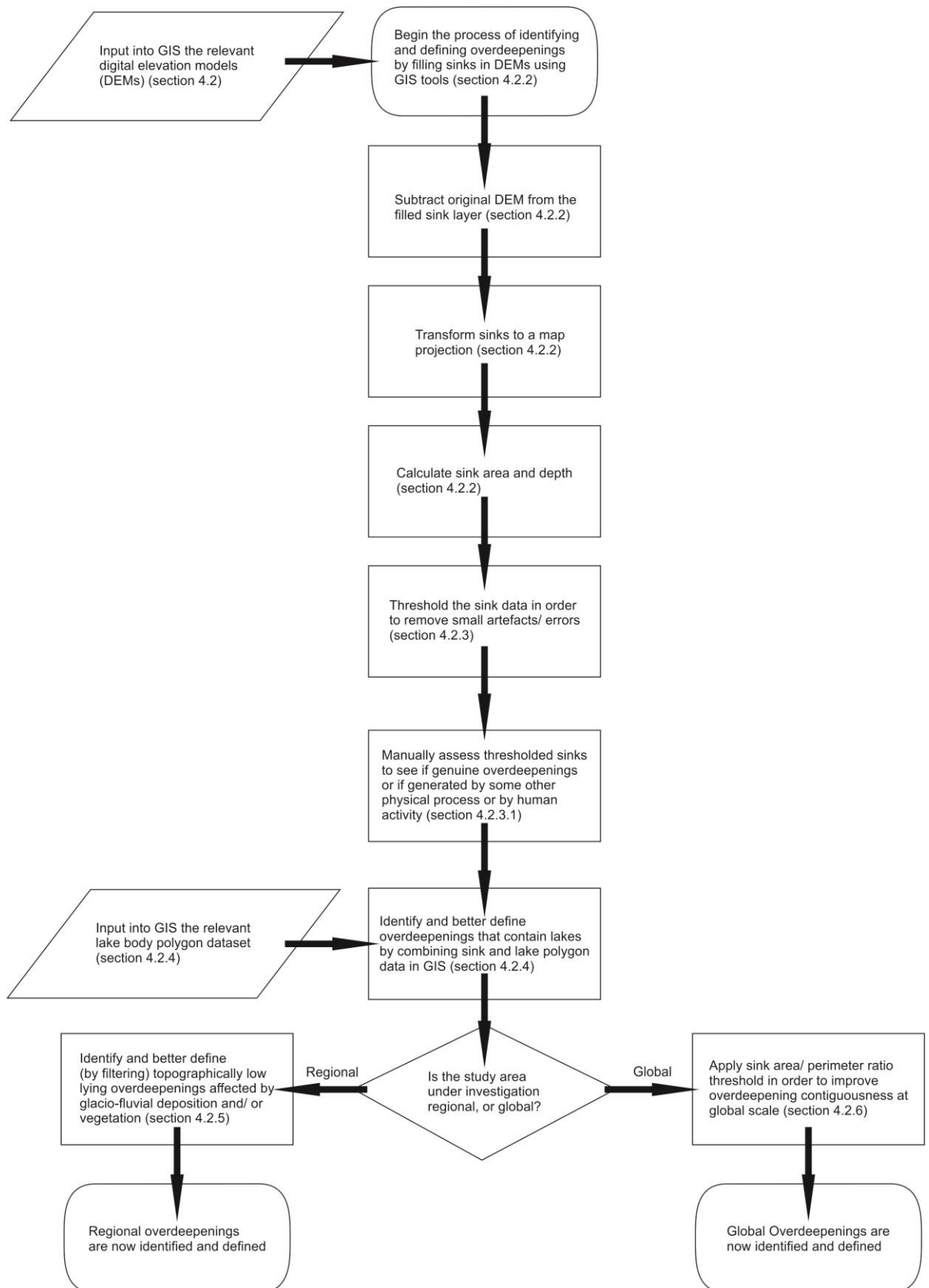


**Figure 18. The main elements of the workflow for overdeepening identification and definition.**

Later elements demonstrate how overdeepening identification and definition is adjusted, where necessary.

## 4.2.2 Identifying sinks, and projection of data

The process of identifying sinks (i.e. potential overdeepenings) utilises a ‘sink fill’ algorithm within the GIS software. This algorithm fills sinks to ‘pour point’ (i.e. to maximum size). The subtraction of the output of this tool from the original DEM, allows sinks to be displayed within the GIS software. The sinks and the DEMs are then projected. Projection converts the units of measure of the horizontal to metres, in common with the vertical height unit of measure. Projection is essential as the analysis of overdeepening metrics and of the relationship between confluence and overdeepenings relies upon the measurement of distance in the horizontal, the assessment of area, and the use of slope maps generated from DEMs. Evaluation of these properties is not possible without suitable projection of data for each of the study regions under investigation. The majority of the datasets used in this analysis are provided in Lat/Long WGS 1984 geographic coordinate system. Data are projected to UTM 20N, UTM 32N and Fuller projection for the study regions (Labrador, Switzerland) and the world map, respectively. Where a dataset is already projected using a different coordinate system (e.g. Swiss geology dataset (Swiss Federal Office of Topography (SwissTopo), 2010), which uses a CH1903 projection) it is re-projected (e.g. Swiss geology dataset, to UTM 32N) to maintain consistency with other datasets. Further simple GIS tools and associated calculations are employed, to derive sink area and sink maximum depth values for use in thresholding analysis (in order to remove small artefacts/errors from sink data), and for use in subsequent analysis of overdeepening metrics.

### 4.2.2.1 Projection accuracy

There is a risk that distortions induced during map projection introduce error into the process of identifying the extent (area and depth) of individual sinks. For study regions where a UTM projection is utilised, this potential error is very small and due to slight shape, area, and distance distortion - true projection of direction is maintained (ESRI Inc., 2008a). The potential error increases slightly where a fuller projection is utilised (i.e. world map) at global scale. The Fuller projection has low overall area, shape and distance distortions, but distorted direction (ESRI Inc., 2008b). It is for these reasons that DEM (and sink) projection occurs after sink identification rather than before in the methodology, thus eliminating the risk of such error. Once sinks have been identified, the distortions induced by map projection are not significant or biased and do not require further consideration, but are discussed here for completeness.

It is possible that small horizontal error is induced (in sinks and in the DEM) by map projection, within the GIS (ESRI) software. This is certain to cause no more than half a pixel horizontal error (e.g. < 45 m horizontal error in the case of SRTM3 land topography data) (ESRI Inc., 2010). Overdeepenings occur on a scale of hundreds of metres to kilometres, in the horizontal plane. As a result, such error is within acceptable limits for the intended application. The majority of this study focuses on overdeepenings located within the SRTM3 dataset.

The effect of map projection upon vertical error (in sinks and in the DEM) is less easy to quantify. The sink fill algorithm is applied to the DEM(s) prior to projection, in order to produce as accurate a representation of sinks as possible. It is then necessary to project both the DEM(s) and the sink data using bilinear interpolation resampling (of vertical cell values). The accuracy of the overall projection is greatest for continuous data, when such interpolation is used. Unfortunately, bilinear interpolation has the effect of smoothing elevation values (ESRI Inc., 2009), which is largely undesirable as this investigation in part analyses sink depths (where it is determined that sinks represent overdeepenings). Bilinear interpolation resampling offers the best compromise (between overall accuracy of projection, and the least smoothing of sink depths) when projecting data. Nearest neighbour interpolation is an alternative resampling method which could have been used instead. Nearest neighbour interpolation maintains cell values (i.e. produces no smoothing) after projection, but this method should not be used on continuous data as the overall accuracy of the projection is poorer than is the case when other interpolation methods are used. Cubic convolution interpolation is another alternative resampling method, but results in even greater smoothing (than is the case when bilinear interpolation is used) and frequently results in dataset output containing vertical cell values outside the range of the input raster (ESRI Inc., 2009), which would be totally unacceptable for the purposes of this investigation.

By way of further explanation as to the smoothing effect that bilinear interpolation has upon elevation values, and why this is undesirable - an unfortunate consequence of projection is that the process will change the individual vertical cell values (of a DEM and of sink data), relative to the values in the original unprojected data. This change (of, perhaps, several metres) alters the sink depth values observed within a projected sink. As a consequence, on occasion, the value (and sometimes therefore the location) of greatest sink depth that is identified during subsequent analysis may be erroneous. Although it is of course essential that optimal overall projection accuracy is maintained by the resampling method for a given DEM, it is also vital that the smoothing of cell values is minimised in order that the accuracy of sink depth is preserved. In GIS parlance, this has been achieved by the removal of zero values (prior to projection), surrounding sinks in the sink dataset. The zero values indicate where there is no sink within the dataset, and therefore where there is no difference between the sink dataset and the original

DEM. When zero values are removed (i.e. nulled, converted to noData values) the subsequent projected cell values within the sink dataset are resampled more accurately (i.e. with less smoothing), as only data values within the sinks are projected and interpolated. Consequently the impact of smoothing error becomes negligible, and the resultant sink data are suitable for use in analyses of sink metrics. The only drawback to this solution is that, although the projected sink dataset and the DEM remain horizontally cell aligned (having undergone the same projection using the same interpolation method), the vertical cell values do not correspond because of the lesser degree of bilinear smoothing (resampling) of sinks compared with the DEM. This is not an ideal scenario, but is acceptable because this investigation does not require that vertical cell values match between sink data and DEM, as analysis is not undertaken directly between these two datasets or upon DEM vertical cell values alone after projection. Analyses focus only upon the relationships between the confluence dataset, sink data, and the geology overlay.

#### **4.2.3 Removal of small artefacts/errors from sink data (thresholding)**

Small artefacts/errors are present in DEMs (and consequently in sink data). These are a product of the topographical mapping process itself. Thresholding of sink data (for the Labrador study region, and separately for the world map) removes such noise, so that it is not considered in further analysis. Thresholding consists of assessing the number of sinks of any given discrete area (based on raster DEM pixel size) that have 1 m depth. There is a high degree of certainty that such sinks are artefacts/errors because of the vertical accuracy specification of the datasets used in this investigation (section 4.1.4). The procedure makes apparent the optimal sink area threshold that is necessary in order to remove as many artefacts/errors from a given dataset as possible, whilst retaining good data that may be potential overdeepenings. This is because the frequency of sinks with 1 m depth will decrease significantly as sink area is systematically increased. The optimal position for the threshold can therefore be identified by the sink area where there is the most significant decrease in number of sinks with 1 m depth.

For SRTM3 (Labrador land topography) data, 0.0357 km<sup>2</sup> is the optimal area threshold value, with less than 25 % of sinks of this area having depths of 1 m. For GEBCO (Labrador) bathymetry data an area threshold of 2.3546 km<sup>2</sup> is optimal, with less than 14.5 % of sinks of this area having depths of 1 m. A depth threshold value of 5 m has been determined as being optimal within the study region, on the basis of respective depth accuracies of each dataset, and on the basis that this is a reasonable minimum depth at which an overdeepening might typically begin to be visually identifiable in the field (and therefore be a significant enough example of overdeepening to warrant further analysis). Thresholded data are displayed as polygon and point shapefile data within the ESRI ArcGIS software.

For the GEBCO (world map at LGM) topography and bathymetry data an area threshold of 3.0545 km<sup>2</sup> is the optimal threshold value for sinks within the limit of the LGM, with less than 9.5 % of sinks of this area having depths of 1 m. However an area threshold of 76.3619 km<sup>2</sup> has been implemented, on the basis that the smaller (optimal) value is too detailed to be useable at the global scale of hard copy maps displaying an overview of significant overdeepenings. A depth threshold of 50 m has been implemented for the world map, again for reasons of scale but also for reasons of depth accuracy limitations of some source data (e.g. DCW, BEDMAP).

#### ***4.2.3.1 Manual analysis of thresholded sinks: Assessing glacial origin***

Manual analysis of thresholded sinks is subsequently undertaken. This allows a judgement to be made regarding whether a sink can be asserted as being an overdeepening (with a good degree of certainty), or whether some other physical process (e.g. tectonic evolution of a basin, a meteor impact creating a crater, volcanic activity creating a caldera) or anthropogenic activity (e.g. the construction of a man-made reservoir, or a harbour) can be asserted as being responsible for the formation of the sink, and therefore whether the sink should be removed from the dataset (in the case of the Labrador data) or labelled (colour coded) appropriately (in the case of the world map). The high threshold value that is used for sink data for the world map eliminates potentially anthropogenic sinks without manual analysis being necessary.

#### ***4.2.4 Defining overdeepenings that contain lakes, within sink data***

Overdeepenings sometimes contain lakes. When such overdeepenings are topographically mapped (at regional or global scale), the corresponding sinks sometimes appear fragmented (in terms of sink area, appearing speckled in the DEM). In comparison, sinks corresponding to overdeepenings that are free of lakes will show no such fragmentation, and will be quite contiguous in appearance. For overdeepenings which contain lakes, sink area fragmentation is a consequence of radar backscatter from the surface of the water, which occurs during mapping (i.e. data collection). The backscatter effect reduces the likelihood of a contiguous lake surface being detected. Of the DEMs utilised in this investigation, backscatter is an issue that is most relevant to those that have greatest resolution.

When overdeepenings containing lakes are mapped, the corresponding maximum sink depths and the location of these (as derived from the resulting DEM) are unlikely to be correct. This is because the detected maximum depth value and location is likely to be only a reflection from the lake surface. Consequently, these metrics will be erroneous and need to be removed.

In order to reduce area fragmentation, and remove erroneous depths/ depth locations in overdeepenings which contain lakes, sink and lake body are combined. Lake bodies are obtained from the inland water bodies dataset. Combining sink and lake defines potential overdeepenings more contiguously than would otherwise be the case (figure 19), for use in subsequent analysis. The resulting combined sink/lake polygons are assigned arbitrary depth values of 0 (i.e. depths of these overdeepenings are unknown).

In order that some sink data (coincident with lake bodies) are not thrown away, unthresholded sink data are utilised in this task. By using unthresholded data, fine detail (occurring on the periphery of a combined sink/lake) is considered, which is likely to constitute a valid part of an overdeepening, and which would otherwise be removed by the thresholding process. In all subsequent analyses, thresholded sink data are utilised in order that small artefacts/errors cannot be considered. Following the combination of sinks and lakes, area thresholding is applied using the same thresholds as detailed in the previous section. Further, manual analysis of the combined dataset is undertaken (as for thresholded sinks), to examine whether some physical process or human activity other than overdeepening is responsible for sink/lake formation. If an overdeepening does not contain a lake then the corresponding sink will be unaltered by the process that combines sinks and lakes.

The area of a combined sink/lake polygon may differ from that of the lake body alone (as obtained from the inland water bodies dataset). This difference may be due to an overdeepening being only partially filled with water, and the corresponding sink consequently being larger than the lake body. The difference in area may otherwise/ also (particularly for the world map) be due to temporal and further seasonal variations in the extent of water bodies as depicted by topographical datasets, when compared to the extent depicted in the inland water bodies dataset.

Occasionally (in the world map), because of the significant difference in horizontal resolution between sink data and lake data in some cases, sinks may not coincide properly with their respective lake body. In such instances lake data are down-sampled (using nearest neighbour sampling) to match the resolution of the sink data, and coincidence then occurs.

Sometimes, when an overdeepening has been totally filled by a lake, the lake will be apparent in the inland water bodies dataset, but there will be no corresponding sink in the DEM. In such instances the lake body is included (unaltered) in the combined sink/lake dataset, for use in subsequent analysis. Using this method, entirely water filled overdeepenings are included in the dataset that may otherwise be almost undetectable. Entirely sediment filled overdeepenings unfortunately remain undetectable.

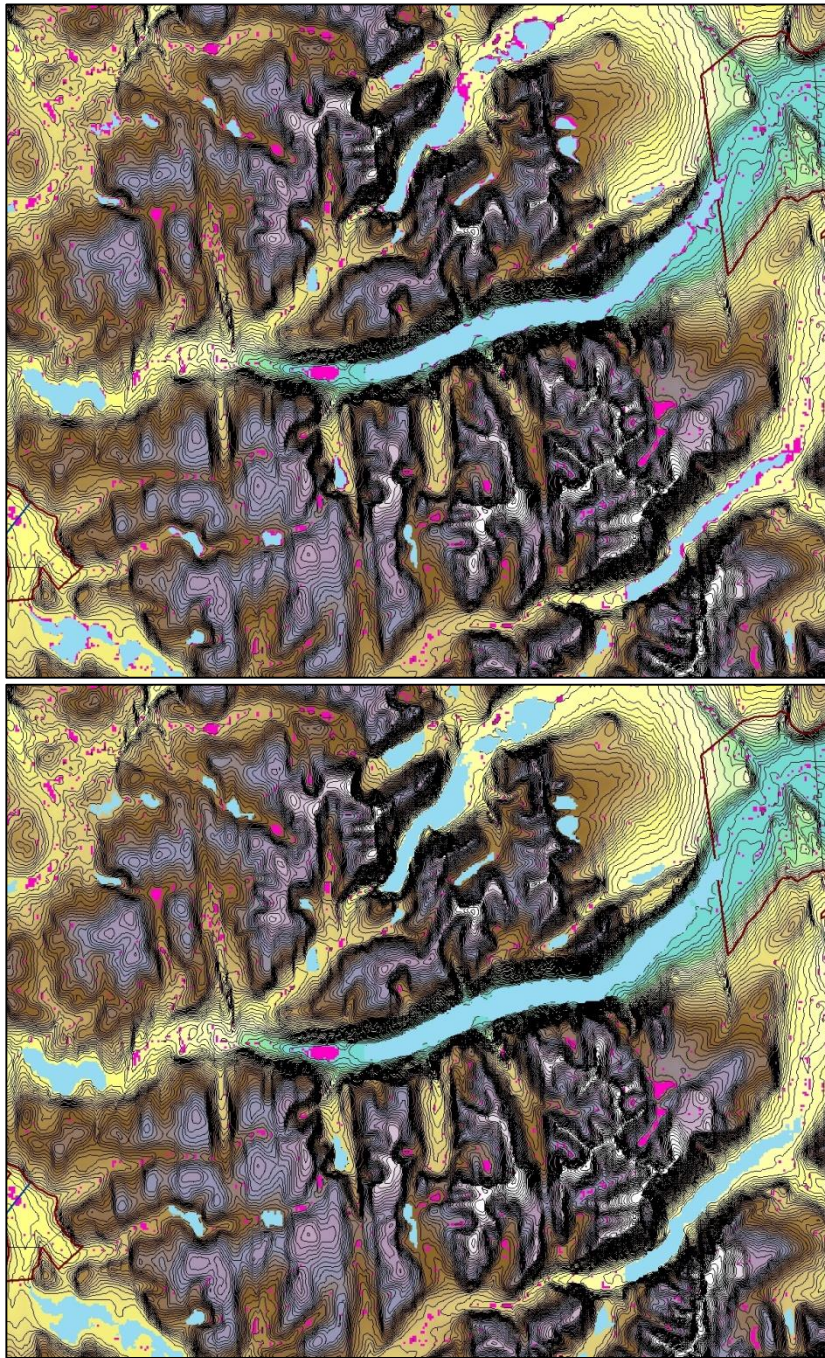


Figure 19. Defining overdeepenings that contain lakes, within sink data (for Labrador study region, and for world map).

For overdeepenings which contain lakes (for the Labrador study region, and for world data), in order to reduce area fragmentation (due to radar backscatter from the surface of lake water), and to remove erroneous depths/ depth locations (due to reflection from the surface of lake water), sink (magenta) and lake (light blue) (top image) are combined (bottom image). Lake bodies are obtained from the inland water bodies dataset. Combined sink/lakes are depicted as 'enlarged' lakes (light blue). Combining sink and lake defines overdeepenings more contiguously than would otherwise be the case, for use in subsequent analysis. If an overdeepening does not contain a lake then the corresponding sink will be unaltered by this process. The DEM is SRTM3 topography data, for the Labrador study region (ll coord 59.0, -64.6 DD), depicted using ESRI ArcGIS 'elevation' colour scale. Contours are placed at 20 m intervals (black lines).

#### 4.2.5 Defining topographically low lying overdeepenings, within sink data (filtering; applied to regional study only)

Overdeepenings sometimes accumulate localised superficial glacio-fluvial deposits and/or are colonised by vegetation. This is particularly common in some empty/ partially sediment filled overdeepenings located in topographically low lying valleys and other low lying areas. When such overdeepenings are mapped, the area of corresponding sinks will often appear fragmented. In comparison, sinks corresponding to overdeepenings that are free of such influences will show no such fragmentation, and will be quite contiguous in appearance. Fragmentation occurs for much the same reason as has been discussed for overdeepenings which contain lakes. Superficial deposits and vegetation will cause a radar backscatter effect during mapping. The backscatter effect reduces the likelihood of a contiguous overdeepening being detected. Fragmentation is an issue that is most noticeable where DEMs are of high resolution, hence the issue is especially evident within the Labrador study region (i.e. SRTM3 dataset).

The greater accumulation of superficial deposits and/or vegetation in topographically low lying valleys/areas, relative to that found up-tributary, is a consequence of greater sediment availability in low lying valleys/areas brought about by fluvial depositional and reworking processes that prevail in the lower tracts of river systems following a deglaciation. Fluvial valley longitudinal profiles naturally tend towards a graded profile in order to erode down to base level, and consequently fluvial erosion is greatest in the upper tract and fluvial deposition is greatest in the lower tract of a river system. Additionally, fluvial processes will rework glacial sediments deposited in topographically low lying coastal valleys, especially at and downstream of the (palaeo) ELA of former glaciers, where such glacial sediments are usually most abundant and where overdeepenings most frequently occur and are of greatest size. In contrast, in formerly glaciated valleys at higher elevations (i.e. located up-tributary), in the upper tracts of river systems, fluvial erosional processes usually prevail and the abundance of glacial sediments is usually lower. Overdeepenings are therefore more likely to accumulate superficial deposits and/or vegetation in low lying valleys/areas.

In order to reduce the area fragmentation of overdeepenings located in low lying valleys/areas, the corresponding sinks are filtered. This process defines overdeepenings more contiguously than would otherwise be the case (figure 20), for use in subsequent analysis. A low pass 3 x 3 filter is applied in a single pass. Only a single pass is applied, so as not to over-process/artificially inflate overdeepening area. Thresholded sink data are utilised in this task, in order that small artefacts/errors are not amplified by filtering. The low pass filter is not applied to lakes, as these are mostly significantly larger and more contiguous than other sinks.

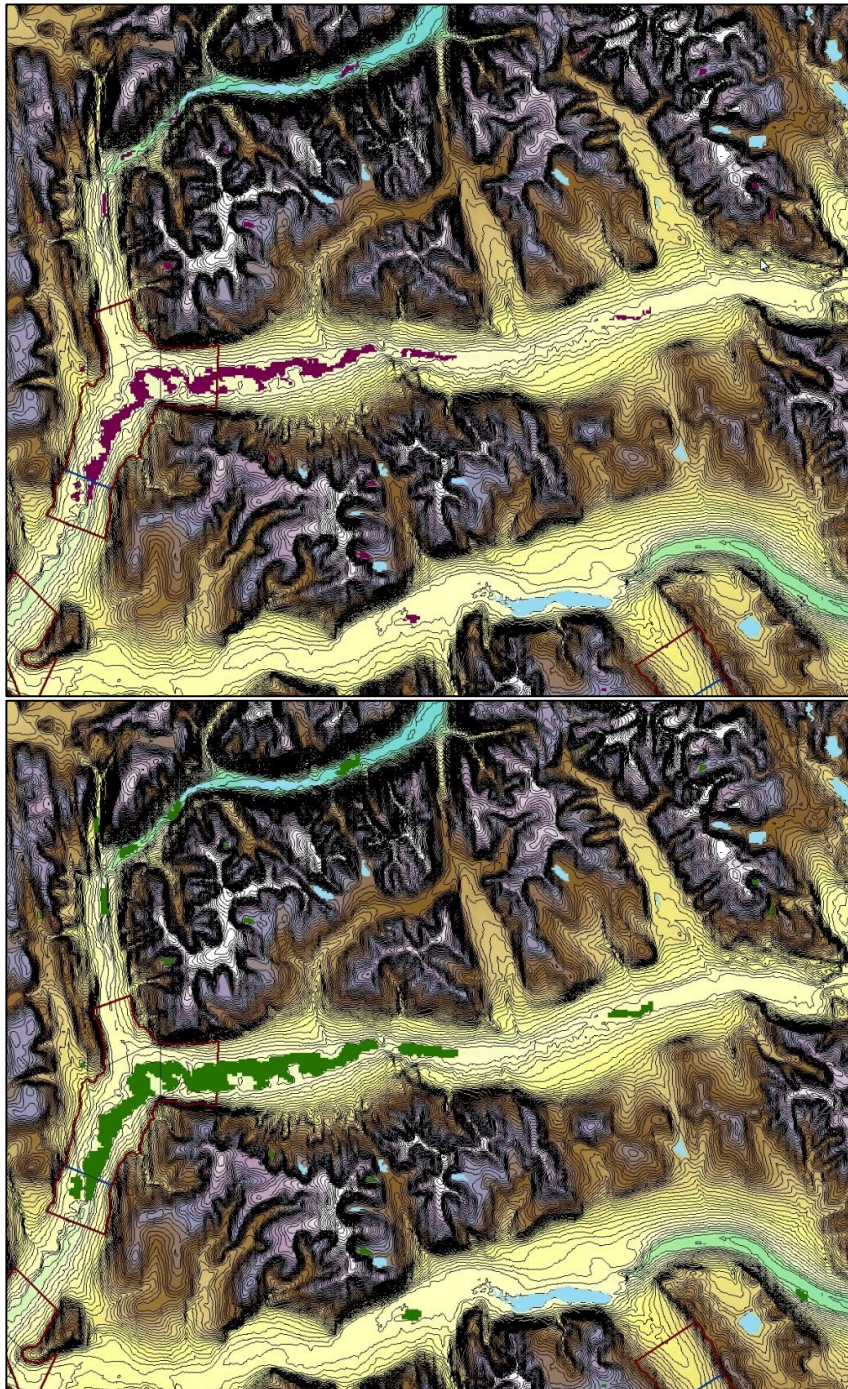


Figure 20. Defining topographically low lying overdeepenings, within sink data (filtering; for Labrador study region only).

For overdeepenings located in topographically low lying valleys and other low lying areas (for the Labrador study region), in order to reduce area fragmentation (caused by radar backscatter from accumulations of superficial deposits and/or vegetation), sinks are filtered. Corresponding sinks (maroon, top image) are made as contiguous as possible by the use of a low pass 3 x 3 filter, applied in a single pass (filtered sinks are presented in dark green, bottom image). Filtering defines overdeepenings more contiguously than would otherwise be the case, for use in subsequent analysis. The low pass filter is not applied to lakes (depicted in light blue, top and bottom image), as these are mostly significantly larger and more contiguous than other sinks. The DEM is SRTM3 topography data, for the Labrador study region (ll coord 58.6, -64.2 DD), depicted using ESRI ArcGIS 'elevation' colour scale. Contours are placed at 20 m intervals (black lines).

The filtering process does not alter the depth values within affected sinks. Original depth values are retained. The additional sink area that is added to (or 'grown' around) sinks by the low pass filter is assigned the arbitrary depth value of 0. In these peripheral positions the depth of the overdeepening is considered to be unknown, but as depth is invariably shallower at these locations than at the (known) positions of maximum sink depth the additional arbitrary depth values are of no consequence to subsequent analysis.

Overdeepenings are considered to be topographically low lying if any part of the corresponding filtered sink is situated below an empirically selected elevation threshold of 345 m a.s.l. Where the entirety of a filtered sink is located at or above 345 m a.s.l the overdeepening is not considered to be low lying and consequently the non-filtered sink is utilised in subsequent analysis instead.

The elevation threshold has been carefully selected, based on visual inspection of the DEM for the Labrador study region. The threshold is effective at identifying the major coastal valley networks and other topographically low lying areas, as a consequence of the well defined natural break in topography (i.e. the fjords) which occurs within this province of Canada at regional scale (figure 21). This simplistic type of threshold would almost certainly not be so effective in identifying regional scale valley networks in DEMs of some other parts of the world, where there is little or no natural break in topography into coastal valleys. For Labrador, a threshold such as this is favoured as it is simple and effective. The alternative would be to either devise a more complicated way of spatially defining a 'valley' in a DEM, in order to isolate sinks within, or to apply a smoothing filter to all sinks regardless of elevation. Devising a more sophisticated way of spatially defining a valley would be too time consuming and is unnecessarily complex for the needs of this investigation. Applying a smoothing filter to all sinks in the Labrador dataset would be undesirable, as it would have the effect of artificially inflating area for many small up-tributary overdeepenings, the majority of which are far less affected by the accumulation of superficial deposits and/or vegetation than are their counterparts in major coastal valleys, for reasons discussed previously in this section.

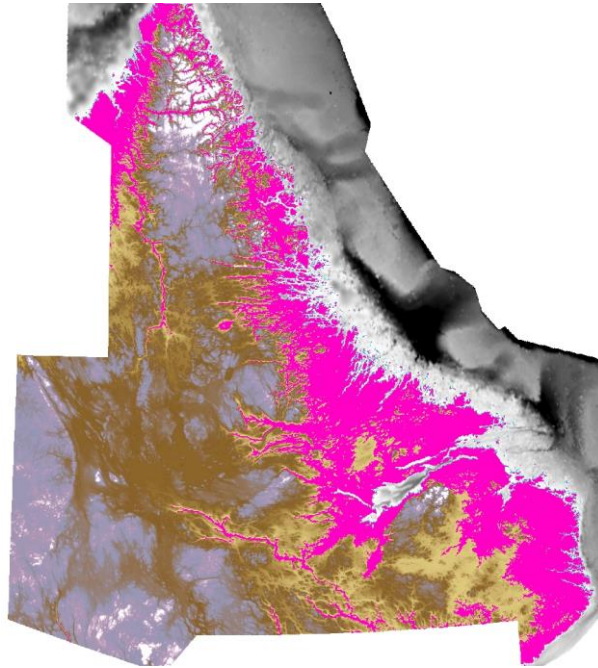


**Figure 21. Defining topographically low lying overdeepenings, elevation threshold (Labrador study only).**

An elevation threshold (of 345 m a.s.l) is used to identify topographically low lying valleys and other low lying areas, within the Labrador study region (ll coord 52.0, -67.8 DD). This has been carefully selected, based on visual inspection of the DEM. The threshold is effective at identifying the major coastal valleys and other low lying areas, as a consequence of the well defined natural break in topography (i.e. the fjords) which occurs within this province of Canada at regional scale. Land topography elevation values below the elevation threshold of 345 m a.s.l are displayed in pink. SRTM3 land topography data are shown in ESRI ArcGIS 'elevation' colour scale. Scale ranges from 345 m a.s.l (light brown) to ~1600 m elevation a.s.l (white). GEBCO bathymetry data are shown in greyscale. Scale ranges from sea level (white/grey) to ~ -1700 m depth (black).

#### **4.2.6 Defining overdeepenings, within sink data (further thresholding; applied to global study only)**

In large, lower resolution datasets (i.e. GEBCO, world map) sink area fragmentation does not occur as much as it does in small, higher resolution datasets (i.e. SRTM3, Labrador). Consequently, for the world map an alternative method is used to consider the contiguousness of overdeepenings, which focuses on sinks in the whole study region rather than only those specifically in low lying valleys and other low lying areas. The technique involves assessing sink area/sink perimeter ratio, in order to determine sink contiguousness. Any sink which is found to have an area/perimeter ratio of less than 1 is not considered further in analysis. The sink area/ perimeter ratio technique improves the quality of global overdeepenings in the dataset, by removing sinks that have poor contiguousness. For large, lower resolution datasets, over large geographical areas, the sink area/ perimeter ratio technique is a computationally inexpensive and reliable way of assessing overdeepening contiguousness at regional to continental scale.

### 4.3 Identifying glacial valley confluences (for regional study) (Objective 2)

In order to investigate all hypotheses within this study, glacial valley confluences must be identified and defined within relevant DEMs. Glacial valley confluences (each comprising a pair of tributary valleys, and a trunk valley) can be considered to be point locations of maximum ice velocity (i.e. a focus of glacial erosion) within glaciated and/or formerly glaciated regions. However, this study considers each (discrete, or unique) confluence as an *area* of influence, in order that individual confluence extent (area) can be defined and in order that the control of individual confluences upon overdeepenings can be assessed. Additionally, in the initial parts of testing both the topographical and the geological hypotheses, confluences are considered as a *single* area of influence (i.e. overlapping confluences are merged to become one confluence 'zone'), in order that the coincidence of glacial confluence with overdeepenings, and coincidence of geological zone with glacial confluence, can be assessed. Figure 22 displays the Labrador study region, and associated confluences and overdeepenings. Confluences and overdeepenings within the Swiss study region are examined in the later stages of the investigation as an exploratory exercise in order to observe whether some results obtained in the Labrador study are reproducible elsewhere. The main elements of the workflow for confluence identification and definition are summarised in figure 23.

A trunk valley is defined as the glacial valley situated immediately downstream of a pair of joining tributary valleys, within a confluence. The trunk valley is the receiving valley for glacial ice, supplied by the tributary pair, within the confluence.

#### 4.3.1 Confluence identification, criteria, and certainty

Some landforms are relatively easy to identify and define in DEMs. One such example is that of overdeepenings, which can be identified and defined simply by delimiting the extent of the depression in the landscape (with some further processing – section 4.2). Other landforms, such as confluences, are more difficult to identify and define because boundaries are fuzzy; i.e. the landform has a vague spatial extent (Fisher, et al., 2004). As yet, delimitation of many such landforms is mainly manual, using visual identification: automation of the process remains a research frontier, with acceptable success rates somewhat elusive (Evans, 2012). Classification of a whole land surface is more difficult than extraction of specific landforms from it (Evans, 2012).

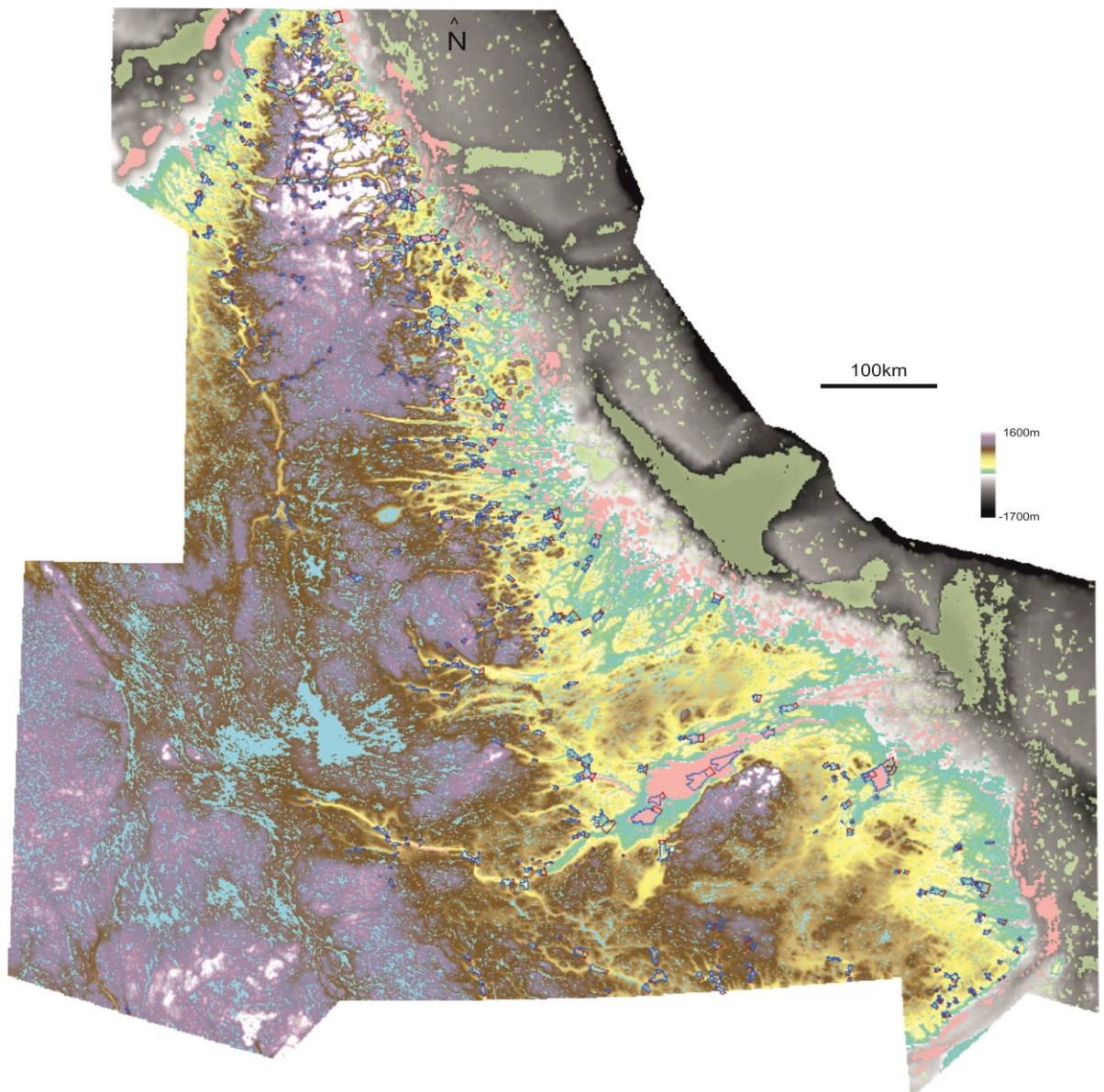


Figure 22. The study region (Labrador, Canada and surrounding region).

Glacial confluences (perimeters denoted in blue), are shown with their liberal extensions (perimeters denoted in dark red) (see section 4.3 for identification method). The general population of overdeepenings (see section 4.2 for identification method) are shown in rose (empty/partially sediment filled) and light blue (totally/partially water filled). The perimeter of the study region (for analysis purposes) is 26 km away from the eastern coast of Labrador (see section 4.5.1.1). The perimeter is defined on the map by a change in the colour (from rose to green) of overdeepenings within the bathymetry. Several large (ice-sheet scale) overdeepenings can be seen in the GEBCO bathymetry data. SRTM3 land topography data (ll coord 52.0, -67.8 DD) are shown in ESRI ArcGIS 'elevation' colour scale. Scale ranges from sea level (turquoise) to ~1600 m a.s.l (white). GEBCO bathymetry data are shown in greyscale. Scale ranges from sea level (white/grey) to ~ -1700 m depth (black).

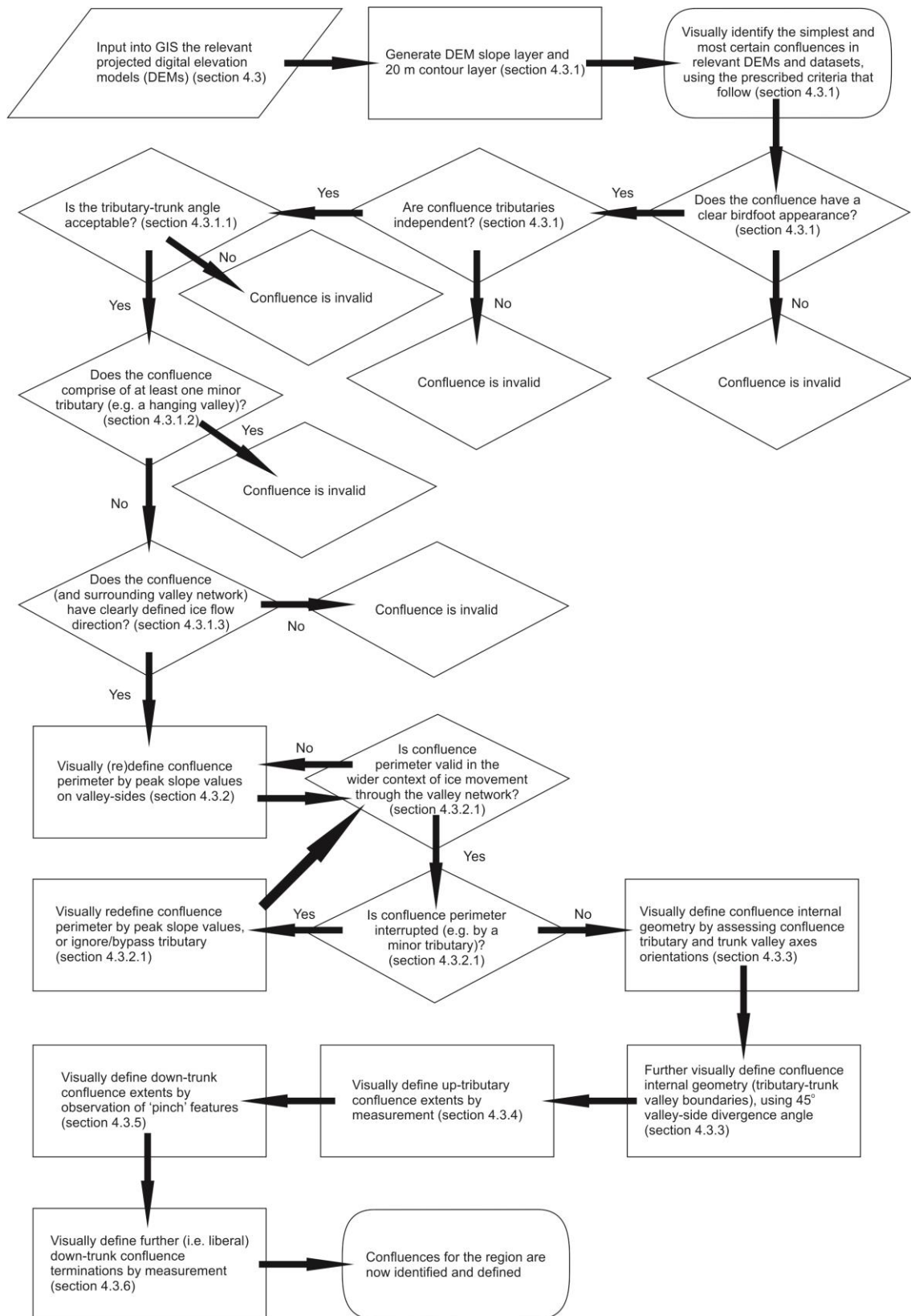


Figure 23. The main elements of the workflow for confluence identification and definition.

Workflow elements demonstrate the criteria with which the simplest and most certain confluences are visually identified for study. Further, elements demonstrate the process by which confluence perimeter is iteratively defined, and the process by which confluence internal geometry, and up-tributary and down-trunk extents are defined. This process allows subsequent assessment of valley cross-sectional area (CSA) change through each confluence.

The development of GIS technology has underlined the need for more detailed and explicit formalisation of the terrain analysis process (Argialas, 1995). Unfortunately, most researchers focus on the methodological aspect (automation) at the expense of the conceptual background of land surface segmentation; with many researchers preferring more readily automated concepts, which are not necessarily the best (Minar & Evans, 2008). Progress is being made with both supervised and unsupervised classification of DEMs (Seijmonsbergen, et al., 2011), but the sophistication of current algorithms is limited. Constraints most relevant to the identification of glacial landforms include the scale at which a land surface classification operates (i.e. window size, multi-scale analysis), the number of classes used, and the thresholds employed during such classification (e.g. slope and curvature tolerances). These variables are currently crucial to feature identification, and small differences can change the nature of detected features significantly (Ehsani & Quiel, 2008). Minar & Evans (2008) note that a general theoretical unification of the many concepts utilised by land surface classification algorithms is needed.

In exploring possible methodologies for confluence identification in this investigation, semi-automatic fuzzy land surface classification has been considered; using Landserf software as developed by Joseph Wood (1996; 2002). This is in order to determine land surface membership to a set of six distinct classes (pits, channels, passes, ridges, peaks, and planar regions) in sample DEMs of formerly glaciated terrains. These classes are widely used in geomorphometry (e.g. Fisher, et al. (2004); Wood (1996); Evans (1980); Peucker & Douglas (1974)) to define local surface form (Fisher, et al., 2004). Preliminary investigation has determined that such classification is unacceptable for the identification of valleys (and hence confluences) as distinct landforms. The classification limit of six classes is inflexible and appears to be better suited to the definition of landforms that are less fuzzy (e.g. river channels and valley-floors), perhaps in fluvial rather than glacial environments. Ehsani & Quiel (2008) note that Wood's method assumes that pits, peaks and passes occur where the local slope is zero; but in reality when neighbourhood is considered, land surfaces usually have overall inclination. Ehsani & Quiel (2008) comment that this assumption may result in output consisting mainly of channels and ridges. The channel class was indeed a significant output in preliminary investigation. The other problem with Wood's method, as stated by Ehsani & Quiel (2008), is that planar features have a zero value of maximum, minimum and cross-sectional curvatures. In reality, most have some curvature, resulting in outcomes that depend strongly on the selected values of slope and curvature tolerances (Ehsani & Quiel, 2008). This dependency accounts for the success of the method at identifying valley-floors during preliminary investigation.

To successfully identify and define confluences it is most important that lateral (confluence) valley extent is clearly delimited. For this to occur it is necessary that valley-sides are clearly defined. Because it is well documented that current land surface classification algorithms perform somewhat poorly, identification and definition of glacial valley confluences has proceeded manually within each study region explored in this investigation, via visual inspection of the DEM (elevation values), and by use of DEM slope map(s) and DEM 20 m contours. DEMs are presented for visual analysis using the adaptive colour stretched ('elevation') ArcGIS colour scheme, available within the software (data is displayed within 2 standard deviations of the mean elevation value, for any given display extent). This setting enables maximum visualisation of detail at any given scale of observation, and therefore facilitates visual identification of the maximum possible number of confluences, within the limits of DEM resolution.

Confluences are identified using the criteria that follow in this section. Confluence perimeter is then defined iteratively, according to a ruleset (section 4.3.2). Confluence internal geometry (section 4.3.3), and up-tributary (section 4.3.4) and down-trunk valley confluence extents (section 4.3.5) are subsequently defined. Confluence certainty (i.e. the degree of confidence with which each confluence might be regarded) is then assessed, based upon how well each confluence meets all criteria (i.e. a value of 0 is assigned to a confluence where it is regarded with less certainty, where several criteria are met with less than total satisfaction; a value of 1 is assigned where a confluence is regarded with more certainty, but where one or more criterion is still met with less than complete satisfaction; and a value of 2 is assigned where a confluence is regarded as very certain, fulfilling all criteria satisfactorily). Potential confluences that have poor overall certainty are considered invalid, and are not recorded for further analysis. Such confluences will totally fail to satisfy at least one criterion.

A potential confluence must be visually apparent within *all* of DEM elevation, slope and contour data, appearing visually unambiguous and well defined (i.e. the confluence should be clear at the position where tributaries meet, perhaps appearing something like a birdfoot in plan), with clear direction and continuity of ice flow (i.e. the transverse profile of the tributaries where they meet, and the longitudinal profile of each tributary, should be reasonably well preserved) (figure 24). Tributaries should appear independent of one another.

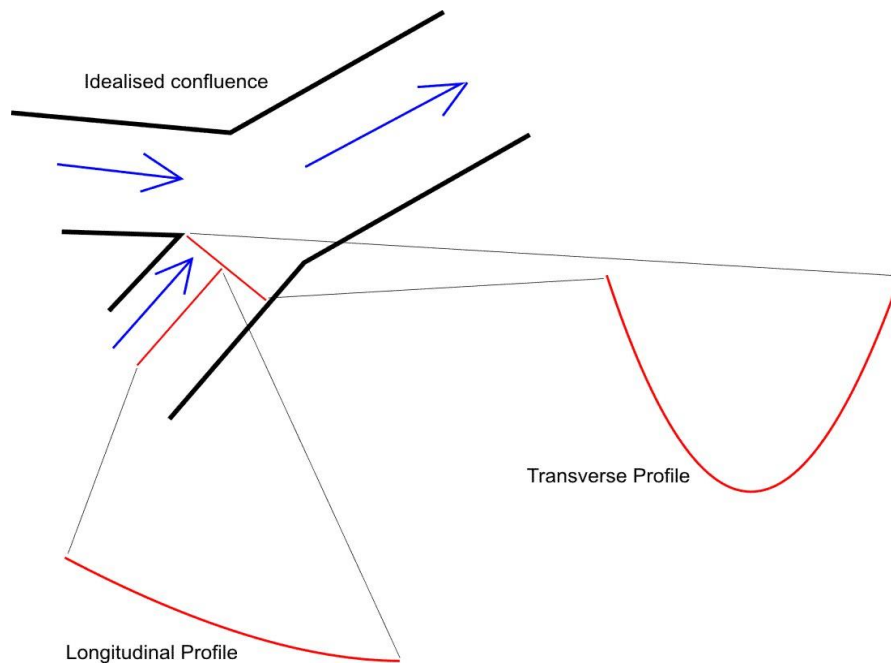


**Figure 24. Schematic plan of an idealised confluence.**

**Ice flow direction is denoted by blue arrows. Idealised schematic transverse and longitudinal profiles (not to scale) depicted in red.**

#### 4.3.1.1 Tributary-Trunk angle

An idealised confluence (with respect to tributary-trunk angle) is shown in figure 25 (top). Where one or both tributaries within a potential confluence appear visually unnatural or spatially discontinuous, the confluence is considered to have very poor certainty and is therefore considered invalid. A common example of such invalidity is where the angle between the tributary and the trunk valley is very acute (i.e. confluence geometry appears visually unnatural) (figure 25, middle). The threshold at which such an angle is deemed unacceptable is not precisely defined in this investigation (although it is usually where the angle is approximately at  $90^\circ$ , figure 25, bottom), as the minimum angle that may be perceived to allow a viable confluence probably varies according to specific confluence geometry. Where uncertainty exists regarding the acceptability of the angle, assessment of confluence validity is made using other criteria (and the confluence is likely regarded as a lower confidence example).

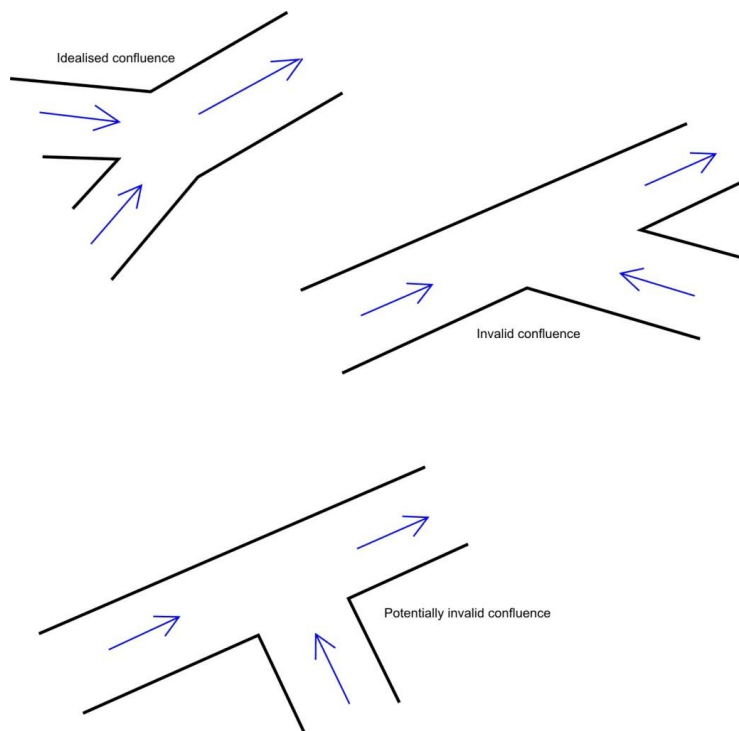
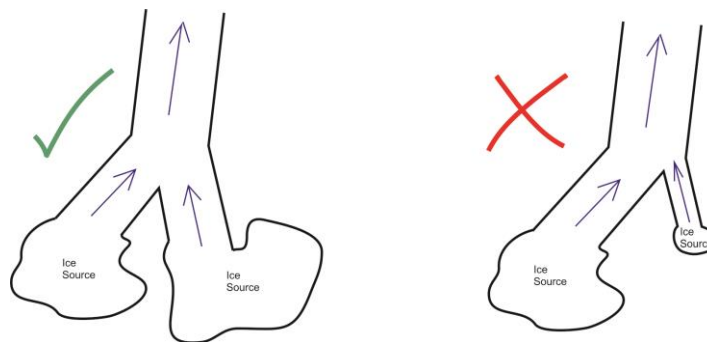


Figure 25. Schematic plans of confluences: Tributary-Trunk angle.

**(Top)** Schematic plan of an idealised, valid, confluence; **(Middle)** A potential confluence that is invalid, after assessment of the (acute) angle between the potential tributary and the trunk valley; **(Bottom)** A potential confluence that is possibly invalid, after assessment of the (right) angle between the potential tributary and the trunk valley (see text). Where uncertainty exists regarding the acceptability of the angle, assessment of confluence validity is made using other criteria. Ice flow direction is denoted by blue arrows.

#### 4.3.1.2 Major and minor tributaries

Tributaries belonging to a potential confluence should be visually balanced. The term 'balanced' means that tributaries should be of the same approximate order of magnitude width and/or CSA as each other in the locality where tributaries meet. Each tributary should form an arterial route for ice at the scale of the valley network in the locality of the potential confluence (i.e. the ice source for each tributary should be significant at this scale) (figure 26). Where a pair of tributaries conform to these rules they are termed major tributaries. Major tributaries form a pair, along with a trunk valley, in a valid confluence. Tributaries that do not conform to these rules (and/or do not meet other criteria, as outlined elsewhere in section 4.3) are considered to be minor tributaries and do not form part of a valid confluence. It is doubtful whether minor tributaries can provide adequate channel constriction (i.e. ice velocity speed up) within a potential confluence, in order that overdeepenings may develop via the confluence control. Consequently, there is very poor certainty for potential confluences where minor tributaries form a part.



**Figure 26. Schematic plans of confluences: Major and minor tributaries.**

**Schematic plan of confluence examples, depicting valid (green tick) and invalid (red cross) potential confluences, after consideration of the relative order of magnitude of each tributary within, and the status of each tributary as an arterial route for ice (at the scale of the surrounding valley network). Tributaries should provide adequate channel constriction (i.e. ice velocity speed up) within a confluence, in order that overdeepenings may develop. Ice flow direction is denoted by blue arrows.**

A potential confluence is considered to have very poor certainty, and is therefore considered invalid, where a hanging valley is observed. Hanging valleys are considered to be minor tributaries. A hanging valley occurs within a potential confluence where ice flow through one tributary has been dominant over ice flow through the other tributary, and consequently where glacial erosion through the dominant tributary (and trunk channel) has left the other tributary hanging (figure 27, top). A hanging valley will be identifiable where a tributary joins a trunk valley, and where very high slope values occur relative to those within the adjacent tributary. The hanging tributary will have considerable vertical discontinuity with the trunk valley (figure

28), and confluence tributaries will be poorly proportioned relative to one another (i.e. the confluence will not be balanced). Where tributaries hang, any associated overdeepening is likely to have developed via an alternative control (i.e. by valley-floor perturbation), rather than by glacial confluence. For this reason, hanging valleys should be the focus of separate study.

Much like a hanging valley, a valley step can show quite high slope values (relative to those within the adjacent tributary) where a tributary joins a trunk valley in a potential confluence (figure 27, bottom), but in these instances it is possible to have confidence in the confluence as it will appear better proportioned, with tributaries appearing visually natural and more spatially continuous in longitudinal valley profile. Hence the confluence will appear balanced and will therefore be valid (figure 29).

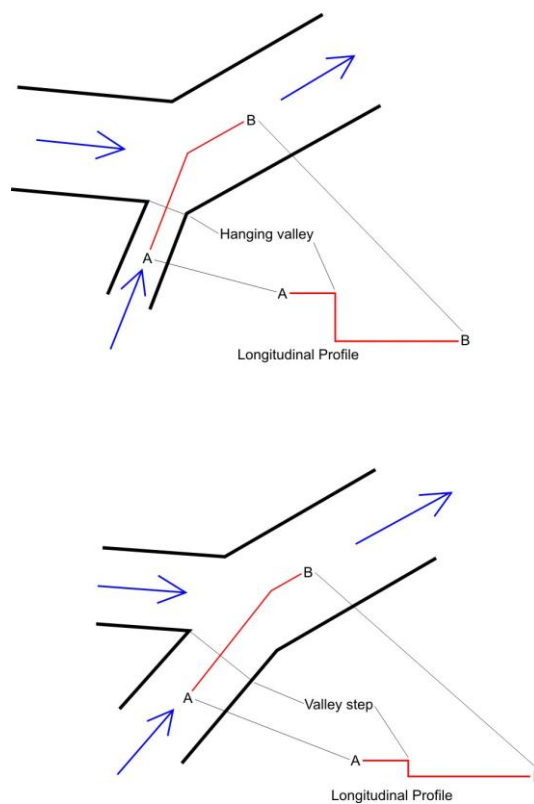
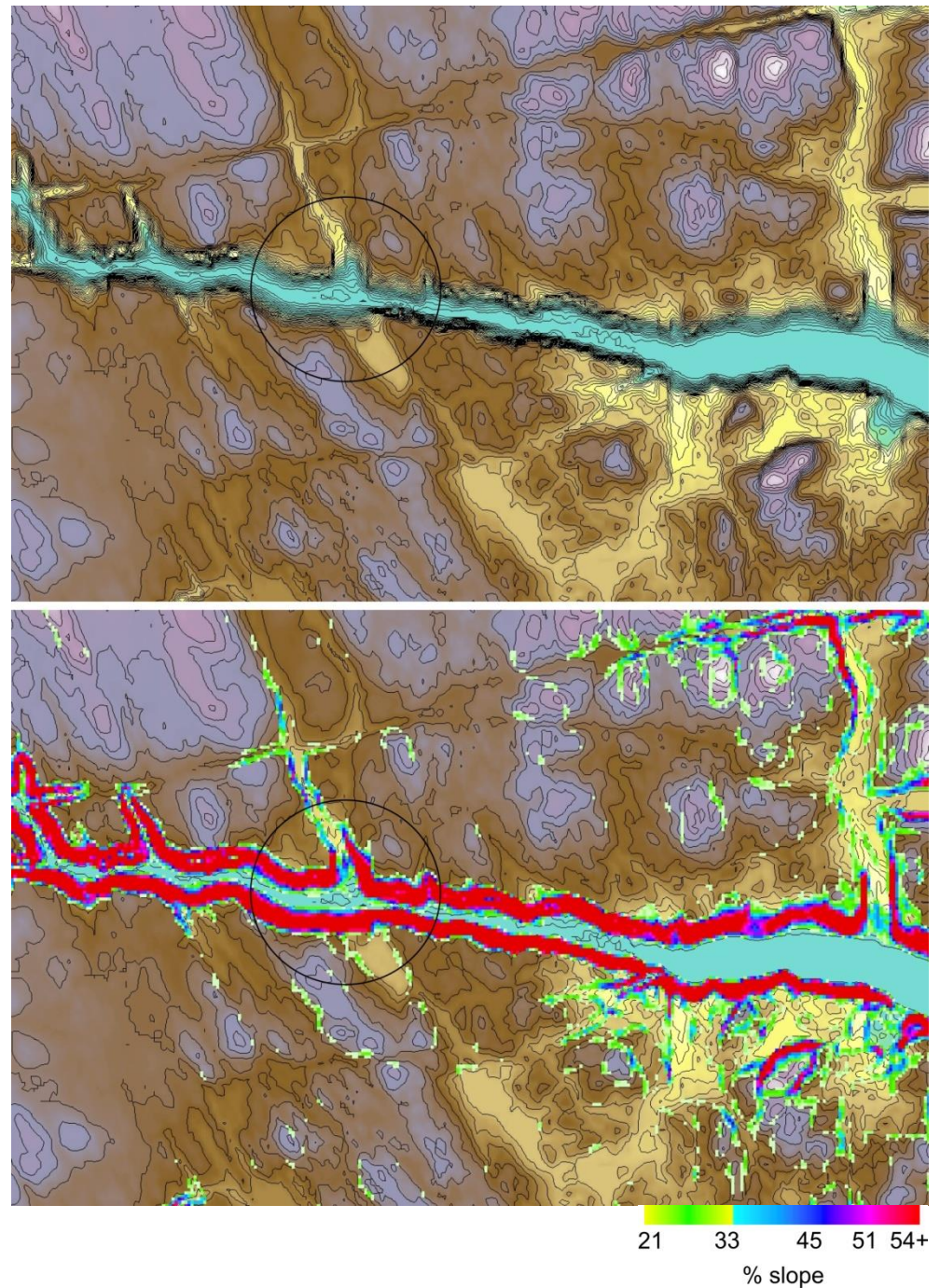


Figure 27. Schematic plans of confluences: Hanging valley & stepping valley.

Schematic plan and longitudinal profile of a potential confluence that is (Top) considered invalid, after assessment of hanging tributary, where tributary joins the trunk valley. At this location there is considerable vertical discontinuity and an ‘unbalanced’ confluence appearance (see text); (Bottom) considered valid, after assessment of stepping tributary, where tributary joins the trunk valley. At this location there is some vertical discontinuity, but an overall ‘balanced’ confluence appearance (see text). Ice flow direction is denoted by blue arrows. Longitudinal profiles (not to scale) are depicted in red.



**Figure 28. Example of hanging valley.**

(Top) An example of an invalid potential confluence (ringed) within the Labrador study region, due to a hanging tributary valley. At this location (ll coord 56.7, -63.1 DD) there is considerable vertical discontinuity and an ‘unbalanced’ confluence appearance (see text). Other less significant hanging valleys are also visible along the main valley. (Bottom) The same invalid confluence with partial slope map superimposed (i.e. displaying highest percentage slope values only). The hanging tributary has associated high slope values relative to adjacent tributary. SRTM3 land topography data are shown in ESRI ArcGIS ‘elevation’ colour scale. SRTM3 derived slope data are shown in a modified ESRI ArcGIS ‘aspect’ colour scale. Contours are placed at 20 m intervals (black lines).

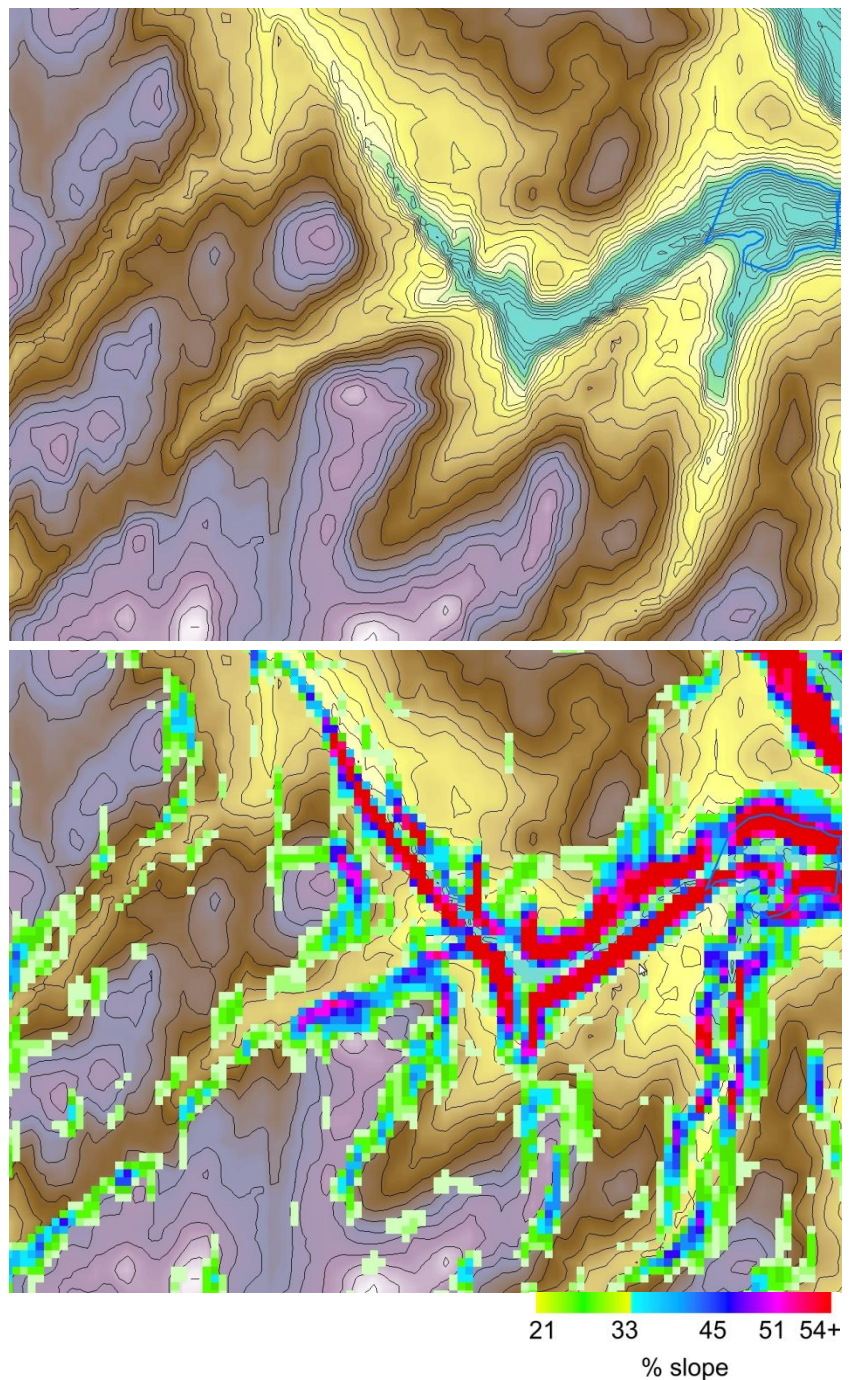


Figure 29. Example of stepped valley.

(Top) An example of a valid potential confluence (perimeter shown in blue) within the Labrador study region, after consideration of a stepped tributary valley. At this location (ll coord 55.0, -62.4 DD) there is some vertical discontinuity, but an overall ‘balanced’ confluence appearance (see text). (Bottom) The same valid confluence with partial slope map superimposed (i.e. displaying highest percentage slope values only). The valley step has associated moderate slope values relative to adjacent tributary. SRTM3 land topography data are shown in ESRI ArcGIS ‘elevation’ colour scale. SRTM3 derived slope data are shown in a modified ESRI ArcGIS ‘aspect’ colour scale. Contours are placed at 20 m intervals (black lines).

#### 4.3.1.3 Ice flow direction within valley networks

Ice flow direction is considered within each potential confluence, and then between adjoining confluences within valley networks (by consideration of former ice divides, and analysis of tributary longitudinal profiles via the use of valley contours). Ice flow direction should not be opposing between two adjoining confluences if both confluences are to be valid (figure 30). Where ice flow direction between two (potential) adjoining confluences is found to be opposing, confluence validity of one or other confluence is reconsidered.

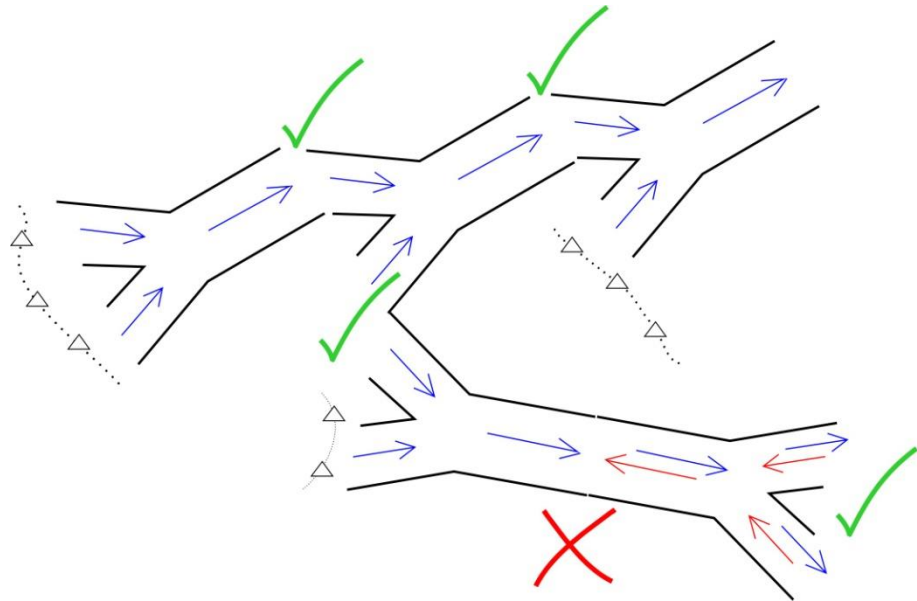


Figure 30. Schematic plan of ice flow direction within a valley system.

Ice flow direction within a valley system, after consideration of former ice divides, and analysis of tributary longitudinal profiles via the use of valley contours. Idealised potential confluences are shown, depicting valid (green tick) ice flow direction (blue arrows) between adjoining confluences and diffluences (where flow direction has good certainty) and invalid (red cross) ice flow direction (red arrows) between adjoining confluences (where flow direction has very poor certainty). Ice divides at ridges and summits are denoted by dotted lines with triangles.

#### 4.3.1.4 Poorly defined confluences within the landscape: Glacial erosion

Where the landscape experiences significant areal scouring and selective linear erosion (by warm based ice), and/or experiences successive phases of valley glacier, ice cap, and ice sheet erosion to form a composite erosional landscape (Sugden & John, 1976; Sugden, 1978), some confluences may be obliterated or appear very poorly defined within the landscape (figure 31, see section 2.6). In such instances a potential confluence will be visually ambiguous in one or all of DEM elevation, contour and slope maps, and will have unclear direction and continuity of flow (i.e. the longitudinal profile of tributaries will not be well preserved). Tributaries may also

not appear independent of one another. In such instances potential confluences will have very poor certainty and no confluence is recorded.

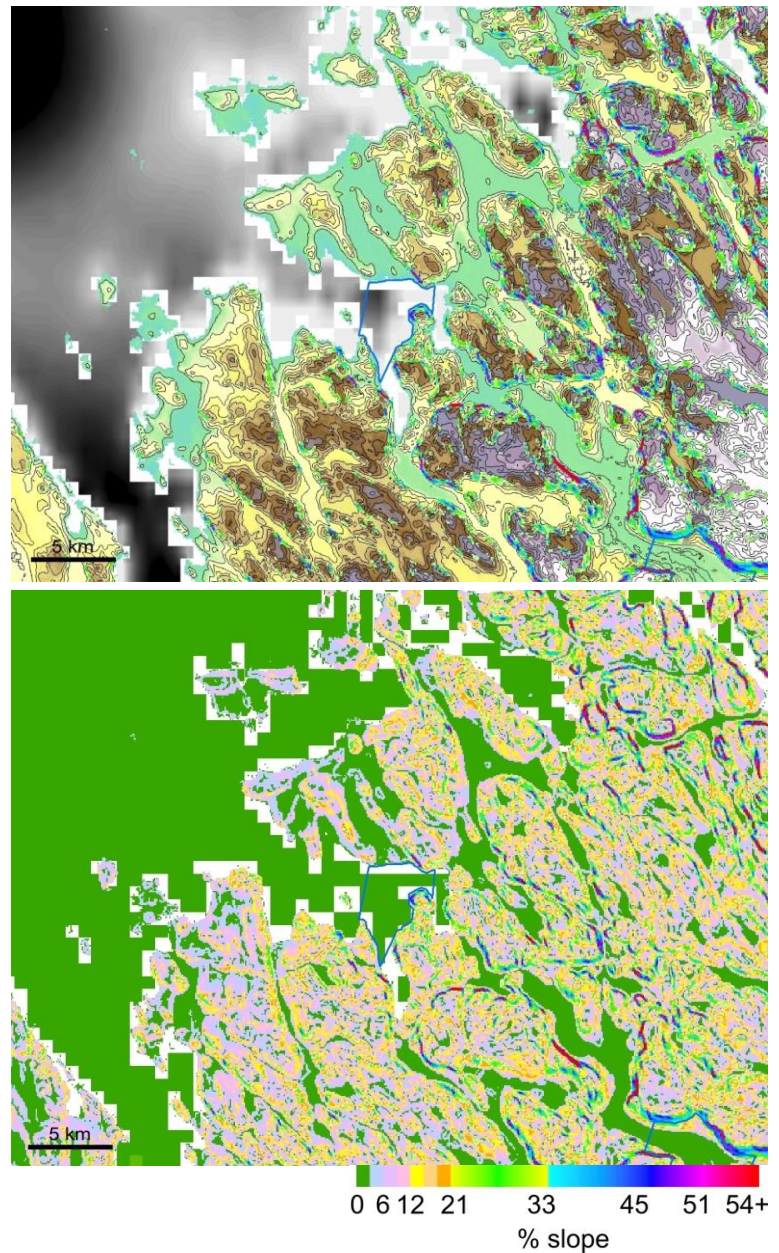


Figure 31. Poorly defined confluences: Glacial erosion.

(Top) An example locality within the Labrador study region, where the landscape has experienced significant areal scouring and selective linear erosion, and/or experienced successive phases of glacial erosion to form a composite erosional landscape (Sugden & John, 1976; Sugden, 1978). In this locality (ll coord 58.7, -66.2 DD), only two confluences can be defined (perimeters shown in blue), as all other potential confluences have been semi-obliterated. There are many other potential confluences. All demonstrate poorly preserved valley longitudinal profiles, and tributaries that are often not independent of one another, up-tributary. Because such confluences cannot be well defined, they have very poor certainty and so are not recorded. (Bottom) The same locality with slope map superimposed. Low slope values are associated with many potential confluences, making them indistinct and therefore of very poor certainty. SRTM3 land topography data are shown in ESRI ArcGIS 'elevation' colour scale. GEBCO bathymetry data are shown in greyscale. SRTM3 and GEBCO derived slope data are shown in a modified ESRI ArcGIS 'aspect' colour scale. SRTM contours are placed at 20 m intervals (black lines).

### 4.3.2 Defining confluence extent (perimeter)

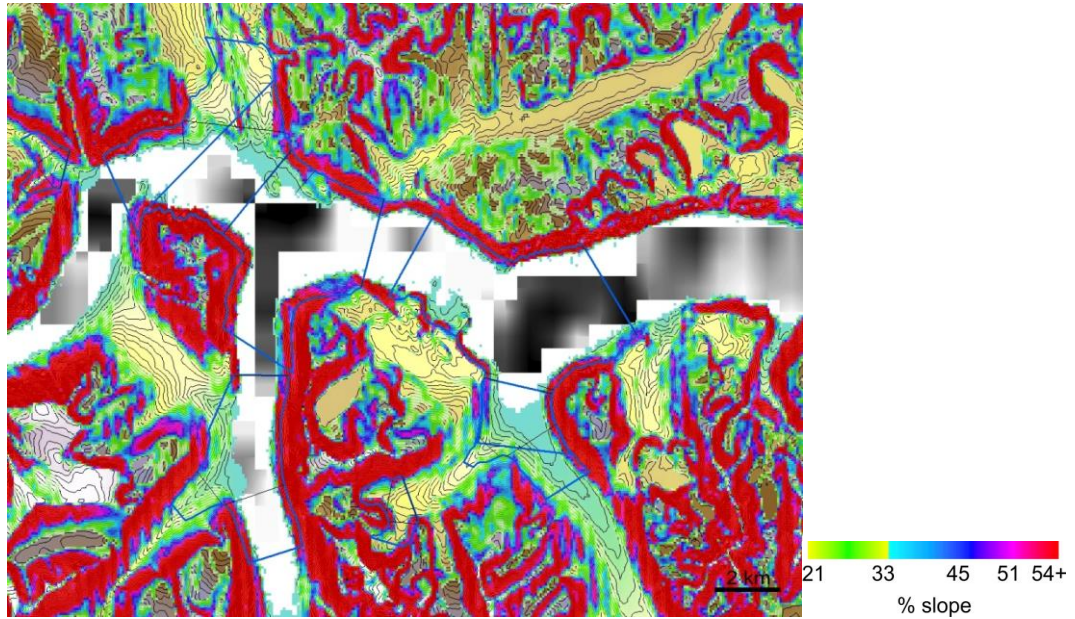
Later on (section 4.5.2), the lateral extent of valleys will be used to calculate CSAs. But what constitutes the edge of a valley? How is it defined? There are likely many different definitions and no 'correct' answer. It is therefore considered important to at least use a consistent method for defining the edge of valleys. Confluences that are identified as valid are manually defined (digitised) in extent using the criteria that follow in this section (see figure 23 for a summary of the main elements of the workflow for confluence identification and definition). In this way, confluences are recorded for subsequent analysis.

The calculation of the slope of a landscape is effective at depicting most terrain features, especially significant features such as valleys. The calculation of slope is computationally inexpensive, is effective at detecting fine scale/ regional relief, and performs well at a variety of scales (Grohmann, et al., 2011). Slope is calculated using the appropriate GIS tool, using the average maximum technique and a 3 x 3 window (ESRI Inc., 2008c).

For any given glacial valley, the slope map of the valley-side is a proxy for glacial erosion of the valley-floor (i.e. higher slope values mean greater glacial erosion). Slope values can therefore be employed as a guide to delineate the outline (or perimeter) of a confluence (figure 32a).

The perimeter of a potential confluence is loosely defined using peak slope values of valley-sides as a guide. A single optimal contour line is then selected (from the 20 m contours of the DEM), which is used to exactly define perimeter. The selected contour line is a 'best-fit' of peak slope values for all valley sides within the confluence (figure 32b). A horizontal glacier top surface is assumed by the use of this method. The contour line is selected for each confluence individually.

a



b

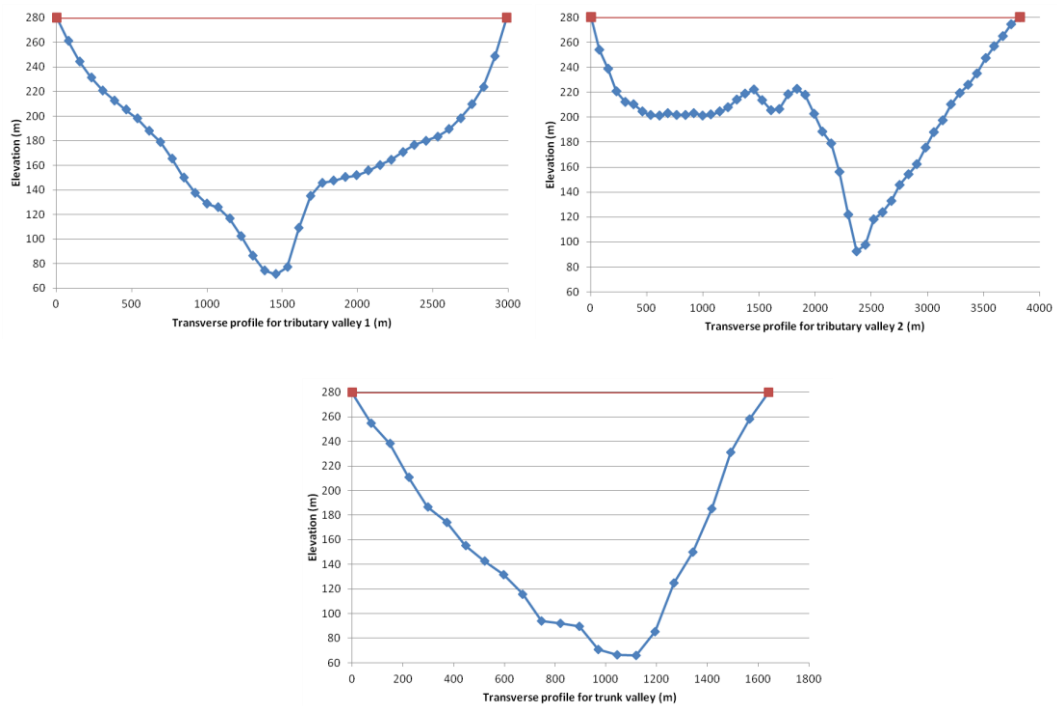


**Figure 32. Defining confluence extent (perimeter).**

(a) DEM of part of the Labrador study region (ll coord 58.9, -64.0 DD), with partial slope map superimposed (i.e. displaying highest percentage slope values only). For any given glacial valley, slope values of the valley-side are a proxy for glacial erosion of the valley-floor. Peak slope values are employed as a guide to define the perimeter of confluences. Perimeter is exactly defined (blue outline) via an optimal ‘best fit’ 20 m contour (see text). SRTM3 land topography data are shown in ESRI ArcGIS ‘elevation’ colour scale. GEBCO bathymetry data are shown in greyscale. SRTM3 derived slope data are shown in a modified ESRI ArcGIS ‘aspect’ colour scale. SRTM contours are placed at 20 m intervals (black lines). (b) Cross-sectional transverse profiles, showing the ‘best-fit’ contour line (280 m a.s.l) across (Top) each tributary and (Bottom) the trunk valley, for an example confluence within the Labrador study region. The selected contour line fits peak slope values for all valley sides within the confluence in question, thereby optimally representing confluence extent.

#### 4.3.2.1 Dealing with 'interrupted' confluence perimeters

Where tributaries other than the major tributary pair (e.g. a minor tributary, or a major tributary belonging to an overlapping confluence) join any part of a potential confluence, the perimeter of the confluence might be interrupted or appear overly crenulated. This is because in these circumstances the best-fit contour line (selected to define perimeter) will deviate away from the confluence along valley-sides of the interrupting tributary. In such circumstances where possible an alternative adjacent contour line is selected to define confluence perimeter (figure 33). Although this measure will usually allow realistic confluence area to be maintained for subsequent analysis, sometimes the interruption or over-crenulation of confluence perimeter cannot be resolved using this method. The alternative perimeter would be so far removed from the best-fit contour line that confluence validity (as assessed using slope map and other confluence identification criteria) would be questionable. In such instances the interrupting tributary is ignored (i.e. bypassed by perimeter) and the perimeter (defined by the best-fit contour line) is retained (figure 33). Where an interrupting tributary is bypassed, confluence perimeter crosses contours at approximately 90° to the tributary valley axis, at the boundary between the tributary and the trunk valley (see section 4.3.3.1 for explanation of tributary valley axis, and tributary-trunk valley boundary).

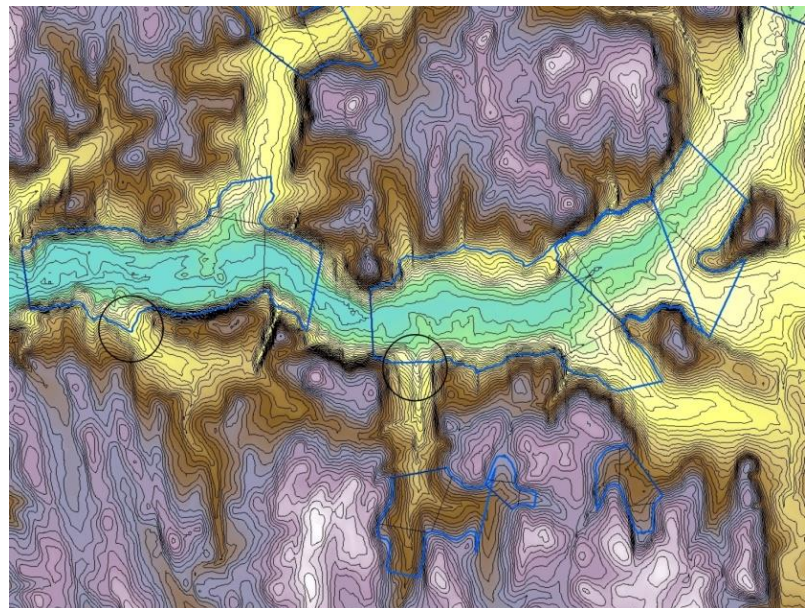


Figure 33. Dealing with 'interrupted' confluence perimeters.

Where a tributary other than the major tributary pair joins any part of a potential confluence, confluence perimeter (blue) is sometimes interrupted or appears overly crenulated. When this scenario arises an alternative adjacent perimeter is selected (left ringed example), thus allowing realistic confluence area to be maintained for subsequent analysis. Sometimes, such problems cannot be resolved using this method (see text). In such instances the interrupting tributary is ignored (i.e. bypassed by perimeter; right ringed example) and the perimeter (defined by the best-fit contour line) is retained. SRTM3 land topography data for Labrador study region (ll coord 58.5, -64.6 DD) are shown in ESRI ArcGIS 'elevation' colour scale. Contours are placed at 20 m intervals (black lines).

The validity of confluence perimeter is further considered in the wider context of the movement of ice through the valley network surrounding the potential confluence. Difffluence should not occur immediately up-tributary of a confluence, at the lateral extent of tributary valleys defined by the best-fit contour line (i.e. confluence perimeter). An alternative adjacent contour line is selected to define perimeter in order to eliminate up-tributary difffluence where possible (figure 34). Where the alternative perimeter is far removed from the best-fit contour line the confluence is invalid. If a valid confluence perimeter cannot be ascertained using this method, where another up-tributary valley is apparent that can provide an alternative and independent source of ice (into one of the major tributaries), a confluence will be valid (but of low certainty) despite the occurrence of difffluence. This is provided that perimeter is not far removed from the best-fit contour line.

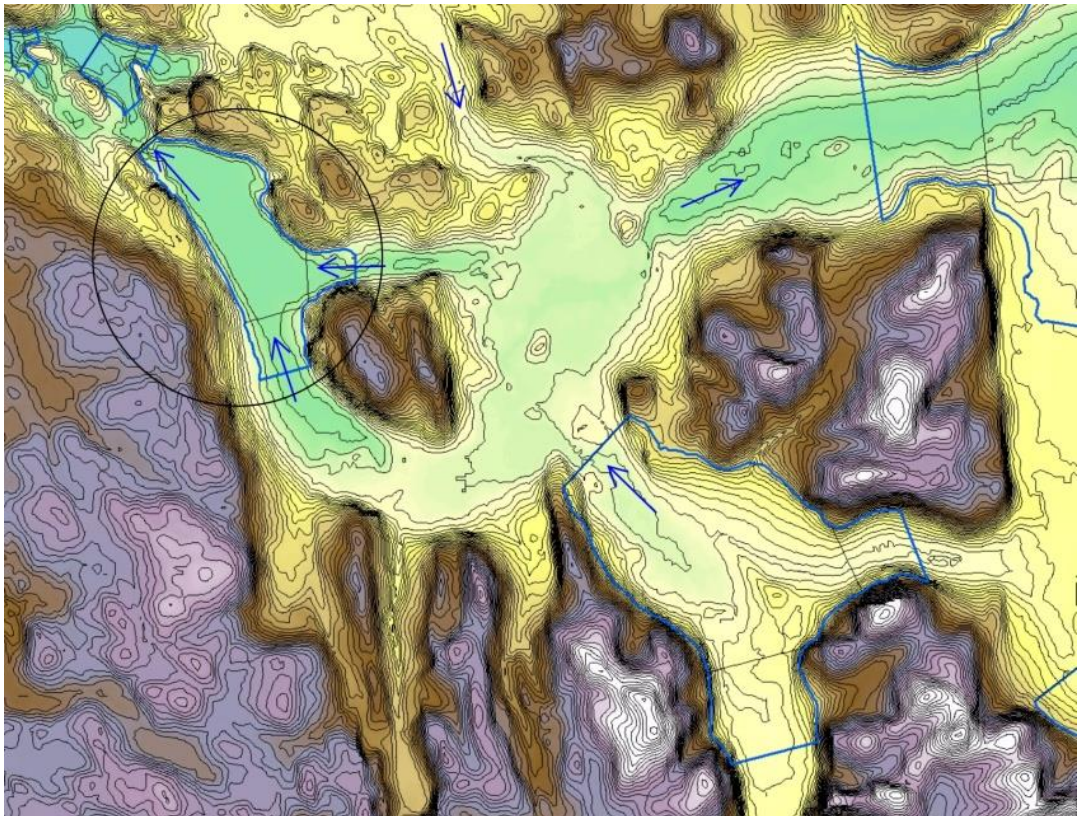


Figure 34. Validity of confluence perimeter, in the context of the surrounding valley network.

Difffluence should not occur immediately up-tributary of a confluence, at the lateral extent of tributary valleys defined by the best-fit contour line (i.e. confluence perimeter). An alternative adjacent contour line is selected to define confluence perimeter in order to eliminate up-tributary difffluence where possible (see text; see ringed example). Glaciation (by warm based ice) has significantly eroded this locality (ll coord 59.6, -65.0 DD). This has most likely removed the topographical divide, which would have once existed at the head of one or both valleys that form the tributary pair in the example confluence. The up-tributary difffluence is a consequence of this erosion. The confluence remains well enough preserved that it can be identified and defined with some confidence, via the criteria. Valley ice flow directions are shown with blue arrows. SRTM3 land topography data for the Labrador study region are shown in ESRI ArcGIS 'elevation' colour scale. Contours are placed at 20 m intervals (black lines).

### 4.3.3 Defining the internal geometry of confluences

It is necessary to identify the transition from the tributary valley into the trunk valley (i.e. a boundary line). This is used in the definition of up-tributary confluence extent (see figure 23 for a summary of the main elements of the workflow for confluence identification and definition). This boundary line also acts as a standardised position where a transverse profile is taken in order to assess down-tributary valley CSA. This contributes towards the assessment of CSA change through a confluence, which in turn allows confluence relationship with overdeepening and overdeepening metrics to be analysed.

#### 4.3.3.1 Defining the tributary-trunk valley boundary (DTT)

The boundary line that denotes the transition between the tributary valley and the trunk valley of a confluence is termed the down-tributary termination (DTT) (figure 35). The DTT is manually positioned at 90° to tributary valley axis, where contour lines (which define confluence perimeter) on each tributary valley-side ultimately diverge (down-tributary, by >45°) relative to each other. The 45° angle is termed the valley-side divergence angle threshold. The DTT will typically occur immediately up-tributary of where a tributary joins with an adjacent tributary and the trunk valley, and where this is visually clearly identifiable at selected confluence extent.

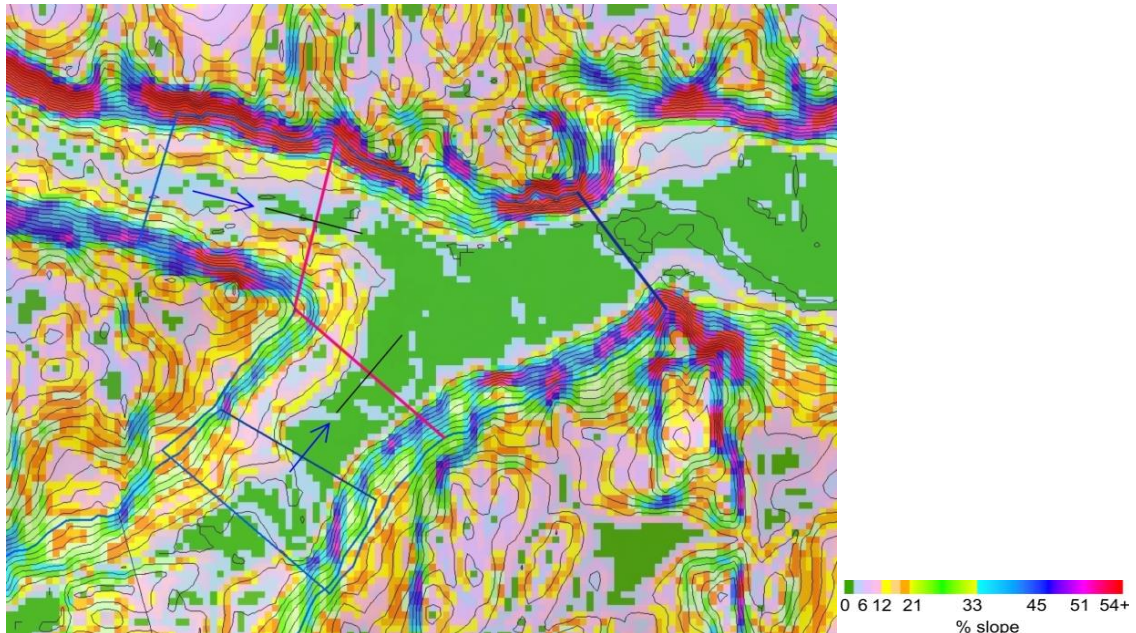


Figure 35. Defining the down-tributary termination (DTT).

The down-tributary termination (DTT; pink) is positioned at 90° to tributary valley axis (thick black line), where contour lines (which define confluence perimeter) on each tributary valley-side ultimately diverge (down-tributary, by >45°) relative to each other. SRTM3 derived slope data for the Labrador study region are shown in a modified ESRI ArcGIS 'aspect' colour scale (ll coord 56.1, -62.9 DD). Confluence perimeters are presented in blue. Ice flow direction is denoted by blue arrows. SRTM contours are placed at 20 m intervals (black lines).

#### 4.3.3.1.1 Defining valley axis

The valley axis is important because it is the trending direction of the course of a valley, and because it is an acceptable proxy for ice flow direction through the valley. Valley axis is defined as the mean trending direction of valley-sides, at selected valley extent (defined by confluence perimeter). Valley axis direction is assessed visually.

For tributary valleys in potential confluences, where the valley is reasonably straight in its down-tributary reach (i.e. the trending direction of valley-sides remains reasonably constant along much of the tributary) a long-term mean trending direction of valley-sides (along down-tributary valley length, to the approximate location of the DTT) is taken as being representative of valley axis at the DTT (figure 36, top). However, for many tributary valleys, the trending direction of valley-sides changes significantly (and sometimes near continuously) along the course of the tributary (i.e. where a valley meanders). In such instances a long-term average cannot represent the valley axis correctly at the DTT. Therefore a much shorter-term mean trending direction (along down-tributary valley length, but only in close proximity to the approximate location of the DTT) is taken as being representative of valley axis at the DTT (figure 36, bottom). Which average is most appropriate for a given tributary is decided by visual assessment.

Occasionally, for some tributary valleys within particular confluence geometries, the trending direction of valley-sides (and, in turn, the direction of the valley axis) will change about the position of the DTT on one flank of the tributary (i.e. on one side of the valley) (figure 37). In this situation, DTT position will have been successfully determined for one flank of the tributary (by the method already defined). However, on the other flank the method will not have been able to absolutely determine DTT position, and the DTT will have a range of potential positions. In such instances, the position of the DTT on the flank where it is known is retained. The position of the DTT on the other flank is sited as far up-tributary as is possible according to the range of potential positions determined by the method. Positioning the DTT in this way most accurately defines the trending direction of valley-sides (and the direction of the valley axis) in the down-tributary reach of a tributary. It also reflects down-tributary valley-width most accurately, for subsequent analysis.

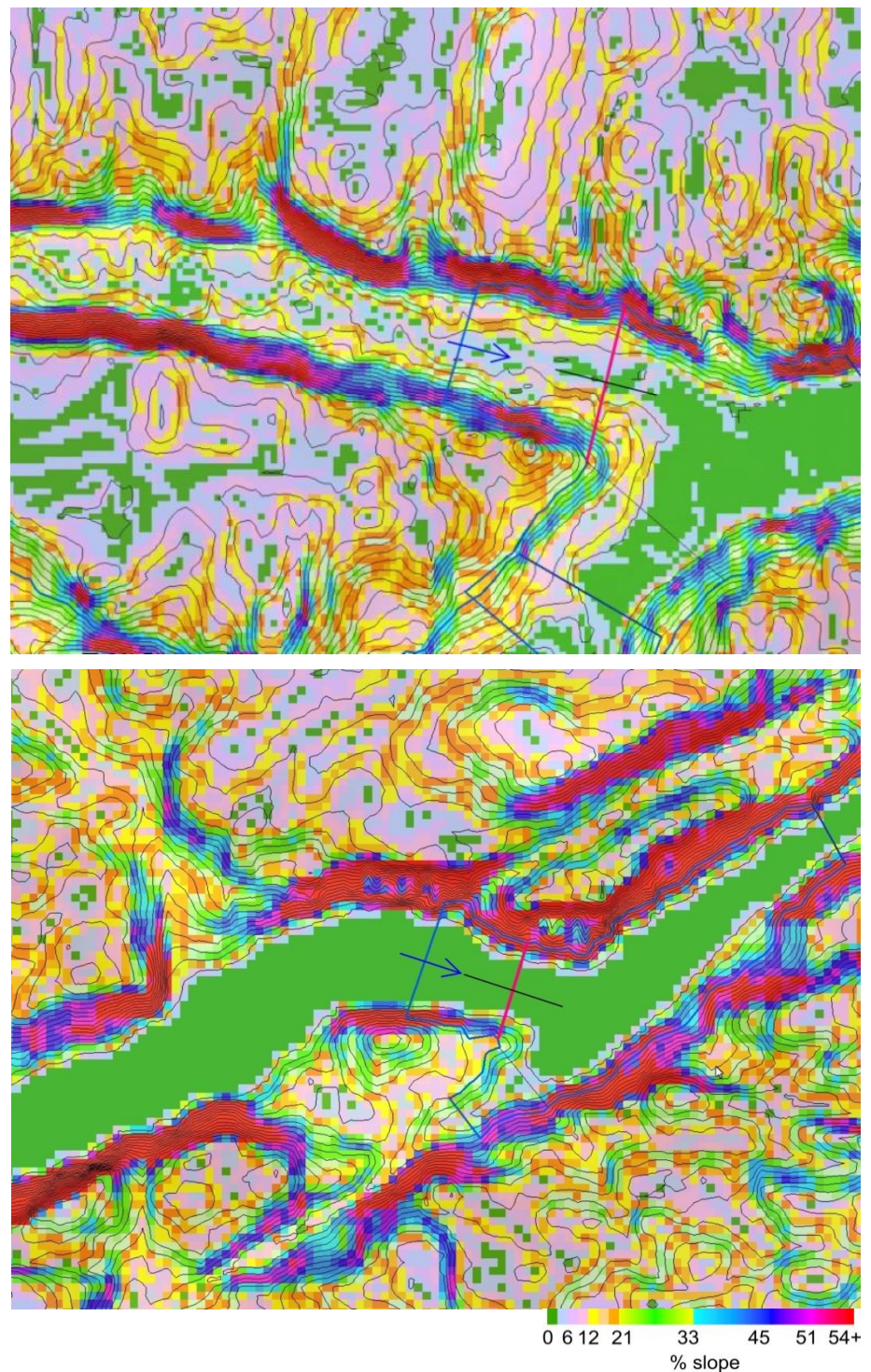


Figure 36. Defining the trending direction of tributary valley-sides in order to define valley axis.

(Top) For tributary valleys in potential confluences, where the valley is reasonably straight in its down-tributary reach a long-term mean trending direction of valley-sides is taken as being representative of valley axis (thick black line) at the DTT (pink; see text) (ll coord 56.1, -63.0 DD). (Bottom) For many tributary valleys, the trending direction of valley-sides changes significantly along the course of the tributary. In such instances a long-term average cannot represent the valley axis correctly at the DTT. Therefore, a much shorter-term mean trending direction of valley-sides is taken as being representative of valley axis at the DTT (see text) (ll coord 55.1, -61.6 DD). SRTM3 derived slope data for the Labrador study region are shown in a modified ESRI ArcGIS 'aspect' colour scale. Confluence perimeters are presented in blue. Ice flow direction is denoted by blue arrows. SRTM contours are placed at 20 m intervals (black lines).

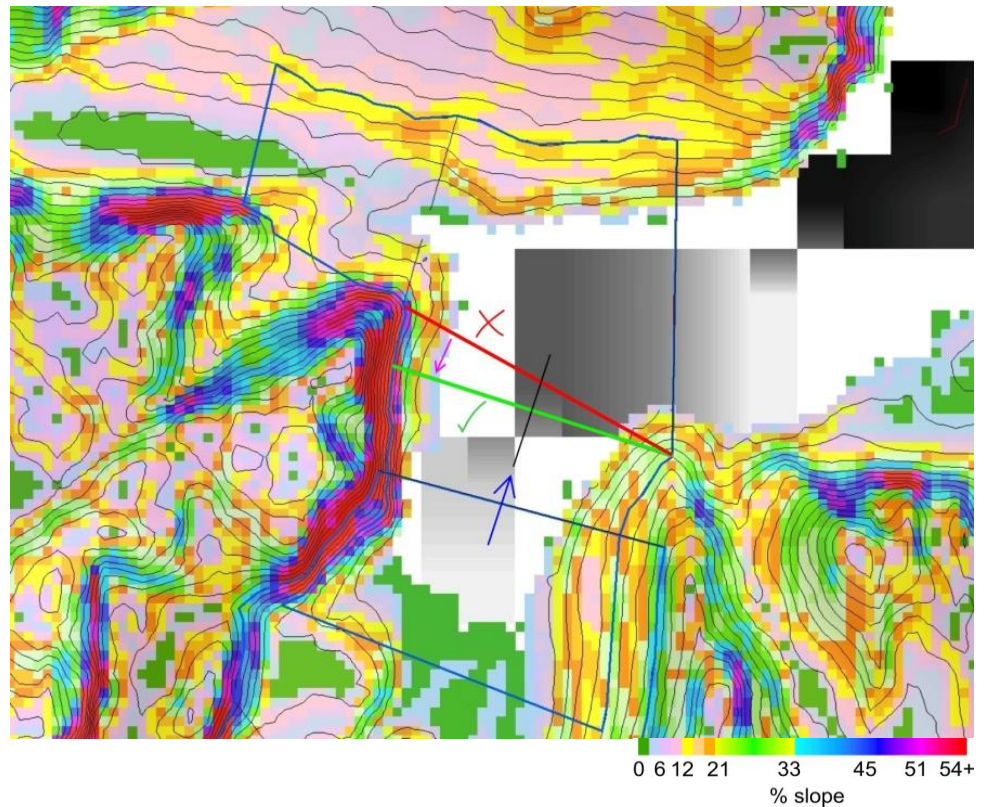


Figure 37. Dealing with change in the trending direction of tributary valley-sides about the position of the DTT on one tributary flank.

Sometimes the trending direction of tributary valley-sides will change about the position of the DTT on one side (flank) of the valley. In this situation, DTT position will have been successfully determined for one flank of the tributary. However, on the other flank of the tributary the method will not have been able to absolutely determine DTT position, and the DTT will have a range of potential positions (potentially resulting in the DTT denoted by the red line). In such instances the position of the DTT on the flank where it is known is retained. The position of the DTT on the other flank is sited as far up-tributary as is possible according to the range of potential positions determined by the method (resulting in the DTT denoted by the green line). Positioning the DTT in this way most accurately defines the trending direction of valley-sides (and the direction of the valley axis, denoted by thick black line) in the down-tributary reach of a tributary. It also reflects down-tributary valley-width most accurately. SRTM3 derived slope data for the Labrador study region are shown in a modified ESRI ArcGIS 'aspect' colour scale (ll coord 57.9, -62.7 DD). GEBCO bathymetry data are shown in greyscale. The confluence perimeter is shown in blue. Tributary ice flow direction is denoted by a blue arrow. SRTM contours are placed at 20 m intervals (black lines).

Occasionally, non-glacial processes operating on the valley-sides of a tributary at very local scales can make the trending direction of valley-sides difficult to identify (i.e. contours appear very irregular). In turn, this makes it difficult to accurately identify the valley axis of a tributary. In such instances an alternative adjacent contour line is selected to define confluence perimeter (figure 38). Selecting the alternative perimeter increases overall confidence in the confluence because there is better certainty to confluence internal geometry. Valley axis is more accurately identified, and the position of the DTT is properly determined. If irregular contours occur at all

alternative perimeters or if the nearest (regular) perimeter is far removed from the best-fit contour line (so that confluence validity is questionable) then the mean trending direction of multiple adjacent contour lines are used to assess trending direction, and the rest of this modification to the rule is not applied.

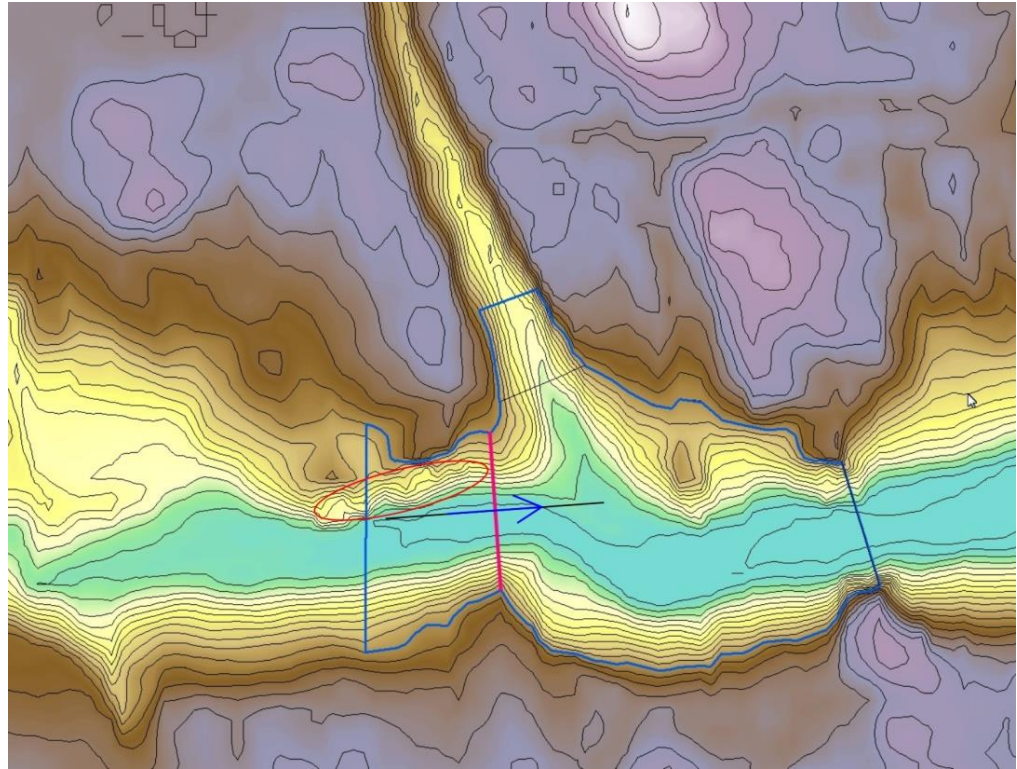


Figure 38. Identifying the trending direction of tributary valley-sides where irregular.

Non-glacial processes operating on the valley-sides of a tributary at very local scales can make the trending direction of valley-sides difficult to identify (i.e. contours appear very irregular, ringed). This makes it difficult to accurately identify valley axis. In such instances an alternative adjacent contour line (blue) is selected to define confluence perimeter. Selecting the alternative perimeter increases overall confidence in the confluence because valley axis (thick black line) is more accurately identified, and the position of the DTT (pink) is properly determined. SRTM3 land topography data for the Labrador study region are shown in ESRI ArcGIS 'elevation' colour scale (ll coord 56.5, -63.2 DD). Tributary ice flow direction is denoted by a blue arrow. SRTM contours are placed at 20 m intervals (black lines).

#### 4.3.3.1.2 Valley-side divergence angle

The valley-side divergence angle threshold of 45° has been chosen to define DTT positions, partly because of its visual simplicity when manually measuring and assessing many hundreds of potential confluences.

The 45° divergence threshold has also been chosen because it is large enough to commonly visually pre-empt (i.e. to occur immediately up-tributary of) where a tributary joins (visibly, at selected confluence extent) with an adjacent tributary and the trunk valley, within a confluence. For explanation of the geometrical reasons for this please refer to the Appendix. The position of the DTT is consequently well suited to indicate the transition from the tributary valley into the trunk valley. The 45° angle is smaller than the minimum angle possible when calculating the true geometrical boundary between a tributary and trunk valley. This minimum angle might best be termed the minimum *absolute* valley-side divergence angle, and is used to define the *absolute* down-tributary termination (ADTT) geometrically and definitively. The method to determine ADTTs is complex and so has not been used in this investigation (see Appendix for further explanation regarding these concepts).

Further to the above, the 45° valley-side divergence angle threshold is large enough that DTTs are placed sufficiently down-tributary so as to avoid measuring unrepresentative valley-width and CSA measurements which might be observed in the up-tributary extent of confluences. In the up-tributary reach of tributaries, and often in the up-tributary extent of confluences, valley-width (and consequently CSA) is commonly not the same as that observed in the down-tributary reach of a tributary, especially near to the DTT within a confluence. It is therefore important that a representative, reliable and repeatable method is used to position DTTs, so that valley-width and CSA in the down-tributary reach of tributaries within confluences are accurately defined.

As a consequence of employing a 45° valley-side divergence angle, DTTs are near optimally positioned to indicate the transition from the tributary valley into the trunk valley within each confluence, and to also provide a representative measure of valley-width (and CSA), within the down-tributary reach of a tributary within a confluence. This would almost certainly not be the case if a different divergence angle threshold were utilised, resulting in DTTs being placed further upstream or downstream within confluences.

#### 4.3.3.1.3 Maintaining realistic internal confluence geometry

This investigation defines confluence first and foremost by a confluence perimeter criterion which (necessarily) ignores/ bypasses tributaries that interrupt the perimeter (e.g. minor tributaries and/or tributaries belonging to overlapping confluences) in order to define a contiguous confluence. However, in order to define other aspects of a confluence, a partly contrary rule is required. When determining DTT position (for a given tributary valley within a confluence) it is important that interrupting tributaries are not ignored in order to maintain realistic internal confluence geometry and so to have satisfactory confidence in confluence up-tributary extent and valley-width and CSA measurements. Consequently, DTTs are always positioned so as to not be coincident with interrupting tributaries (figure 39). Where coincidence occurs, a DTT is re-positioned as far up-tributary as is necessary in order to avoid such coincidence. The new DTT position otherwise adheres to the DTT positioning method.

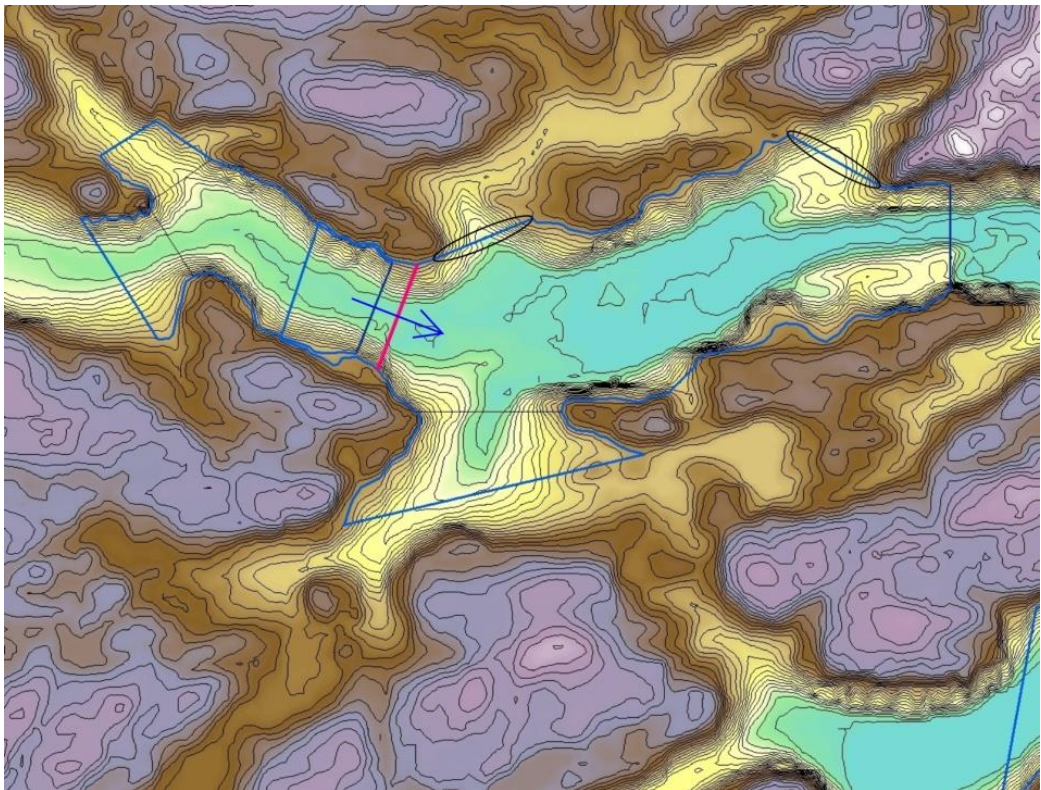


Figure 39. Maintaining realistic internal confluence geometry.

When determining DTT position it is important that interrupting tributaries (a minor tributary in this example, ringed) are not ignored (see text). Where the position of a DTT is coincident with an interrupting tributary, the DTT is re-positioned (pink) as far up-tributary as is necessary in order to avoid such coincidence. The new DTT position still otherwise adheres to the DTT positioning method. SRTM3 land topography data for the Labrador study region are shown in ESRI ArcGIS 'elevation' colour scale (ll coord 57.4, -63.2 DD). Confluence perimeters are presented in blue. Tributary ice flow direction is denoted by a blue arrow. SRTM contours are placed at 20 m intervals (black lines).

#### 4.3.4 Defining confluence extent (up-tributary valley)

Up-tributary valley confluence extent is defined by a boundary line which is termed the up-tributary termination (UTT; figure 40; see figure 23 for a summary of the main elements of the workflow for confluence identification and definition). This is manually placed one tributary width up-tributary from the DTT. Tributary valley-width is measured at the DTT. The distance upstream is measured along each valley-side, along the contour line that defines confluence perimeter.

The UTT is placed one tributary width upstream from the DTT, for the reason that horizontal ice surface velocity data from field studies, numerically modelled vertical ice velocity calculations (verified by the use of field data) and remote sensed ice surface velocity observations (Gudmundsson, et al., 1997; Berthier, et al., 2003; Gudmundsson, 1999; Byrd Polar Research Center, Remote Sensing Laboratory, 2001a) indicate that confluence (i.e. channel constriction) has an influence on ice flow for some distance up-tributary (figure 41). Findings are supported by initial empirical observations of up-tributary overdeepening associations with confluence, in DEMs employed in this study. Confluence influence on ice flow therefore provides the potential for overdeepening initiation up-tributary. Ice velocity measurements (Gudmundsson, et al., 1997; Berthier, et al., 2003; Gudmundsson, 1999; Byrd Polar Research Center, Remote Sensing Laboratory, 2001a) also indicate that confluence is not a significant control on ice flow at more than one tributary width up-tributary from the DTT (figure 41). Further observations made during visual inspection of DEMs used in this study support this finding. Confluences are too far removed to have a significant effect on ice flow in localities situated two or more tributary widths up-tributary from a DTT (figure 40). Consequently at such localities confluence cannot influence overdeepening initiation, and presumably other controls dominate.

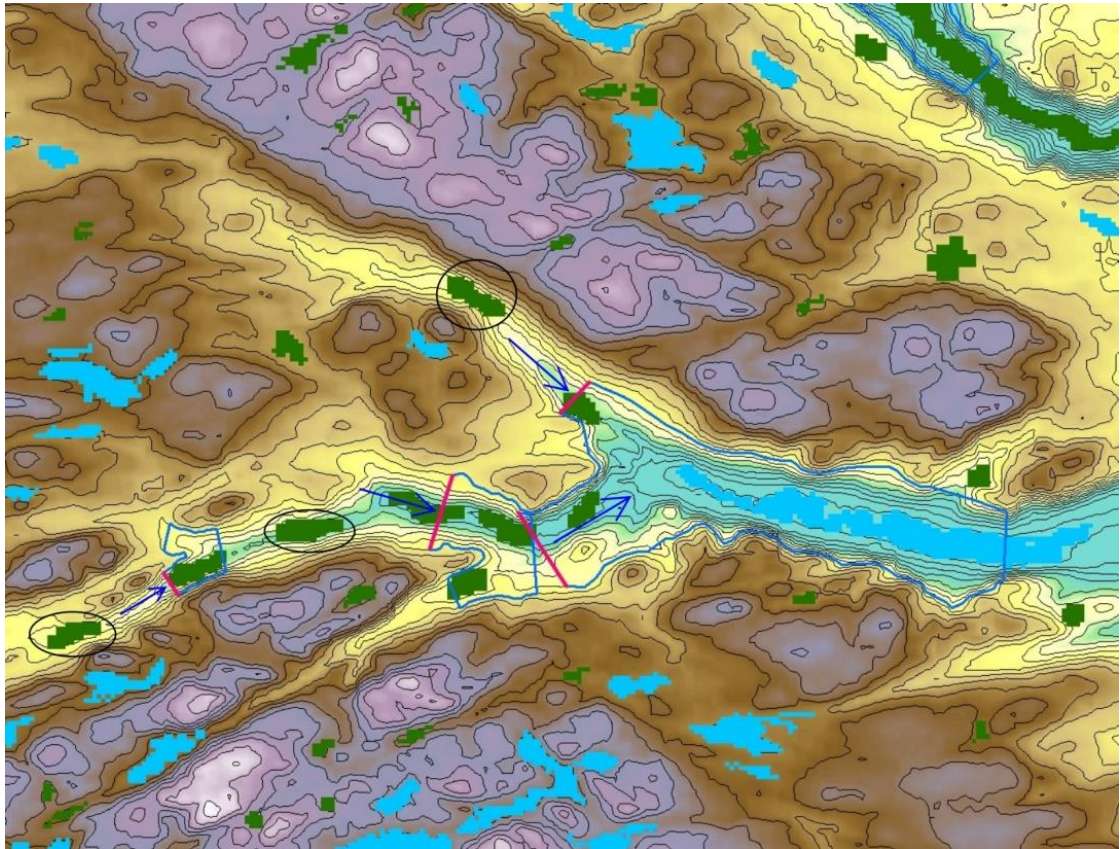


**Figure 40. Defining the up-tributary termination (UTT).**

The up-tributary termination (UTT, pink) of a confluence (denoted by blue perimeter) is placed one tributary width up-tributary from the DTT (see text). Empty/ partially sediment filled overdeepenings are depicted in dark green. Water filled overdeepenings are shown in light blue. Overdeepenings (ringed) that are situated two or more tributary widths up-tributary from a DTT are undoubtedly too far removed to be affected by change in ice flow resulting from the influence of confluence. Consequently overdeepening initiation cannot be influenced by confluence in such locations. SRTM3 land topography data for the Labrador study region are shown in ESRI ArcGIS 'elevation' colour scale (ll coord 53.3, -61.2 DD). Ice flow direction is denoted by blue arrows. SRTM contours are placed at 20 m intervals (black lines).

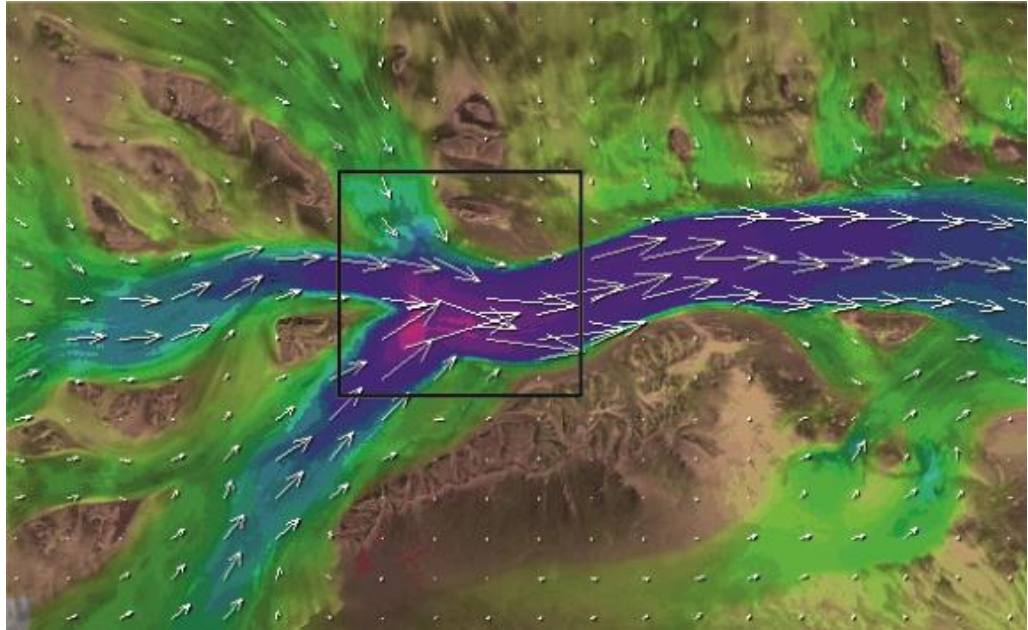


**Figure 41. Surface ice velocity vectors for the Lambert Glacier, Antarctica.**

Vectors acquired from RadarSat SAR imagery (Byrd Polar Research Center, Remote Sensing Laboratory, 2001a). The areas of no motion (yellow) are either exposed land or stationary ice. The smaller confluent glaciers have generally low velocities (100-300 m per year, green) which gradually increase as they flow down the rapidly changing continental slope into the upper reaches of the faster flowing Lambert Glacier. Most of the Lambert Glacier has velocities between 400-800 m per year (blues) (Byrd Polar Research Center, Remote Sensing Laboratory, 2001b). This example demonstrates that glacial confluence has an influence on ice flow for some distance up-tributary; a significant localised increase in ice flow velocity (900-1,000 m per year, pinks) can be seen at the junction of the Lambert, Mellor and Fisher Glaciers (boxed). Further, the ice velocity map shows that glacial confluence is not a significant control on ice flow at more than approximately one tributary width (as measured at DTT) upstream from the estimated location of DTTs within the confluence.

In some confluences, up-tributary perimeter is not visually well constrained (bounded) by topography (contour lines) at furthest up-tributary end. This situation arises where the tributary is immediately downstream of a plateau (for example). In this scenario, confluence area is significantly truncated (i.e. confluence appears ‘squashed’ up-tributary) and/or confluence perimeter is not valid (i.e. the perimeter crosses itself up-tributary, and thus appears unnatural) (figure 42). For such confluences, where possible an alternative adjacent contour line is selected to define perimeter, in order to increase confidence in the confluence. Usually however, there is no alternative perimeter that will remove up-tributary area truncation and/or perimeter invalidity, without the alternative being so far removed from the best-fit contour line that confluence validity becomes questionable. In such circumstances an additional criterion is implemented. Up-tributary of the position where perimeter is not well constrained, the perimeter is instead defined by a straight line that runs parallel to tributary valley axis at the furthest position up-tributary where the valley is well constrained. The straight line defines perimeter until the appropriate distance up-tributary (i.e. one valley-width, as measured at DTT) has been

measured to the UTT. The furthest position up-tributary where a valley is well constrained, is defined by where valley-side contour lines ultimately diverge (upstream, by  $\geq 90^\circ$ ) relative to each other.

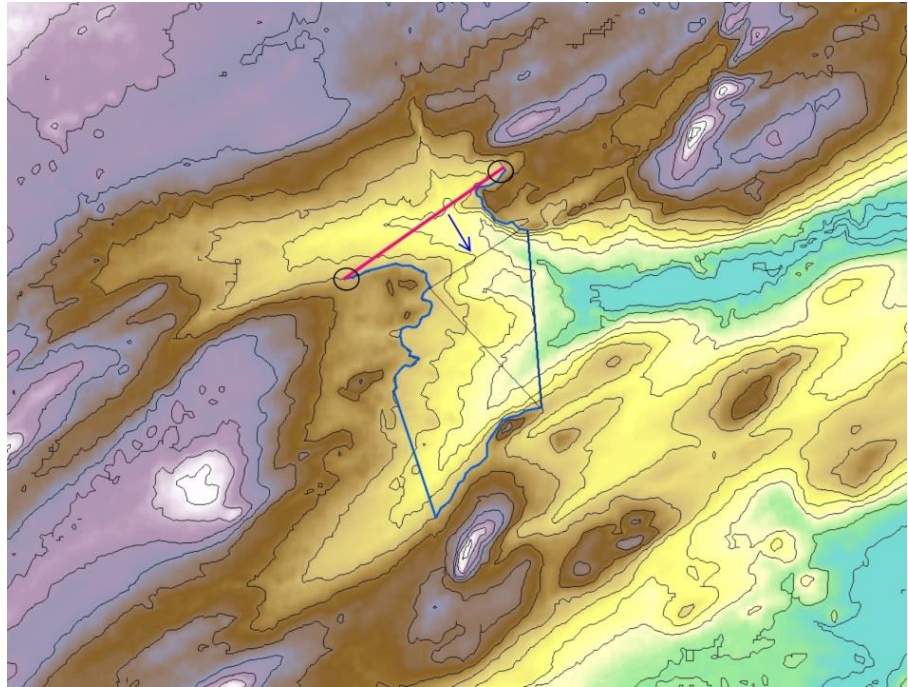


**Figure 42. Dealing with problems that arise where UTT is not well constrained by topography.**

**This example of confluence (blue perimeter) demonstrates some lack of constraint by topography, up-tributary (ringed locations). Consequently the confluence displays minor up-tributary area truncation and demonstrates how up-tributary perimeter may cross itself where lack of constraint is more severe. In this example the confluence remains viable, and so implementation of the criterion (see text) to deal with this problem is not necessary. SRTM3 land topography data for the Labrador study region are shown in ESRI ArcGIS 'elevation' colour scale (ll coord 54.3, -58.9 DD). The UTT is shown in pink. The DTT is denoted by a thin black line. Tributary ice flow direction is denoted by a blue arrow. SRTM contours are placed at 20 m intervals (thick black lines).**

In some smaller confluences the up-tributary end of a confluence may occur closer than one tributary width up-tributary from the DTT, at selected confluence extent. In this circumstance the contour lines which define each valley-side of a tributary will join together at furthest up-tributary end. In such instances the UTT is positioned as far up-tributary as possible (figure 43).

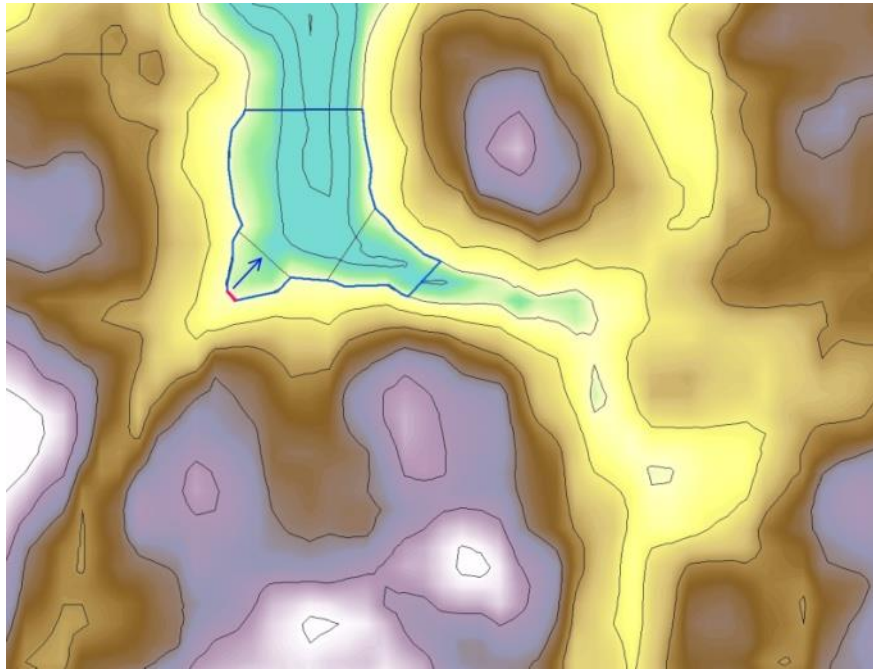


**Figure 43. Dealing with the scenario where the up-tributary end of a confluence occurs close to the DTT.**

**In this example (ll coord 53.1, -60.8 DD), the up-tributary end of a confluence (confluence denoted by blue perimeter) occurs closer than one tributary width up-tributary from the DTT (thin black line). Consequently the UTT (pink) has been positioned as far up-tributary as possible. SRTM3 land topography data for the Labrador study region are shown in ESRI ArcGIS 'elevation' colour scale. Tributary ice flow direction is denoted by a blue arrow. SRTM contours are placed at 20 m intervals (thick black lines).**

#### 4.3.5 Defining confluence extent (down-trunk valley)

Down-trunk valley confluence extent is defined by a boundary line which is termed the down-trunk termination (figure 44, see figure 23 for a summary of the main elements of the workflow for confluence identification and definition). This is manually placed at 90° to trunk valley axis at the position where a ‘pinch’ (constriction) is visible in the confluence trunk valley, at selected confluence extent.

The down-trunk termination acts as a standardised position where a transverse profile is taken in order to provide a representative measure of down-trunk valley width and CSA. This contributes towards the assessment of CSA change through a confluence, which in turn allows confluence relationship with overdeepening and overdeepening metrics to be analysed.

An effective decrease in channel CSA is typically observed through glacial valley confluences as tributaries join the trunk valley. This most often manifests itself visually as a pinch (constriction) at the downstream end of the confluence in the trunk valley. It can be reasoned that glacial erosion, within glacial valley confluences, works to balance the sum of tributary channel CSAs with trunk channel CSA (i.e. confluence allometry may naturally reach an equilibrium steady-state in which ice speed up will no longer occur). However, from visual analysis of landscapes I suggest that valley confluences seldom reach this state over glacial timescales (most probably because the process is self-limiting), and that the pinch feature of glacial trunk valleys (within confluences) is the result of this (figure 44, top; see later for further discussion of this phenomena).

The pinch feature is commonplace within most examples of confluence, although sometimes it is not so clearly apparent. In such instances the down-trunk termination is placed at the most upstream position where trunk valley-width is observed to be relatively uniform, as this is a suitable approximation for where the pinch is usually observed (figure 44, bottom). Upstream trunk valley-width can be highly variable, in contrast to downstream trunk valley-width, and so assessment of the uniformity of trunk valley-width is straight-forward.

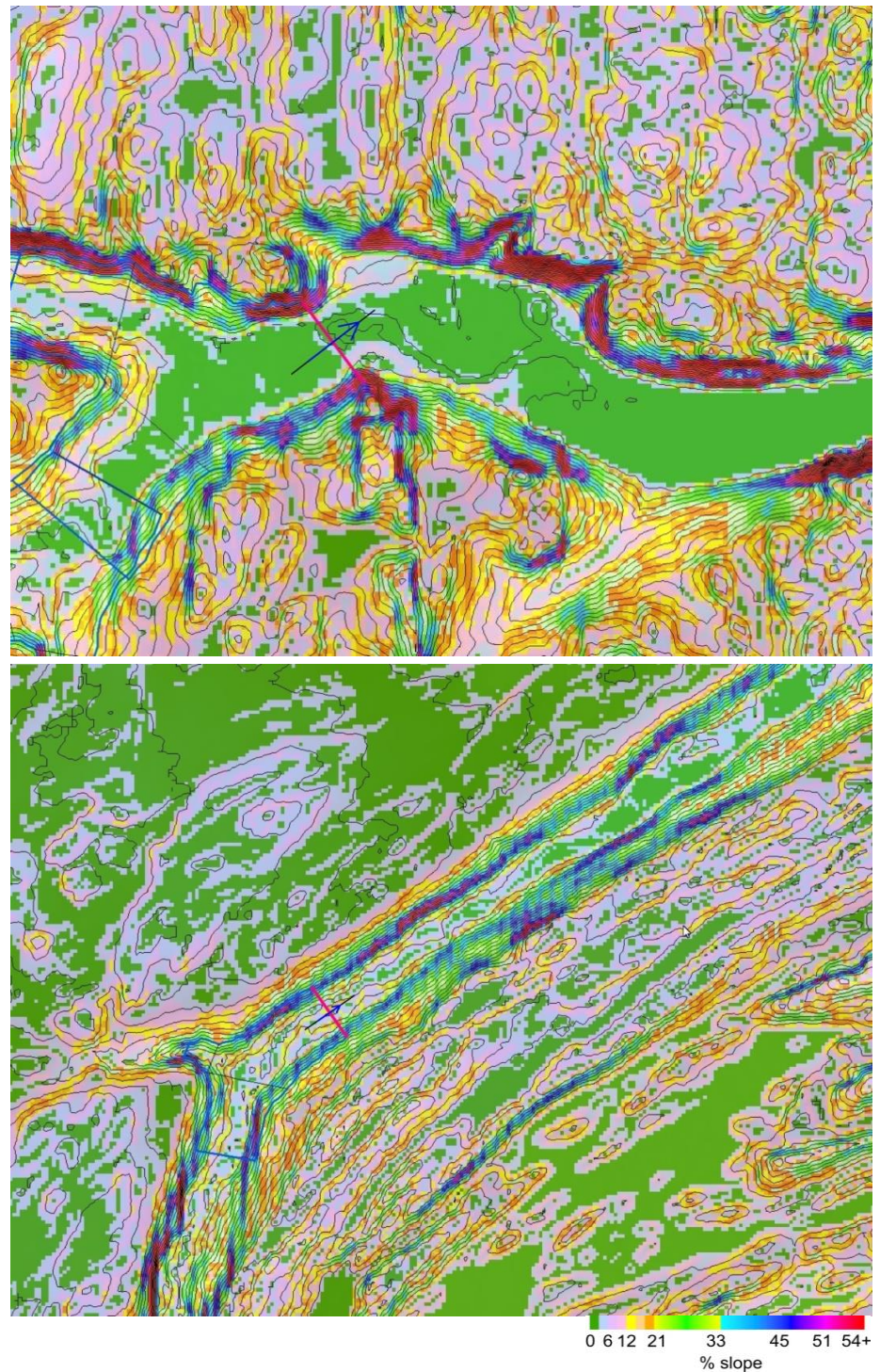


**Figure 44. Defining the down-trunk termination.**

(Top) The down-trunk termination (pink) is placed at 90° to trunk valley axis (thick black line) at the position where a ‘pinch’ (constriction) is visible in the confluence trunk valley, at selected confluence extent (blue perimeter; see text) (ll coord 56.1, -62.9 DD). (Bottom) The pinch feature is not clearly apparent in this confluence. Hence the down-trunk termination is placed at the most upstream position where trunk valley-width is observed to be relatively uniform, as this is a suitable approximation for where the pinch is usually observed (see text) (ll coord 54.4, -62.5 DD). SRTM3 derived slope data for the Labrador study region are shown in a modified ESRI ArcGIS ‘aspect’ colour scale. Ice flow direction is denoted by blue arrows. SRTM contours are placed at 20 m intervals (black lines).

The valley axis of the downstream end of a trunk valley is defined by the mean trending direction of valley-sides at the location of the pinch feature, at selected confluence extent (figure 45, top). If pinch position is unclear then a short term mean trending direction, around the locality where pinch is to be placed (i.e. where valley-width is relatively uniform), is used to fix pinch position exactly (figure 45, bottom). This average is visually assessed.

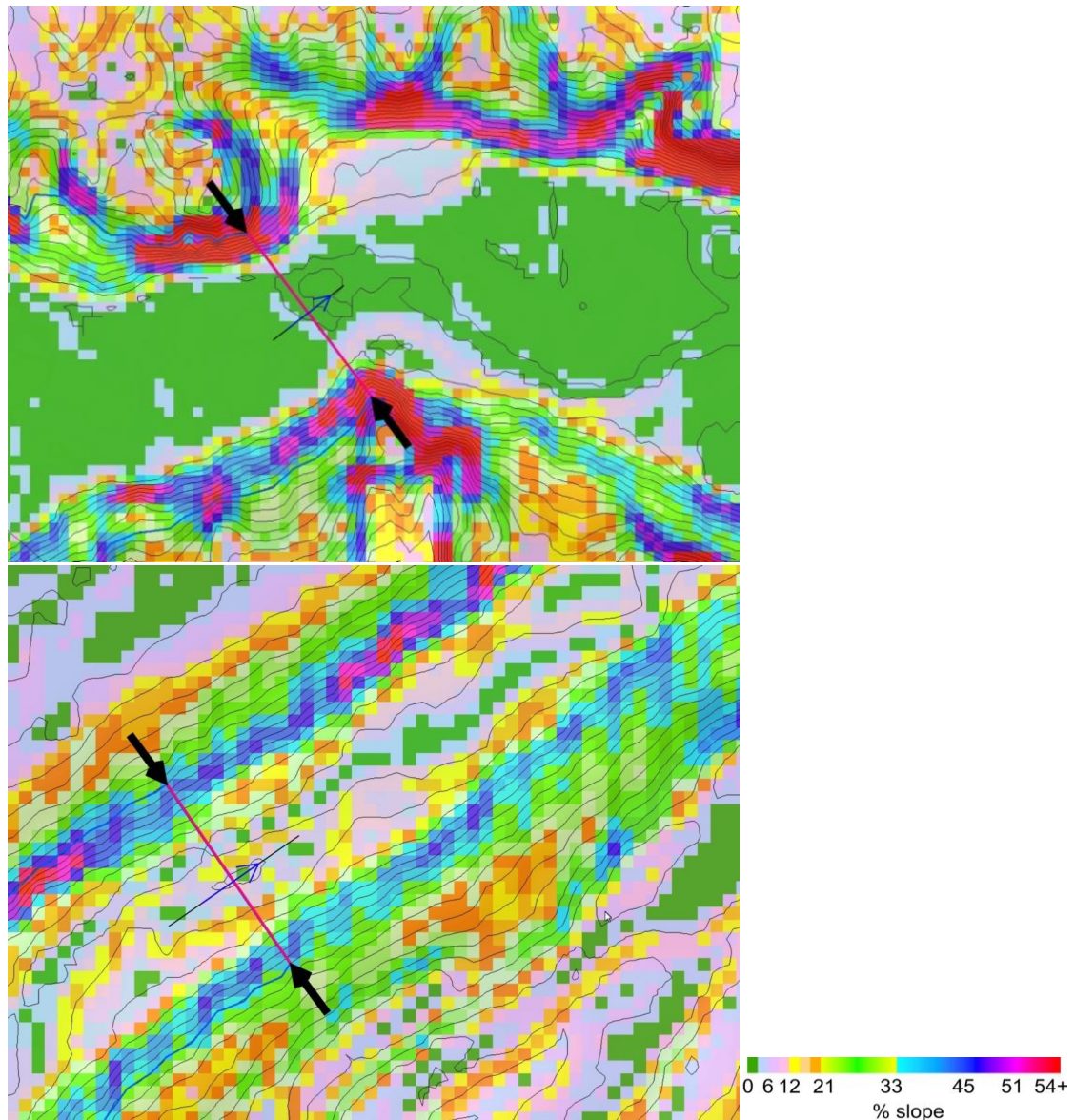


Figure 45. Defining the trending direction of trunk valley-sides in order to define valley axis.

(Top) The valley axis (thick black line) of the downstream end of a trunk valley is defined by the mean trending direction of valley-sides at the location of the pinch feature (pink, emphasised by black arrows), at selected confluence extent (blue perimeter) (ll coord 56.1, -62.8 DD). (Bottom) Pinch position is unclear in this example. Hence a short term mean trending direction of valley-sides, around the locality where pinch is to be placed, is used to fix pinch position exactly (ll coord 54.5, -62.4 DD). SRTM3 derived slope data for the Labrador study region are shown in a modified ESRI ArcGIS ‘aspect’ colour scale. Ice flow direction is denoted by blue arrows. SRTM contours are placed at 20 m intervals (black lines).

#### 4.3.6 Defining further 'liberal' down-trunk terminations

Two datasets have been created, containing the confluence data. These allow the evaluation of how co-location relationships between confluence and overdeepening are affected by the use of a conservative, and a more liberal definition of down-trunk termination. This is necessary because there is some uncertainty in defining confluence extent. Hence varying downstream confluence extent allows differences in analysis to be assessed. The first dataset contains confluences as defined using the identification and definition criteria detailed previously in section 4.3. These are termed 'conservative' confluences. The second dataset contains the same confluences, but extended downstream (from conservative down-trunk termination) by trunk valley-width at the conservative down-trunk termination (figure 46). These are termed 'liberal' confluences. The downstream extension is measured along contour lines on each valley-side, at selected confluence extent (see figure 23 for a summary of the main elements of the workflow for confluence identification and definition). The use of conservative and liberal datasets to evaluate confluence extent is a form of landform identification (see section 4.3.1).

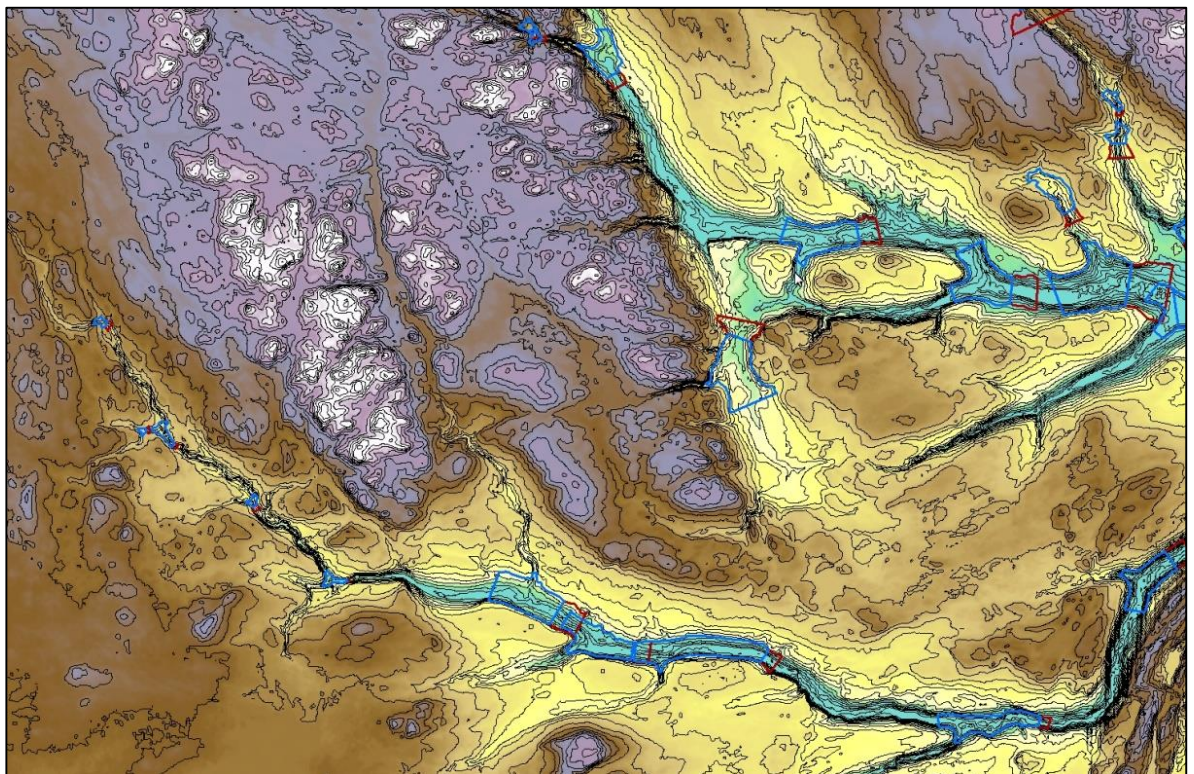


Figure 46. Defining 'conservative' and 'liberal' down-trunk terminations.

Example conservative confluences (blue perimeter), as defined using the identification and definition criteria, showing corresponding liberal downstream extensions (dark red perimeter). These allow evaluation of how co-location relationships between confluence and overdeepening are affected by the use of a conservative, and a more liberal definition of downstream confluence extent (see text). Liberal confluences are extended downstream (from the conservative down-trunk termination) by trunk valley-width at the conservative down-trunk termination. The DEM is SRTM3 topography data (ll coord 54.4, -63.5 DD), for the Labrador study region, depicted using ESRI ArcGIS 'elevation' colour scale. Contours are placed at 20 m intervals (black lines).

The criteria used to identify and define liberal confluence perimeters are the same as those applied to conservative perimeters. However, in some confluences, liberal perimeter (in the downstream extension) is not visually well constrained (bounded) by topography (contour lines) at furthest down-trunk end. This situation arises where the trunk is immediately upstream of a plain (for example). Confluence area will appear significantly truncated (i.e. confluence appears 'squashed' downstream) and/or confluence perimeter will not be valid (i.e. perimeter crosses itself, and thus appears unnatural downstream). In such circumstances (similar to those previously discussed for some up-tributary confluence perimeters) an additional criterion is applied. Down-trunk of where perimeter is no longer well constrained, the perimeter is instead defined by a straight line that runs parallel to valley axis at the conservative down-trunk termination. The straight line defines perimeter until the appropriate distance down-trunk (i.e. one valley-width, as measured at the conservative down-trunk termination) has been measured to liberal down-trunk termination (figure 47). The furthest down-trunk position where a liberal confluence extension is well constrained is defined by where valley-side contour lines ultimately diverge (downstream, by  $\geq 90^\circ$ ) relative to each other.

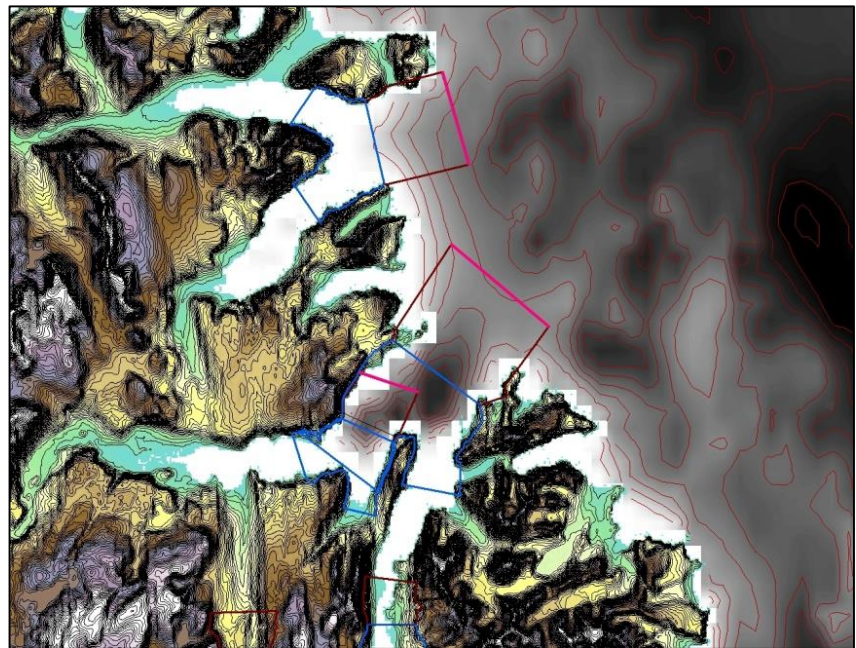


Figure 47. Dealing with problems that arise where the liberal perimeter is not well constrained by topography.

Examples of confluence where the liberal perimeter (in the downstream extension; dark red) is not visually well constrained (bounded) by topography (valley-side contour lines) at furthest down-trunk end (see text). Down-trunk of where perimeter is no longer well constrained, the perimeter is instead defined by a straight line that runs parallel to valley axis at the conservative down-trunk termination. The straight line defines perimeter until the appropriate distance down-trunk has been measured to liberal down-trunk termination (pink line). The DEMs utilised are SRTM3 topography data and GEBCO bathymetry data for the Labrador study region, depicted using ESRI ArcGIS 'elevation' colour scale and greyscale respectively (ll coord 58.8, -63.5 DD). Conservative confluence perimeters and conservative down-trunk terminations are shown in blue. Contours are placed at 20 m intervals (SRTM, black lines; GEBCO, red lines).

## **4.4 Sensitivity testing in order to justify parameter choices**

Various parameter choices have been outlined throughout the method in order to define overdeepenings (section 4.2) and confluences (section 4.3). Consideration is given here to the sensitivity of research outcomes to such parameter choices. Some parameters are considered to be insensitive and fixed, whilst others require more formal sensitivity testing to explore the effect they have. Both cases are discussed below. The discussion, and outcomes of sensitivity testing (section 5.1), show that there is no cause for concern regarding the issue of sensitivity in this investigation. Research outcome sensitivity to operator variability in parameter choices is acceptable.

### **4.4.1 Dataset visualisation parameters**

The DEMs and datasets used are of much higher resolution than the scale of valleys investigated, and are thus deemed to be of sufficient resolution for investigating the landforms (i.e. confluences and overdeepenings; see section 4.1). No sensitivity testing for grid size was thus performed. Elevation data is presented for visual analysis, within 2 standard deviations of the mean elevation value for any given display extent. This enables optimal visualisation of detail at any given scale of observation and therefore facilitates identification of the maximum possible number of confluences and overdeepenings.

### **4.4.2 Overdeepening parameters**

The justification for selecting threshold parameters for removing small artefacts and errors from sink data are discussed in detail in section 4.2.3 and so are not considered further here.

#### *4.4.2.1 Topographically low lying overdeepenings (regional study)*

When defining topographically low lying overdeepenings within the sink data, a low pass 3x3 filter is utilised in a single pass to 'grow' overdeepening area (see section 4.2.5). This parameter choice has been made because it is the minimum amount of processing and smallest window size that can be applied to the data in order that overdeepenings appear more contiguous in appearance. Such filtering is necessary in low lying valleys, where overdeepenings are affected by superficial glacio-fluvial deposits and/or colonisation by vegetation, but has been used sparingly. A single pass 3x3 window is the only option, for this parameter, that produces overdeepenings of realistic scale relative to valley size. All other possible parameter choices (i.e 5x5, 7x7, double pass, triple pass, etc) are found to produce overdeepenings that are too large.

An elevation threshold value of 345 m a.s.l was selected to define topographically low lying areas where it is expected that overdeepenings will be particularly affected by sediment deposition and vegetation (section 4.2.5). The threshold is effective at identifying the major coastal valley networks and other topographically low lying areas that occur within Labrador, bearing in mind that the purpose of the threshold is to identify overdeepenings associated with, rather than to definitively define such valleys. The threshold is effective as a consequence of the well-defined natural break in topography (i.e. the fjords) which occurs at regional scale. This break is apparent in the frequency distribution of elevation values for the region (Figure 48, red bracket) and was chosen for this reason. Visual investigation of the dataset shows that alternative elevation threshold values simply do not identify low lying valleys well, if they are far away from the small range of values that are plausible after consideration of the frequency distribution. Of this plausible range of values (which can be no more than +- 10 m, and are more likely to be +- 5 m), where valley relief is moderate or large (as is the case within much of the study region), variation in the threshold has a negligible effect upon the definition of low lying valley networks (figure 49 top), and consequently upon overdeepened area. This is because contours are usually close together and so the area set by the threshold changes little. In turn, the overdeepened area that is subject to low pass filtering must show negligible change. However, where valley relief is small (i.e. in areally scoured zones, zones of selective linear erosion, and/or zones that have experienced successive phases of glaciation on a variety of scales) such variation in the threshold could potentially influence the definition of low lying valley networks, and so overdeepened area.

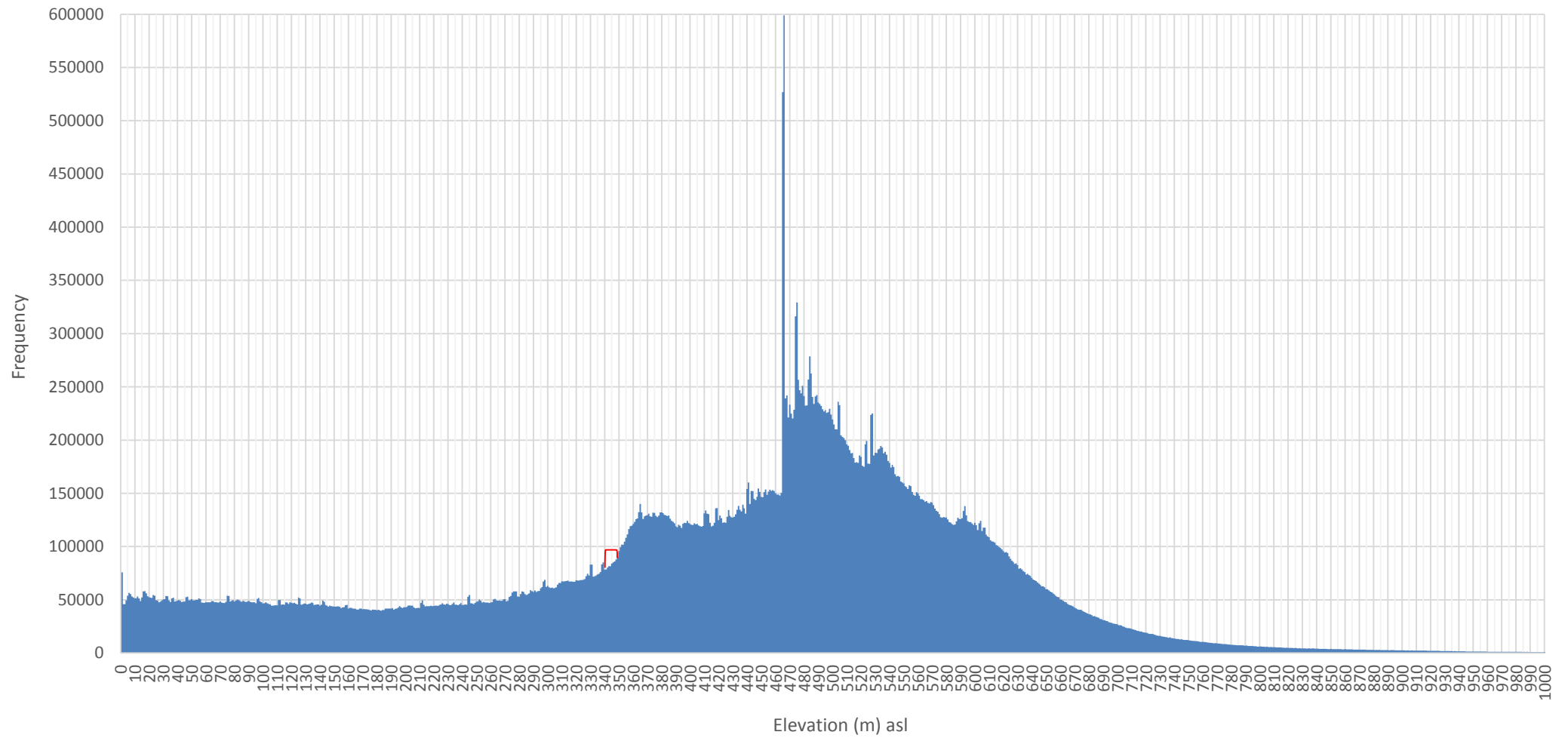


**Figure 48.** The frequency distribution of elevation values for the Labrador study region.

An elevation threshold value of 345 m a.s.l has been selected in order to define topographically low lying areas, where it is expected that overdeepenings will be particularly affected by sediment deposition and vegetation. The red bracket indicates the plausible range of values where the elevation threshold should be placed (after visual investigation of the DEM of the region, and appraisal of the frequency distribution)

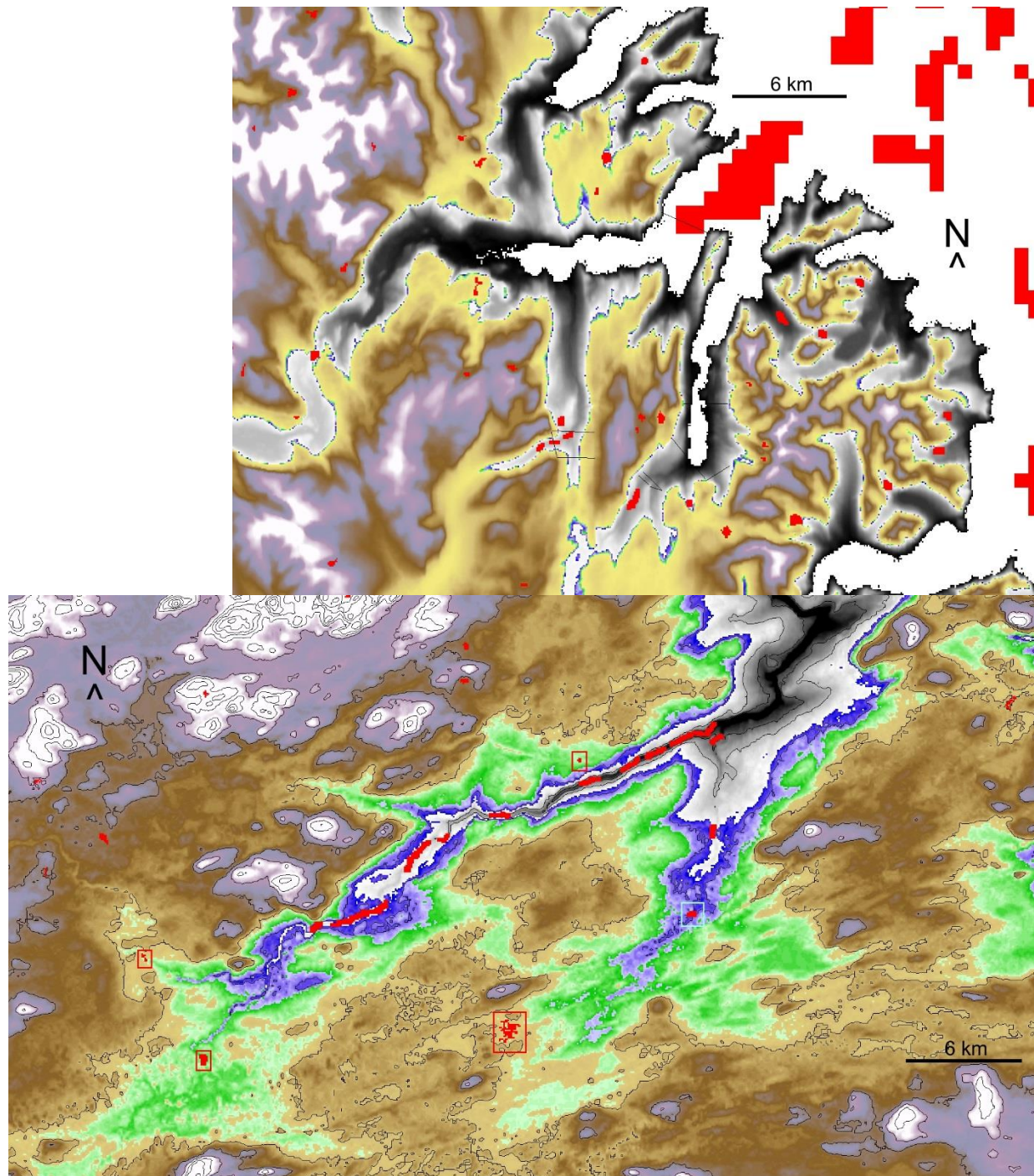


Figure 49. Considering the sensitivity of overdeepened area to variation of the elevation threshold.

(Top) The elevation threshold (345 m a.s.l) identifies low lying valley networks (and so associated overdeepened area) very well across the study region. Where valley relief is moderate or large (as is the case within much of the study region), variation (of  $\pm 10$  m) in the threshold has a negligible effect upon the definition of low lying valley networks, and consequently upon associated overdeepened area (ll coord 58.7, -63.6 DD). Land topography elevation values below 335 m a.s.l are displayed in greyscale (335 m a.s.l, black, to sea level, white), 336-345 m a.s.l in dark to light blue, 346-355 m a.s.l in dark to light green. Overdeepenings are depicted in red; (Bottom) Where valley relief is small (see text; contours at 20 m intervals, black lines), variation in the threshold (of  $\pm 10$  m) produces unacceptable definitions of valley networks, including plateau areas lying below and valley heads lying above the threshold, with consequent undesirable inclusion (red boxes) or exclusion (light blue box) of overdeepened area (ll coord 52.8, -58.9 DD). SRTM3 land topography data are shown in ESRI ArcGIS 'elevation' colour scale. Scale ranges from 355 m a.s.l (light brown) to  $\sim 1600$  m elevation a.s.l (white).

Where valley relief is small, if the threshold is made smaller (by 10 m or more) then it becomes visually apparent that parts of valley networks lie above the threshold value, which is unacceptable as this can result in some valley overdeepenings being excluded from filtering (figure 49 bottom, light blue box). If the threshold value is made larger (by 10 m or more) then extensive inland plateau areas are included within the area set by the threshold. This is unacceptable because it leads to overdeepenings being included in filtering which are clearly not part of low lying valley networks (or other low lying areas; figure 49 bottom, red boxes). Hence, even in regions where valley relief is small, the threshold value cannot be varied by more than  $\sim \pm 5$  m without unacceptable consequences. Whilst extensive sensitivity testing of the effect (upon overdeepening area) of this small variation in elevation threshold could be undertaken, we do not investigate this issue further. This is because so few overdeepenings are affected by such variation, and because those overdeepenings that are affected are inherently very small in area (being situated up-valley). Thus, importantly, acceptable variation (of  $\sim \pm 5$  m) in the threshold value yields insignificant impact upon overdeepened area, even in areas of small relief.

#### *4.4.2.2 Further thresholding of sink data (global study)*

An area/ perimeter ratio threshold value of 1 was chosen in order to remove sinks that have poor contiguousness from the global overdeepening dataset (section 4.2.6). Whilst sensitivity testing of the effect of varying this threshold upon sink contiguousness/removal could be undertaken, it is unnecessary given that the purpose of the resulting world maps is simply to inform future studies as to the location of potential overdeepenings at (small) regional to continental scales, for the purpose of further research.

### 4.4.3 Confluence parameters (regional study)

#### 4.4.3.1 Tributary-trunk angle

As the purpose of the investigation was to find whether there is any relation between variations in confluence ice velocity and overdeepening, the simplest forms of confluence were sought. Typical ‘birds foot’ y-shaped junctions are ideal for this (figure 50 top), whereas angular complications (such as in figure 50 middle) were rejected. A simple 90° tributary-trunk angle was used as a threshold to filter undesired confluences (figure 50 bottom). Assessment of variation in this threshold was not considered necessary given that the aim here is to seek the simplest confluences for investigation.

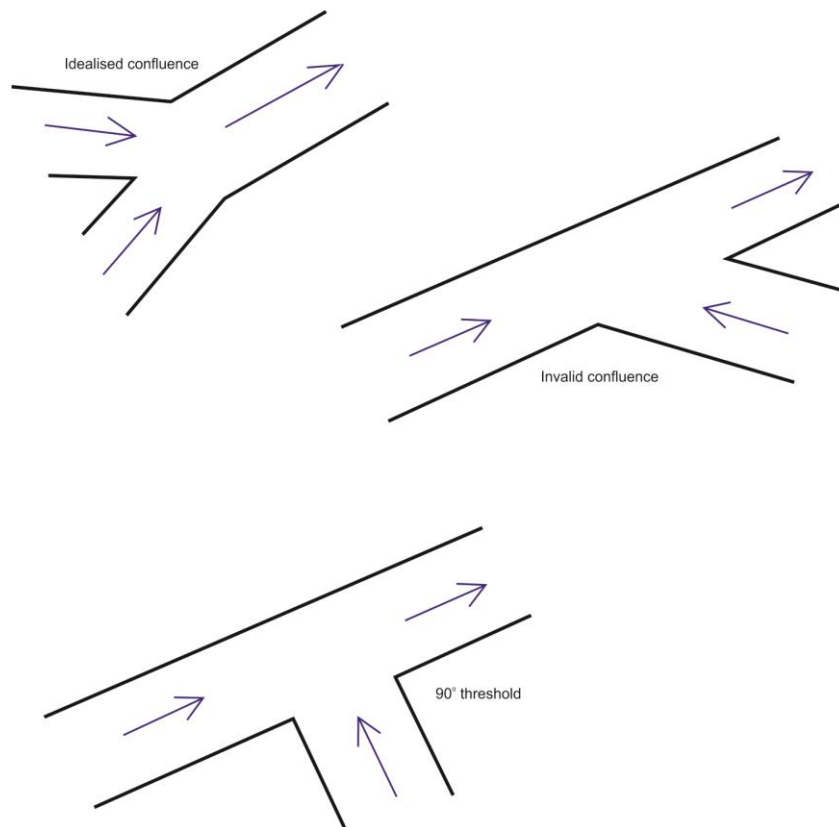


**Figure 50. Schematic plans of confluences: Tributary-Trunk angle.**

(Top) Schematic plan of an idealised, valid, confluence; (Middle) An undesired (invalid) confluence, after assessment of the angle between tributary and trunk valley; (Bottom) The 90° tributary-trunk angle threshold, used to filter undesired confluences. Ice flow direction is denoted by blue arrows (modification of figure 25).

#### 4.4.3.2 *Hanging valleys and stepped valleys*

A tributary can join a valley with a large step evident at the join (i.e. a hanging valley, figure 51), say of  $\geq 20\%$  of the total valley relief, or it can do so with a smaller or no step. For the simplest experimental design only clear cases of simple confluences were used (i.e. with small or no step), with hanging valleys excluded by visual analysis.

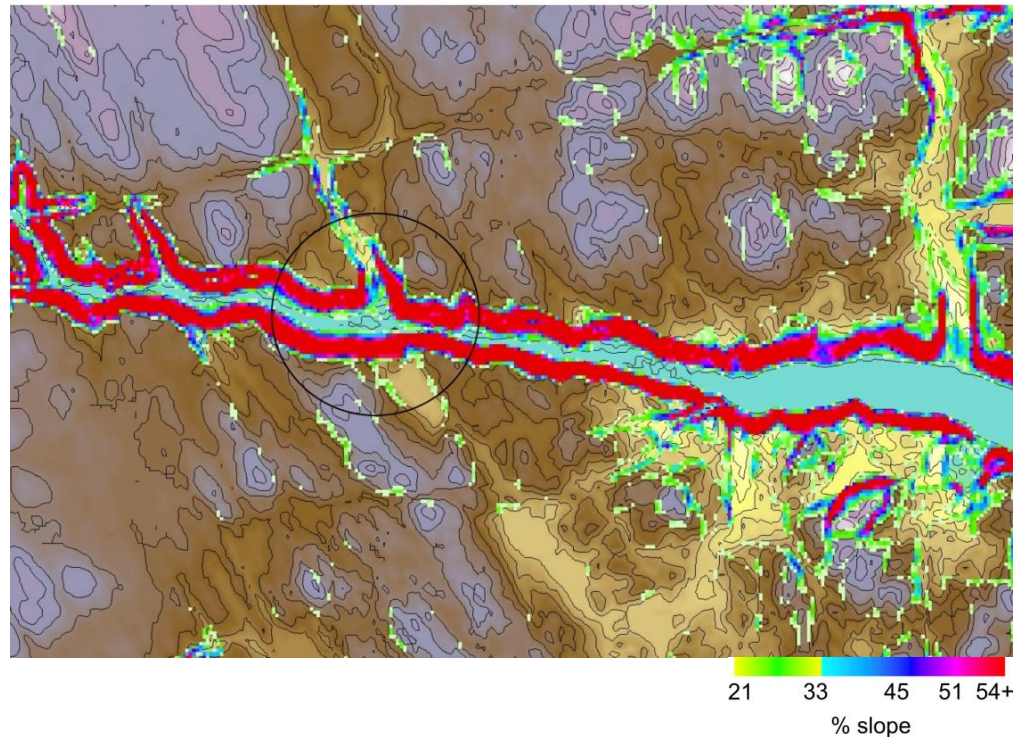


**Figure 51.** Example of a hanging valley.

An example of an invalid confluence (ringed), due to a hanging tributary valley, with partial slope map superimposed (i.e. displaying highest percentage slope values only). At this location (ll coord 56.7, -63.1 DD) there is considerable vertical discontinuity. The hanging tributary has associated high slope values where it joins with the trunk valley, relative to corresponding slope values in the adjacent tributary. SRTM3 land topography data are shown in ESRI ArcGIS 'elevation' colour scale. SRTM3 derived slope data are shown in a modified ESRI ArcGIS 'aspect' colour scale. Contours are placed at 20 m intervals (black lines; modified reproduction of figure 28).

#### **4.4.3.3 Confluence extent (lateral perimeter) & down-tributary termination (DTT) location**

##### **4.4.3.3.1 To what extent does the working definition of confluence affect confluence speed-up ratio?**

The parameters used to define the lateral perimeter of confluences (section 4.3.2) and the location of down-tributary terminations within confluences (section 4.3.3) have a direct influence on the measurement of valley cross-sectional area. However, because the ratio of cross-sectional area is assessed in this investigation, it might be that any sensitivity to the parameter choice does not matter much. Nevertheless, it was considered worth exploring the sensitivity of ratio results to variations in threshold parameters.

Given that we have created a ruleset (sections 4.3.2 and 4.3.3) in order to define confluence extent and internal geometry, we undertake an analysis of this ruleset in order to assess the sensitivity of confluence speed-up ratio to variations in confluence definition, as might be caused by operator variability. The issue here, is that small variations in how confluence is defined might have large consequences on confluence valley cross-sectional area (above and below the confluence) which could undermine the speed-up ratio that is subsequently calculated. Thus, we test for this using sensitivity analysis.

The underpinning approach is to vary the lateral extent of confluence by a percentage of confluence relief, only for confluences where the topography permits such variation. Where topography does not permit an increase or decrease in extent for a particular confluence, the ruleset will be broken and the confluence will consequently not exist at that scale. However, more commonly, topography will permit variation in confluence extent, and so the ruleset will not be broken. In such a scenario a confluence will exist in the topography at a variety of scales. Further, the internal geometry of confluence is varied where necessary, in order to assess the influence of down tributary termination (DTT) position and tributary valley axis orientation upon valley cross-sectional area. Rather than performing sensitivity testing on the entire population of confluences, we have chosen a sample from the Labrador study region.

The extent of each case study confluence was varied by +- 10 % of maximum valley relief (using elevation values) within the confluence (figure 52).

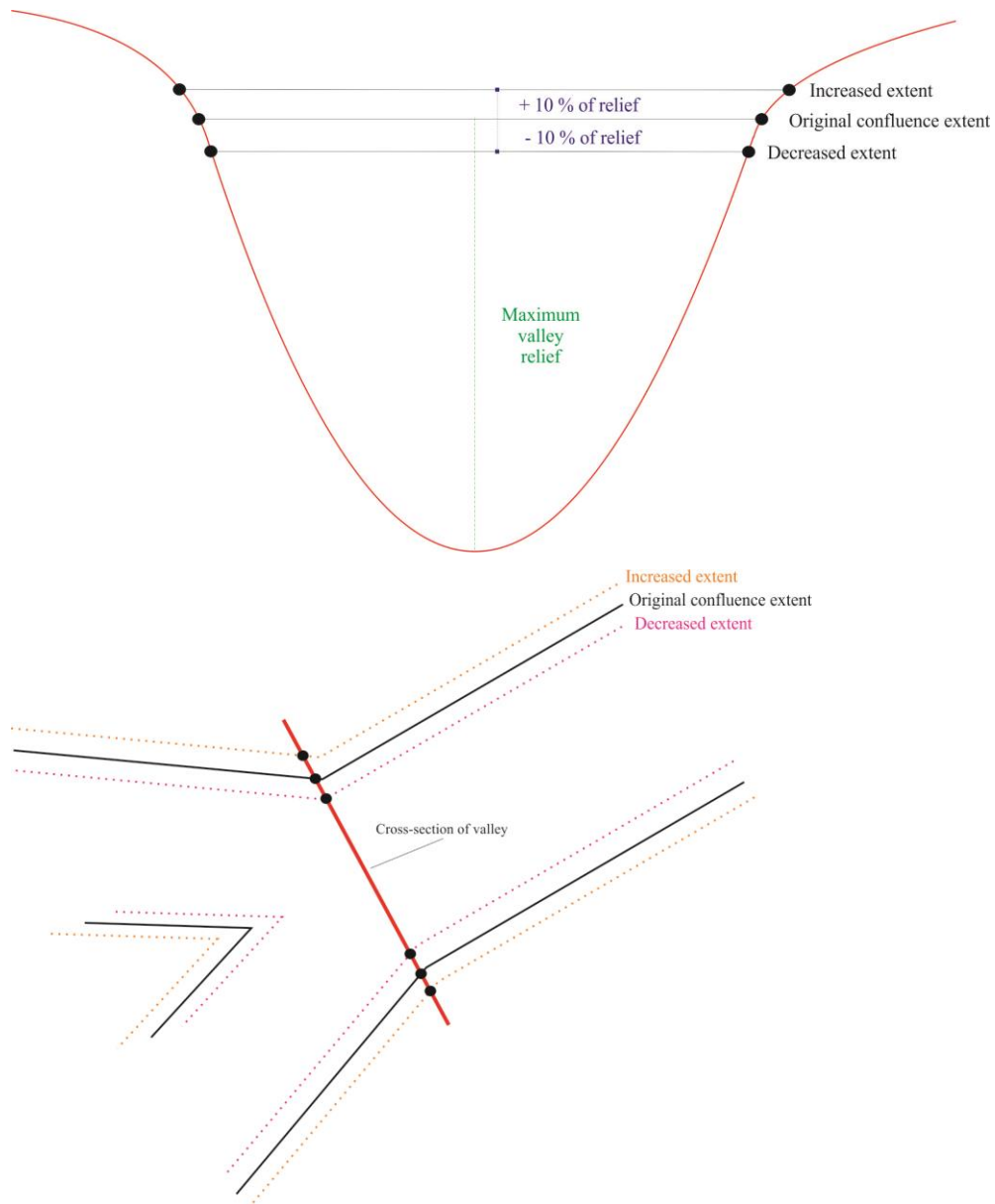


**Figure 52. Testing the sensitivity of confluence speed-up ratio to change in (lateral) confluence extent.**

**(Top) Schematic cross-section of a valley at the position of maximum relief within a confluence. Confluence extent is varied by  $\pm 10\%$  of maximum valley relief (see text); (Bottom) Schematic of an idealised confluence, showing the cross section (in plan) and increase (orange) and decrease (purple) in lateral confluence extent.**

It is apparent from visual consideration of confluences in Labrador that a  $10\%$  relief variation (typically tens of metres in real terms) provides as large enough lateral variation in extent to approximate any operator variability that might exist. Variations larger than this would result in many confluences breaking the ruleset. Such confluences would cease to be valid (figure 53). For this reason, operator variability rapidly becomes irrelevant when larger thresholds are considered.

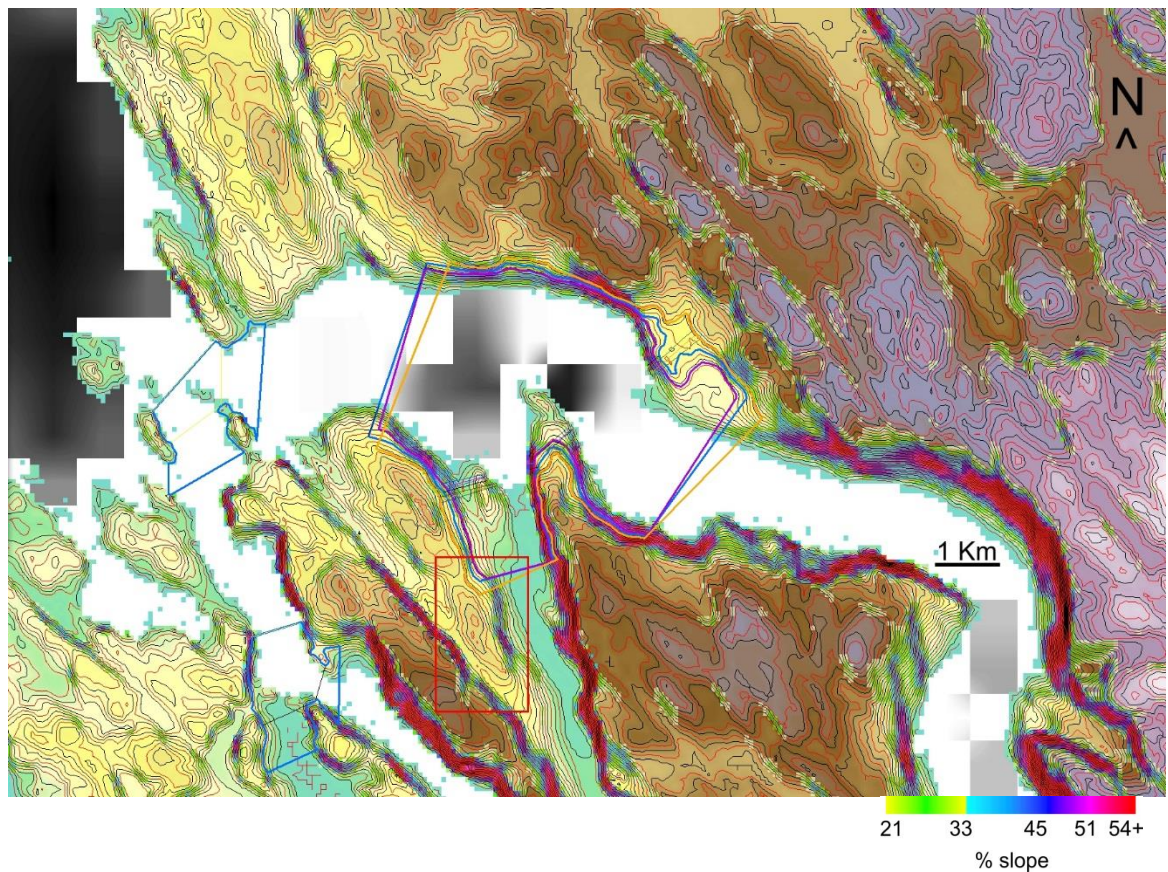
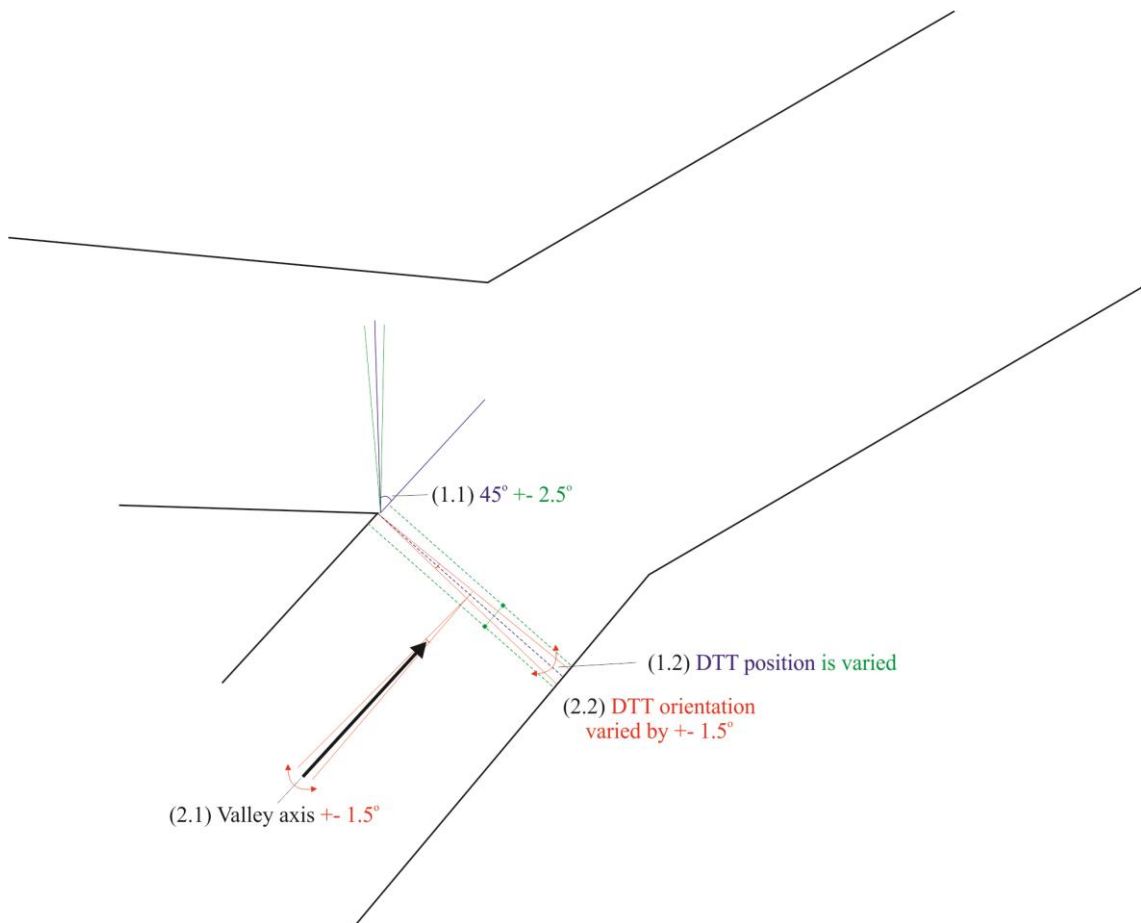


Figure 53. Considering the optimal relief threshold, with which to test the sensitivity of confluence speed-up ratio to change in (lateral) confluence extent.

This case study (ll coord 59.4, -65.4 DD) is a large relief fjordal confluence (extent denoted in blue, + 10 % in orange, - 10 % in purple) within a valley network, which has undergone some areal scouring (or similar, see sections 2.6 and 4.3.1.4). The confluence is typical of many in the landscape, and demonstrates how if the relief threshold is increased by more than 10 % (i.e. extent is increased beyond that denoted in orange), the confluence becomes invalid. Invalidity occurs in at least two ways, (1) Difffluence/ Non-contiguosness is apparent at several localities (denoted by the red box), and (2) Peak slope values for the confluence (used as a guide to define extent) are largely exceeded (especially on the south-west side of the confluence). SRTM3 land topography data are shown in ESRI ArcGIS 'elevation' colour scale. SRTM3 derived slope data are shown in a modified ESRI ArcGIS 'aspect' colour scale. GEBCO bathymetry data are shown in greyscale. Contours are placed at 10 m and 20 m intervals (red and black lines respectively).

In order to test the sensitivity of confluence speed-up ratio to change in down-tributary termination (DTT) position and tributary valley axis orientation, DTT position is moved up/down the longitudinal profile of tributary valleys by varying the 45° valley-side divergence angle threshold by  $\pm 2.5^\circ$  (figure 54). Further to this, DTT orientation across tributary valleys is varied by  $\pm 1.5^\circ$  (about the vertical (yaw) axis, figure 54). This is in order to simulate variation in the orientation of the valley axis.



**Figure 54. Testing the sensitivity of confluence speed-up ratio to change in down-tributary termination (DTT) position and tributary valley axis orientation.**

Schematic plan of an idealised confluence. By varying the  $45^\circ$  valley-side divergence angle threshold by  $\pm 2.5^\circ$  (1.1), DTT position is moved up/down the longitudinal profile of tributary valleys (1.2). A  $\pm 1.5^\circ$  variation in valley axis orientation is simulated (2.1), by varying DTT orientation across tributary valleys by  $\pm 1.5^\circ$  about the vertical (2.2).

The DTT position and orientation angle thresholds for sensitivity testing have been selected by visual consideration of the internal geometry of confluences. The use of a  $\pm 2.5^\circ$  threshold provides a large variability with which an operator might feasibly define the valley-side divergence angle (the position of which is usually very obvious and thus easy to define in most cases). For most examples of confluence in the study region, the divergence angle threshold will be reached at the same (DTT) position in the tributary, regardless of whether the threshold used is  $42.5^\circ$  through to  $47.5^\circ$ , such is the insensitivity of DTT position to this parameter (figure 55, left). A larger threshold value has not been selected because, when such thresholds are utilised, the DTTs of many confluences become positioned in unrealistic locations up and down valley. In such circumstances a transverse profile (taken at the DTT) is visually unrepresentative of down-tributary valley-width and cross-sectional area (figure 55, right). Such positions are

therefore beyond those which could be allowed by the ruleset, and so cannot be feasible by operator variability.

The parameter choice that is likely to have a more significant influence upon DTT location (and consequently valley cross-sectional area and in turn confluence ratio) is the orientation of the valley axis (i.e. the orientation of the DTT, for the purpose of testing). Visual consideration of confluences demonstrates that, if confluence DTT orientations are varied by greater than  $\pm 1.5^\circ$ , many DTTs become oriented unrealistically. Such orientations clearly do not reflect the valley axis position (figure 55), and are therefore beyond those which can be considered feasible by operator variability.

The sensitivity testing provides many combinations of confluence extent, down-tributary termination (DTT) positions, and tributary valley axis orientations, for each case study. This is in order to fully test operator variability upon valley cross-sectional area, and the subsequent effect upon confluence ratio. The sensitivity testing is addressed using 9 case studies, which are qualitatively considered to be typical of confluences in the landscape. The case studies consider confluences distributed evenly across the Labrador study region, in a variety of geological settings, with a variety of (plan) areas, reliefs (45-385 m), and cross-sectional area ratio values (i.e. from low (1.26) to very high (6.08)).

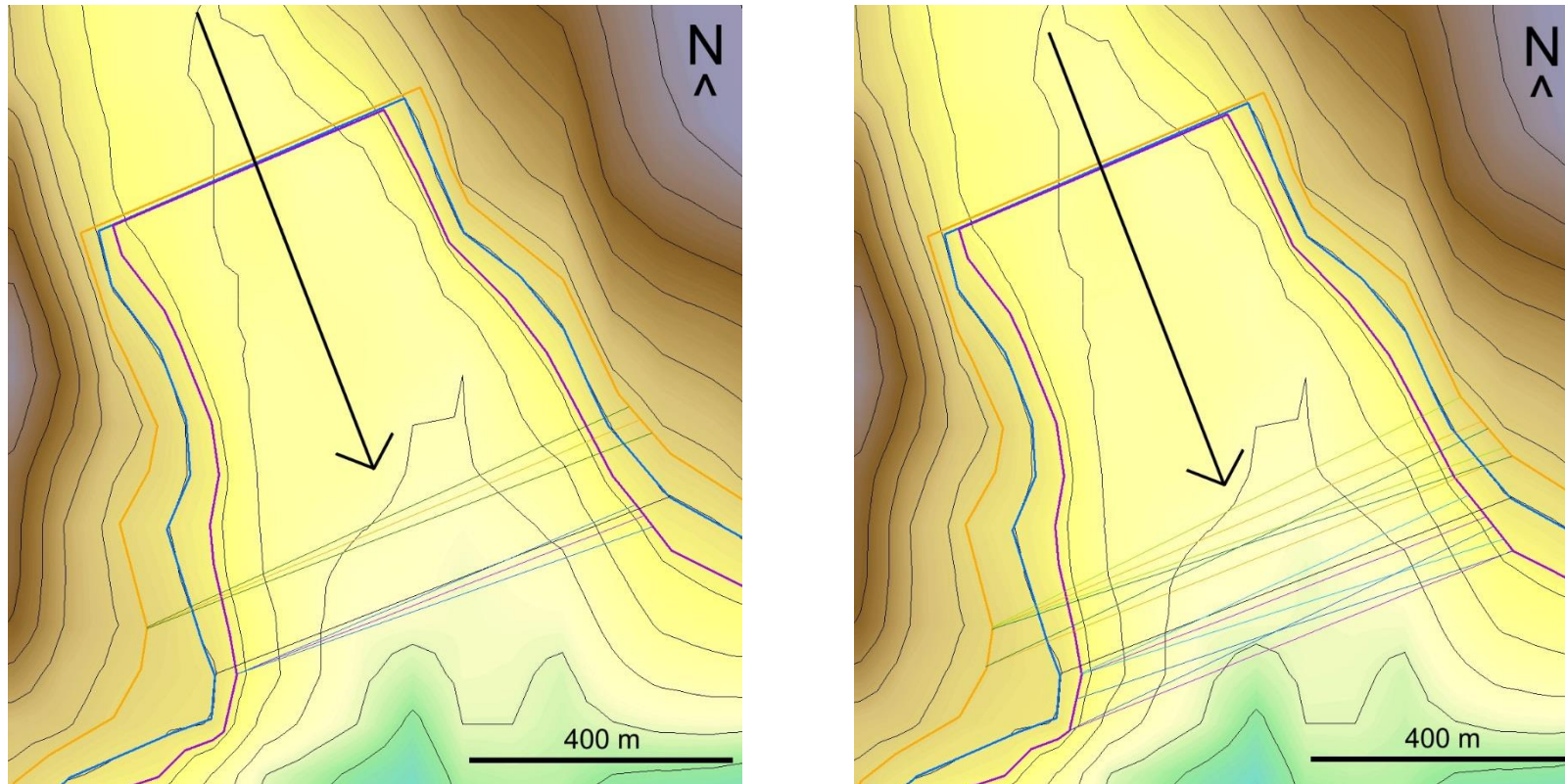


Figure 55. Considering optimal angle thresholds, with which to test the sensitivity of confluence speed-up ratio to change in down-tributary termination (DTT) position and tributary valley axis orientation.

(Left) In the typical case depicted here (ll coord 55.17, -61.9 DD) DTT position is quite insensitive to divergence angle, being the same (at each confluence extent) regardless of angle used (through 42.5° to 47.5°). Confluence extent is denoted in blue, DTT by black line; increased extent and DTT in orange; decreased in purple. Ice flow direction through the tributary is denoted by the arrow. When DTT orientations are varied by  $\pm 1.5^\circ$  they appear visually realistic, reflecting the valley axis position reasonably accurately; depicted here in dark green (at increased extent) and blue (at decreased). Variation of the divergence angle by  $\pm 2.5^\circ$ , and of the orientation angle by  $\pm 1.5^\circ$  in testing is considered optimal.

(Right) Larger angle thresholds cause DTTs in many confluences to become unrealistically located, beyond those feasible by the ruleset and so by operator variability, and are therefore sub-optimal. In this example, the divergence angle is varied by  $\pm 5^\circ$ . When a 40° divergence angle is utilised, DTT position remains the same as when 42.5°-47.5° angles are used (at each confluence extent). However, a 50° angle positions the DTT further down-valley (at each extent). Here, down-tributary valley-width is not properly represented. Further, DTT orientation is varied by  $\pm 3^\circ$ . Consequently DTTs are oriented unrealistically, not reflecting a plausible valley axis position; depicted in dark green where a 50° divergence angle is used, light green where 40° is used (at increased extent), and blue where 50°, light blue where 40° (at decreased extent). SRTM3 land topography data are shown in ESRI ArcGIS 'elevation' colour scale. Contours are placed at 20 m intervals (black lines).

#### 4.4.3.3.2 To what extent does the working definition of confluence affect confluence co-location with overdeepenings or geological zone?

Operator variability in how confluences are defined may influence (lateral and longitudinal) confluence extent, which will affect confluence (plan) area and may (in turn) influence confluence co-location with overdeepening (section 4.5) or geological zone (section 4.6). However, as demonstrated in the earlier sensitivity study (section 4.4.3.3.1), variations in confluence extent determined by varying the key relief threshold yield only small variations in lateral extent (for example in figure 53). For this reason the sensitivity of co-location (area) metrics to confluence definition is not considered further.

#### 4.4.3.4 *Down-trunk termination location*

By definition, the down-trunk termination (section 4.3.5) is placed at the position (and orientation) where minimum valley width is observed in the trunk valley and is usually visually very pronounced, occurring as a ‘pinch’ feature (figure 56, top). In the minority of examples where pinch position is not clear it is because valley width does not vary (perhaps due to erosion) in this location. In such examples the down-trunk termination is placed at the most upstream position where trunk valley-width is observed to be relatively uniform (figure 56, bottom). Negligible operator variability in location of the down-trunk termination can occur in this scenario because it is very clear where the trunk valley ceases to be of uniform width in the up-valley direction. Even if a little operator variability in location were to occur in such circumstances, it can have only an insignificant effect upon the trunk valley-width and down-trunk valley cross-sectional area that is measured at this position, because (in such circumstances) valley-width is so uniform in this part of the confluence. Hence, whether the pinch feature is visually pronounced or not, operator variability will be insignificant in its effects at the down-trunk termination, other than by the indirect influence of varying the lateral extent of confluences (which is investigated separately). Consequently, sensitivity testing for this parameter is redundant.

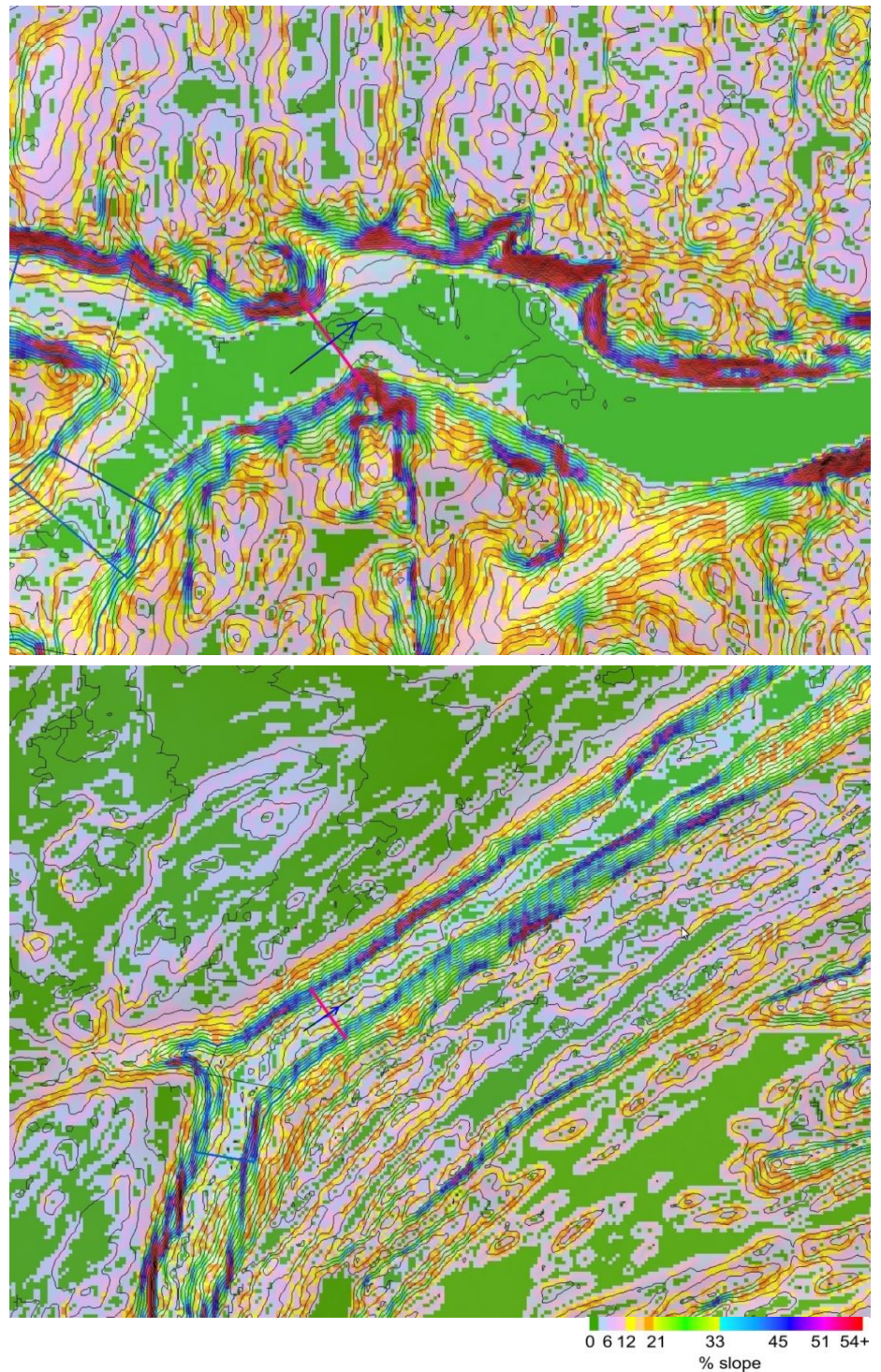


Figure 56. Considering operator variability in the location of the down-trunk termination.

(Top) The down-trunk termination (pink) is positioned where the pinch is apparent in the confluence trunk valley (see text). Consequently there can be no operator variability in termination location. Confluence extent is denoted in blue, trunk valley axis by thick black line (ll coord 56.1, -62.9 DD); (Bottom) There may be operator variability in termination location where the pinch is not apparent. However, this will be negligible (see text). Here, there can be only an insignificant effect upon measured down-trunk valley cross-sectional area, because valley-width is so uniform in this part of the confluence (ll coord 54.4, -62.5 DD). SRTM3 derived slope data for the Labrador study region are shown in a modified ESRI ArcGIS 'aspect' colour scale. Ice flow direction is denoted by blue arrows. SRTM contours are placed at 20 m intervals (black lines; modified reproduction of figure 44).

#### 4.5 Investigating ice velocity hypotheses (1 & 2); Assessing the co-location of glacial confluence and overdeepenings, for Labrador study region (Objective 3)

A GIS tool has been used to assess the co-location of glacial confluence and overdeepenings (figure 57). This is in order to examine the first and second hypotheses, regarding whether overdeepenings are preferentially located at glacial valley confluence and whether overdeepening size will be larger in confluences where there is greater ice velocity speed up. Further GIS analysis has been undertaken upon the resulting intersection datasets (using appropriate automated and manual GIS tools), which has provided basic statistics regarding confluences (both conservative and liberal) and co-located overdeepenings. Confluence and co-located overdeepening metrics have been assigned to these datasets. The metrics that have been considered in relation to the first and second hypotheses are confluence ratio, overdeepening area, and overdeepening maximum depth. Statistics are discussed in the results chapter.

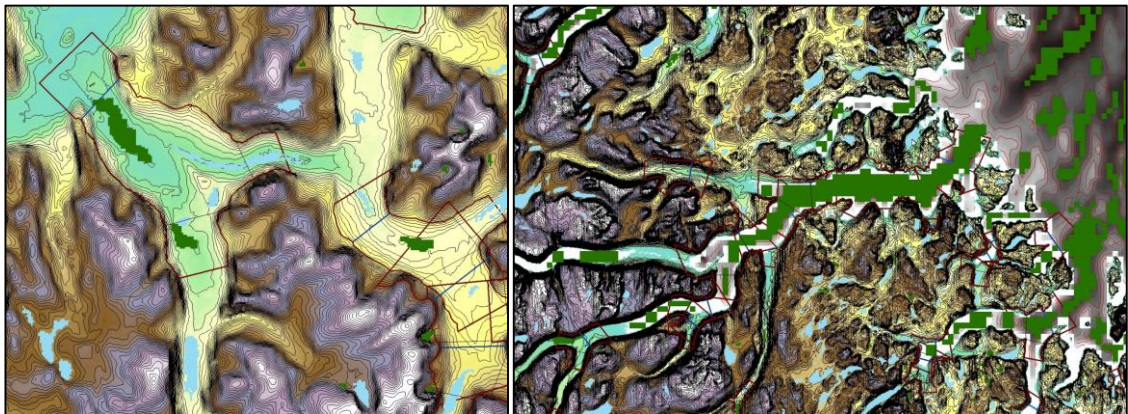


Figure 57. Assessing co-location of glacial confluence and overdeepenings using a GIS.

The co-location of glacial confluence (conservative, blue perimeter; liberal, dark red perimeter) with overdeepenings (empty/partially sediment filled, dark green; water filled/ partially water filled, light blue) has been assessed using a GIS. Further analysis has provided basic statistics. The DEMs utilised are SRTM3 topography data and GEBCO bathymetry data, for the Labrador study region, depicted using ESRI ArcGIS 'elevation' colour scale, and greyscale respectively (left image ll coord 59.5, -64.8 DD; right image 57.9, -63.6 DD). Contours are placed at 20 m intervals (SRTM, black lines; GEBCO, red lines).

##### 4.5.1 Evaluating the strength of the co-location relationship between glacial confluence and overdeepenings

In order to evaluate the strength of co-location relationships within the study region (for various hypotheses, see objectives 3, 7-10), area statistics are required, and these need to be compared to any co-location that might occur purely by chance. For this reason overall size of the study

region is important as well as the total overdeepened area, and the total area of confluence (considered as a single area of influence, for each of conservative and liberal confluence extents) within the study region.

#### 4.5.1.1 *Defining study region extent*

The overall size of the study region has been defined by a buffer zone (figure 58), which includes the SRTM topography data and GEBCO coastal bathymetry. Buffer zone extent is set well within the bounds of the GEBCO dataset because the majority of the bathymetry contains no discernible confluences. In order to make accurate area assessments, and so evaluate the strength of co-location relationships correctly, bathymetry and overdeepenings should be included in the study region only if there is a possibility of co-location with confluence. Where there are no confluences there can be no such possibility. The precise extent of the study region can therefore only be defined once the extent of confluence occurrence is known.

A buffer zone extent of 26 km has been identified as optimal, as this distance encompasses the marine area occupied by coastal overdeepenings that are coincident and not coincident with confluences; whilst excluding extraneous overdeepenings that are more distal, where there are no confluences. The buffer zone extends from the mainland of the study region without considering surrounding islands, as the most distal confluences are located in the fjords and bays of the mainland coast.

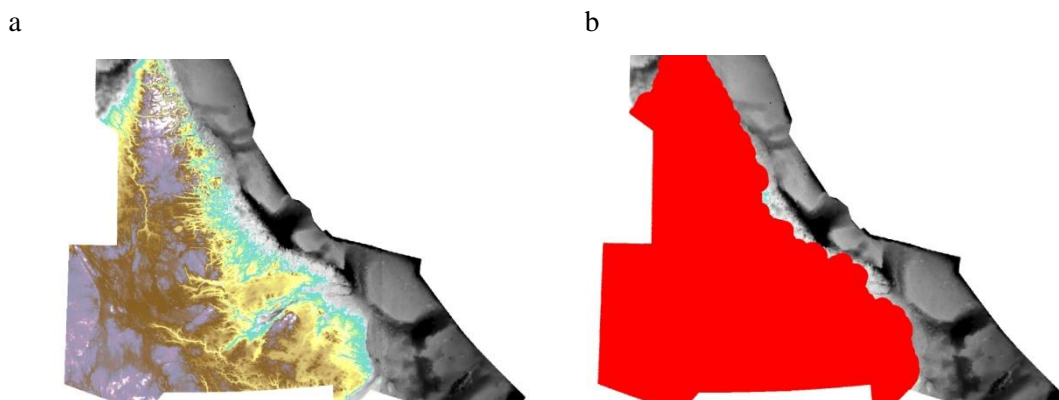


**Figure 58. Defining the precise extent of the Labrador study region.**

**a) The study region, and surrounding bathymetry (ll coord 52.0, -67.8 DD); b) A 26 km buffer zone, applied around the mainland topography (buffer mask, red).**

#### ***4.5.1.2 Calculating total area of study region, overdeepenings and confluence***

The overall size of the study region, the total overdeepened area, and the total area of confluence within the study region has been determined by the use of appropriate automated GIS tools. The total area of the study region is 450,406 km<sup>2</sup> (i.e. all SRTM3 topography and GEBCO bathymetry, inside of the buffer mask). The total overdeepened area is 64,295 km<sup>2</sup>. The total area of confluence is 7,458 km<sup>2</sup>, and 9,743 km<sup>2</sup> (calculated for conservative and liberal confluences, respectively).

Because entirely sediment filled overdeepenings are not identifiable, total overdeepened area may be underestimated within the study region. It is reasonable to assume that the majority of sediment filled overdeepenings will be located within valley networks, as this is where most sediment transfer will take place within the landscape. Consequently, the effect of such underestimation is likely to be a conservative appraisal of the strength of co-location between confluence and overdeepenings, which is satisfactory.

#### ***4.5.1.3 Actual co-location of glacial confluence with overdeepenings, versus expected (random) co-location of glacial confluence with overdeepenings***

The actual area of overdeepenings that are coincident (co-located) with area of glacial confluence within the Labrador study region has been compared with the expected area of overdeepenings that should be coincident with area of confluence by random chance. Only the overdeepened area that intersects with area of confluence is considered, not the whole area of the overdeepenings in question. This is in order that accurate overdeepened area versus study region and confluence area can be maintained in calculations.

The comparison allows assessment of the strength of the co-location relationship between glacial confluence and overdeepenings, making it possible to determine whether actual co-location of confluence and overdeepening in the study region can be attributed purely to random occurrence (i.e. that the two variables are statistically wholly independent of one another), or whether actual co-location demonstrates a relationship that is significantly stronger (i.e. that one variable is potentially statistically dependent upon the other). Chi-squared testing is also employed.

The expected (random) overdeepened area that should be coincident with area of confluence is calculated on the basis of the total area of the study region, the total overdeepened area within the study region, and the total area of confluence within the study region. The expected overdeepened area randomly coincident with confluence area in the study region is given by:

$$\left( \frac{\text{Total overdeepened area within study region}}{\text{Total area of study region}} \right) * \text{Total confluence area within study region}$$

If there is no relationship between confluence and overdeepening (i.e. coincidence is random, occurring purely by chance) then actual coincidence will be (less than or) similar to the calculated expected area. However, if there is a relationship between confluence and overdeepening then actual coincidence will be considerably greater than the expected area, and subsequent research will be required to provide evidence to support or oppose a causal relationship.

#### 4.5.2 Measuring valley cross-sectional area change through glacial confluences (Objective 4)

The measurement of valley CSA change through glacial confluences allows the quantification of the extent to which valley CSA change through a confluence affects overdeepening location and overdeepening metrics. This allows the causality of any relationship between confluence and overdeepening within the study region to be assessed. CSA change through a confluence is determined by the calculation of a confluence ratio. This is in order to examine the first and second hypothesis, regarding whether overdeepenings are preferentially located at glacial valley confluence and whether overdeepening size will be larger in confluences where there is greater ice velocity speed up.

The measurement is achieved by assessment of the CSA of the tributaries and the trunk valley within each confluence, at downstream terminations (i.e. at the DTT for tributaries, and at the conservative confluence down-trunk termination for the trunk valley). Measurements are taken using the 'interpolate line' tool from within the 3D Analyst extension of the ArcGIS 9.3.1 software. This tool makes use of bilinear interpolation (smoothing, 2 x 2 weighted average) on continuous raster data (i.e. the DEMs used in this investigation), and produces a transverse profile across each valley, situated at each downstream termination, which can be exported into Microsoft Excel 2007 software for further editing and analysis.

By the use of Excel software, a trapezoid rule calculation is performed on the profile for any given valley, in order to calculate the area under the curve. An identical type of calculation is performed on (the straight line of) a notional second profile, which is drawn from the first to the last data point of the (original) profile. The difference between the calculated area values of the

two profiles is the CSA of the valley. The CSA ratio for a given confluence is then calculated by:

$$(CSA \text{ of tributary 1} + CSA \text{ of tributary 2}) / CSA \text{ of trunk}$$

The CSA ratio can be described in various ways. It is a scale independent measure of:

- the difference between the CSAs of the sum of the tributary valleys, and the CSA of the trunk valley within a confluence (i.e. valley CSA change through a confluence)
- the difference between ice input/output of a confluence (i.e. ice through-put), if constant ice velocity is assumed (not realistic)

In the context of this investigation the CSA ratio might be best described as the ‘speed up factor’ of ice flow through a confluence (i.e. the greater the decrease in channel CSA of the confluence trunk, relative to the tributaries, the greater the consequent localised ice flow acceleration), as per the confluence CSA change hypotheses (hypotheses 1 and 2). Confluence ratio is therefore used as an index of ice velocity speed up within confluence.

Ratio values are 1 when there is parity of ice flow within a confluence (i.e. no ice speed up, valley CSA maintained through the confluence). Ratio values are more than 1 when ice flow is required to increase through a confluence (i.e. ice speed up, valley CSA decreases through the confluence). Ratio values are less than 1 when ice flow decreases through a confluence.

#### **4.5.3 Evaluating the influence of confluence cross-sectional area change upon overdeepening location (Objective 5)**

Comparison of the frequency distribution of confluence ratio for subsets of confluences co-located and not co-located with overdeepenings, allows the determination of the extent to which valley CSA change through a confluence affects overdeepening location within the study region.

The analysis (within Excel software) allows the causality of any relationship that has been observed between confluence and overdeepening location to be assessed. If a strong co-location relationship is found between confluence and overdeepening within the study region, and if a significantly greater number of confluences that are co-located with overdeepenings demonstrate ice speed up (i.e. ratios greater than 1) than is the case for confluences not co-located, then this provides evidence in support of a causal relationship. This is the final step in addressing the first hypothesis, regarding whether overdeepenings are preferentially located at glacial valley confluence.

#### *4.5.3.1 Quality control of the confluence/overdeepening datasets*

Prior to analysis, confluence co-located overdeepenings undergo a quality control process. This removes up-tributary overdeepenings from the intersection dataset. The quality control process allows a more accurate evaluation of the influence of confluence ice velocity speed up upon overdeepening location because, following quality control, there can be greater certainty that confluence ratios assessed in this test represent confluences that are co-located with overdeepenings most proximal to where valley CSA change may be influencing ice flow.

There is less certainty that ice flow at up-tributary positions is influenced by confluence. Other controls may have greater influence upon up-tributary overdeepenings. Up-tributary overdeepenings are therefore retained in the intersection datasets only if they extend downstream into the confluence trunk (figure 59), as it is only then that there can be a high degree of certainty that ice flow proximal to the overdeepening is influenced by the confluence (i.e. a decrease in trunk valley CSA, and associated increase in ice velocity), as supported by initial visual evidence from this study and by ice velocity calculations in other studies (Gudmundsson, et al., 1997; Berthier, et al., 2003; Gudmundsson, 1999; Byrd Polar Research Center, Remote Sensing Laboratory, 2001a).

The removal of up-tributary overdeepenings has insignificant influence upon the total area of overdeepenings within confluences, because the area of removed overdeepenings is small. Consequently, the influence of quality control upon co-location relationship strength (previously determined in section 4.5.1.3) is minimal. Any strong co-location relationship will remain; irrespective of whether up-tributary overdeepenings are included in, or excluded from analysis.

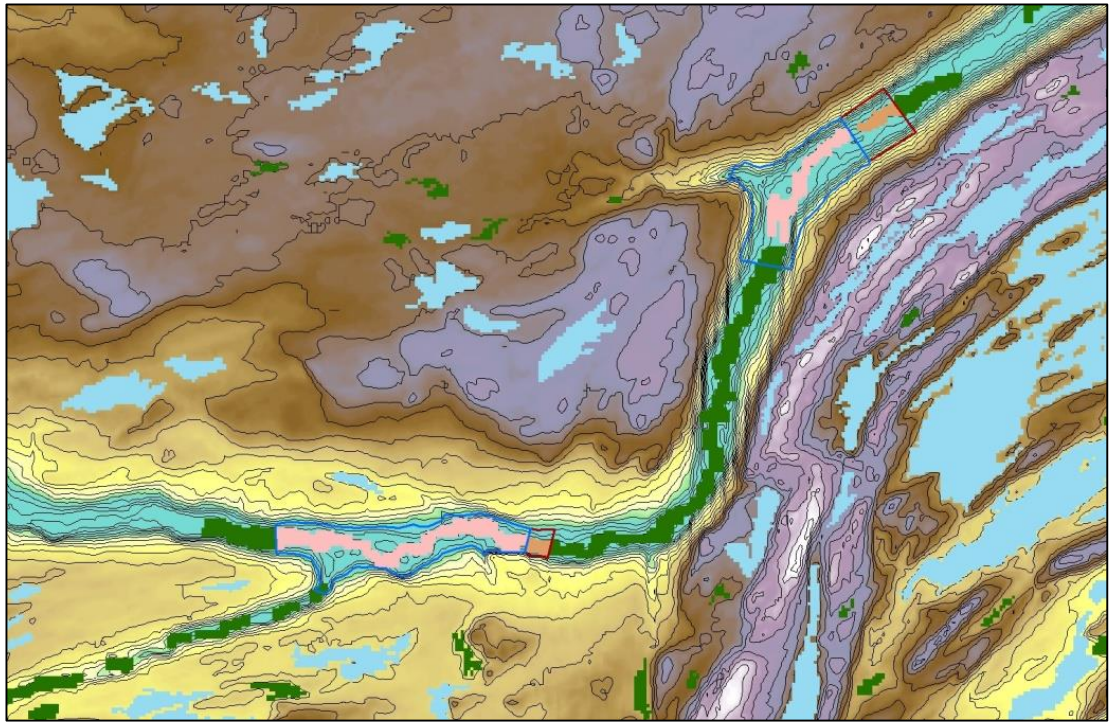


Figure 59. Quality control of the confluence/overdeepening datasets.

Up-tributary overdeepenings are retained in the confluence/overdeepening intersection datasets only if they extend downstream into the confluence trunk, as it is only then that there can be a high degree of certainty that ice flow proximal to the overdeepening is influenced by the confluence (see text). Confluences (conservative, blue perimeter; liberal, dark red perimeter), and overdeepenings (empty/partially sediment filled, dark green; water filled/ partially water filled, light blue), are presented with the confluence/overdeepening intersection datasets superimposed (conservative, rose; additional liberal, light brown). The DEM is SRTM3 topography data, for the Labrador study region, depicted using ESRI ArcGIS 'elevation' colour scale (ll coord 54.4, -62.7 DD). Contours are placed at 20 m intervals (black lines).

Rarely, there may be visual evidence of ice flow direction reversal in a confluence. In such instances, there may be uncertainty as to whether one or more co-located overdeepenings are sited up-tributary or down-trunk valley. Such overdeepenings are retained in the intersection datasets. Confluences where this occurs are considered to be of lower confidence (figure 60). Reversal of ice flow direction in a confluence may be observed in the longitudinal profile of valleys (i.e. contours), by the internal geometry of the confluence (i.e. the angle between tributaries and trunk valley), and/or by other indicators of ice flow direction within the surrounding topography (i.e. the situation of the confluence within the landscape, contours and direction of ice flow in other proximal confluences, and the position and orientation of adjacent overdeepenings) at selected confluence scale.

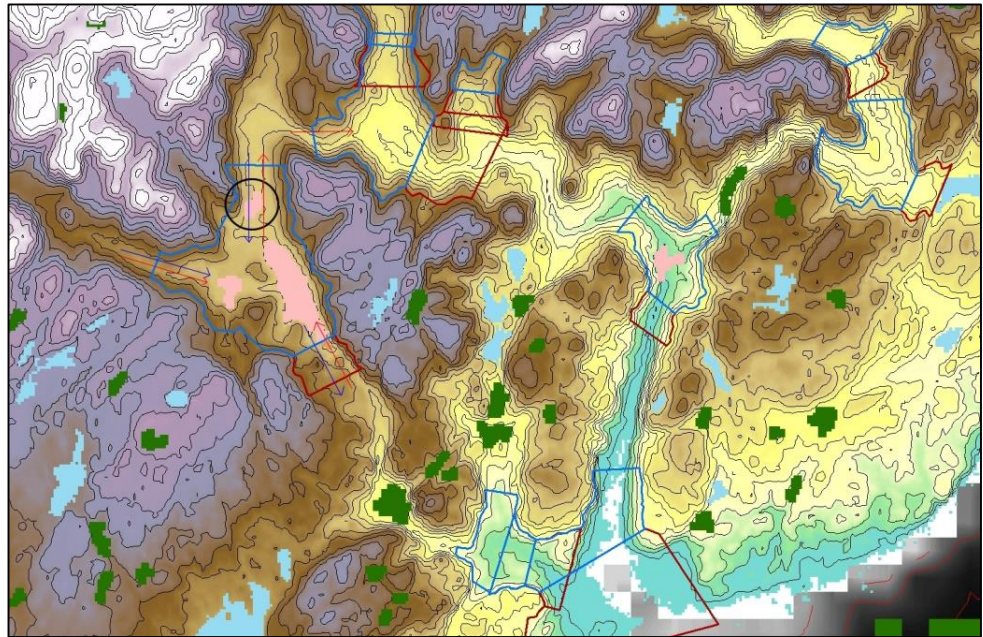


Figure 60. Dealing with ice flow direction reversal in confluences.

Where there is visual evidence of ice flow direction (blue arrows) reversal (red arrows) in a confluence there may be uncertainty as to whether one or more co-located overdeepenings (ringed) are sited up-tributary or down-trunk valley. Such overdeepenings are retained in the intersection datasets (see text). Confluences (conservative, blue perimeter; liberal, dark red perimeter), and overdeepenings (empty/partially sediment filled, dark green; water filled/ partially water filled, light blue), are presented with the confluence/overdeepening intersection datasets superimposed (conservative, rose; additional liberal, light brown). The DEMs utilised are SRTM3 topography data and GEBCO bathymetry data, for the Labrador study region, depicted using ESRI ArcGIS 'elevation' colour scale, and greyscale respectively (ll coord 51.6, -57.0 DD). Contours are placed at 20 m intervals (SRTM, black lines; GEBCO, red lines).

After quality control, the conservative confluence/overdeepening intersection dataset contains 462 overdeepenings. The liberal equivalent contains 660 overdeepenings.

#### 4.5.4 Evaluating the influence of confluence cross-sectional area change upon overdeepening size (Objective 6)

Analysis of the relationship between confluence ratio and co-located overdeepening metrics allows the determination of the extent to which valley CSA change through a confluence affects co-located overdeepening size within the study region.

Analysis involves the separate assessment of scatter plots of confluence ratio plotted against the various overdeepening metrics for confluence co-located overdeepenings. This allows the causality of any relationship to be assessed. Scatter plot relationships are assessed via linear regression analysis (using least squares method), undertaken in Excel software. The trend and strength of relationships are assessed, using adjusted  $r^2$  value and significance level. Because

this analysis assesses the relationship between speed up in confluences and the metrics of overdeepenings, confluences which demonstrate no ice velocity speed up or a decrease in ice velocity (i.e. ratio values  $\leq 1$ ) are excluded. If a strong co-location relationship is found between confluences and overdeepenings, and statistically significant relationships are also found between confluence ratio and overdeepening metrics for confluences that are co-located with overdeepenings within the study region, then this provides evidence in support of a causal relationship between confluence and overdeepening size. This is the final step in addressing the second hypothesis, regarding whether overdeepenings size will be larger in confluences where there is greater ice velocity speed up.

#### **4.5.4.1 Further quality control of the confluence/overdeepening datasets**

Further quality control removes very small and very large overdeepenings (relative to valley scale) from the dataset. Confluences that are less well defined at valley scale (according to the identification and definition criteria) are also removed. The quality control process allows a more accurate evaluation of the influence of confluence ice velocity speed up upon overdeepening size because, following quality control, there can be greater certainty that metrics assessed in this test represent overdeepenings that occur at, and confluences best defined at valley scale.

Although the procedure thus far identifies overdeepenings that are co-located with confluence, it has no criteria of scale and consequently sometimes yields very small and very large overdeepenings (by area) that cannot be considered to be influenced *primarily* by valley scale controls. Consequently, whilst valley scale controls will influence such overdeepenings (it has been assessed that very large overdeepenings in the dataset always contain valley scale overdeepenings within the co-located confluence), corresponding overdeepening metrics are unlikely to accurately reflect the influence of valley scale controls. Therefore, prior to analysis the scales of overdeepenings in the intersection datasets are assessed. Very small and very large overdeepenings are excluded from this analysis.

Further to this, confluence ratios are considered in analysis only for those confluences where there is most confidence that confluence extent and geometry is best defined at valley scale (i.e. that all identification and definition criteria have been met). Confluences of lower certainties in the intersection datasets are excluded from this analysis.

When assessing the scale of overdeepenings in the intersection dataset, a certainty is assigned to each overdeepening as to whether maximum extent of the overdeepening occurs at valley scale.

Certainties are assigned from 0 to 2 with 2 being the most certain. A low certainty (i.e. a certainty of 0) is manually assigned to an overdeepening (using GIS tools) when the overdeepening occurs at the wrong scale to have been primarily influenced by controls operating at valley scale (i.e. the overdeepening is very large, figure 61, top; or very small, figure 61, bottom). Low certainty overdeepenings are excluded from analysis.

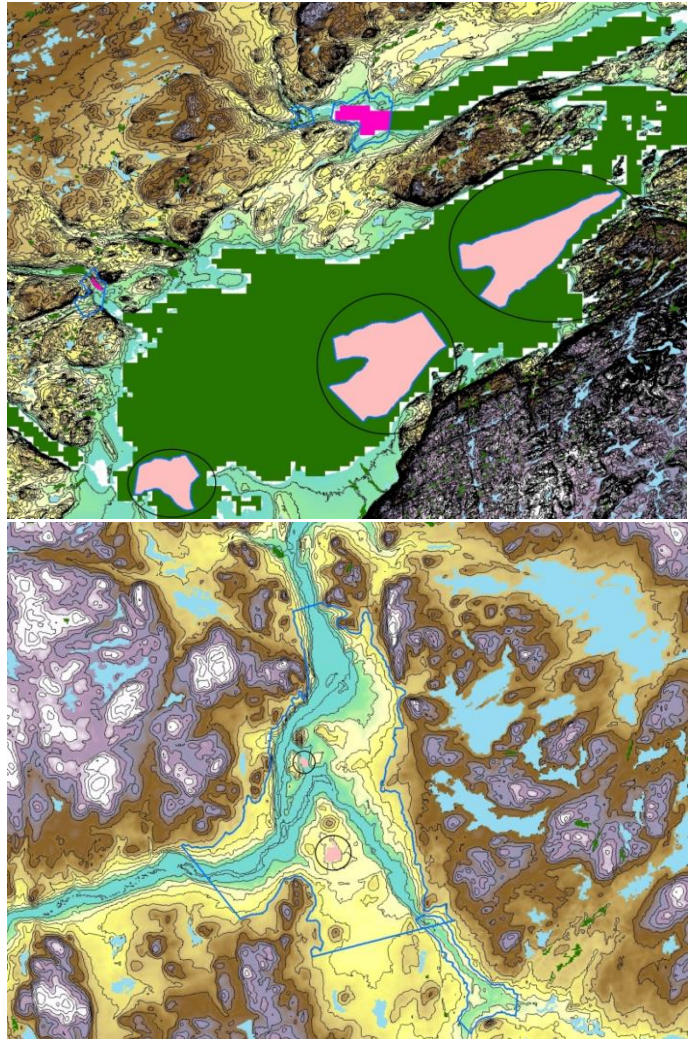


**Figure 61. Further quality control of the confluence/overdeepening datasets: Overdeepening scale, low certainty.**

**(Top)** An example of an overdeepening that is very large, relative to the area of the co-located confluences. The overdeepening (dark green) is a regional scale terminal overdeepening, the scale of which far exceeds that of the 3 confluences (ringed) with which it is co-located. The confluences each contain valley scale overdeepenings (ll coord 53.5, -60.4 DD). **(Bottom)** Two very small overdeepenings (ringed), relative to the size of the co-located confluence (blue perimeter) (ll coord 55.8, -65.0 DD). The DEMs utilised are SRTM3 topography data and GEBCO bathymetry data, for the Labrador study region, depicted using ESRI ArcGIS 'elevation' colour scale, and greyscale respectively. Overdeepenings (empty/partially sediment filled, dark green; water filled/ partially water filled, light blue) are presented with the conservative confluence/overdeepening intersection dataset superimposed (rose). Overdeepenings with assigned certainties of 2 within the intersection dataset are displayed in pink. Contours are placed at 20 m intervals (SRTM, black lines; GEBCO, red lines).

Where a small (i.e. non-valley scale) overdeepening is defined as being of low certainty, this may be supported by other indicators. An example of this is where the position of the overdeepening clearly suggests the primary influence of a specific non-valley scale control (figure 62).

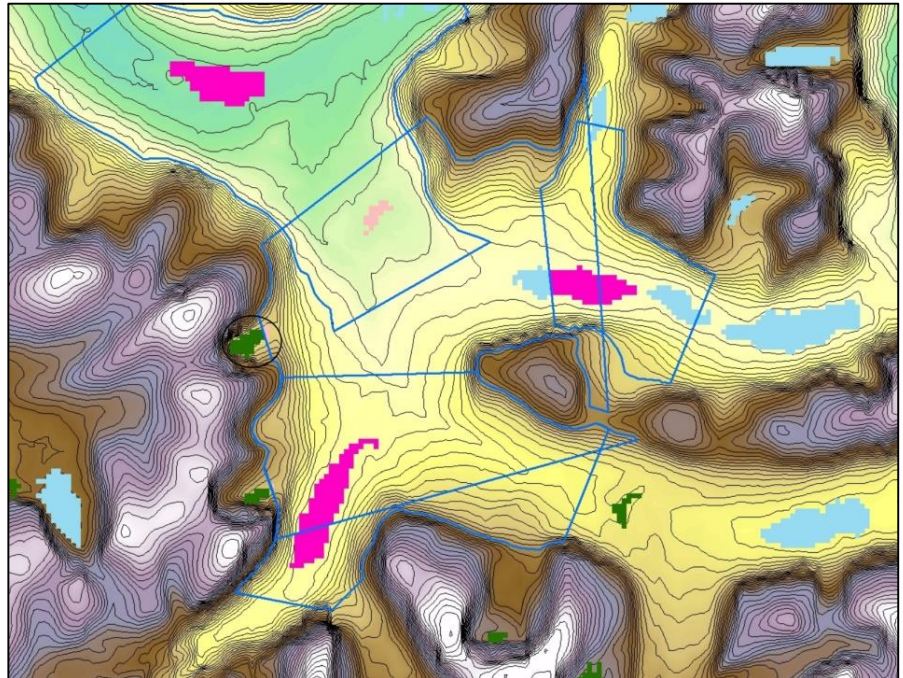


**Figure 62. Further quality control of the confluence/overdeepening datasets: Overdeepening scale, low certainty, other indicators.**

In this example (ll coord 59.5, -64.5 DD), a small cirque overdeepening (ringed) is situated on the edge of a much larger confluence (blue perimeter). The position of the overdeepening clearly suggests the primary influence of a cirque control that is not operating at the scale of the main valley. The DEM is SRTM3 topography data, for the Labrador study region, depicted using ESRI ArcGIS 'elevation' colour scale. Overdeepenings (empty/partially sediment filled, dark green; water filled/ partially water filled, light blue) are presented with the conservative confluence/overdeepening intersection dataset superimposed (rose). Those overdeepenings with assigned certainties of 2 within the intersection dataset are displayed in pink. Contours are placed at 20 m intervals (black lines).

A moderate certainty (i.e. a certainty of 1) is assigned to an overdeepening where there is some ambiguity as to whether the overdeepening occurs at valley scale (i.e. the overdeepening is quite small, figure 63). Moderate certainty overdeepenings are excluded from analysis.

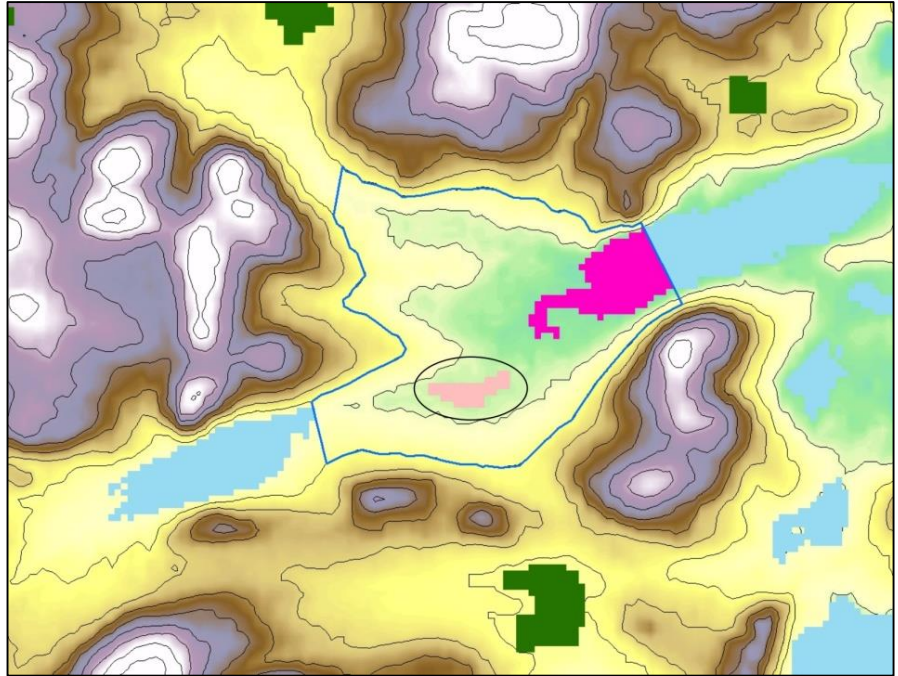
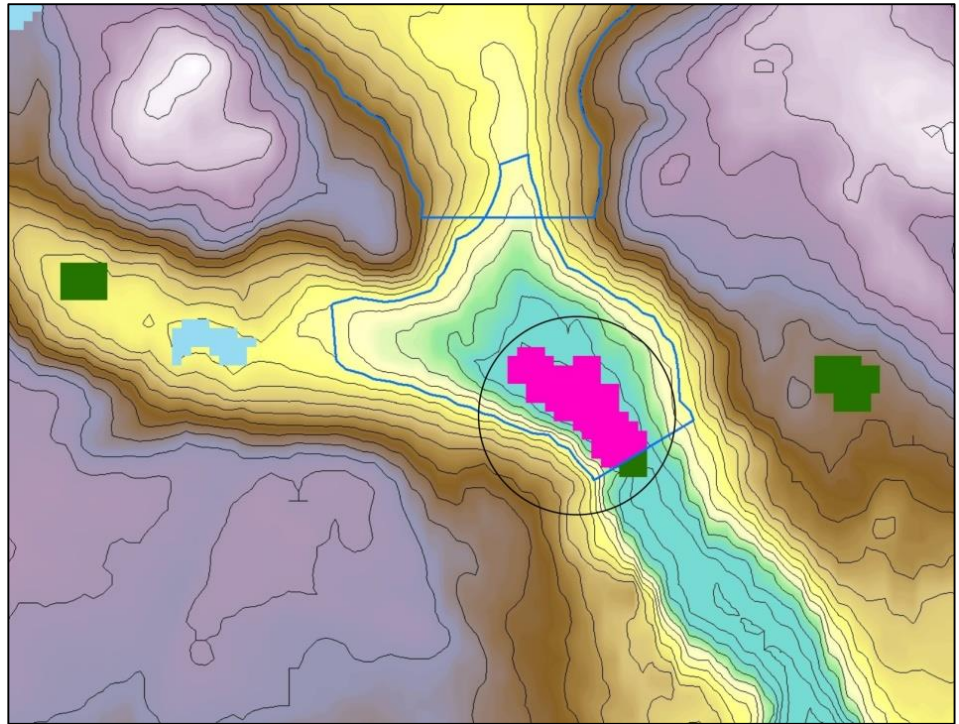


Figure 63. Further quality control of the confluence/overdeepening datasets: Overdeepening scale, moderate certainty.

In this example (ll coord 52.3, -56.2 DD), the overdeepening (ringed) is quite small relative to the size of the co-located confluence (blue perimeter). The DEM is SRTM3 topography data, for the Labrador study region, depicted using ESRI ArcGIS 'elevation' colour scale. Overdeepenings (empty/partially sediment filled, dark green; water filled/ partially water filled, light blue) are presented with the conservative confluence/overdeepening intersection dataset superimposed (rose). Overdeepenings with assigned certainties of 2 within the intersection dataset are displayed in pink. Contours are placed at 20 m intervals (black lines).

A high certainty (i.e. a certainty of 2) is assigned to an overdeepening where it occurs at valley scale (figure 64). Overdeepenings with high certainty are used in analysis.



**Figure 64. Further quality control of the confluence/overdeepening datasets: Overdeepening scale, high certainty.**

In this example (ll coord 51.9, -56.2 DD) the overdeepening (ringed) occurs at valley scale within the confluence (blue perimeter). The DEM is SRTM3 topography data, for the Labrador study region, depicted using ESRI ArcGIS 'elevation' colour scale. Overdeepenings (empty/partially sediment filled, dark green; water filled/ partially water filled, light blue) are presented, with the conservative confluence/overdeepening intersection dataset (with assigned certainties of 2) superimposed in pink. Contours are placed at 20 m intervals (black lines).

After further quality control, the conservative confluence/overdeepening intersection dataset contains 127 overdeepenings.

#### **4.6 Investigating bedrock erosion hypotheses (3 & 4); Assessing the co-location of geological zones and glacial confluence, for Labrador study region (Objective 7)**

The methodology that has been used earlier has been modified and repeated in order to assess the co-location of geological zones and glacial confluence, and to evaluate the strength of these relationships. This is in order to examine the third and fourth hypotheses, regarding whether overdeepenings will more frequently occur in confluences with weaker bedrock and whether overdeepening size will be larger in confluences with weaker bedrock.

Confluence (conservative) co-location with geological zones (i.e. igneous, metamorphic, sedimentary, and structural - shear and/or fault zones) has been assessed, using the appropriate automated and manual GIS tools and the Geological map of Labrador, 1:1,000,000 scale, dataset (Wardle, et al., 1997). Assigned geological zones for co-located confluences have been incorporated (using GIS tools) into the attribute table of corresponding confluence/overdeepenings, which also contains previously defined confluence/overdeepening metrics. The metrics that have been subsequently considered are geological zone, confluence ratio, overdeepening area, and overdeepening maximum depth.

##### **4.6.1 Evaluating the strength of the co-location relationship between geological zones and glacial confluence**

In order to evaluate the strength of co-location relationships within the geological study region, area statistics are required. It is necessary to calculate the total area of the study region (for which geological data is available), the total area of each geological zone, and the total area of confluence (considered as a single area of influence) within the geological study region.

###### **4.6.1.1 Defining study region extent, and calculating total area of geological zones and confluence, for geological analysis**

Coverage of the geological map of Labrador (Wardle, et al., 1997) is limited to within the political boundary of the province of Labrador (figure 65). The area of the study region for the purposes of geological analysis (termed the 'geological study region') is therefore smaller than that defined for the wider study region. Confluences outwith the geological study region are excluded from analysis. Segments of confluences which are split by the geological map perimeter, but which are located within the province, are considered in the evaluation of total confluence area. Segments of confluences which are split by the perimeter, but which are located outwith the province, are disregarded in evaluation of total confluence area. This is in

order that accurate total confluence area versus geological study region and geological zone area can be maintained. GIS tools are used to calculate area statistics. The total area of the geological study region is 293,453 km<sup>2</sup> (i.e. all SRTM3 topography within the bounds of the geological map). The total area of the igneous zone within the geological study region is 117,759 km<sup>2</sup>. The total area of the metamorphic zone is 87,010 km<sup>2</sup>. The total area of the sedimentary zone is 16,139 km<sup>2</sup>. The total area of the structural zone is 72,545 km<sup>2</sup>. The total area of confluence within the geological study region is 4,412 km<sup>2</sup>.

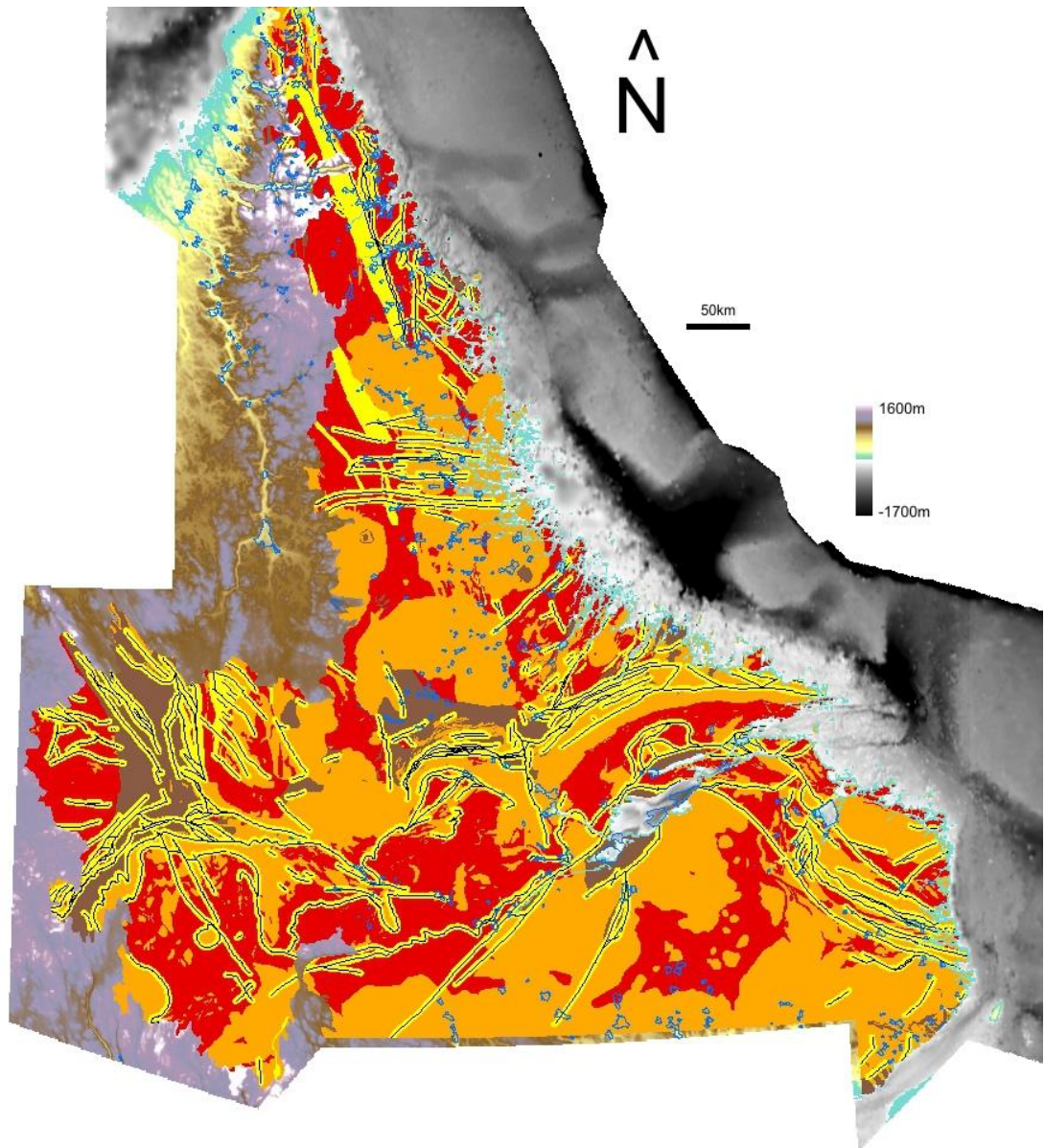


Figure 65. The study region (Labrador, Canada and surrounding region), with the geological zones for the province of Labrador (modified from Wardle, et al., 1997) superimposed.

The geological zones are igneous (orange), metamorphic (red), sedimentary (brown), and structural (shear and fault zones indicated in yellow, main fault lines indicated in black). The geological zones indicate the extent of the study region, for the purpose of geological analysis. SRTM3 land topography data are shown in ESRI ArcGIS 'elevation' colour scale (ll coord 52.0, -67.8 DD). Scale ranges from sea level (turquoise) to ~1600 m elevation a.s.l (white). GEBCO bathymetry data are shown in greyscale. Scale ranges from sea level (white/grey) to ~ -1700 m depth (black). Glacial (conservative) confluence perimeters are shown in blue.

#### *4.6.1.2 Defining confluence co-location with geological zones*

By the use of GIS tools, confluences are classified by the lithological zone within which each occurs. Where a confluence is at all co-located with a structural zone, the confluence is instead classified as belonging to the structural zone. Confluences that are not co-located with a structural zone, and which extend between two or more lithological zones, are classified as boundary confluences and are excluded from analysis due to the fact that geological boundaries have no quantifiable area (i.e. a boundary is a line, rather than a zone of influence). Boundary confluences are not suitable for area analysis. Lithological and structural zones have quantifiable area and so it is possible to assess actual versus random co-location of geological zone and glacial confluence, for co-located confluences.

Confluences which are co-located with a structural zone are classified as belonging to the structural zone regardless of the extent to which they are co-located (and the lithology in which they otherwise occur), as it is assumed that structural shear/fault zones will be the dominant geological control upon erosion in confluences (i.e. rather than lithology) where such zones are encountered. It is reasonable to assume that the presence of a shear or fault zone will be the overriding geological control upon erosion, where encountered (if such a control is found to exist at all, via hypothesis testing), as such zones will be significantly less competent than any lithological zone in which confluences may occur. It is likely that topographical processes (initially) and glacial processes (subsequently) will preferentially exploit the weakest geology.

Segments of confluences which are split by the perimeter of a structural zone, and which are located within the zone are considered in the evaluation of confluence area within the structural zone. Segments of confluences split by the perimeter, but which are located outwith the zone, are disregarded in the evaluation of confluence area within (and outwith) the structural zone. This is the case in order that accurate confluence area versus geological study region and geological zone area can be maintained. After exclusion of boundary confluences, and exclusion of segments of structural zone co-located confluences that are outwith the structural zone, the total area of confluence within the geological study region is 3,103 km<sup>2</sup>.

#### *4.6.1.3 Defining structural fault zone extent*

Ductile structural shear zones are defined within the geological map of Labrador (Wardle, et al., 1997) dataset (as zones with quantifiable area). However, brittle structural fault line data within the dataset are delineated (as lines with no quantifiable area) without consideration as to the fault zone of influence which surrounds them (i.e. sympathetic faulting, the zone of complex brittle deformation that is associated with main fault planes). Further, the geological dataset details only major structural features for the Labrador region, at regional scale (i.e. 1:1,000,000 scale). For these reasons a buffer zone of appropriate size (see below) to approximate the zone of influence for such faults is applied around each fault line (figure 66).

Visual assessment of DEMs and of the geology dataset has determined that valley networks tend to follow major structural fault features, at regional scale, within the Labrador study region. As topographical (and other) controls will presumably exploit zones of structural fault weakness in order to initiate and develop valleys, the zone of influence of the structural faults can be considered to occur on a similar scale to that of valleys, at regional scale. Consequently, buffer zone size is set to an extent compatible with the scale of confluence trunk valley widths within the study region, as these valley width metrics are known. The selected buffer zone extent is three times the mean valley-width, at confluence trunk pinch (i.e. down-trunk termination width), of only those confluences within the bounds of the geology dataset. This methodology provides a reasonable estimate of the potential zone of influence of faults within the study region, at regional scale, as it ensures that the full width of all valleys that are coincident with structural faults are included within the structural fault zone, provided that valleys are broadly parallel with fault line features (figure 66). Where valleys and fault line features are coincident but are not broadly parallel (or are simply not coincident), presumably controls other than structural fault weakness will have greater influence upon valley location/orientation and development. Mean valley-width for confluences within the bounds of the geology dataset is 1.89 km. Buffer zone value is therefore set to 2.835 km either side of each fault line feature, as this facilitates a zone of three times valley-width (5.67 km) in total, about each fault line. The ductile structural shear zones in the geology dataset are combined with the brittle structural fault (buffer) zones, resulting in a unified structural zone for which total area can be calculated and with which further analysis can take place.

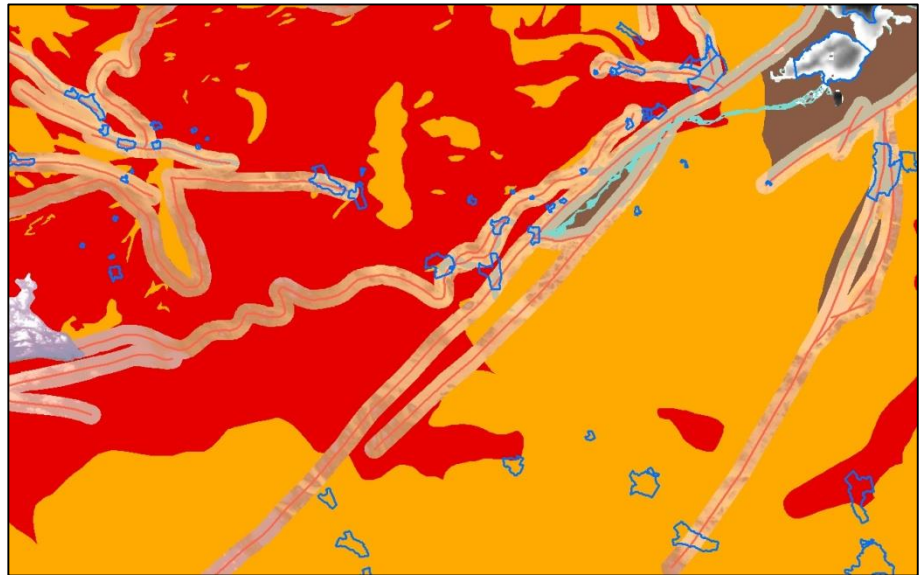


Figure 66. Defining structural fault zone extent.

Ductile structural shear zones are defined within the Geological map of Labrador, 1:1,000,000 scale, dataset (Wardle, et al., 1997). However, brittle structural fault line data are delineated without consideration as to the fault zone of influence which surrounds them. Further, the geological dataset details only major structural features for the Labrador region, at regional scale. Consequently, a buffer zone of appropriate size (see text) to approximate the zone of influence for such faults is applied around each fault line. The geological zones are igneous (orange), metamorphic (red) and sedimentary (brown). Additionally, the figure depicts structural shear zones combined with (buffered) structural fault zones (semi transparent, fault lines indicated by red lines). SRTM3 land topography data are shown in ESRI ArcGIS 'elevation' colour scale, with GEBCO bathymetry data shown in greyscale (ll coord 52.1, -63.7 DD). Confluence perimeters are shown in blue.

#### 4.6.1.4 *Actual co-location of geological zones with glacial confluence, versus random co-location*

The actual area of glacial confluence that is co-located with each geological zone within the geological study region (calculated using area statistics in sections 4.6.1.1 and 4.6.1.2, and the appropriate automated GIS tools) is compared to the area of confluence which should be co-located with a given geological zone by chance. The comparison allows assessment of the strength of the co-location relationship beyond that expected by chance. Chi-squared testing is also used.

The expected area of confluence which should be coincident with a given geological zone by chance is calculated on the basis of the total area of the geological study region, the area covered by each geological zone within the study region, and the area covered by confluence within the geological study region. The expected area of confluence coincident with a geological zone is given by:

$$\left( \begin{array}{c} \textit{Total confluence area} \\ \textit{within geology} \\ \textit{study region} \\ \\ \textit{Total area of geology} \\ \textit{study region} \end{array} \right) * \textit{Total area of geological zone within geology study region}$$

#### 4.6.2 Assessing the co-location of geological zones and overdeepenings (Objective 8)

The above methodology, used to assess the co-location of geological zones and glacial confluence, and used to evaluate the strength of these relationships, has been modified and repeated in order to assess the co-location of geological zones and overdeepenings within the study region, and to evaluate the strength of these relationships. This is in order to examine the third and fourth hypotheses, regarding whether overdeepenings will more frequently occur in confluences with weaker bedrock and whether overdeepening size will be larger in confluences with weaker bedrock. Overdeepening co-location with geological zones has been assessed using the appropriate automated and manual GIS tools. After exclusion of boundary overdeepenings, and exclusion of segments of structural zone co-located overdeepenings that are outwith the structural zone, the total area of overdeepening within the geological study region is 23,196 km<sup>2</sup>.

#### 4.6.3 Assessing the co-location of glacial confluence and overdeepenings, per each geological zone (Objective 9)

An automated GIS tool has been used to assess the strength of the co-location relationship between glacial confluence and overdeepenings for each geological zone within the Labrador study region. The methodology is the same as that used above other than regarding the division of the study region into geological zones. Multiple applications of the methodology were therefore required, one for each geological zone.

##### 4.6.3.1 Assigning geological zones to confluence/overdeepenings

The influence of valley CSA change will be localised to the topographical feature within which it occurs (i.e. the confluence). The influence of bedrock mass strength change is not localised to confluence. Confluences occur within significantly larger geological zones.

Bedrock mass strength change presumably operates in both similar and dissimilar modes (to that which it may do within confluence) at a variety of spatial scales (including at regional or

regional valley network scale). Bedrock mass strength change (along with other controls) may therefore have an unpredictable influence upon the location and size of overdeepenings that are co-located with confluence. This influence will presumably become greater as overdeepenings become larger, and as parts of overdeepenings consequently become more distal to the confluence.

Accordingly, the strength of further co-location relationships (i.e. sections 4.6.3 and 4.6.4), and the influence of bedrock mass strength upon confluence co-located overdeepening location and size, is assessed using the geological zones assigned to the respective confluence (see section 4.6; rather than those assigned to overdeepenings in the co-location strength test, section 4.6.2). This allows accurate assignment of geological zones to confluences (i.e. at valley scale). Confluences are locations within geological zones for which ice velocity speed up is known, and where overdeepenings are co-located.

#### **4.6.4 Assessing the co-location of geological zones and glacial confluence co-located with overdeepenings (Objective 10)**

In order to assert that any co-location relationship found between geological zone and confluence is applicable specifically for confluences that are co-located with overdeepenings (within a given geological zone), the assessment of the strength of the co-location relationship between geological zone and glacial confluence has been repeated for only those confluences co-located with overdeepenings, for each geological zone within the study region. An automated GIS tool has been used. The methodology is the same as that used earlier. After exclusion of boundary confluences, and exclusion of segments of structural zone co-located confluences that are outwith the structural zone, the total area of confluence (co-located with overdeepening) within the geological study region is 2,650 km<sup>2</sup>.

#### **4.6.5 Evaluating the influence of confluence bedrock mass strength upon overdeepening location (Objective 11)**

Analysis of the frequency distribution of confluence ratio for subsets of confluences with overdeepenings within each geological zone and within the remainder of the geological study region, allows the determination of the extent to which change in bedrock mass strength affects confluence co-located overdeepening location within the study region.

The comparison, performed in Excel, allows the causality of any relationship between geological zone and quality controlled confluence/overdeepenings (as detailed in section 4.5.3.1) to be assessed. If strong co-location relationships are found between a given geological

zone and confluence and between the same geological zone and overdeepenings (in addition to strong co-location relationships as described in sections 4.6.3 and 4.6.4), and if (for the geological zone) a significantly greater number of confluences co-located with overdeepenings demonstrate ice speed up (i.e. ratios greater than 1) than is the case for confluences co-located with overdeepenings within the remainder of the geological study region, then this provides evidence in support of a causal relationship between geological zone and confluence co-located overdeepening location, within the study region. This is the final step in addressing the third hypothesis, regarding whether overdeepenings will more frequently occur in confluences with weaker bedrock.

For the geological study region, the (quality controlled) conservative confluence/overdeepening intersection dataset contains 407 overdeepenings.

#### **4.6.6 Evaluating the influence of confluence bedrock mass strength upon overdeepening size (Objective 12)**

Analysis of the relationship between confluence ratio and co-located overdeepening metrics within each geological zone, allows determination of the extent to which bedrock mass strength affects overdeepening size.

Analysis involves the separate assessment of scatter plots of confluence ratio plotted against the various overdeepening metrics for confluence co-located overdeepenings (i.e. intersection dataset) for each geological zone within the study region. This allows the causality of any relationship between geological zone and confluence co-located overdeepening size within the study region to be assessed. Scatter plot relationships are assessed via linear regression analysis (using least squares method), undertaken in Excel software. The trend and strength of relationships are assessed, using adjusted  $r^2$  value and significance level. If a strong co-location relationship is found between both a specific geological zone and confluence, and the same geological zone and overdeepenings within the study region (in addition to strong co-location relationships as described in sections 4.6.3 and 4.6.4), and statistically significant relationships are also found between confluence ratio and overdeepening metrics for confluence co-located overdeepenings that occur within the geological zone in question (which are not apparent for those confluence co-located overdeepenings that occur within the remainder of the geological study region), then this provides evidence in support of a causal relationship between geological zone and confluence co-located overdeepening size. This is the final step in addressing the fourth hypothesis, regarding whether overdeepening size will be larger in confluences with weaker bedrock.

Prior to analysis, confluences and respective co-located overdeepenings in the intersection dataset undergo a further process of quality control. This further criterion is in addition to the quality control processes already detailed (in section 4.5.3.1 and 4.5.4.1).

#### *4.6.6.1 Further quality control of the confluence/overdeepening datasets (geology)*

As discussed in section 4.6.3.1, the unpredictable influence of bedrock mass strength change upon confluence co-located overdeepenings (at greater than valley scale) presumably become greater as overdeepenings become larger, and as parts of overdeepenings consequently become more distal to the confluence.

Because of the above, some large overdeepenings are found to be co-located with two or more confluences, which are in turn (as a group) co-located with two or more different geological zones. Consequently corresponding overdeepening metrics cannot be attributed to one geological zone. Such overdeepenings are excluded from analysis. Omitting these few large overdeepenings improves confidence that overdeepening metrics assessed in this test can most accurately represent the influence of bedrock mass strength change (at valley scale) upon overdeepening size in confluences, should this occur.

After further quality control, the conservative confluence/overdeepening intersection dataset, for the geological study region, contains 100 overdeepenings (of which 44 are co-located with a lithological zone, 48 are co-located with a structural zone, and 8 are co-located with a lithological boundary).

## 4.7 Testing reproducibility: A supplementary (Swiss) study region (Objective 13)

In order to determine whether some of the outcomes from analyses for the Labrador study region are replicated elsewhere, some methodologies used thus far are repeated for a smaller group of confluences and overdeepenings within the Swiss Alps, as an exploratory exercise. This study region (figure 67) has a significant glacial record. The datasets used are SRTM3 land topography data (ESRI Inc./ US NASA, 2006), and the Geological Map of Switzerland; 1:500,000 scale (Swiss Federal Office of Topography (SwissTopo), 2010).

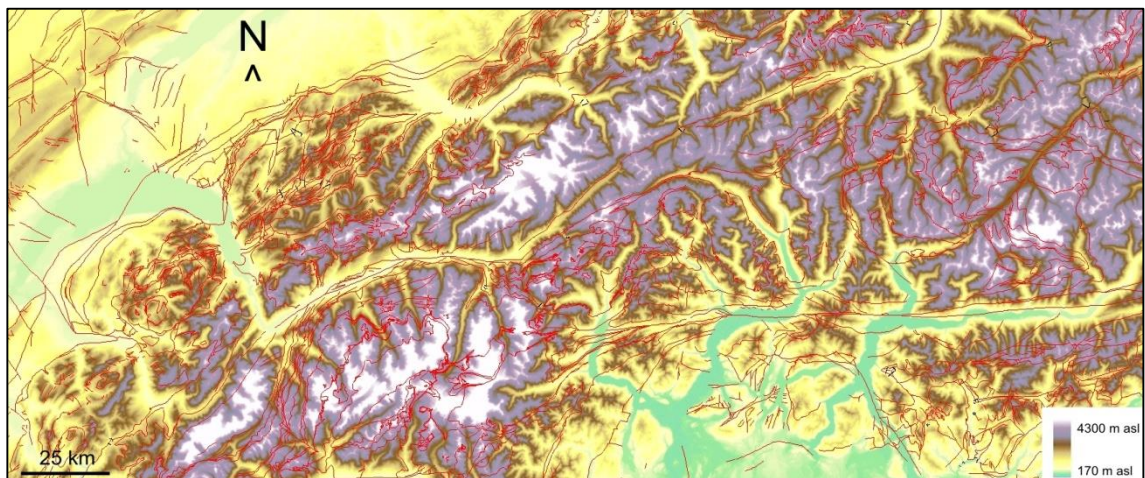


Figure 67. The Swiss study region.

Some methodologies are repeated for a smaller group of confluences and overdeepenings within the Swiss Alps. SRTM3 land topography data (ESRI Inc./ US NASA, 2006) are shown in ESRI ArcGIS 'elevation' colour scale (ll coord 6.0, 45.7 DD). Scale ranges from 170 m a.s.l (turquoise) to ~4300 m elevation a.s.l (white). Geological data are derived from the Geological Map of Switzerland; 1:500,000 scale (Swiss Federal Office of Topography (SwissTopo), 2010). Fault lines are denoted by red lines.

### 4.7.1 Defining structural fault zone extent, within structural geology zone

As was the case for the Labrador study region, structural fault lines within the Swiss geology dataset (Swiss Federal Office of Topography (SwissTopo), 2010) are delineated without consideration as to the fault zone of influence which surrounds them (i.e. sympathetic faulting, the zone of complex brittle deformation that is associated with main fault planes). The same methodology that is applied during analysis of the Labrador study region is applied in the Swiss analysis, to define fault zone extent.

Two different buffer zone extents have been assessed, in order to characterise the zone of influence of faults within the study region, at regional scale (figure 68). The first assessment

uses the (Labrador derived) buffer zone extent of three times the mean valley-width at confluence trunk pinch (i.e. down-trunk termination width), of only those confluences within the bounds of the (Labrador) geology dataset. Mean valley-width for such confluences is 1.89 km. The second assessment also uses a buffer zone extent of three times the mean valley-width at confluence trunk pinch (i.e. down-trunk termination width), but the buffer zone extent that is used is derived from a Swiss confluence dataset (produced for this investigation) which, whilst being more relevant to the study region in question, is a significantly smaller dataset and is therefore potentially less accurate than its Labrador counterpart. Mean valley-width for Swiss confluences is 0.98 km. Labrador buffer zone extent is derived from a mean average of some 440 confluence valley-widths at confluence trunk pinch. Swiss buffer zone extent is derived from a mean average of only 15 confluence valley-widths at confluence trunk pinch. However, the methodology can be used with confidence because a reasonable estimate of the zone of influence of faults within the Swiss study region, at regional scale, is the result whichever of the two buffer zone extents are used to characterise the zone of influence. When either buffer zone size is utilised, the full width of all valleys that are coincident with structural faults are included within the structural fault zone, provided that valleys are broadly parallel with fault line features. Where valleys and fault line features are coincident but are not broadly parallel (or are simply not coincident), presumably controls other than structural fault weakness have greater influence upon valley location/orientation and development.

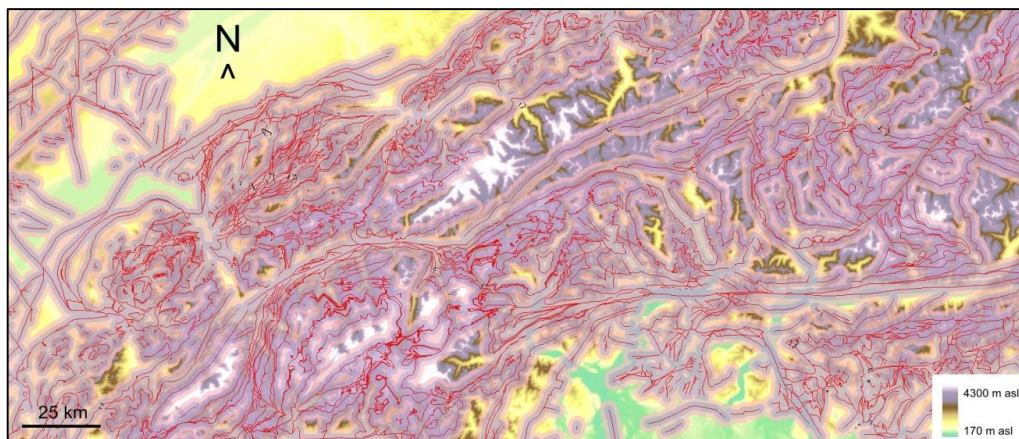


**Figure 68. Defining structural fault zone extent (Swiss study region).**

A buffer zone has been applied around each fault line within the Swiss study region, to approximate the zone of influence of each fault zone. Two different buffer zone extents have been assessed, in order to characterise the zone of influence of faults within the study region, at regional scale (see text). The Swiss derived fault zone of influence is displayed (semi transparent blue) within the (larger) Labrador derived fault zone of influence (semi transparent rose). SRTM3 land topography data (ESRI Inc./ US NASA, 2006) are shown in ESRI ArcGIS 'elevation' colour scale (ll coord 6.0, 45.7 DD). Scale ranges from 170 m a.s.l (turquoise) to ~4300 m elevation a.s.l (white). Geological data are derived from the Geological Map of Switzerland; 1:500,000 scale (Swiss Federal Office of Topography (SwissTopo), 2010). Fault lines are denoted by red lines.

#### **4.8 Identifying probable overdeepenings within limits of the LGM, globally (Objective 14)**

In view of the lack of availability of systematic data regarding the location of overdeepenings (at a global scale), this investigation has produced a series of maps (Section 5.6, figure 86 a-h) which provide an overview of topographical depressions within the limits of the Last Glacial Maximum (LGM), emphasising localities of likely glacial overdeepening. Depressions associated with small mountain glaciers are not examined within this assessment. The maps will be useful for future investigation of overdeepening, and as a test of numerical models of glacial erosion.

In production of the maps, some care has been taken, both to ensure that the finished maps are an accurate record of depressions within the limit of the LGM, and also to differentiate those depressions that are known or likely overdeepenings, from depressions which are known or likely geological basins (but which probably contain overdeepenings), and from other depressions (such as impact craters or calderas, which might possibly contain overdeepenings). Geological basin locations are derived from Meyer, et al. (2007). Whilst identification of depressions within the maps can be looked upon with a good degree of confidence, the categorisation is of course more subjective.

The maps are presented using the Fuller projection, which is optimised for low overall area, shape and distance distortions. Distance scale is true along tangent lines (i.e. particular lines of longitude and latitude), used during the projection process. Distortions increase away from tangent lines. Generally, directions are distorted, depending on the orientation of a tangent line (ESRI Inc., 2008b). Details of datasets and methods used in the production of the maps can be found in section 4.1 and 4.2.

## 5 Results

*This chapter presents outcomes of the investigation. Results of sensitivity testing are considered for research outcomes potentially susceptible to parameter choices made in overdeepening and confluence definition. Outcomes are then considered from general qualitative analysis of the Labrador study region, formal testing of ice velocity and bedrock erosion hypotheses, and systematic assessment of the location of known/likely overdeepenings at global scale. Results are considered for each of the study areas investigated; Labrador, the supplementary Swiss, and world (within the limits of the LGM).*

### 5.1 Sensitivity testing in order to justify parameter choices

#### 5.1.1 To what extent does the working definition of confluence affect confluence speed-up ratio? (regional study)

The sensitivity of confluence speed-up ratio to variations in confluence definition (by operator variability) has been assessed (see figure 69 for a map of confluence case study locations, and table 4 for a summary of the results). Analysis shows that small variations in how confluences are defined (i.e. lateral extent, DTT position, and valley axis orientation, see sections 4.3.2 and 4.3.3) have little to negligible impact upon valley cross-sectional area (and so confluence speed-up ratio) when confluence relief is large (table 4, figure 70). When relief is large it is most likely that the contours which define confluence are close together, and so impact is minimal. Relief is greatest in well-defined valley networks, especially where confluences are fjordal (e.g. case studies 1-6, figure 69; case study 3, figure 71). Analysis shows that when the definition of confluence is varied where confluence relief is small there can be a significant impact upon confluence valley cross-sectional area (table 4, figure 70). The contours that define confluence are most likely to be far apart in such a scenario. Smallest relief is most often encountered in confluences that are fairly isolated, situated away from valley networks, and/or where confluences are located in areally scoured zones, zones of selective linear erosion, and/or zones that have experienced successive phases of glaciation on a variety of scales (e.g. case studies 8 and 9 particularly, figure 69; case study 9, figure 71). It is noted that the case studies with the largest ratio values (i.e. case studies 8 and 9) have poorest performance in the sensitivity testing because they are low relief confluences. The impact of such cases is not considered to be significant in this study because most confluences in the Labrador and Swiss studies have moderate or greater relief.

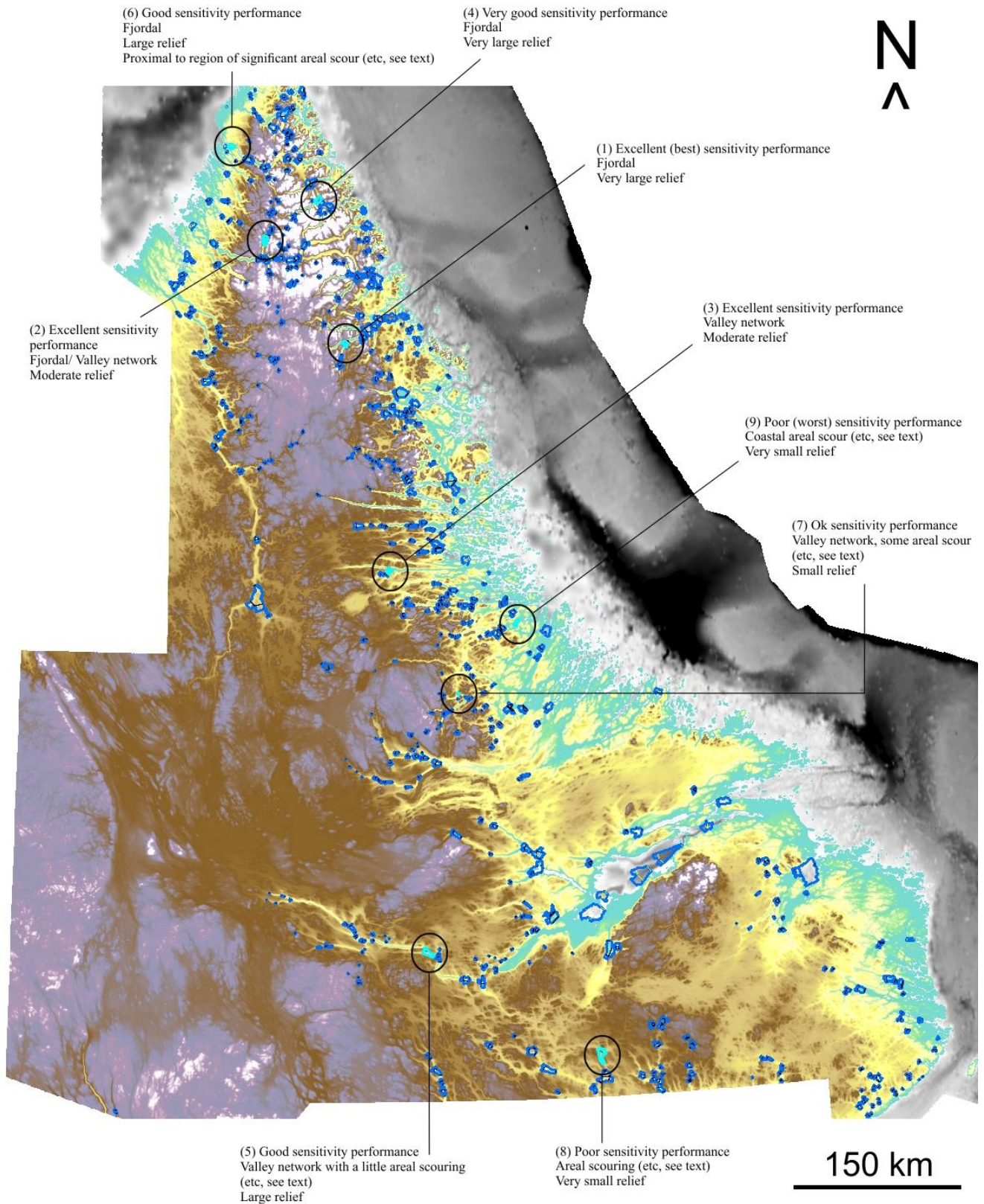


Figure 69. Sensitivity testing. Map of confluence case study locations.

Confluence case studies for sensitivity testing are ringed, annotated with further information (see table 4), and highlighted in light blue. Other confluences in the study region are denoted in blue. SRTM3 land topography data are shown in ESRI ArcGIS 'elevation' colour scale (ll coord 52.0, -67.8 DD). Scale ranges from sea level (turquoise) to ~1600 m a.s.l (white). GEBCO bathymetry data are shown in greyscale. Scale ranges from sea level (white/grey) to ~ -1700 m depth (black).

Confluence data						Results of sensitivity testing			
Confluence case study	'Speed-up' ratio (R)	Area (km <sup>2</sup> )	Relief (m)	10% of relief (m)	Comment	End member (offset) R values	Range of (offset) R values	No. of results within +- 0.05 of R	Performance
1	1.52	15.32	384	38	Moderate area, very large relief	1.50 1.53	0.03	12 of 12	Excellent
2	1.71	26.29	200	20	Large area, moderate relief	1.67 1.73	0.06	8 of 8	Excellent
3	2.07	16.44	183	18	Moderate area, moderate relief	2.01 2.09	0.08	11 of 12	Excellent
4	1.26	20.42	386	39	Moderate-large area, very large relief	1.24 1.35	0.11	4 of 8	Very Good
5	2.16	36.68	238	24	Large area, large relief	2.01 2.17	0.16	5 of 8	Good
6	1.27	18.91	236	24	Moderate-large area, large relief	1.06 1.29	0.24	4 of 8	Good
7	2.94	2.57	132	13	Small area, small relief	2.80 3.08	0.28	1 of 8	Ok
8	4.72	56.13	63	6	Very large area, very small relief	4.34 5.00	0.66	0 of 8	Poor
9	6.08	11.87	46	5	Moderate area, very small relief	5.74 6.56	0.81	0 of 8	Poor

**Table 4. Results of testing the sensitivity of confluence ratio to change in the working definition of confluence (extent and internal geometry), sorted in order of performance.**

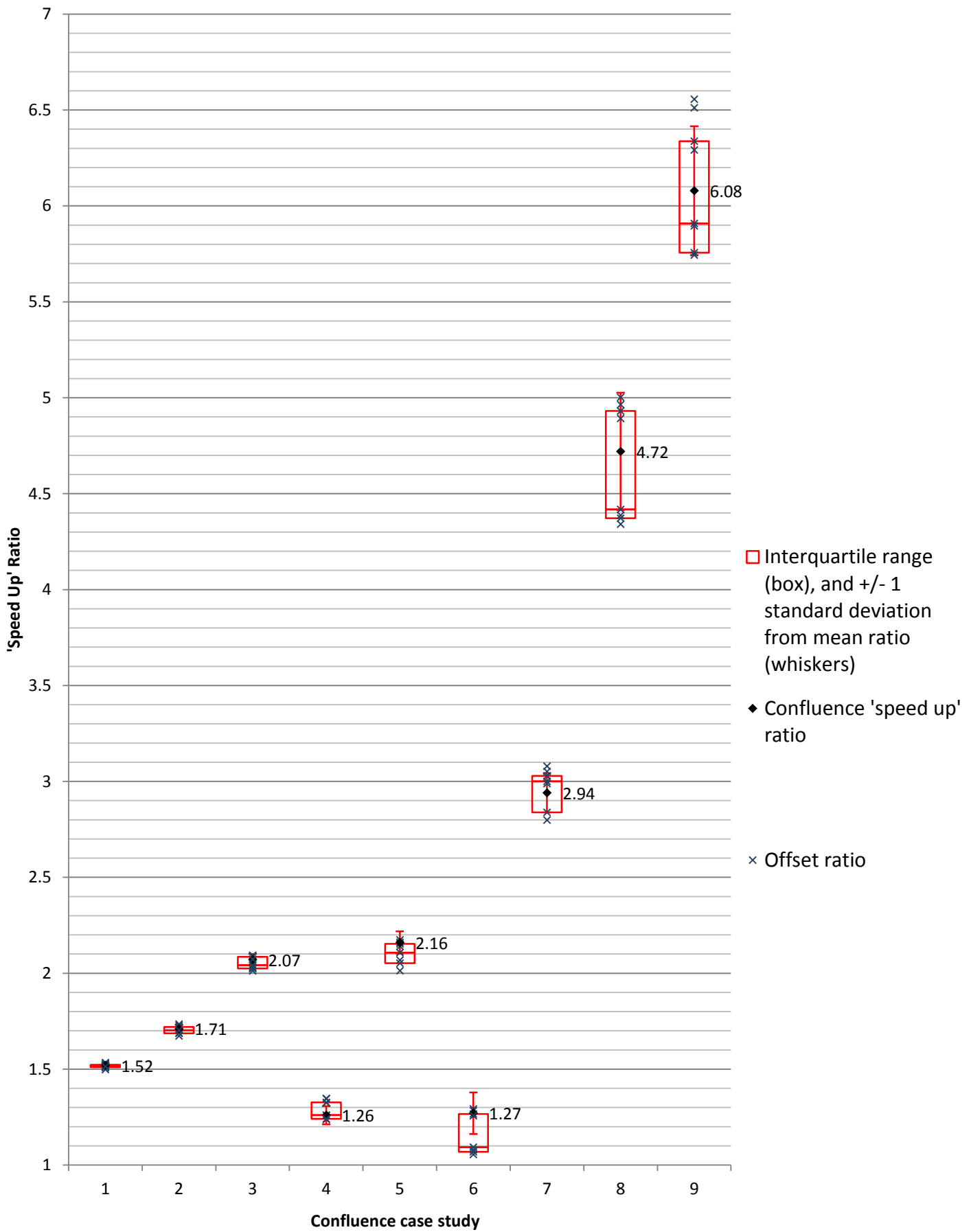


Figure 70. Results of testing the sensitivity of confluence ratio to change in the working definition of confluence (extent and internal geometry), sorted in order of performance, showing each case study and the range of each corresponding ratio value.

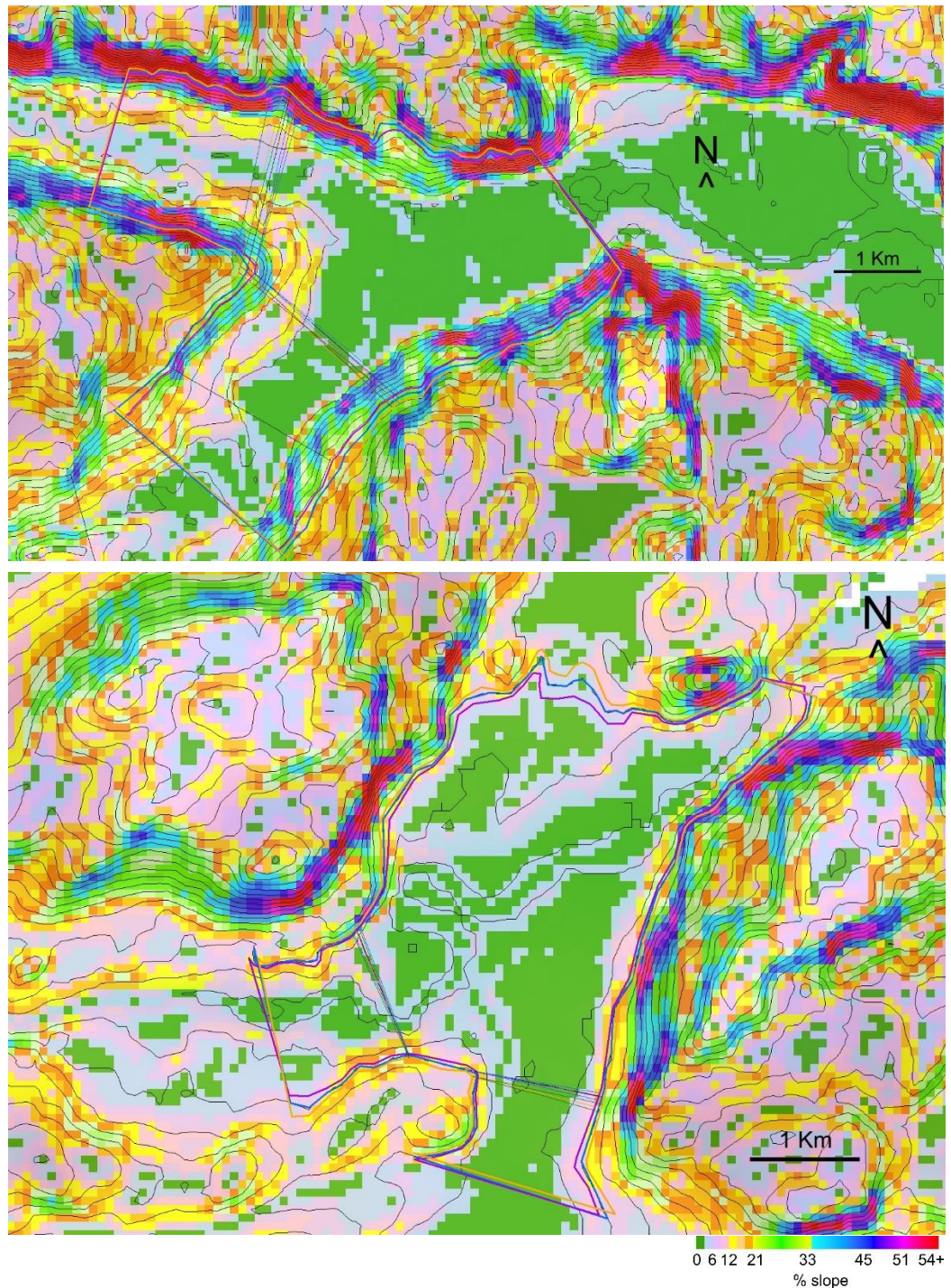


Figure 71. Confluence case studies 3 and 9, demonstrating excellent and poor outcomes (respectively) to testing of the sensitivity of confluence ratio to change in the working definition of confluence (extent and internal geometry).

(Top) Confluence case study 3 (ll coord 56.1, -62.9 DD), part of a well defined valley network (see text), with moderate relief; (Bottom) Confluence case study 9 (ll coord 55.7, -61.1 DD), coastal and areally scoured (see text) with very small relief. SRTM3 derived slope data are shown in a modified ESRI ArcGIS 'aspect' colour scale. Confluence extents are presented in blue, increased extents and corresponding down-tributary terminations (DTTs) are presented in orange, decreased extents and DTTs in purple. Variations in DTT position/orientation are presented in green and red (for increased extents) and blue (for decreased extents). SRTM contours are placed at 20 m intervals (black lines).

Because most confluences occur in well-defined valley networks where confluence relief is moderate or greater, the analysis predominantly uses the 'best' confluences (in terms of sensitivity to operator variability) where it is critical (i.e. hypothesis testing). Results show that, for such confluences, the sensitivity of confluence ratio to change in confluence extent and internal angles (by operator variability) is acceptable (i.e. the range in ratio value is small).

## 5.2 Qualitative analysis of the Labrador study region

The Labrador study region is a landscape of mountains, plateaus, and plains. Mountains are of moderately high elevation and have significant relief, especially in the north/ north-east (the Torngat Mountain Range), although there are areas of significant elevation (and less relief) in the south and south-west (e.g. the Mealy Mountains, and the Red Wine Mountains). Plateaus are of moderate elevation and are situated inland, to the west. Plains are of low elevation and are situated towards the coast, mainly to the east. The landscape shows evidence of significant glacial erosion (areal scouring and selective linear erosion). There are pronounced valley networks, particularly associated with the Torngat Mountain Range, and with Lake Melville (an estuary) in the south. Many of these valleys form fjords into the Labrador Sea (to the east) or Ungava Bay (to the north-west).

There are hundreds of glacial confluences apparent, which are primarily distributed within the valley networks. Although confluences are possibly the most easily identifiable exemplar of valley CSA decrease within landscapes, the narrowing of a valley (perhaps due to some lithological constriction or similar) is theoretically the simplest case example (figure 10). Simple valley narrowing however, is not obvious within the landscape.

Tens of thousands of overdeepenings are apparent, occurring at various scales. Hundreds of large (ice sheet, and large valley to regional scale) overdeepenings are apparent in the shallow bathymetry that surrounds most of Labrador, with significantly more numerous smaller (cirque and valley scale) overdeepenings apparent inland. Many lakes (from cirque to regional scale, most of which are overdeepenings) are also apparent in the interior of Labrador, especially in the inland plateaus. The location and variation in scale of the overdeepenings, suggests overdeepening initiation occurs by a variety of controls. There is a co-location relationship superficially visible between confluence and overdeepenings, especially within fjords.

For overdeepenings co-located with confluences, the majority of overdeepenings appear to occur at the approximate position of peak ice velocity within confluence. The approximate position of peak ice velocity has been suggested by empirical observations (i.e. Gudmundsson, et al., 1997; Berthier, et al., 2003; Gudmundsson, 1999; Byrd Polar

Research Center, Remote Sensing Laboratory, 2001a), see sections 2.7.2 and 4.3.4. Most other overdeepenings occur downstream of this position (typically at a mean distance of a few hundred metres). Upstream overdeepenings do occur, but are far less common and tend to be observed closer to the position of peak ice velocity than is the case for downstream examples of the phenomenon. The position of maximum overdeepening depth is typically situated downstream of the position of peak ice velocity, at a mean distance of a few kilometres.

The landscape has complex (mostly igneous and metamorphic) geology, with significant structural faulting in the mountains, plateaus, and plains. The structural faulting is largely east-west, and north-west to south-east trending in the north; with north-west to south-east, and some south-west to north-east trending faulting in the south. There is a convincing co-location relationship apparent between structural faulting and valley networks (and consequently also between structural faulting and confluences, with associated overdeepenings), especially within fjords.

### 5.3 Investigating ice velocity hypotheses (1&2) for Labrador study region

Outcomes of the first and second hypotheses are presented here, regarding whether overdeepenings are preferentially located at glacial valley confluences and whether overdeepening size is larger in confluences where there is greater ice velocity speed up. Summary statistics for the dataset are displayed in table 5.

	Km <sup>2</sup>
Total area of Labrador study region	450,406
Total overdeepened area within study region	64,295
Total overdeepened area (excluding lakes) within study region	20,172
Total confluence area within study region	7,458
Total confluence area within study region, liberal	9,743

**Table 5. Summary statistics for the Labrador study region.**

### 5.3.1 Evaluating the strength of the co-location relationship between glacial confluence and overdeepenings

The *actual* area of overdeepenings that are co-located with area of glacial confluence (considered as a single area of influence) has been compared with the *expected* area of overdeepenings that should be co-located by random chance. The comparison allows assessment of the strength of the co-location relationship, making it possible to determine whether actual co-location can be attributed purely to random occurrence (i.e. that the two variables are statistically wholly independent of one another), or whether actual co-location demonstrates a relationship that is significantly stronger (i.e. that one variable is potentially statistically dependent upon the other). Summary statistics of the co-location relationship, for subsets of overdeepenings, are shown in table 6.

Overdeepened area co-located with confluence	Km <sup>2</sup>	As a % of total overdeepened area in study region	As a proportion of expected value
Expected (random)	1065	1.66	1.0x
Actual	1792	2.79	1.7x
Expected (random), liberal	1391	2.16	1.0x
Actual, liberal	2268	3.53	1.6x
Expected (random), lakes excluded	334	1.64	1.0x
Actual, lakes excluded	1457	7.22	4.4x
Expected (random), liberal, lakes excluded	436	2.17	1.0x
Actual, liberal, lakes excluded	1840	9.12	4.2x

**Table 6. Summary statistics showing the area co-location relationship between glacial confluence and overdeepenings, for subsets of overdeepenings within the Labrador study region.**

The co-location relationship using a conservative down-trunk confluence perimeter is shown un-highlighted; using a liberal down-trunk confluence perimeter, in yellow; using a conservative perimeter but with water filled overdeepenings (i.e. lakes) excluded, in light blue; and using a liberal perimeter with lakes excluded, in dark yellow.

The statistics show that observed (actual) co-location is 1.7 times higher than is expected, were co-location to occur as a result of random chance (table 6; figure 72, top). This indicates a relationship between confluence and overdeepening location that is worthy of further investigation. The outcome of the chi-squared test of independence for this relationship is shown in table 7, confirming a statistically significant relationship.

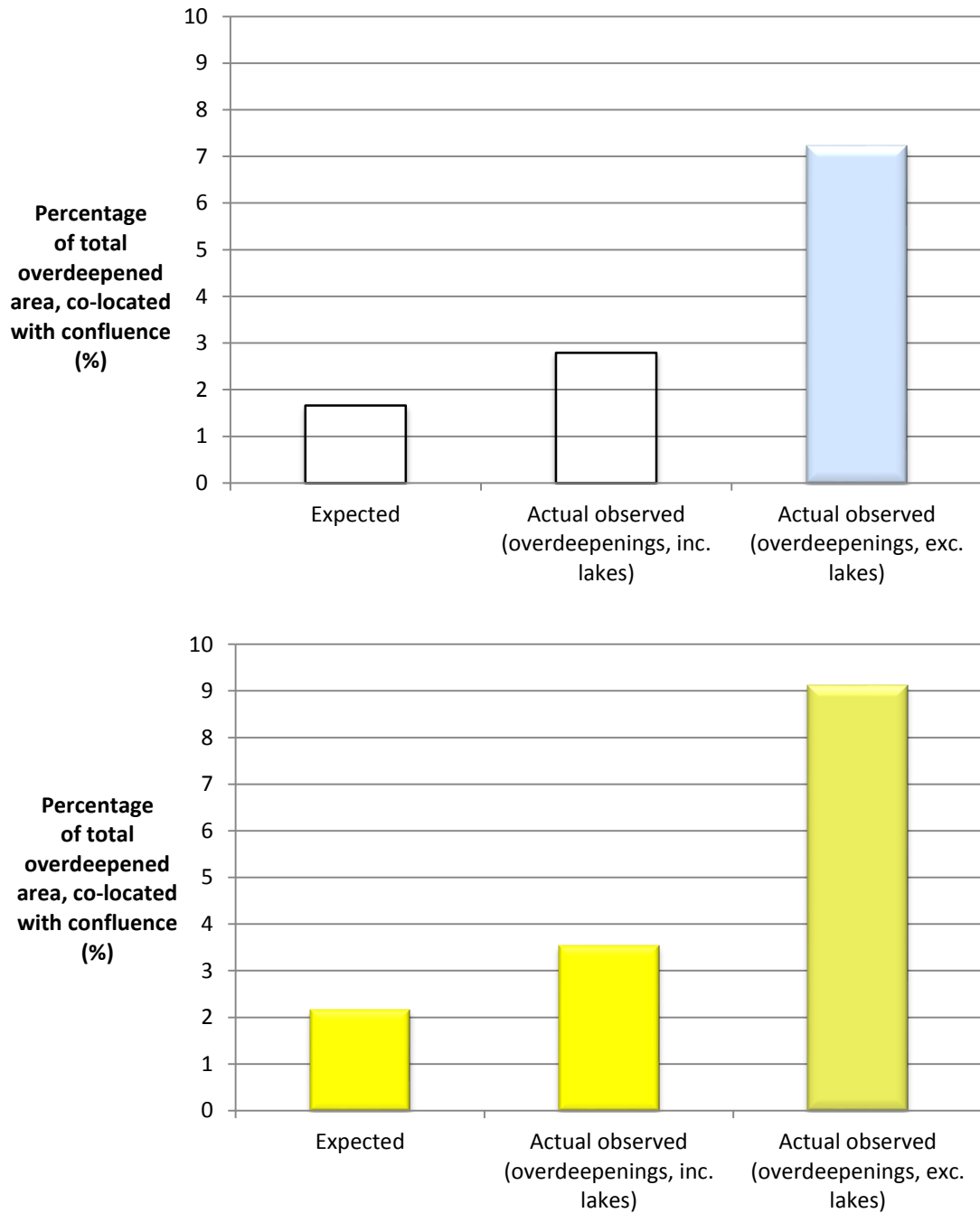


**Figure 72. Evaluating the strength of the area co-location relationship between glacial confluence and overdeepenings.**

**A comparison of the expected 'random' and the actual observed percentage of total overdeepened area within the Labrador study region, that is co-located with confluence, (Top) using a conservative down-trunk confluence perimeter, and (Bottom) using a liberal down-trunk confluence perimeter.**

For the more liberal down-trunk confluence perimeter, observed co-location is 1.6 times higher than expected by random chance (table 6; figure 72, bottom). This similarly indicates a relationship between liberal confluence and overdeepening location, albeit not as strong as that above.

If water filled overdeepenings (i.e. lakes) are ignored in calculations so that we deal just with those for which there can be most certainty, the difference is even greater. Observed co-location is 4.4 times higher than expected (table 6; figure 72, top). This indicates a significantly stronger co-location relationship when lakes are excluded. For the more liberal down-trunk confluence perimeter, observed co-location is 4.2 times higher than expected (table 6; figure 72, bottom). This similarly indicates a significantly stronger co-location relationship when lakes are excluded, albeit (again) not as strong as when a conservative down-trunk confluence perimeter is employed.

Visual assessment of DEMs indicates that many water filled overdeepenings occur at regional scale, and that many are located away from valley networks. This suggests that the dominant controls upon location and size of water filled overdeepenings will most likely occur at regional scale (away from valley networks, i.e. non-confluence related), rather than at the localized glacial valley scale associated with confluences. Further, water filled overdeepenings have less certainty (of being an overdeepening) than partially sediment filled and/or empty overdeepenings. This uncertainty implies possible (non-overdeepening related) controls upon lake location and size, especially away from valley networks. This suggests that the *expected* strength of the co-location relationship between water filled overdeepenings and confluence is likely to be overestimated in the calculation (due to an inflated *total* overdeepened area being considered), with the result that any actual co-location relationship is obscured. The consequence of this is that the strength of any co-location relationship between overdeepenings and confluence, when lakes are included, is significantly reduced (as shown in figure 72). Nevertheless, it is highly likely that many water filled overdeepenings are co-located with confluences, and so inclusion of water filled overdeepenings in analysis is important if the study is to be realistic.

<b>Observed Frequencies</b>	Area (Km <sup>2</sup> )		Total
	Within confluence	Outwith confluence	
Associated with overdeepening	1,792	62,503	64,295
Not Associated with overdeepening	5,666	380,445	386,111
<b>Total</b>	<b>7,458</b>	<b>442,948</b>	<b>450,406</b>

<b>Expected Frequencies</b>	Within confluence	Outwith confluence
Associated with overdeepening	1,065	63,230
Not Associated with overdeepening	6,393	379,718

<b>Alpha</b>	0.05
<b>df</b>	1
<b>Critical chi-square</b>	3.841458821
<b>P-Value</b>	3.2525E-130
<b>Observed chi-square</b>	> 70

**Table 7. The chi-squared test of independence for the relationship between confluence and overdeepening, within the Labrador study region.**

There is a statistically significant relationship between confluence and overdeepening. The observed chi-square value is much greater than the critical value required. The probability (P-value) of the observed chi-square value being a chance occurrence is much smaller than the pre-supposed level of significance (Alpha).

#### ***5.3.1.1 Evaluating conservative and liberal confluence perimeters, in order to best define the down-trunk extent of confluences***

Conservative down-trunk confluence perimeters better define the extent of confluences when compared with the liberal alternative. Visual inspection of conservative and liberal confluence perimeters support this statement. Conservative perimeters clearly provide a more natural representation of glacial confluence, but both definitions are explored as a sensitivity to this issue.

### 5.3.2 Co-location of individual confluences with overdeepenings

Simple GIS analysis (after some quality control, i.e. the removal of up-tributary overdeepenings from confluences, where too far removed from trunk valley, see section 4.5.3.1) provides basic statistics regarding the co-location of individual confluences with overdeepenings. These are shown in table 8.

	Confluences co-located with overdeepenings
Confluences with conservative perimeter	312 (56.2 %)
Confluences with liberal perimeter	361 (65.0 %)
Confluences with conservative perimeter, lakes excluded	224 (40.4 %)
Confluences with liberal perimeter, lakes excluded	268 (48.3 %)
Confluences with conservative perimeter, non-lakes excluded	128 (23.1 %)
Confluences with liberal perimeter, non-lakes excluded	156 (28.1 %)

**Table 8. Summary statistics showing the co-location of individual confluences with overdeepenings, for subsets of overdeepenings within the Labrador study region.**

The statistics show the number and percentage of individual confluences that are co-located with overdeepenings, out of a total of 555 confluences found in the study region. Where a conservative down-trunk confluence perimeter is used the statistic is shown un-highlighted; where conservative but with water filled overdeepenings (lakes) excluded from analysis, in light blue; where conservative but with empty and partially sediment filled overdeepenings (non-lakes) excluded, dark blue; where a liberal perimeter is used, yellow; where liberal with lakes excluded, dark yellow; and where liberal with non-lakes excluded, brown.

Results show that the majority of individual confluences are co-located with overdeepenings, regardless of which down-trunk confluence perimeter is utilised. This is expected because of the strong area co-location relationship that is observed between confluence and overdeepenings. Individual co-location is diminished when only those overdeepenings for which there can be most certainty are analysed (i.e. when water filled overdeepenings – lakes – are excluded), and is further significantly diminished when water filled overdeepenings are considered alone. Empty/ partially sediment filled overdeepenings (non-lakes) constitute most confluence co-located overdeepenings, but many water filled overdeepenings are also co-located and form an important part of the co-location dataset, which should be included in analysis if the study is to be realistic.

### 5.3.3 Co-location of individual overdeepenings with confluence

Viewed in the other direction, the percentage of individual overdeepenings that are co-located with glacial confluence (table 9) is relatively low. It can therefore be inferred that glacial confluence is (at best) only one of perhaps numerous controls that initiate overdeepenings (see sections 2.1 and 2.7). The location and variation in scale of overdeepenings apparent in the landscape suggests that other controls are likely to be of greater influence upon the phenomenon. Other controls are not restricted to (localised) glacial valleys (unlike the potential confluence control) and operate at a variety of spatial scales.

	Overdeepenings co-located with confluence
Confluences with conservative perimeter	411 (0.91 %)
Confluences with liberal perimeter	553 (1.22 %)
Confluences with conservative perimeter, lakes excluded	273 (1.49 %)
Confluences with liberal perimeter, lakes excluded	363 (1.99 %)

**Table 9. Summary statistics showing the co-location of individual overdeepenings with confluence, for subsets of overdeepenings within the Labrador study region.**

The statistics show the number and percentage of individual overdeepenings that are co-located with confluence, out of a total of 45,358 overdeepenings (or 18,270 when water filled overdeepenings – lakes – are excluded) found in the study region.

### 5.3.4 Investigating ice velocity hypothesis (1): Evaluating the influence of confluence cross-sectional area change upon overdeepening location

Comparison of the frequency distribution of confluence CSA ratio (ice velocity speed up) for subsets of individual confluences, co-located and not co-located with overdeepenings, allows the determination of the extent to which valley CSA change through a confluence affects overdeepening location.

As previously demonstrated, a strong co-location relationship is found between confluence and overdeepenings. Further to this, speed up as revealed by the CSA ratio is found more often in confluences where an overdeepening is present than where an overdeepening does not occur (figures 73 and 74).

The frequency distribution of confluence speed up ratio is shown in figure 73. A summary of these distributions (to allow comparison), including the distribution of confluence ratio for all confluences in the study region (regardless of overdeepening co-location) is shown in figure 74.

The majority of confluences demonstrate some degree of speed up (table 10), even when they have no overdeepenings. However, the percentage of confluences that demonstrate speed up is very much higher for confluences co-located with overdeepenings (75.3 %) than for confluences without (56.4 %). Findings are supported by mean, mode, and median ice velocity speed up values, which are significantly higher for confluences with overdeepenings than without.

	<b>Confluences with speed up</b>	Mean ratio	Mode ratio	Median ratio
Confluences co-located with overdeepenings (312 of 555)	235 of 312 (75.3 %)	2.3	1.0	1.3
Confluences not co-located with overdeepenings (243 of 555)	137 of 243 (56.4 %)	1.3	0.8	1.1
All confluences in the study region (555)	372 of 555 (67.0 %)	1.9	1.0	1.2

**Table 10. Summary statistics showing the number, percentage, and average ratio values of confluences demonstrating ice velocity speed up (i.e. a ratio > 1), for subsets of confluences within the Labrador study region.**

When the more liberal down-trunk confluence perimeter is employed, the percentage of confluences that demonstrate speed up for confluences with overdeepenings is 71.8 %. This is a weaker relationship than observed using the conservative perimeter (75.3 %). The conservative down-trunk confluence perimeter is used in all subsequent analysis.

The analysis above provides strong evidence in support of the hypothesis that overdeepenings are preferentially located at glacial valley confluences, because this is where ice velocity speed up (due to change in valley CSA) occurs.

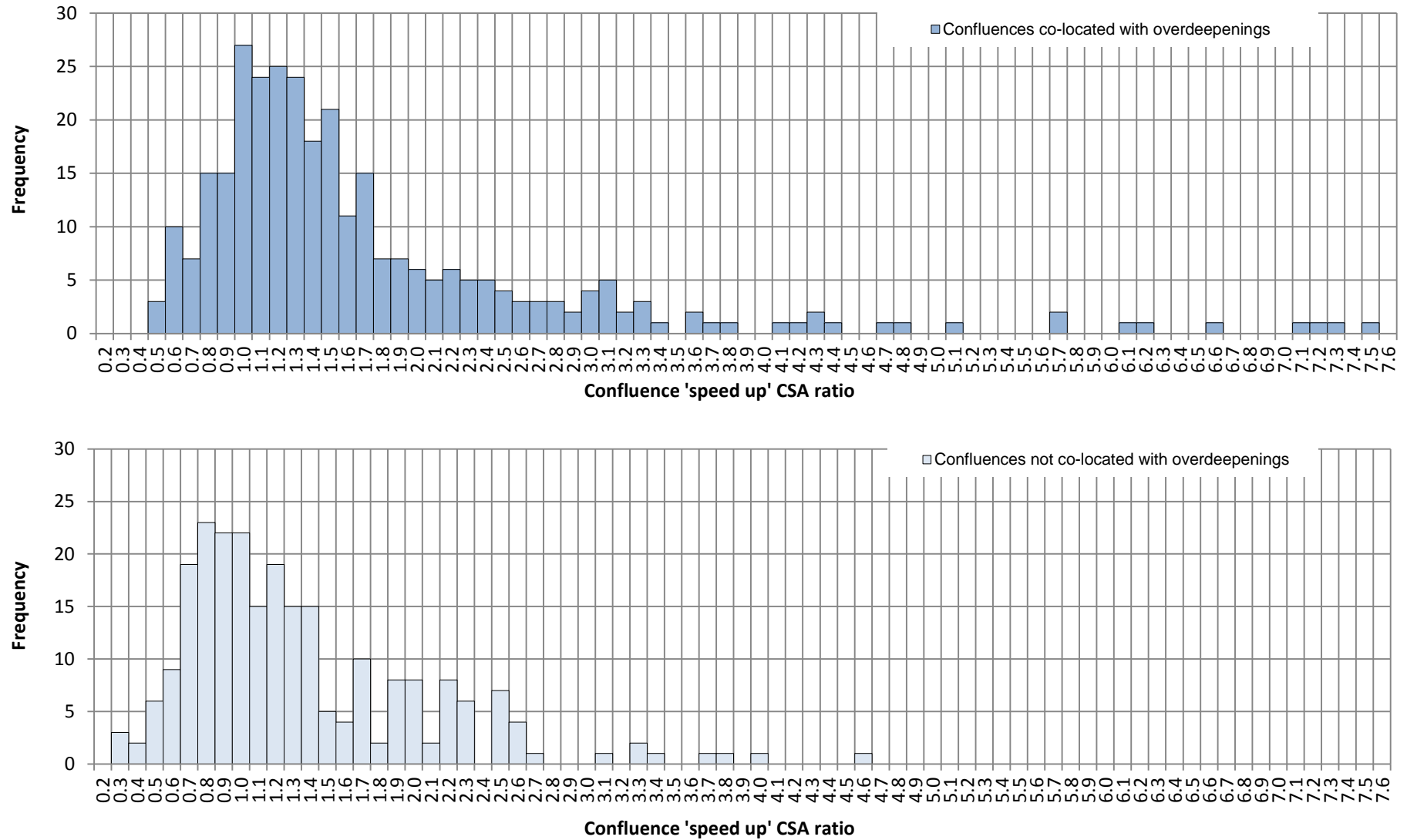


Figure 73. The frequency distribution of confluence 'speed up' ratio, for confluences with and without overdeepenings.

The frequency distribution of confluence 'speed up' ratio, for confluences co-located (blue, top) and not co-located (light blue, bottom) with overdeepenings. (Top) The distribution is unimodal (mode ratio is 1), with significant positive skew. Mean ratio value is 2.3. 75.3 % of confluences co-located with overdeepenings display a speed up ratio greater than 1. (Bottom) In comparison, the distribution for confluences not co-located with overdeepenings is similarly unimodal (mode ratio is lower, 0.8), with less positive skew. Mean ratio value is smaller (1.3). Only 56.4 % of confluences not co-located display a speed up ratio greater than 1. Confluences with overdeepenings show significantly greater speed up than confluences without them. This finding demonstrates that ice velocity speed up (due to change in valley CSA) influences overdeepening location, and so the likelihood of an overdeepening occurring.

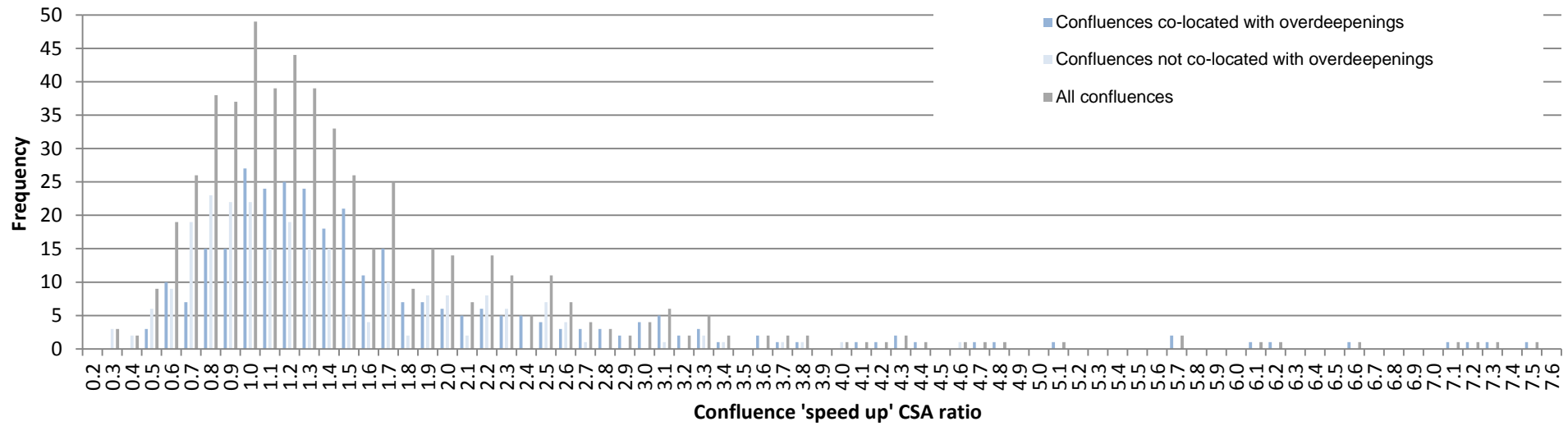


Figure 74. A summary graph of frequency distribution of confluence 'speed up' ratio.

A summary graph (to allow comparison), showing the frequency distribution of confluence 'speed up' ratio for confluences co-located with overdeepenings (blue), confluences not co-located with overdeepenings (light blue), and all confluences regardless of overdeepening co-location (grey) within the Labrador study region.

### 5.3.5 Investigating ice velocity hypothesis (2): Evaluating the influence of confluence cross-sectional area change upon overdeepening size

Analysis of the relationship between confluence CSA ratio at confluences, and co-located overdeepening metrics (after further quality control, i.e. removal of overdeepenings where scale does not match valley, and removal of confluences that are not so well defined at valley scale) allows the determination of the extent to which inferred speed up (via valley CSA change) through a confluence affects co-located overdeepening size.

A strong co-location relationship was earlier found between confluence and overdeepenings. As figures 75 and 76 demonstrates however, there is no relationship between confluence CSA ratio and overdeepening depth.

Interestingly, the relationship between confluence CSA ratio and overdeepening depth has ultimately provided significant outcomes later in this study when examining further subsets of the data pertaining to geological controls, but this initially poor relationship is illustrated fully in this section. The relationship is poor after some quality control (figure 75, see section 4.5.3.1 for details), and remains poor after further quality control (figure 76, section 4.5.4.1). Further, the relationship is weak when SRTM land topography and GEBCO bathymetry data are analysed separately, and when any outlying data are removed (figure 76). Findings are based on the 48 SRTM observations and 20 GEBCO observations (empty/ partially sediment filled overdeepenings) that remain after quality control. Water filled overdeepenings cannot be considered in this particular test, as there is an absence of depth information for these examples.

Analysis of the complete dataset therefore finds no evidence to support the hypothesis that overdeepening depth is larger in confluences where there is greater ice velocity speed up (due to change in valley CSA), because this is where ice erosion should be greatest.

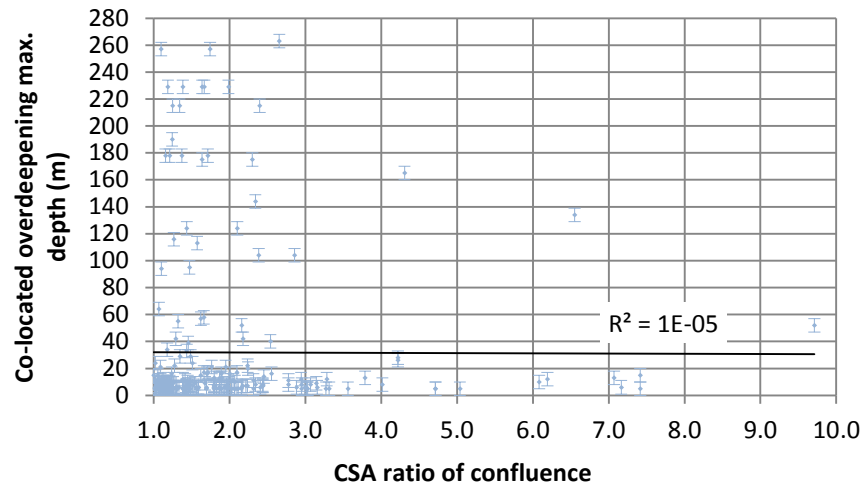


Figure 75. Relationship between confluence CSA ratio and the maximum depth of overdeepenings, after some quality control.

See text for details of quality control. No statistically significant relationship is found. Error bars indicate the largest absolute vertical linear error of the datasets used in this test, for this region. For >90 % of the SRTM land topography data used in this test, absolute vertical linear error is  $\leq 5$  m (Farr, et al., 2007). Absolute vertical linear error for GEBCO bathymetry data is 0.3 m for depths (below sea level) of less than 30 m, and 1 % of depth value for depths greater than 30 m (GEBCO, IHO and IOC, 2014), resulting in a maximum absolute vertical linear error of 2.7 m for GEBCO data in this test. The potential error for CSA ratio values is not easily quantified, but is not likely to limit interpretation of results.

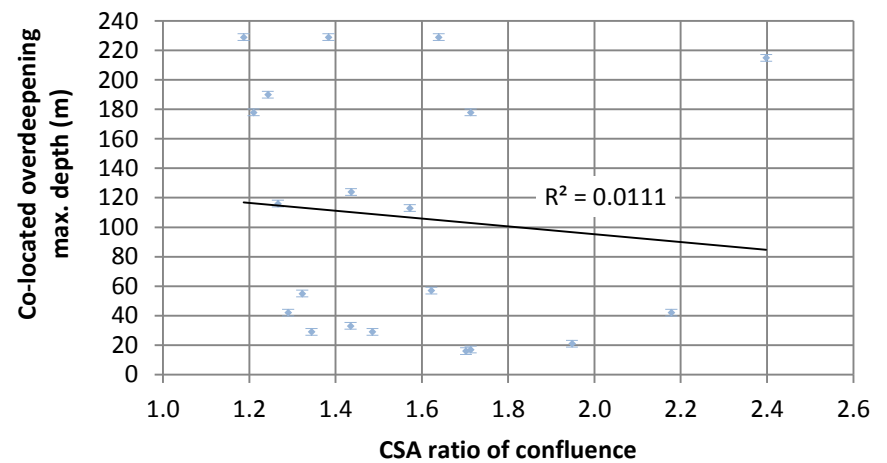
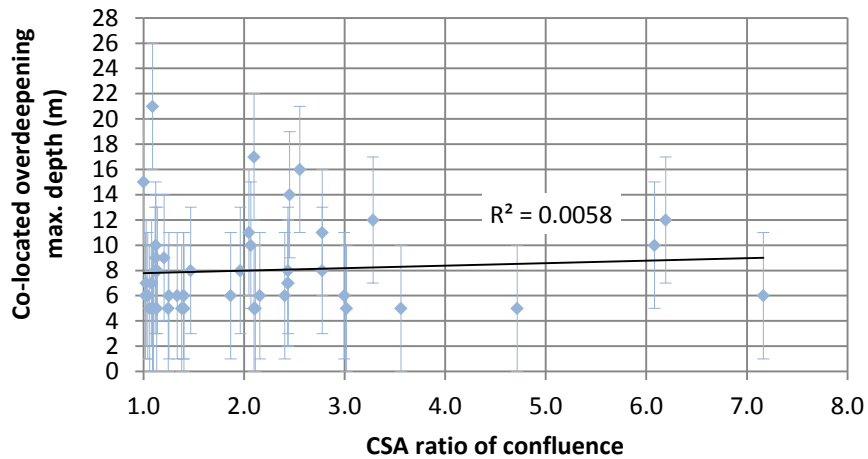
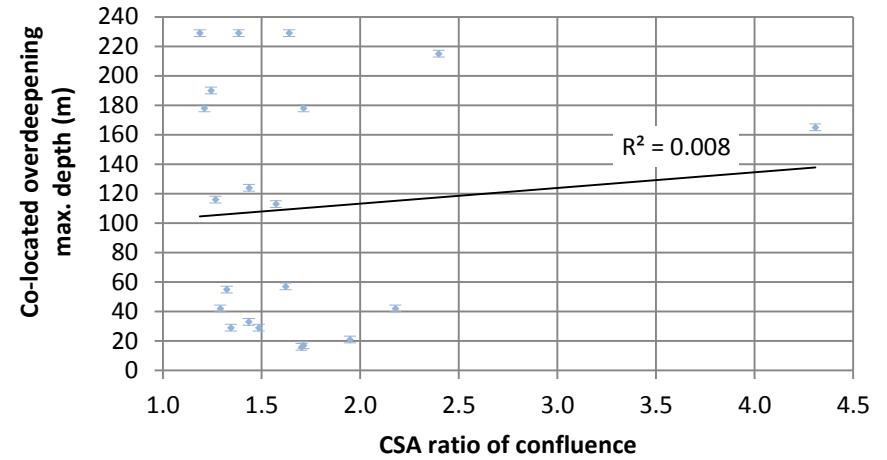
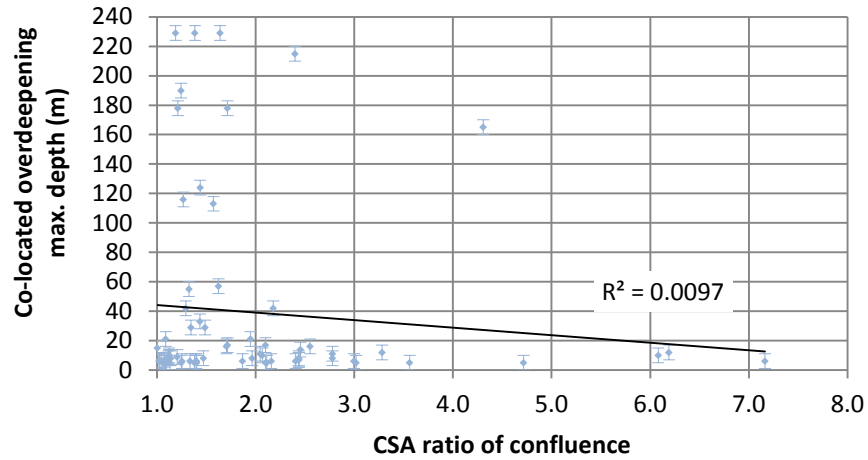


Figure 76. Relationship between confluence CSA ratio and the maximum depth of overdeepenings, after further quality control.

(Top Left) Relationship after further quality control (see text). (Bottom Left) As top left, but displaying SRTM data only. (Top Right) As top left, but displaying GEBCO data only. (Bottom Right) As top right (GEBCO data only), but with outlier removed. The plots demonstrate that no statistically significant relationships are found between confluence CSA ratio (ice velocity speed up) and co-located overdeepening maximum depth. These findings indicate that ice velocity speed up (due to change in valley CSA) does not influence overdeepening depth within the Labrador study region as a whole. Error bars indicate the largest absolute vertical linear error of the datasets used in each test, for this region. For >90 % of the SRTM land topography data used in these tests, absolute vertical linear error is  $\leq 5$  m (Farr, et al., 2007). Absolute vertical linear error for GEBCO bathymetry data is 0.3 m for depths (below sea level) of less than 30 m, and 1 % of depth value for depths greater than 30 m (GEBCO, IHO and IOC, 2014), resulting in a maximum absolute vertical linear error of 2.3 m for GEBCO data in these tests. The potential error for CSA ratio values is not easily quantified, but is not likely to limit interpretation of results.

## 5.4 Investigating bedrock erosion hypotheses (3&4) for Labrador study region

Outcomes of the third and fourth hypotheses are presented here, regarding whether overdeepenings more frequently occur in confluences with weaker bedrock and whether overdeepening size is larger in confluences with weaker bedrock. Summary statistics for the dataset are displayed in table 11.

	Km <sup>2</sup>
Total area of geological study region	293,453
Total area of igneous zone within geological study region	117,759
Total area of metamorphic zone within geological study region	87,010
Total area of sedimentary zone within geological study region	16,139
Total area of structural zone within geological study region	72,545
Total overdeepened area within geological study region (excluding segments of structural zone co-located overdeepenings that are outwith the structural zone, and excluding boundary overdeepenings; see section 4.6.2)	23,196
Total confluence area within geological study region (exclusions the same as above for segments of confluence; section 4.6.1.2)	3,103
Total confluence area co-located with overdeepening within geological study region (exclusions as above)	2,650

**Table 11. Summary statistics for the geological study of the Labrador region.**

### 5.4.1 Evaluating the strength of the co-location relationship between specific geological types and glacial confluence

The area of *glacial confluence* co-located with area of specific *geological types* has been compared against that expected by random chance, and the strength of any relationship assessed. This is to see if there is a preference for particular rock type or structures. Summary statistics are shown in table 12 and represented graphically in figure 77. These statistics indicate that actual co-location of igneous, metamorphic, and sedimentary geological zones with glacial confluence is lower than expected by random chance. Actual co-location of the structural geology zone with glacial confluence is 2.0 times higher than is expected to occur randomly.

Confluence area co-located with geological zone	Km <sup>2</sup>	As a % of total confluence area in study region	As a proportion of expected value
Expected (random), igneous	1245	40.1	1.0x
Actual, igneous	1135	36.6	0.9x
Expected (random), metamorphic	920	29.7	1.0x
Actual, metamorphic	331	10.7	0.4x
Expected (random), sedimentary	171	5.5	1.0x
Actual, sedimentary	77	2.5	0.5x
Expected (random), structural	767	24.7	1.0x
Actual, structural	1559	50.2	2.0x

**Table 12. Summary statistics showing the area co-location relationship between geological zones and glacial confluence within the Labrador study region.**

Statistics for the igneous zone presented in orange; metamorphic, red; sedimentary, brown; structural, yellow.

These results suggest mixed relationships between geological types and confluence location. There appears no control regarding igneous, but a strong avoidance of confluence with sedimentary and metamorphic rock types. There is a strong preference for confluence to be located in the structural zone. The outcome of the chi-squared test of independence for this latter relationship is shown in table 13, confirming a statistically significant relationship. The relationship between the structural zone and confluence is worthy of further investigation.

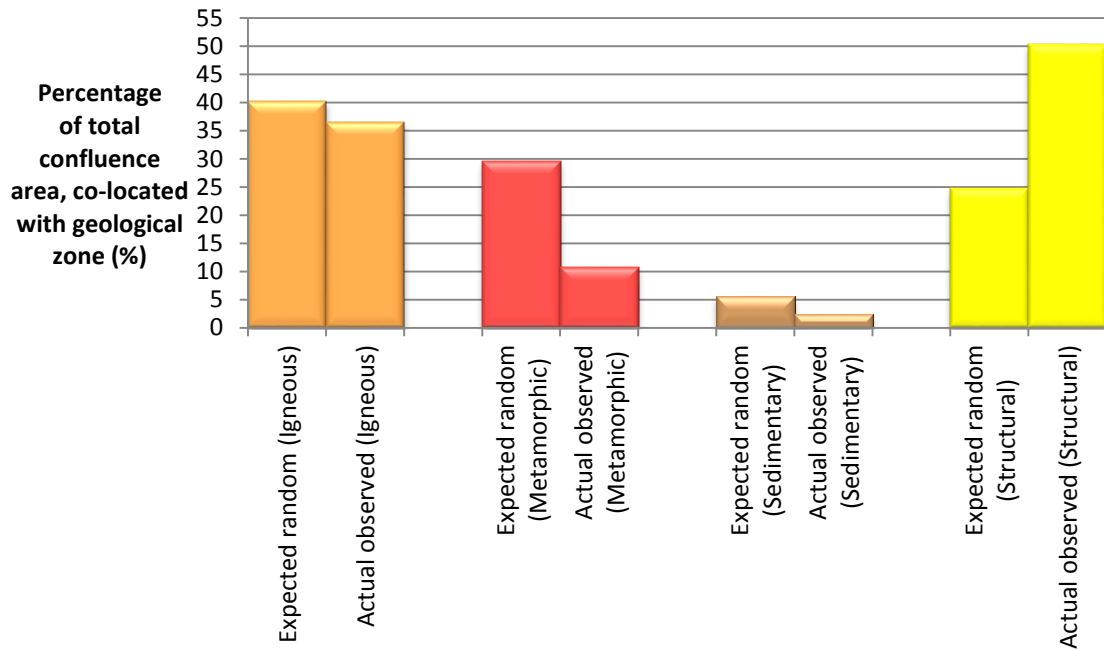


Figure 77. A comparison of the expected 'random' and the actual observed percentage of total confluence area that is co-located with geological zones, within the Labrador study region.

Observed Frequencies	Area (Km <sup>2</sup> )		
	Within ST zone	Outwith ST zone	Total
Associated with confluence	1,559	1,544	3,103
Not Associated with confluence	70,986	219,364	290,350
<b>Total</b>	<b>72,545</b>	<b>220,908</b>	<b>293,453</b>

Expected Frequencies	Within ST zone	Outwith ST zone
	Associated with confluence	767
Not Associated with confluence	71,778	218,572

<b>Alpha</b>	0.05
<b>df</b>	1
<b>Critical chi-square</b>	3.841458821
<b>P-Value</b>	1.1087E-240
<b>Observed chi-square</b>	> 70

Table 13. The chi-squared test of independence for the relationship between structural zone and confluence, within the Labrador study region.

There is a statistically significant relationship between structural (ST) zone and confluence. The observed chi-square value is much greater than the critical value required. The probability (P-value) of the observed chi-square value being a chance occurrence is much smaller than the pre-supposed level of significance (Alpha).

#### 5.4.2 Evaluating the strength of the co-location relationship between geological zones and overdeepenings

Similarly, the actual area of *overdeepening* co-located with area of *geological types* has been compared with that expected by random chance, to assess if rock type exerts a control on overdeepening occurrence. Summary statistics are shown in table 14 and represented graphically in figure 78. Statistics indicate that actual co-location of igneous, metamorphic, and sedimentary geological zones with overdeepening is slightly lower than expected by random chance, suggesting no overall control. Actual co-location of the structural geology zone with overdeepening is 1.6 times higher than is expected to occur randomly. These results suggest no relationship between most geological zones and overdeepening location, but a strong preference for overdeepenings to occur in structural zones, which is worthy of further investigation. The outcome of the chi-squared test of independence for this latter relationship is shown in table 15, confirming a statistically significant relationship.

Overdeepened area co-located with geological zone	Km <sup>2</sup>	As a % of total overdeepened area in study region	As a proportion of expected value
Expected (random), igneous	9308	40.1	1.0x
Actual, igneous	7962	34.3	0.9x
Expected (random), metamorphic	6878	29.7	1.0x
Actual, metamorphic	5495	23.7	0.8x
Expected (random), sedimentary	1276	5.5	1.0x
Actual, sedimentary	805	3.5	0.6x
Expected (random), structural	5734	24.7	1.0x
Actual, structural	8934	38.5	1.6x

**Table 14. Summary statistics showing the area co-location relationship between geological zones and overdeepenings within the Labrador study region.**

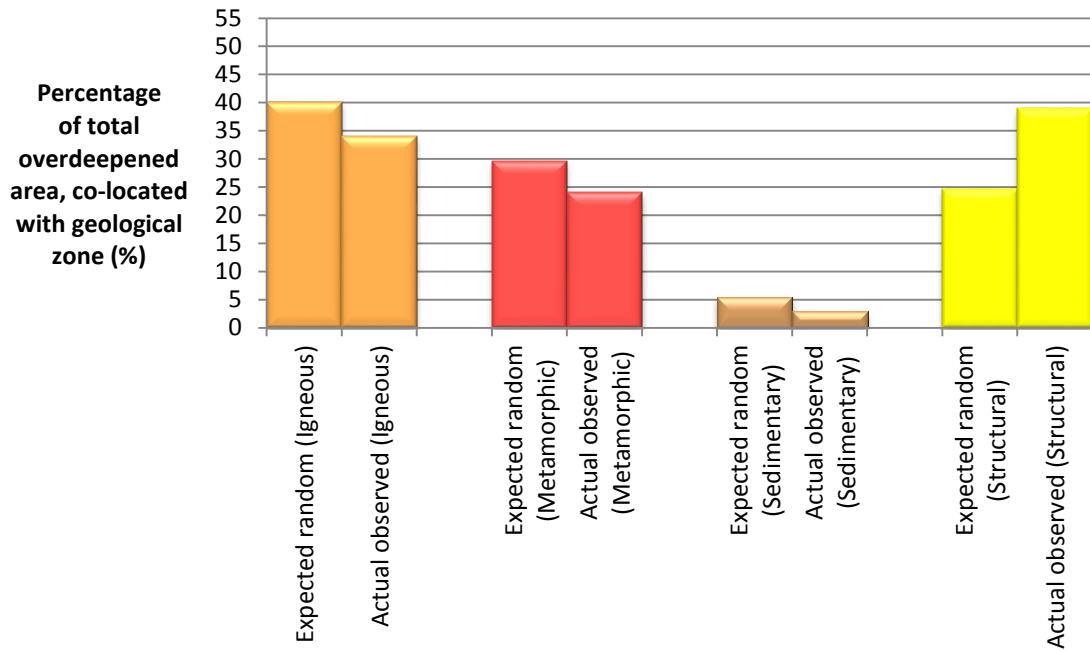


Figure 78. A comparison of the expected 'random' and the actual observed percentage of total overdeepened area, that is co-located with geological zones.

Observed Frequencies	Area (Km <sup>2</sup> )		
	Within ST zone	Outwith ST zone	Total
Associated with overdeepening	8,934	14,262	23,196
Not Associated with overdeepening	63,611	206,646	270,257
<b>Total</b>	<b>72,545</b>	<b>220,908</b>	<b>293,453</b>

Expected Frequencies	Within ST zone	Outwith ST zone
	Associated with overdeepening	5,734
Not Associated with overdeepening	66,811	203,446

<b>Alpha</b>	0.05
<b>df</b>	1
<b>Critical chi-square</b>	3.841458821
<b>P-Value</b>	< 1E-307
<b>Observed chi-square</b>	> 70

Table 15. The chi-squared test of independence for the relationship between structural zone and overdeepening, within the Labrador study region.

There is a statistically significant relationship between structural (ST) zone and overdeepening. The observed chi-square value is much greater than the critical value required. The probability (P-value) of the observed chi-square value being a chance occurrence is much smaller than the pre-supposed level of significance (Alpha).

### 5.4.3 Evaluating the strength of the relationship between glacial confluence and overdeepenings, within the structural geology zone

Because overdeepenings have been shown to preferentially seek out zones of pronounced structural geological weakness, the relationship is here explored further. Within the structural zone, the actual area of overdeepenings co-located with area of glacial confluence has been compared with that expected by random chance. Summary statistics are shown in table 16 and represented graphically in figure 79.

Because many overdeepenings that co-locate with confluence in the structural zone do so immediately off the coast of Labrador in the fjords and bays, this test cannot include them if the structural zone is defined as in the rest of this investigation. The problem here is that geological data stops at the coast of Labrador and does not extend into the bathymetry. Consequently many large overdeepenings that would otherwise contribute to the examined relationship are excluded from analysis; and the test therefore shows only a random relationship between confluence and overdeepening in the structural zone, when in fact the opposite is true.

In order to provide some indication as to the true relationship, expected and actual co-location has been estimated for a structural geology zone of slightly expanded area (which therefore includes said overdeepenings). This is acceptable because it is safe to assume (using available geological data to interpolate) that the structural zone continues across fjords and bays where the zone is apparent on either side of such features. Estimated overdeepened and confluence areas have correspondingly been increased in calculations, as appropriate. Estimated areas are assessed visually. Total overdeepened area in the expanded structural zone increases significantly to ~ 17,000 km<sup>2</sup>, total confluence area increases slightly to ~ 2,000 km<sup>2</sup>, and the size of the structural zone increases to ~ 90,000 km<sup>2</sup>. Actual co-location is conservatively estimated to be 1.5 times higher than expected by random chance. This suggests a strong relationship between confluence and overdeepening location within the structural zone. No chi-squared test of independence is performed on this relationship, because the data used are a best approximation.

Overdeepened area co-located with confluence	Km <sup>2</sup>	As a % of total overdeepened area in (expanded) structural geology zone	As a proportion of expected value
Estimated expected (random)	~ 397	2.2	1.0x
Estimated actual	~ 600	3.4	1.5x

**Table 16. Summary statistics showing the estimated area co-location relationship between glacial confluence and overdeepenings, within the (expanded) structural geology zone.**

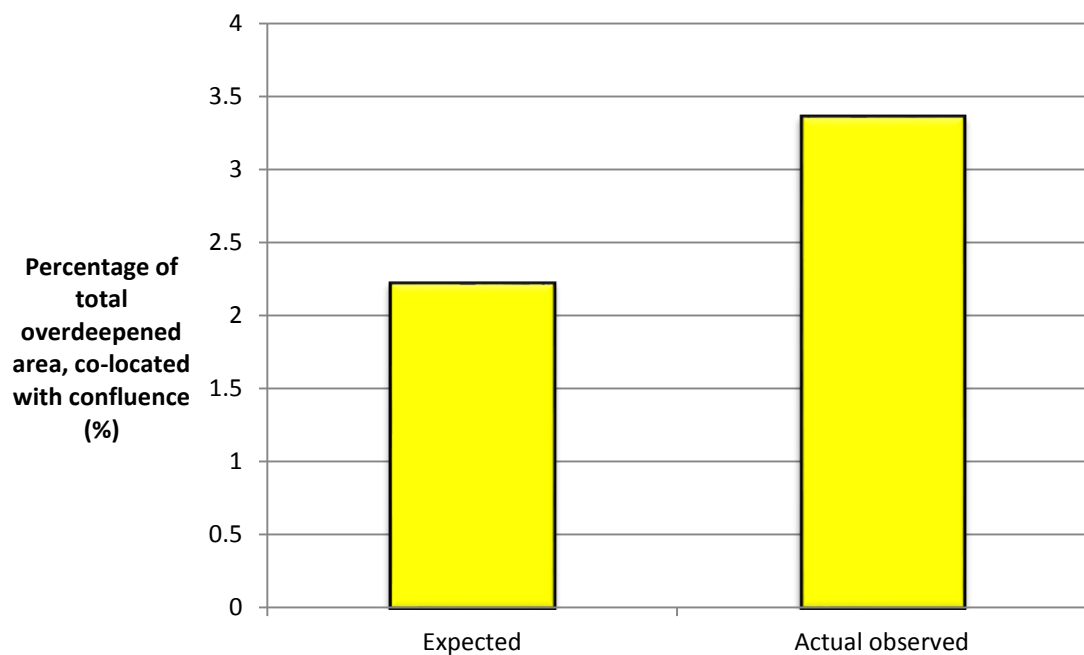


**Figure 79. A comparison of the expected 'random' and the actual observed percentage of total overdeepened area that is estimated to be co-located with glacial confluence within the (expanded) structural geology zone.**

#### 5.4.4 Evaluating the strength of the relationship between the structural geology zone and glacial confluence (for confluences with overdeepenings)

For confluences *with overdeepenings*, the actual area of glacial confluence that is co-located with the structural zone has been compared against that by random chance. Summary statistics are shown in table 17 and represented graphically in figure 80. Actual co-location is 2.0 times higher than expected, were co-location to occur randomly. This suggests a strong relationship between the structural zone and confluence location. The outcome of the chi-squared test of independence for this relationship is shown in table 18, confirming a statistically significant relationship.

Confluence area co-located with structural geology zone	Km <sup>2</sup>	As a % of total confluence area in study region	As a proportion of expected value
Expected (random)	655	24.7	1.0x
Actual	1326	50	2.0x

Table 17. Summary statistics showing the area co-location relationship between glacial confluence and the structural geology zone, for confluences with overdeepenings.

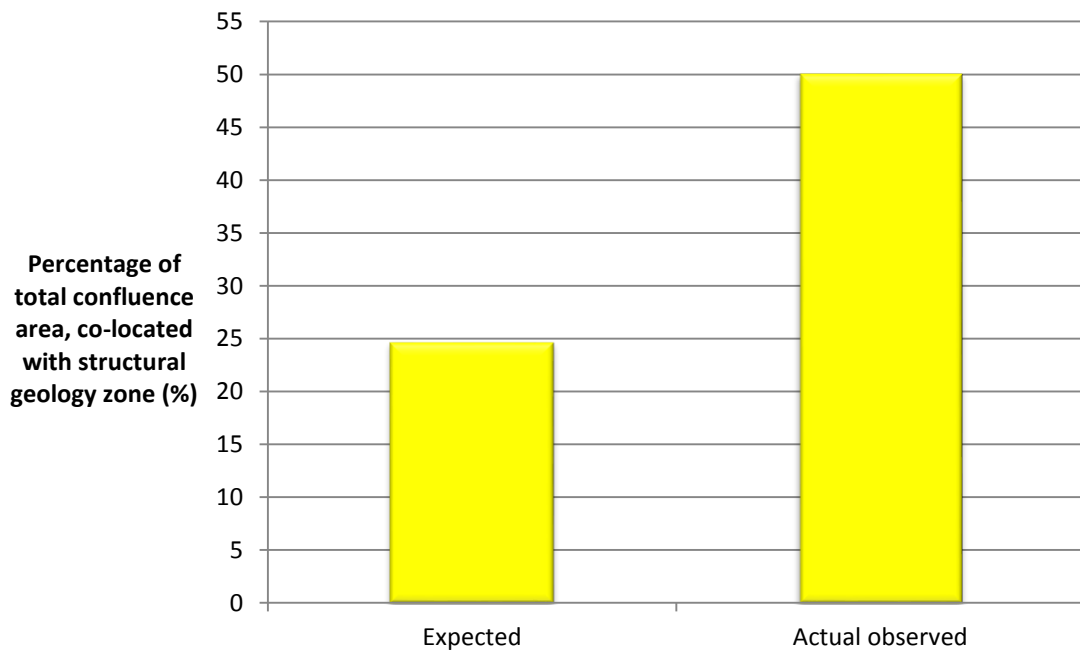


Figure 80. A comparison of the expected 'random' and the actual observed percentage of total glacial confluence area that is co-located with the structural geology zone (for confluences with overdeepenings).

<b>Observed Frequencies</b>	Area (Km <sup>2</sup> )		Total
	Within ST zone	Outwith ST zone	
Associated with confluence (with OD)	1,326	1,324	2,650
Not Associated with confluence (with OD)	71,219	219,584	290,803
<b>Total</b>	<b>72,545</b>	<b>220,908</b>	<b>293,453</b>

<b>Expected Frequencies</b>	Within ST zone	Outwith ST zone
Associated with confluence (with OD)	655	1,995
Not Associated with confluence (with OD)	71,890	218,913

<b>Alpha</b>	0.05
<b>df</b>	1
<b>Critical chi-square</b>	3.841458821
<b>P-Value</b>	2.6888E-202
<b>Observed chi-square</b>	> 70

**Table 18. The chi-squared test of independence for the relationship between structural zone and confluence (for only confluences that contain overdeepenings), within the Labrador study region.**

When only those confluences containing overdeepenings (ODs) are considered, there is a statistically significant relationship between structural (ST) zone and confluence. The observed chi-square value is much greater than the critical value required. The probability (P-value) of the observed chi-square value being a chance occurrence is much smaller than the pre-supposed level of significance (Alpha).

#### **5.4.5 Investigating bedrock erosion hypothesis (3): Evaluating the influence of confluence bedrock mass strength change upon overdeepenings within the structural geology zone**

Comparison of the frequency distribution of confluence CSA ratio (ice velocity speed up) for subsets of individual confluences with overdeepenings within and outwith the structural zone (after some quality control, section 4.5.3.1), allows the determination of the extent to which change in bedrock mass strength affects confluence co-located overdeepening location.

As previously discussed, strong co-location relationships are found between the structural zone and confluence, and between the structural zone and overdeepenings. A significantly greater number of confluences with overdeepenings demonstrate ice speed up than do confluences without. This occurs both within and outwith the structural zone (figure 81). These findings provide evidence of a relationship between confluence and overdeepening location specifically within the structural zone, which further supports the outcome of the first hypothesis, indicating that overdeepenings are preferentially located at glacial valley confluences. Unfortunately, further findings indicate that no greater number of confluences that have overdeepenings demonstrate ice speed up within than outwith the structural zone (figure 82).

The frequency distribution of confluence speed up ratio for confluences with and without overdeepenings, both within and outwith the structural zone, is shown in figure 81. A summary of the frequency distributions (for comparative purposes) for confluences co-located with overdeepenings within and outwith the structural zone is shown in figure 82, and related statistics displayed in table 19. The results show that for confluences with overdeepenings, the percentage that demonstrate speed up within the structural zone (74.4%) is remarkably similar to that observed outwith the structural zone (76.0%), and to that observed in the study region as a whole (75.3%). The percentage of confluences that demonstrate speed up for confluences without overdeepenings, within the structural zone is 52.7 %. Outwith the structural zone this value is 56.8 %.

	<b>Confluences with speed up</b>	Mean ratio	Mode ratio	Median ratio
Confluences co-located with overdeepenings within structural zone (121 of 195)	90 of 121 (74.4 %)	1.6	1.5	1.3
Confluences co-located with overdeepenings outwith structural zone (147 of 245)	112 of 147 (76.0 %)	3.1	1.0	1.4
Confluences co-located with overdeepenings within study region (312 of 555)	235 of 312 (75.3 %)	2.3	1.0	1.3

**Table 19. Summary statistics showing the number, percentage, and average ratio values of confluences demonstrating ice velocity speed up (i.e. a ratio > 1), for subsets of confluences co-located with overdeepenings within the Labrador study region.**

Statistics for within the structural zone presented in yellow; outwith the structural zone, purple; in the wider study region, un-highlighted. 268 confluences are co-located with overdeepenings in the geological study, out of a total of 440 confluences. There are 555 confluences in the wider study region.

Confluences with overdeepenings within the structural zone demonstrate a CSA ratio speed up frequency distribution that has a distinctive characteristic. The frequency distribution is bimodal (major mode ratio is 1.5, minor mode ratio is 1.1, figure 81, top). This characteristic is not apparent in confluences outwith the structural zone (figure 81, bottom) and may be diagnostic of a structural influence upon confluences, and (especially) overdeepenings within confluences. It is suggested that the observed bimodality perhaps indicates a preferred confluence speed up ratio value (of 1.5) where confluences control overdeepening initiation and where there is a structural control, in addition to the (1.0 to 1.1, or thereabouts) speed up ratio value that is common where confluences control overdeepening initiation without a structural control (figure 73).

This analysis finds no evidence to support the hypothesis that overdeepenings more frequently occur in confluences with weaker bedrock, where there is greater potential for erosion and removal of material (due to change in bedrock mass strength).

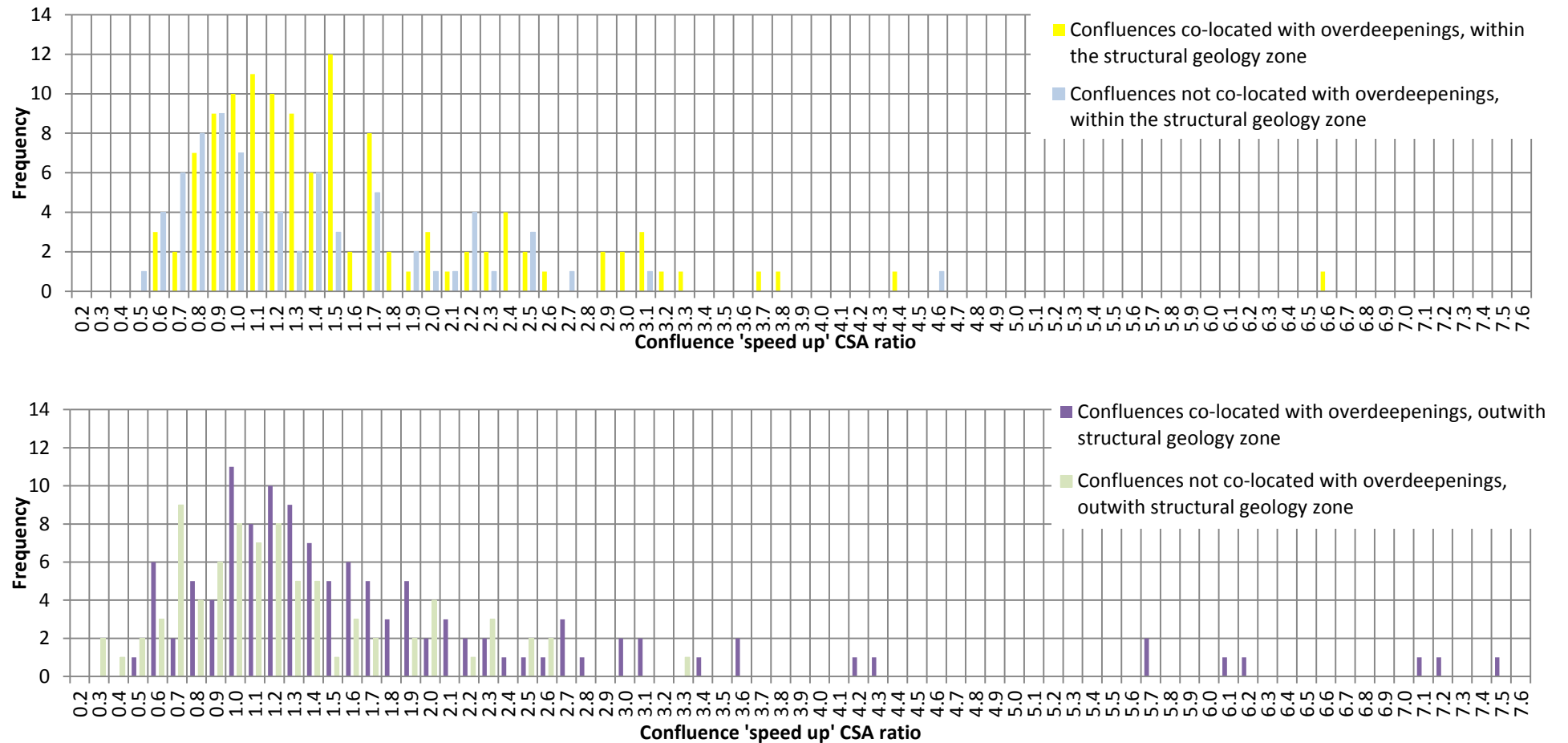


Figure 81. The frequency distribution of confluence 'speed up' ratio, for confluences with and without overdeepenings, within and outwith the structural geology zone.

(Top) Structural geology zone: The distribution for confluences co-located (yellow) and not co-located (light blue) with overdeepenings. The distribution for confluences with overdeepenings is bimodal (major mode ratio is 1.5, minor mode ratio is 1.1), with significant positive skew. Mean ratio value is 1.6. 74.4 % of confluences with overdeepenings display a speed up ratio greater than 1. In comparison, the distribution for confluences without is unimodal (mode ratio is lower, 0.9), with less positive skew. Mean ratio value is smaller (1.3). Only 52.7 % of confluences without display a speed up ratio greater than 1. Confluences with overdeepenings show significantly greater speed up than confluences without. (Bottom) Outwith the structural geology zone: The distribution for confluences co-located (purple) and not co-located (light green) with overdeepenings. The distribution for confluences with overdeepenings is unimodal (mode ratio is 1.0), with significant positive skew. Mean ratio value is 3.1. 76.0 % of confluences with overdeepenings display a speed up ratio greater than 1. In comparison, the distribution for confluences without is similarly unimodal (mode ratio is lower, 0.7), with much less positive skew. Mean ratio value is significantly smaller (1.2). Only 56.8 % of confluences without display a speed up ratio greater than 1. Confluences with overdeepenings show significantly greater speed up than confluences without, both within and outwith the structural zone. This concurs with findings for confluences within the study region as a whole, and provides further evidence that ice velocity speed up (due to valley CSA change) influences overdeepening location both within and outwith the structural zone of the study region.

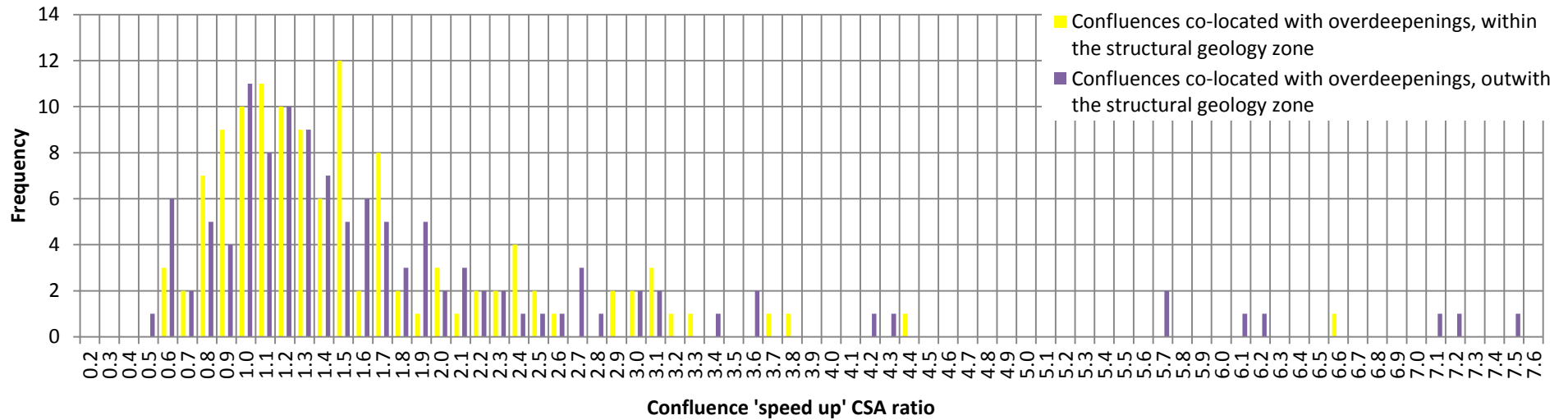


Figure 82. The frequency distribution of confluence 'speed up' ratio for confluences with overdeepenings, within and outwith the structural zone.

The distribution within the structural zone (yellow) is bimodal (major mode ratio is 1.5, minor mode ratio is 1.1) with significant positive skew. Mean ratio value is 1.6. 74.4 % of confluences within the structural zone display a speed up ratio greater than 1. In comparison, the distribution for confluences outwith the structural zone (purple) is unimodal (mode ratio is 1.0) with greater positive skew. Mean ratio value is significantly larger (3.1). 76.0 % of confluences outwith the structural zone display a speed up ratio greater than 1. Confluences co-located with overdeepenings within the structural zone consequently show no greater speed up than confluences co-located outwith the structural zone. These findings indicate that change in bedrock mass strength does not influence confluence co-located overdeepening location within the Labrador study region.

#### 5.4.5.1 *The structural geology zone, further statistics: Co-location with individual confluences and overdeepenings*

Table 20 shows summary statistics for individual confluences, and for those co-located with overdeepenings in the geological study region.

Confluences occurring in the igneous zone	142 of 440
Confluences co-located with overdeepenings in the igneous zone	83 of 268
Confluences occurring in the metamorphic zone	48 of 440
Confluences co-located with overdeepenings in the metamorphic zone	30 of 268
Confluences occurring in the sedimentary zone	12 of 440
Confluences co-located with overdeepenings in the sedimentary zone	8 of 268
Confluences occurring at a lithological boundary	43 of 440
Confluences co-located with overdeepenings at a lithological boundary	26 of 268
Confluences occurring in the structural zone	195 of 440
Confluences co-located with overdeepenings in the structural zone	121 of 268

**Table 20. Summary statistics showing the number of individual confluences in the geological study region that occur within each geological zone, and that are co-located with overdeepenings in each zone.**

Previous results show that actual confluence and overdeepened area within the structural geology zone is significantly greater than is expected by chance. Further, statistics indicate that within the geological study region, the largest group of confluences (49.1 %) occurs within the structural zone (51.8 % after normalisation by geological zone area). 50.0 % of all confluences that contain overdeepenings (after some quality control, section 4.5.3.1) occur within the structural zone (again, the largest group; 51.9 % after normalisation). See table 21.

Of 349 confluence co-located overdeepenings where geological zone classification has high certainty, 150 (43.0 %, the largest group of) overdeepenings are located within the structural zone. See section 6.2, for further discussion.

		After normalisation by geological zone area
Confluences occurring in the structural zone	195 of 397 (49.1 %)	51.8 %
Confluences co-located with overdeepenings in the structural zone	121 of 242 (50.0 %)	51.9 %

**Table 21. Summary statistics showing the number and percentage of individual confluences in the geological study region that occur in the structural zone and that are co-located with overdeepenings in the structural zone.**

The percentage is calculated on the basis of the 397 (of 440) confluences in the geological study region for which co-location with a particular zone can be determined, confluences on the boundary between lithological zones being excluded from analysis; and similarly on the basis of the 242 (of 268) confluences with overdeepenings in the geological study region that are not on a lithological boundary.

#### *5.4.5.2 The structural geology zone, further statistics: Analysis of confluence area and down-trunk valley width*

Statistics indicate that confluences within the structural zone are particularly large (by mean area, 17.3 km<sup>2</sup>) and wide (at trunk valley pinch, mean width 2.2 km) when compared with confluences outwith the structural zone (10.2 km<sup>2</sup> and 1.5 km respectively) and in the study region at large (14.1km<sup>2</sup> and 1.8 km respectively; see table 22 for summary). This is reflected in the significantly lower mean ratio (of 1.6) for confluences co-located with overdeepenings within the structural zone, relative to those outwith the structural zone (for which the ratio is 3.1). Further, groups of confluences co-located with overdeepenings are consistently larger and wider than are groups of confluences where co-location with overdeepenings is not considered (table 22), or where confluences are not co-located. Confluences within the structural zone do not exhibit the pinch feature (i.e. at the conservative down-trunk valley termination) to the same extent as confluences outwith the structural zone. See section 6.2, for further discussion.

Previous results provide no evidence to support a causal relationship between change in bedrock mass strength and confluence co-located overdeepening location. Nevertheless, findings suggest that other relationships between change in bedrock mass strength and overdeepening size should be observed.

Confluence Location	Mean area of confluences (km <sup>2</sup> )	Mean trunk valley width at pinch (km)	Mean 'speed up' ratio of confluences
Within the study region	14.1	1.8	1.9
Within study region (co-located with overdeepenings)	19.1	2.1	2.3
Within the geological study region	13.9	1.9	1.9
Within geological study region (co-located with overdeepenings)	18.3	2.1	2.3
Within structural geology zone	17.3	2.2	1.5
Within structural geology zone (co-located with overdeepenings)	22.3	2.5	1.6
Outwith structural geology zone	10.2	1.5	2.4
Outwith structural geology zone (co-located with overdeepenings)	13.8	1.6	3.1

**Table 22. Statistics, for subsets of confluences within the Labrador study region.**

Statistics for within the study region presented un-highlighted; within the geological study region, grey; within the structural zone, yellow; outwith the structural zone, purple.

#### **5.4.6 Investigating bedrock erosion hypothesis (4): Evaluating the influence of confluence bedrock mass strength change upon overdeepening size within the structural geology zone**

It is fair to presume that due to the high level of faults, joints and other planes of weakness within the defined structural geology zone, that these areas have lower bedrock mass strength and are perhaps more susceptible to glacial erosion. To explore this, analysis was made of the relationship between confluence CSA ratio and overdeepening depth, both within and outwith the structural zone.

The relationship between confluence CSA ratio and the maximum depth of overdeepenings outwith the structural zone is not statistically significant after some quality control (figure 83, top; section 4.5.3.1). The relationship remains not significant after further quality control (figure 83, bottom; section 4.5.4.1 and 4.6.6.1). The findings are based on the 24 SRTM observations that remain after quality control.

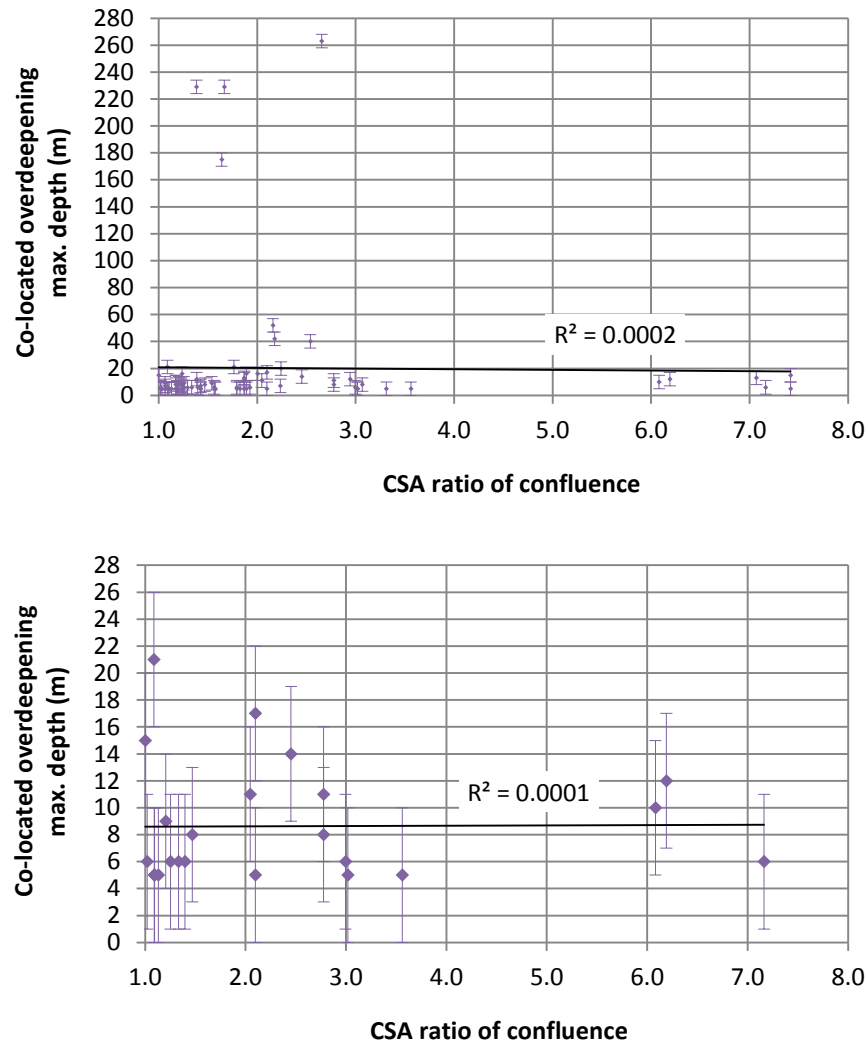


Figure 83. Relationship between confluence CSA ratio and the maximum depth of co-located overdeepenings, outwith the structural geology zone.

(Top) Relationship between ratio and depth of overdeepenings, after some quality control (see text). (Bottom) As top, after further quality control (see text). The plots demonstrate that no statistically significant relationships are found between confluence CSA ratio (ice velocity speed up) and co-located overdeepening maximum depth, outwith the structural geology zone. When considered alongside figure 84, findings indicate that overdeepening depth will be greater in confluences influenced by weaker bedrock (i.e. within the structural geology zone) within the Labrador study region. Error bars indicate the largest absolute vertical linear error of the datasets used in each test, for this region. For >90 % of the SRTM land topography data used in these tests, absolute vertical linear error is  $\leq 5$  m (Farr, et al., 2007). Absolute vertical linear error for GEBCO bathymetry data is 0.3 m for depths (below sea level) of less than 30 m, and 1 % of depth value for depths greater than 30 m (GEBCO, IHO and IOC, 2014), resulting in a maximum absolute vertical linear error of 2.7 m for GEBCO data in this test (top). The potential error for CSA ratio values is not easily quantified, but is not likely to limit interpretation of results.

The relationship between confluence CSA ratio and the maximum depth of co-located overdeepenings within the structural zone is shown in figure 84. The relationship is statistically significant within SRTM land topography data, after all quality control has been undertaken. The relationship is not significant within GEBCO bathymetry data. The findings show a positive linear relationship between the independent and the dependent variable within the SRTM data, with an adjusted  $r^2$  value of 0.265 (a moderately strong value for goodness of fit of a statistical model, when encountered in the natural world) and a significance value (p-value) of 0.024 (i.e. there is confidence that the relationship does not occur by chance, as it is comfortably statistically significant at the 95 % confidence level). Confluence CSA ratio values range from 1.0 to 3.3. The potential error for CSA ratio values is not easily quantified, but is not likely to limit the interpretation of results. Overdeepening depths range between 5m and 16 m, although depths are normally between 6 m and 10 m. Absolute vertical linear error for >90 % of the SRTM land topography data used in this test, for this region is  $\leq 5$  m (Farr, et al., 2007). The findings are based on the 16 SRTM observations and 14 GEBCO observations that remain after quality control.

In summary, strong co-location relationships are found between the structural zone and confluence, and between the structural zone and overdeepenings. Further, as outlined above, a statistically significant relationship is found between confluence CSA ratio and the maximum depth of overdeepenings that occur within the structural zone. Such a relationship is not observed for those overdeepenings outwith the structural zone. This finding of a relationship within the structural zone is interpreted as evidence that *when* bedrock strength is sufficiently weak, overdeepening depth scales with speed up (using the proxy of CSA ratio).

The relationship between confluence CSA ratio and the maximum depth of co-located overdeepenings within the structural zone is modest (in terms of magnitude of overdeepening depths) but statistically significant, and so results are valid but should be treated with caution. The relationship is scale dependent. It is only observed at local (confluence) scale (using SRTM3 land topography data) and is not detected at regional (large valley, to ice sheet) scale (using GEBCO bathymetry data), at which scale presumably other controls upon overdeepening size will dominate.

This analysis provides good evidence in support of the hypothesis that overdeepening size is larger in confluences with weaker (faulted) bedrock, because of the greater potential for erosion and removal of material.

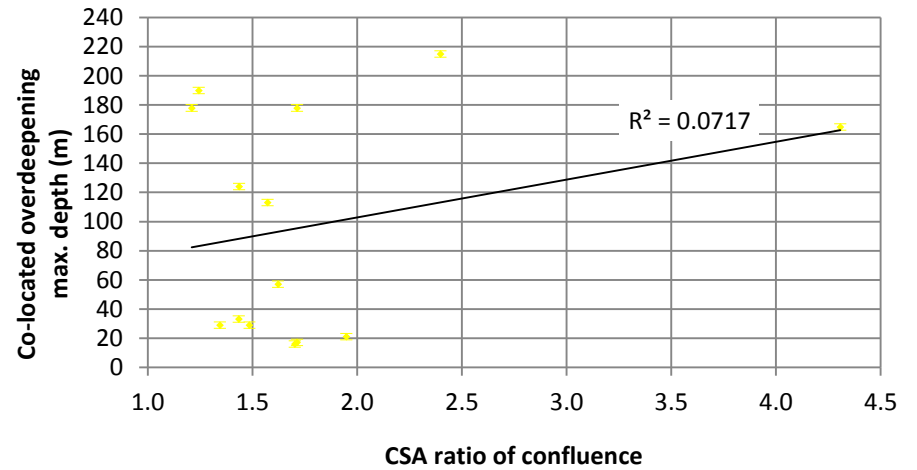
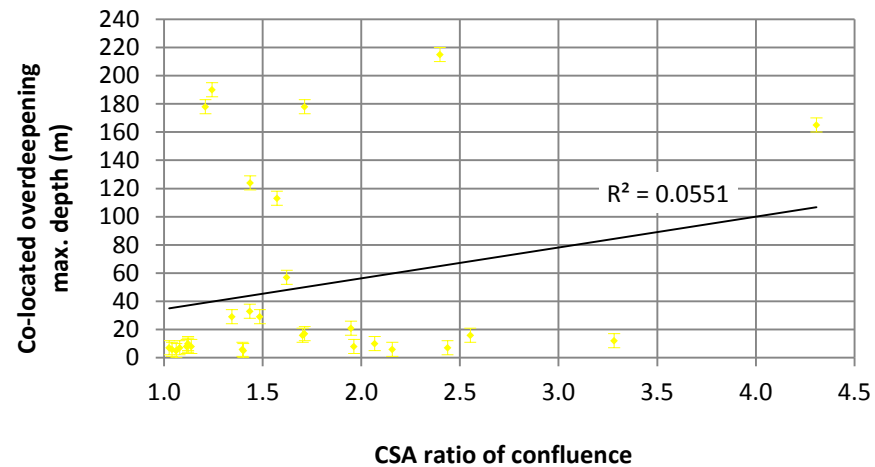
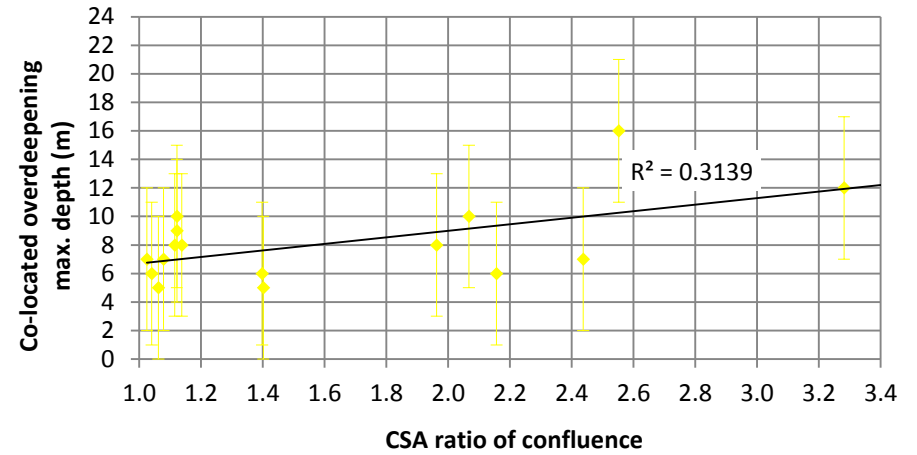
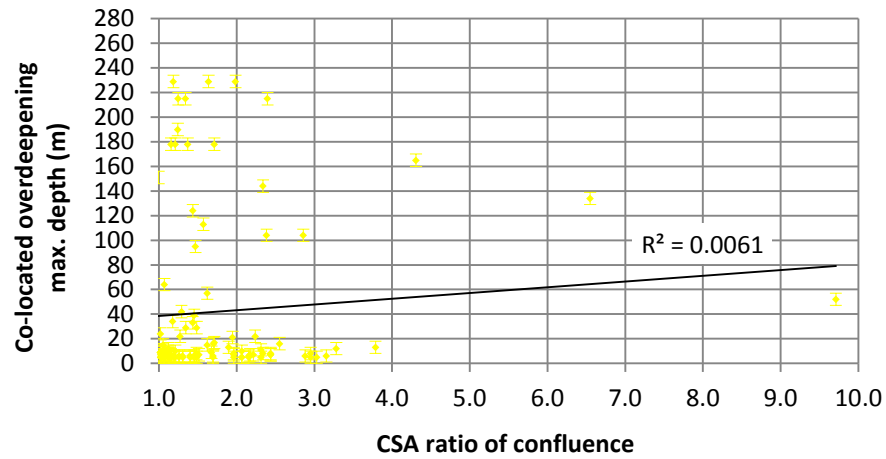


Figure 84. Relationship between confluence CSA ratio and the maximum depth of co-located overdeepenings, within the structural geology zone.

(Top Left) Relationship between ratio and depth of overdeepenings, after some quality control (see text). (Bottom Left) As top left, after further quality control (see text). (Top Right) As bottom left, but displaying SRTM data only. (Bottom Right) As bottom left, but displaying GEBCO data only. The plots demonstrate a statistically significant relationship between confluence CSA ratio (ice velocity speed up) and co-located overdeepening maximum depth, for SRTM data only (see text). When considered alongside figure 83, findings indicate that overdeepening depth will be greater in confluences influenced by weaker bedrock (i.e. within the structural geology zone) within the Labrador study region. Error bars indicate the largest absolute vertical linear error of the datasets used in each test, for this region. For >90 % of the SRTM land topography data used in these tests, absolute vertical linear error is  $\leq 5$  m (Farr, et al., 2007). Absolute vertical linear error for GEBCO bathymetry data is 0.3 m for depths (below sea level) of less than 30 m, and 1 % of depth value for depths greater than 30 m (GEBCO, IHO and IOC, 2014), resulting in a maximum absolute vertical linear error of 2.3 m for GEBCO data in these tests. The potential error for CSA ratio values is not easily quantified, but is not likely to limit interpretation of results.

## 5.5 Testing reproducibility: A supplementary (Swiss) study region

It is useful to examine the extent to which some findings for Labrador are more widely replicable. This is explored by investigation in Switzerland, a region noted for its overdeepenings.

### 5.5.1 Investigating bedrock erosion hypothesis (4): Evaluating the influence of confluence bedrock mass strength change upon overdeepening size

By examining the extent to which outcomes of the bedrock erosion hypothesis (4) for Labrador are more widely replicable elsewhere, we test the replicability of outcomes for the most complex hypothesis postulated in this investigation. This is readily testable as an easy supplementary exercise, using a small group of confluences that contain overdeepenings in the Swiss region. To indicate replicability, the test does not require the identification and definition of many overdeepenings and confluences (unlike that undertaken to fully examine the range of hypotheses explored in the Labrador study), nor does the test require the duplication of much methodology used in the Labrador study. To essentially repeat the entirety of the Labradorian analysis for the Swiss study region would be very time consuming and is consequently outside of the feasible scope of this investigation.

A statistically significant relationship is found between confluence CSA ratio and the maximum depth of overdeepenings that occur within the structural zone of the Swiss study region. This finding supports the outcome of the Labrador study, which tests the hypothesis that overdeepening depth will be greater in confluences influenced by weaker bedrock (i.e. within the structural zone).

The relationship between confluence CSA ratio and the maximum depth of overdeepenings within the structural zone of the Swiss study region is statistically significant, after all quality control has been undertaken as for Labrador (figure 85). The relationship is prominent in most of the data, prior to further quality control, but is ruined by a few outliers which are presumably influenced by other local scale controls. Relative to results of the Labrador study, findings show an improved positive linear relationship between the independent and the dependent variable, with a slightly weaker adjusted  $r^2$  value of 0.230 (nevertheless, this remains a moderately strong value for goodness of fit of a statistical model, when encountered in nature) and a slightly weaker significance value (p-value) of 0.035 (though still comfortably statistically significant at the 95 % confidence level). Confluence CSA ratio values range from 1.1 to 2.7 and so are broadly similar to those encountered in Labrador. Overdeepening depths range between 13 m and 61 m, although depths are normally between 23 m and 43 m. Depth values are therefore

significantly greater in magnitude in the Swiss study region than in the Labrador study region. Absolute vertical linear error for >90 % of the SRTM land topography data used in this test, for this region is  $\leq 10$  m (Farr, et al., 2007), owing to the typically more rugged terrain in this location compared to the terrain in the Labrador study region. The findings are based on the 16 observations that remain after quality control.

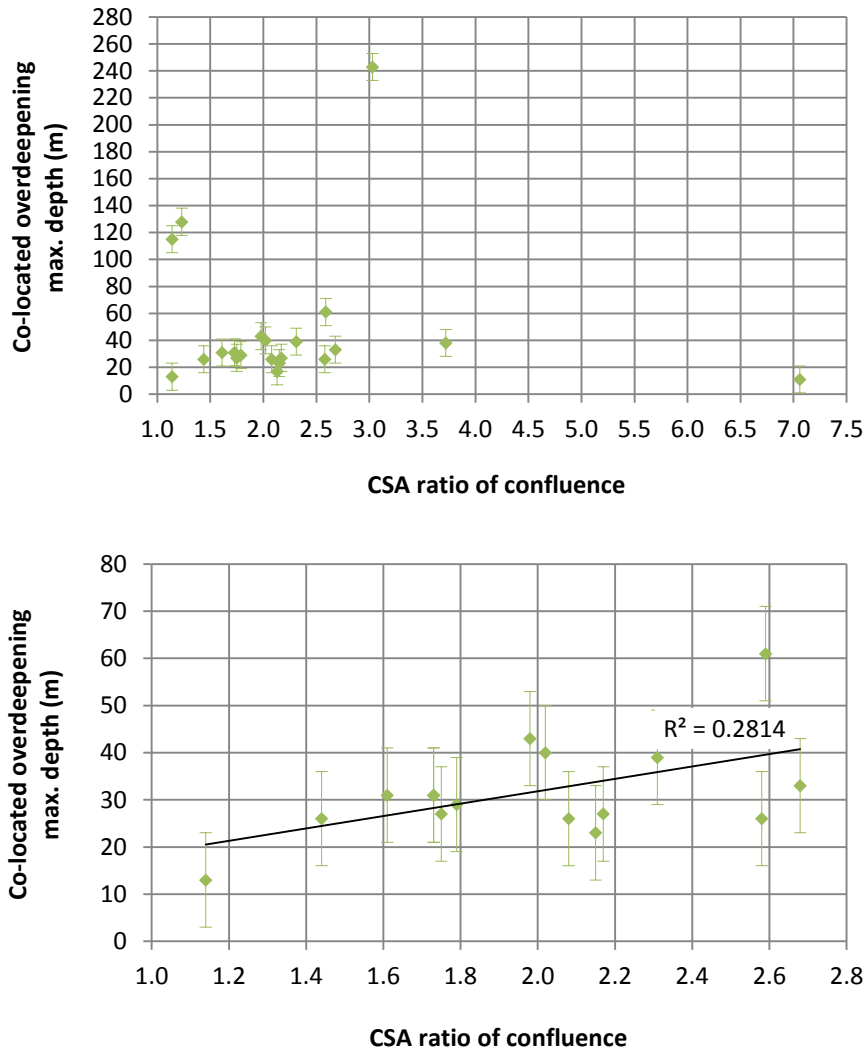


Figure 85. Relationship between confluence CSA ratio and the maximum depth of co-located overdeepenings, within the structural geology zone, Swiss study region.

(Top) Relationship between ratio and depth of overdeepenings, after some quality control (see text). (Bottom) As top, after further quality control (see text, and after removal of outliers). The plots demonstrate a statistically significant relationship between confluence CSA ratio (ice velocity speed up) and co-located overdeepening maximum depth, using SRTM data (see text). This finding supports the outcome of the similar Labrador analysis, which tested the hypothesis that overdeepening depth will be greater in confluences influenced by weaker bedrock (i.e. within the structural geology zone). Error bars indicate the absolute vertical linear error for >90 % of the SRTM land topography data used in these tests, for this region ( $\leq 10$  m) (Farr, et al., 2007). The potential error for CSA ratio values is not easily quantified, but is not likely to limit interpretation of results.

Despite slightly weaker statistical characteristics (i.e. adjusted  $r^2$  value, p-value), relative to the equivalent Labrador result, the relationship between confluence CSA ratio and maximum depth of overdeepenings within the structural zone of the Swiss study region remains comfortably statistically significant, and confirms that the Labrador result is repeatable for an alternative formerly glaciated study region. The relationship is observed at local (confluence) scale (using SRTM3 land topography data), as is the case for the Labrador study. The Swiss result shows a stronger positive trend between confluence CSA ratio and overdeepening depth values than is the case for Labrador. It is suggested that the difference between the magnitudes of observed depth values, for the two sets of overdeepenings can be accounted for by considering the geological and glacial history of the two study regions (see section 6.4 for further discussion).

## 5.6 World map of overdeepenings

The following series of maps (figure 86, a-h) provide an overview of topographical depressions within the limits of the Last Glacial Maximum (LGM), emphasising localities of likely glacial overdeepening. These data will be useful for future investigation of overdeepening, and as a test of numerical models of glacial erosion. Summary statistics for the dataset are displayed in table 23.

	Km <sup>2</sup>	As a % of land area covered by ice at the LGM
Area of known or likely overdeepenings	3,726,744	7.3
Area of known or likely geological basins (which probably contain overdeepenings)	3,271,219	6.4
=	6,997,963	13.7
Area of study region within limits of LGM	51,086,279	100

**Table 23. Summary statistics for the world map of potential overdeepenings.**

There are over 2600 known/ probable overdeepenings globally. Of these nearly 2200 are empty or partially sediment filled, with the remainder being lakes. Further, nearly 100 known basins contain probable overdeepenings. Most of the deepest (i.e. > 1000 m) overdeepenings within the study region occur in Antarctica, with others occurring predominantly in Patagonia and Norway. Overdeepenings are a major feature of the global glacial landscape. There is plentiful evidence throughout the dataset for continental and regional (mountain range) scale patterns of terminal (pure, meltwater abundance) overdeepening at or near the edge of former ice sheets, and also evidence to a lesser extent for equilibrium line (pure, ice velocity) overdeepening on a similar scale. There is evidence of confluence (topographical) overdeepening at more local scales, especially in mountain ranges such as the Alps, Andes, Southern Alps, and elsewhere where valley-scale overdeepenings are abundant. The relatively small scale and topographical (rather than geological) nature of the dataset makes it difficult to comment as to whether the map set shows evidence for the other types of overdeepening (valley-floor perturbation, and bedrock mass strength) discussed in section 2.7.2.

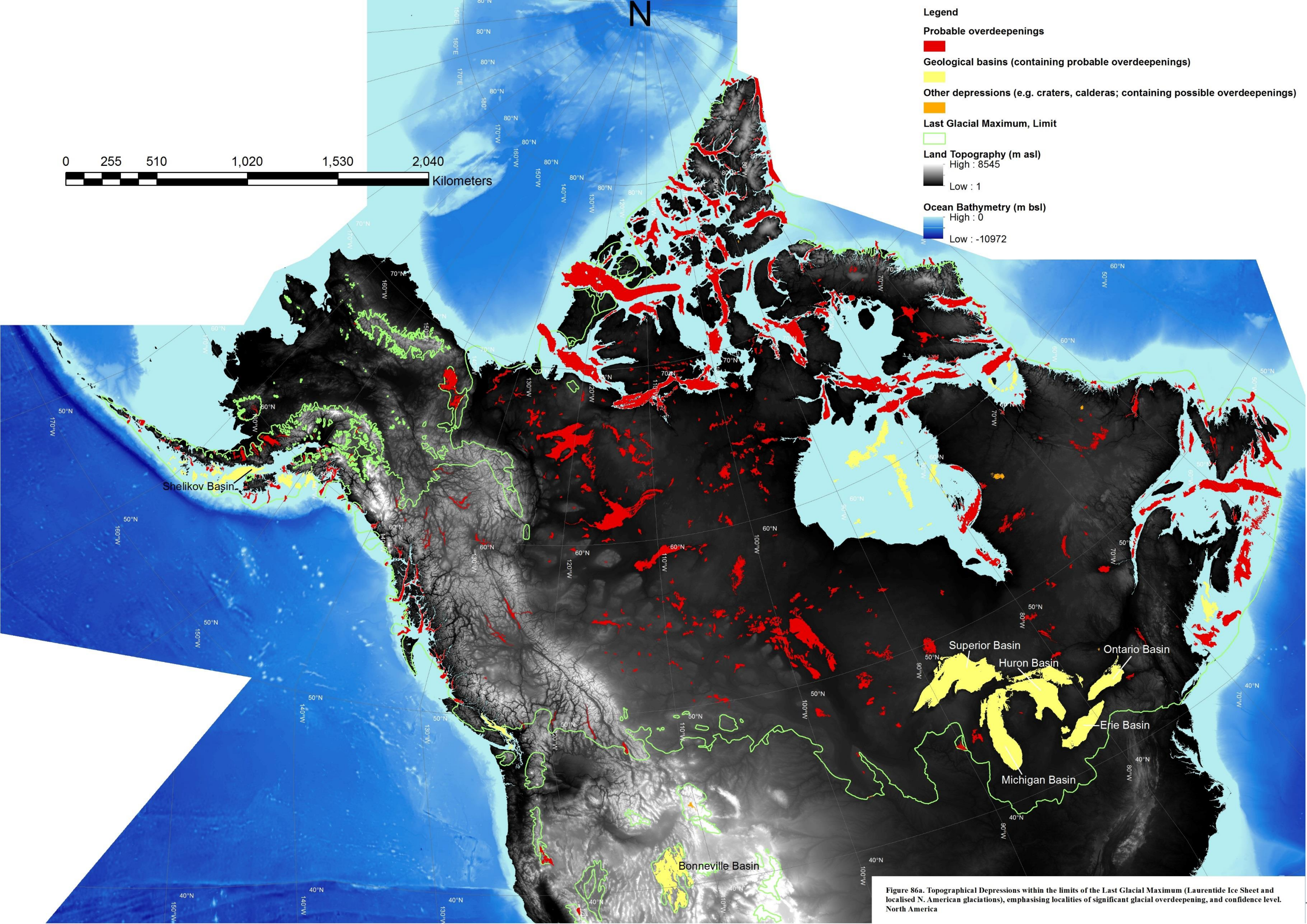


Figure 86a. Topographical Depressions within the limits of the Last Glacial Maximum (Laurentide Ice Sheet and localised N. American glaciations), emphasising localities of significant glacial overdeepening, and confidence level. North America

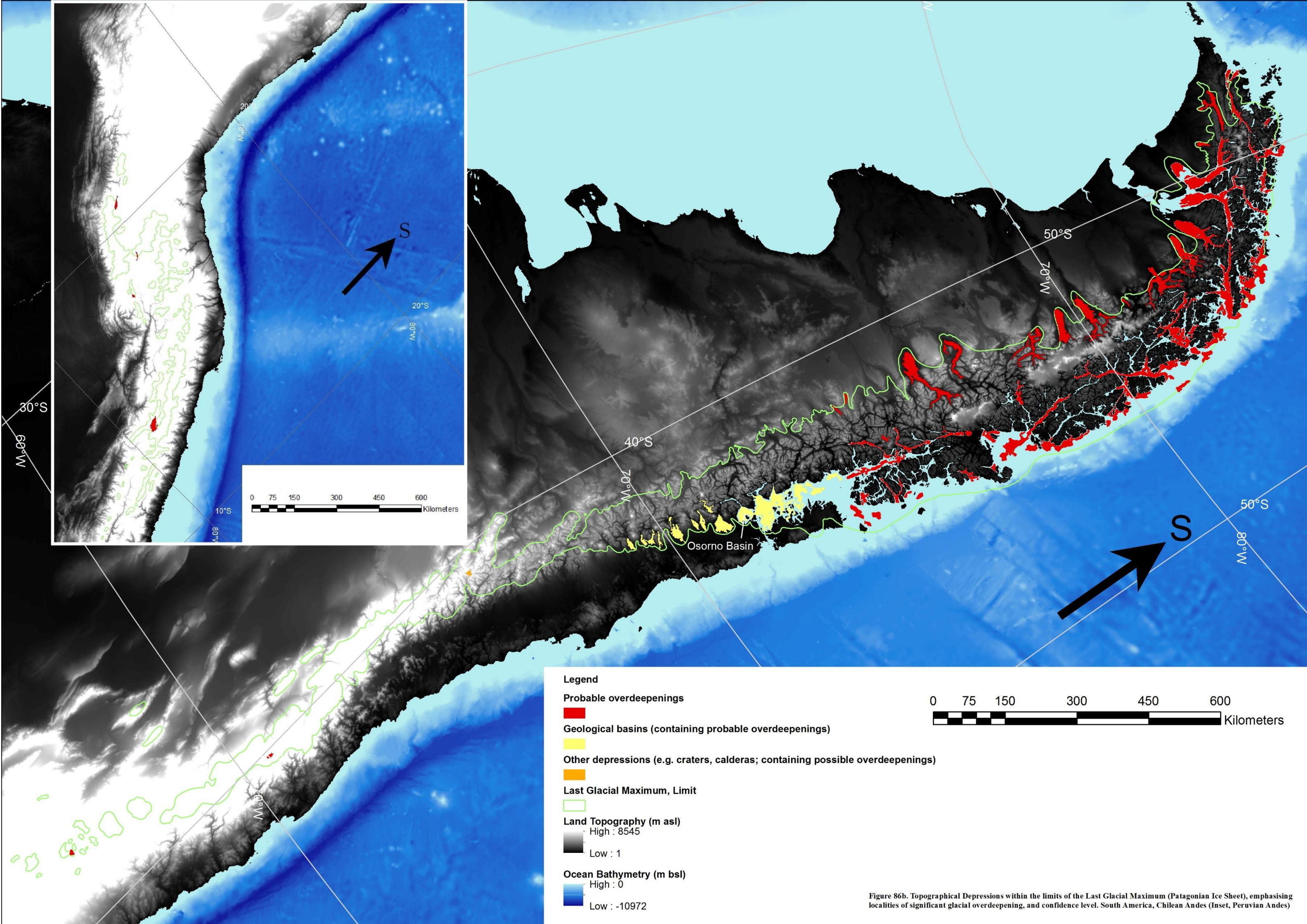


Figure 86b. Topographical Depressions within the limits of the Last Glacial Maximum (Patagonian Ice Sheet), emphasising localities of significant glacial overdeepening, and confidence level. South America, Chilean Andes (Inset, Peruvian Andes)

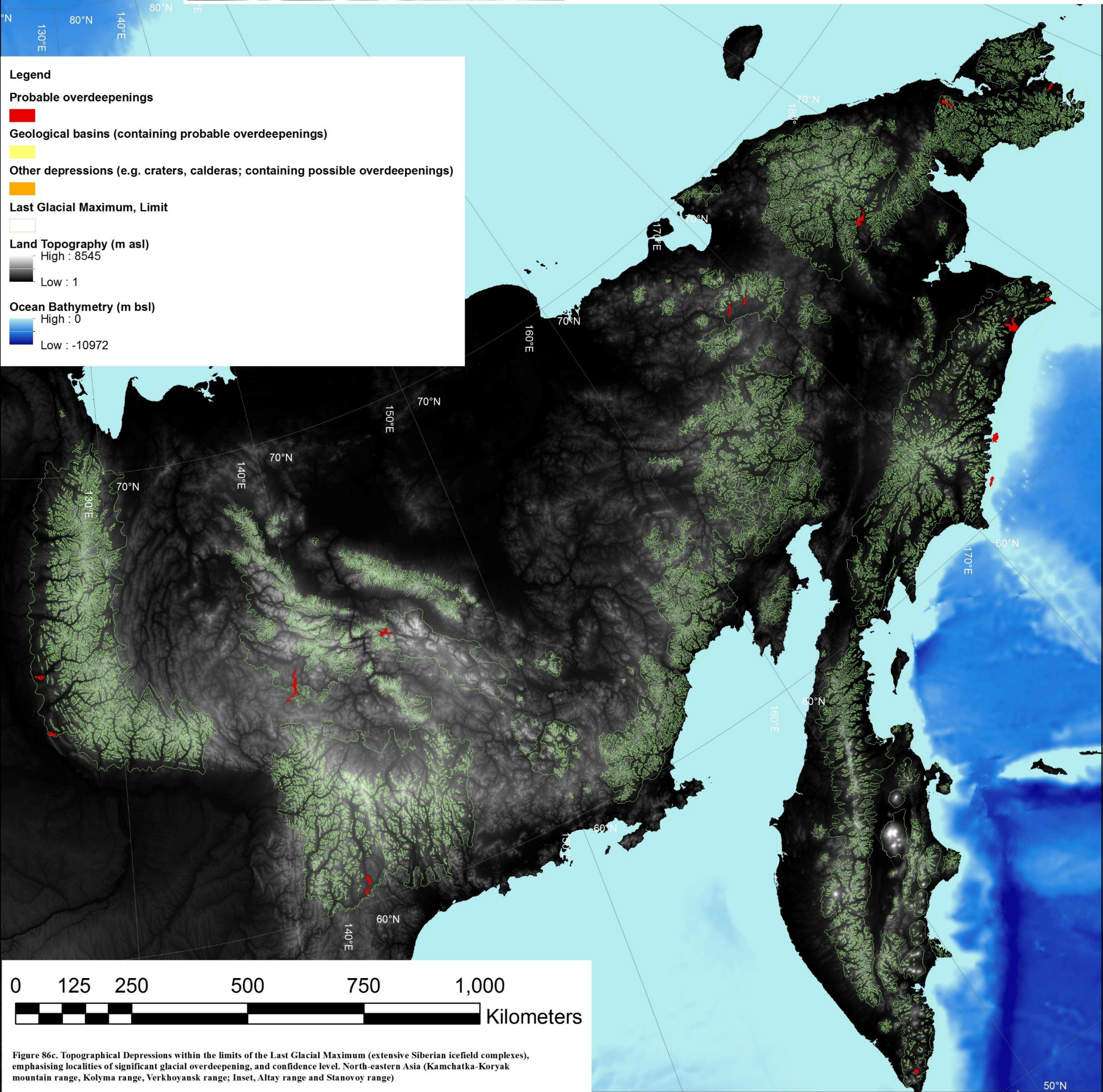
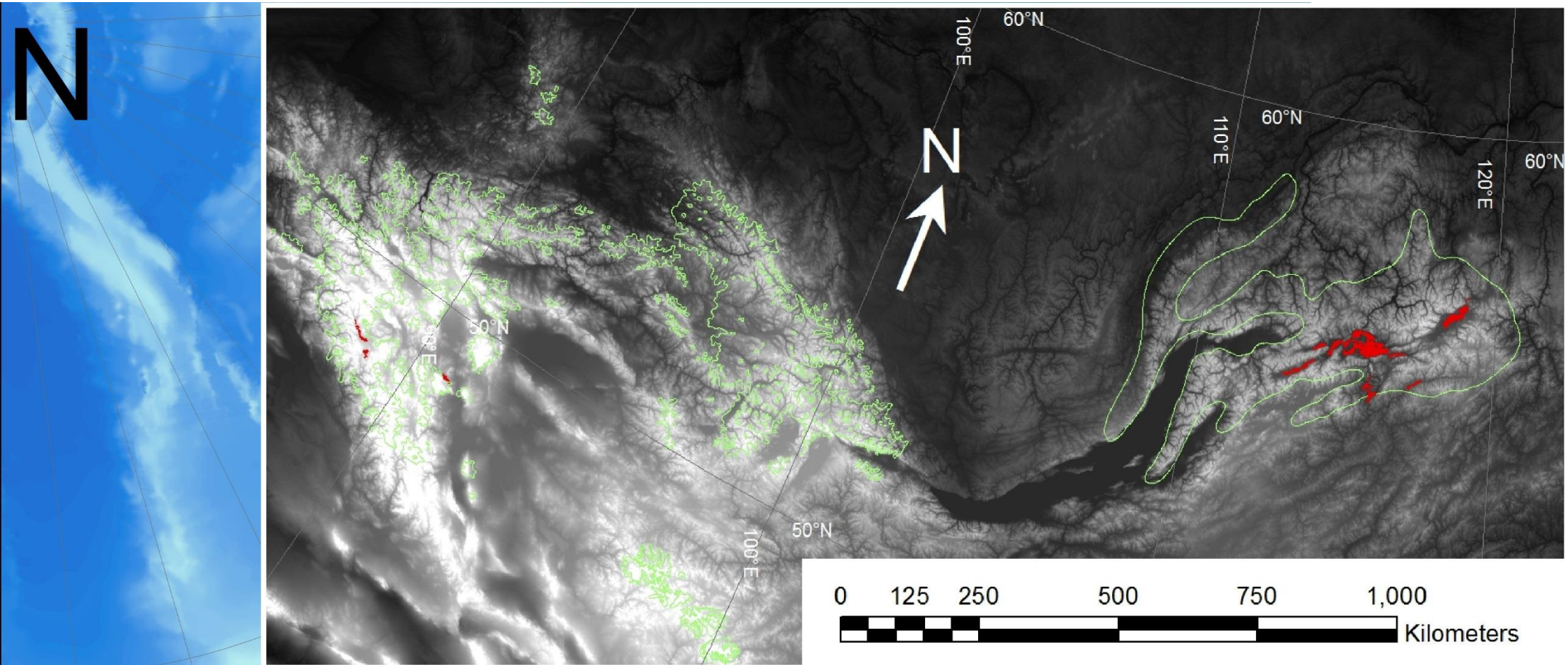
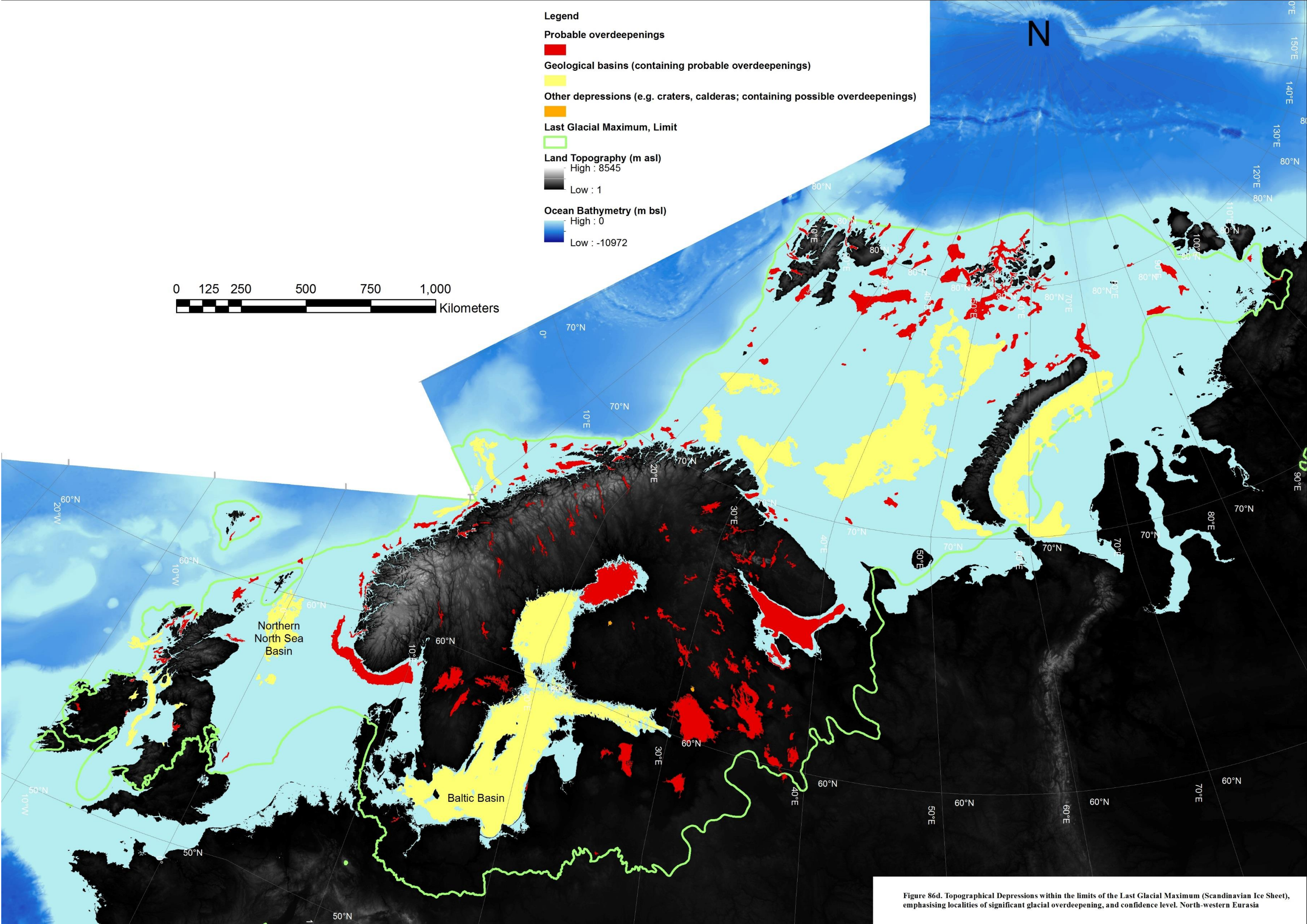


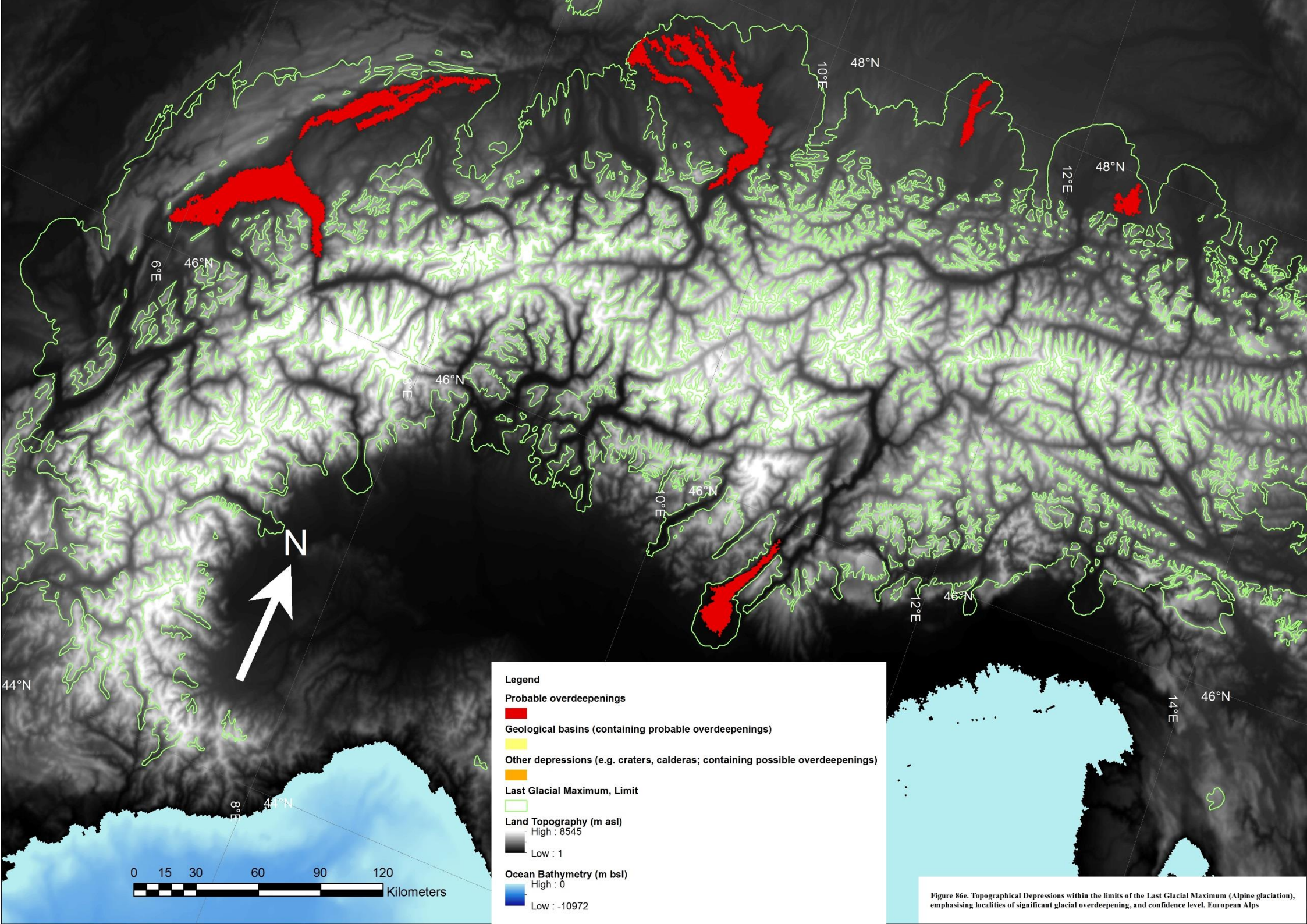
Figure 86c. Topographical Depressions within the limits of the Last Glacial Maximum (extensive Siberian icefield complexes), emphasising localities of significant glacial overdeepening, and confidence level. North-eastern Asia (Kamchatka-Koryak mountain range, Kolyma range, Verkhoyansk range; Inset, Altay range and Stanovoy range)

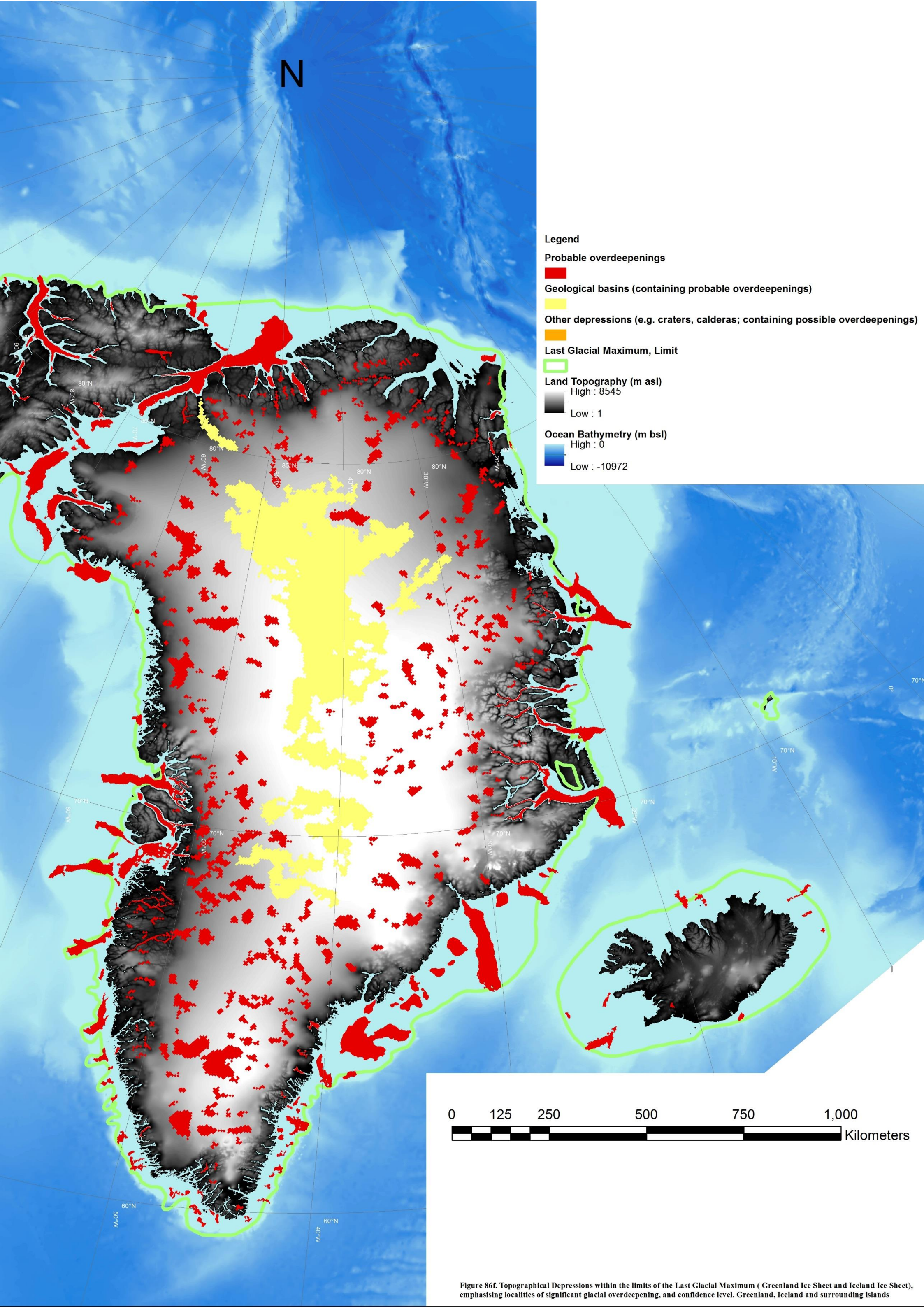


- Legend**
- Probable overdeepenings
    -
  - Geological basins (containing probable overdeepenings)
    -
  - Other depressions (e.g. craters, calderas; containing possible overdeepenings)
    -
  - Last Glacial Maximum, Limit
    -
  - Land Topography (m asl)
    - High : 8545
    - Low : 1
  - Ocean Bathymetry (m bsl)
    - High : 0
    - Low : -10972

0 125 250 500 750 1,000 Kilometers

Figure 86d. Topographical Depressions within the limits of the Last Glacial Maximum (Scandinavian Ice Sheet), emphasising localities of significant glacial overdeepening, and confidence level. North-western Eurasia





**Legend**

Probable overdeepenings



Geological basins (containing probable overdeepenings)



Other depressions (e.g. craters, calderas; containing possible overdeepenings)



Last Glacial Maximum, Limit



Land Topography (m asl)

High : 8545

Low : 1

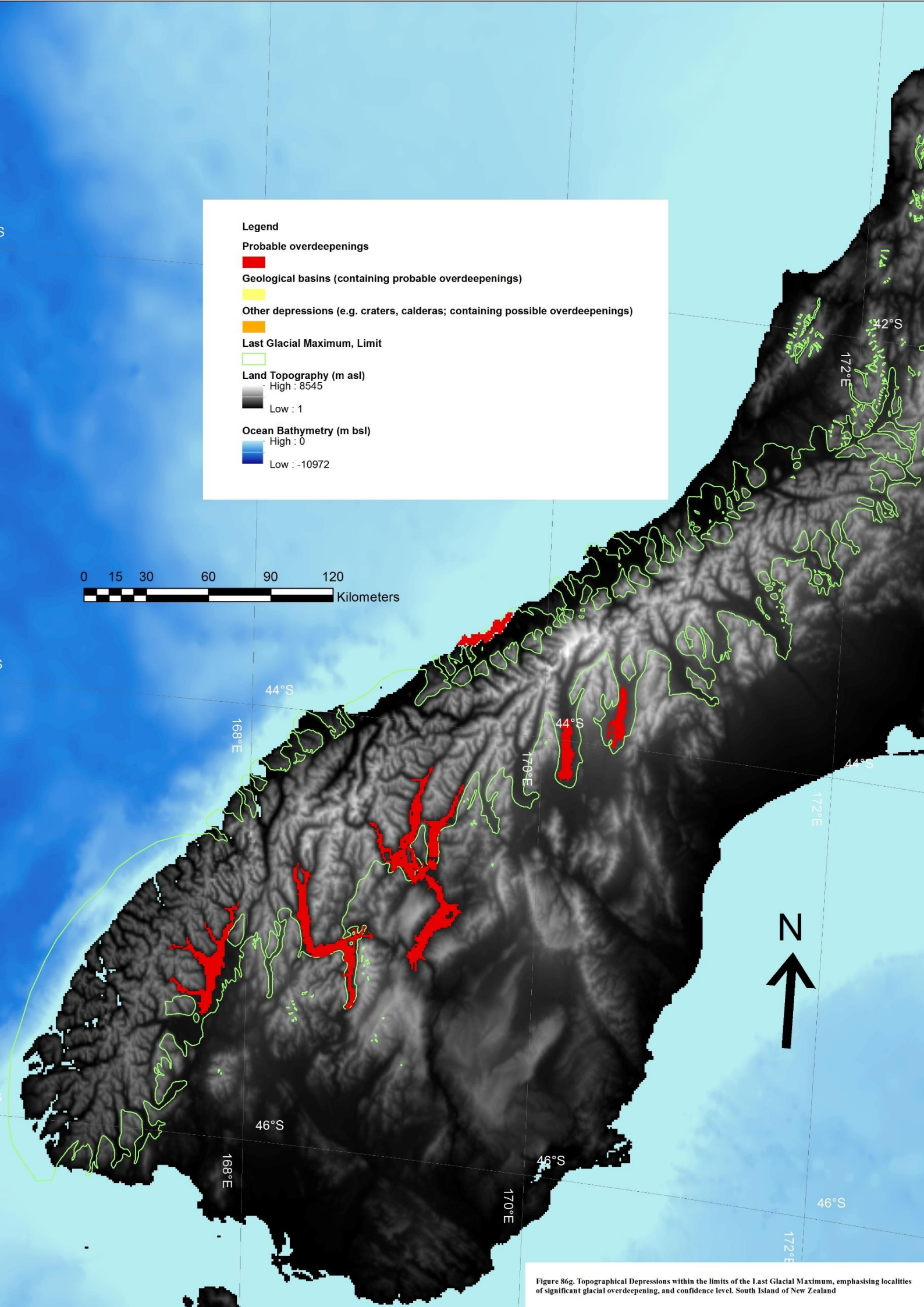
Ocean Bathymetry (m bsl)

High : 0

Low : -10972



Figure 86f. Topographical Depressions within the limits of the Last Glacial Maximum (Greenland Ice Sheet and Iceland Ice Sheet), emphasising localities of significant glacial overdeepening, and confidence level. Greenland, Iceland and surrounding islands



**Legend**

- Probable overdeepenings**
- Geological basins (containing probable overdeepenings)**
- Other depressions (e.g. craters, calderas; containing possible overdeepenings)**
- Last Glacial Maximum, Limit**
- Land Topography (m asl)**  
 High : 8545  

 Low : 1
- Ocean Bathymetry (m bsl)**  
 High : 0  

 Low : -10972

0 15 30 60 90 120  
 Kilometers



Figure 86g. Topographical Depressions within the limits of the Last Glacial Maximum, emphasising localities of significant glacial overdeepening, and confidence level. South Island of New Zealand

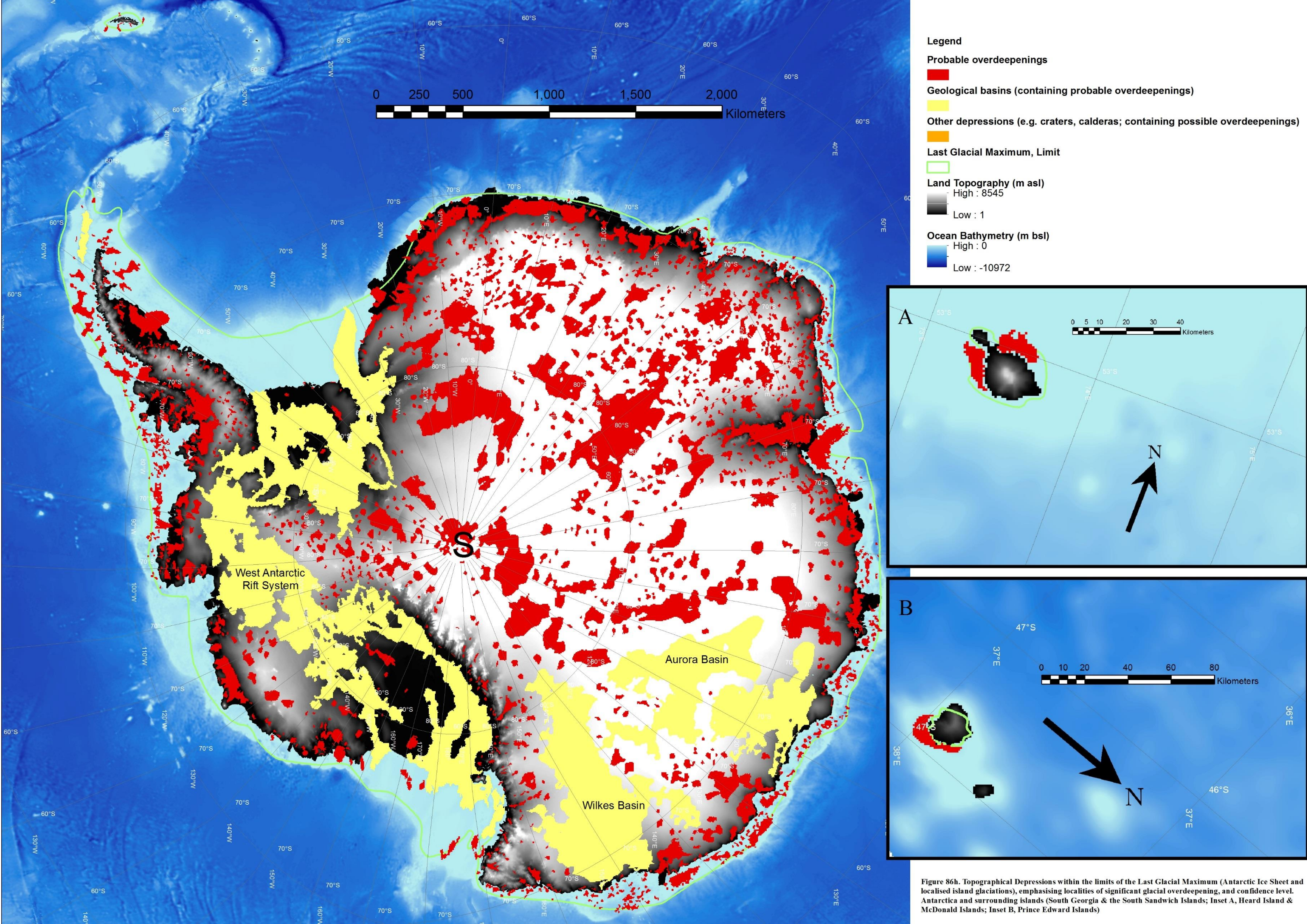


Figure 86h. Topographical Depressions within the limits of the Last Glacial Maximum (Antarctic Ice Sheet and localised island glaciations), emphasising localities of significant glacial overdeepening, and confidence level. Antarctica and surrounding islands (South Georgia & the South Sandwich Islands; Inset A, Heard Island & McDonald Islands; Inset B, Prince Edward Islands)

## 6 Discussion

*This chapter considers the major outcomes and findings of the investigation. Results of testing sensitivity to operator variability are summarised and put into the context of relevant literature. Confluence allometry is explored. The development of Labradorian topography, as a result of topographical and glacial controls upon geology, is discussed. An explanation for the difference in depth of valley overdeepenings in the Labrador structural zone compared to overdeepenings in the Swiss structural zone is examined.*

The results of the hypothesis testing indicate that structural weakness (i.e. faulting) in bedrock is a primary control upon overdeepening depth within glacial confluences, via increase in ice velocity. It can be inferred that glacial erosion (i.e. overdeepening) and the subsequent removal of eroded material is more effective in confluences within zones of structural weakness, only if overdeepenings have been initiated via an increase in ice velocity. Initiation of overdeepenings via an increase in ice velocity is due to change in valley CSA, which is the primary control upon overdeepening location within glacial confluences. The relationship between structural weakness (faulting) in bedrock and (confluence co-located) overdeepening depth is true only at local (confluence) scale. The relationship does not occur at regional scale (i.e. large valley, to ice sheet scale), at which scale presumably other controls upon overdeepening size will dominate.

As discussed by Krabbendam & Glasser (2011), bedrock properties are known to control landforms, but this has rarely been analysed quantitatively. Krabbendam & Glasser (2011), in their analysis of a study region in north-west Scotland, find that rock hardness and joint spacing exert a strong control on sub-glacial erosional landforms and the mechanisms that form them. A lithology with a particular hardness can have highly variable joint spacing, for instance in the vicinity of tectonic faults (Krabbendam & Glasser, 2011). The effect of local variations in joint spacing is well illustrated by studies on glacial erosion of granitic rocks in Yosemite. Matthes (1930) showed qualitatively that densely jointed granite in Yosemite is more susceptible to plucking than less jointed granite - confirmed quantitatively by Duhnforth et al. (2010) using cosmogenic nuclide exposure dating techniques (Krabbendam & Glasser, 2011). The study by Krabbendam & Bradwell (2011) of erosional glacial bedforms (megagrooves) in Britain and Ungava, Canada, reports that bedforms occur on well-stratified or layered bedrock with closely spaced joints. Bedforms do not occur on massive crystalline rocks or thick bedded sedimentary rocks. Quarrying is thought to be a more feasible formation mechanism than glacio-fluvial erosion or abrasion. The formation of such bedforms is strongly controlled by bedrock

properties (Krabbendam & Bradwell, 2011). Findings in this thesis concur with those discussed above. Zones of faulting are shown to allow more effective erosion (resulting in valley widening and deepening) than is the norm within otherwise generally massive crystalline igneous and metamorphic rocks. This implies that quarrying plays a more important role in erosion in zones of structural weakness than does glacial abrasion.

Although it is feasible that ice velocity is the primary process propagating overdeepening depth within the structural geology zone, current process understanding indicates that quarrying (i.e. ice velocity, and sub-glacial meltwater abundance/pressure) is most likely to be the primary process at work for reasons expressed in section 2.7.2 (bedrock mass strength, an external geological control upon overdeepening location and size). Glacial quarrying remains enigmatic despite being long recognized as a primary, perhaps the dominant, process by which glaciers erode bedrock (Hallet, 1996). Recent advances, such as improvements to the Herman and Braun (2008) landscape evolution model, have found sub-glacial hydrology to be profoundly important to the temporal and spatial patterns of sub-glacial erosion (including overdeepening) (Herman, et al., 2011). Consequently, the ice 'speed up' ratio data examined in this investigation, whilst providing new insight into the processes that initiate and develop overdeepenings, may not be sufficiently comprehensive in representing such processes, especially within structural fault zones.

Outcomes of hypothesis testing have identified a set of conditions where the overdeepening process is sensitive to bedrock mass strength. The conditions occur at valley scale, where change in glacial valley CSA in confluence (or presumably any appropriate control) has initiated overdeepening within a structural fault zone. By way of ultimate example of such conditions, Glasser & Ghiglione (2009) infer that the primary control on (overdeepened) fjord development in glaciated areas is geological and not glaciological. Successive glaciations in the Andes of South America have followed the same ice-discharge routes, widening and deepening pre-existing geological structures at the expense of the surrounding terrain to create the fjord landscape (Glasser & Ghiglione, 2009). As discussed by Krabbendam & Glasser (2011), glacial conditions (i.e. ice velocity, ice thickness) can only be inferred from glacial erosional landforms if the effects of bedrock properties are considered.

## 6.1 Sensitivity testing of operator variability in confluence definition

There has been little quantification or discussion of the operator variability that is associated with manual definition of landscape features, since initial discussion of the issue (Podwysocki, et al., 1975; Siegal, 1977) at the advent of modern 'machine aided' mapping and remote sensing during the 1970s. Subsequently, the lack of development of sufficiently accurate automated or semi-automated alternatives to manual analysis (section 4.3.1) has meant that manual methods of identifying and defining confluences remain the most effective, and are therefore preferred and used in this study. Analysis (sections 4.4.3.3.1 and 5.1.1) has shown that the sensitivity of confluence ratio to changes (by operator variability) in the extent and internal angles of confluences in this study is acceptable, thus alleviating concerns regarding sensitivity in this instance. Such concerns are a result of the lack of reproducibility of landform definition between different human operators, as discussed by Podwysocki, et al. (1975) and by Siegal (1977). Operator variability is only recently beginning to be quantified in remote-sensed image interpretation. A recent study of this type (Van Coillie, et al., 2014) quantified operator variability in remote-sensed image interpretation using both thematic and positional accuracy measures, as well as psychological tests, with results that concurred with the operator induced limitations qualitatively expressed in the earlier literature.

## 6.2 Confluence allometry

Change in valley CSA as ice moves from tributaries into a trunk valley has been used as a useful proxy for ice velocity changes in order to aid understanding of the overdeepening process. However, there is some interest in these CSA measurements themselves, putting aside overdeepenings for a while. Figure 87 (reproduced here from section 5.3.4), shows that most (67.0 %) of the confluences have ice velocity speed up ratios actually exceeding the neutral value of one ( $1.0 =$  cases with stable CSA such that no speed up would be expected), telling us that ice in these Labrador valleys should have usually experienced a speed up. A consequence of such speed up should be that glacial erosion is enhanced in the trunk (relative to the tributaries) which should widen and/or deepen the main trunk accordingly. This differential erosion should proceed until the trunk CSA catches up with the sum of tributary CSAs (which might also be growing), thus reaching a value of one. This then, is the steady-state or equilibrium form for a glacial confluence. Confluence allometry may therefore naturally reach an equilibrium steady-state in which ice speed up will no longer occur - a negative feedback on trunk growth. If the confluences in figure 87 were narrowly and normally distributed about the steady-state value of 1.0, it would be possible to conclude that trunk valley adjustment by differential erosion is sufficiently rapid for valleys to reach such a steady-state. On the contrary however, the

distribution is wide and with a lengthy positive tail, from which it is concluded that there has been insufficient time available in the glaciations or that there is some other process that self-limits trunk growth.

Herman and Braun (2008) discuss output from their landscape evolution model for the Southern Alps of New Zealand, and find that a significant increase in glacial erosion efficiency will lead to wider valleys and greater overdeepening. Width and height of valleys are considered highly sensitive to increases in glacial erosion, but even so the resulting landforms cannot be renewed on the time scale of a glacial cycle (Herman & Braun, 2008), taking (they argue) a number of cycles. In the light of this process understanding from modelling, and outcomes (above) from this investigation, I maintain that valley confluences seldom reach equilibrium over glacial timescales, and that confluences therefore become preferred places for the development of overdeepenings via speed up. This helps explain why overdeepenings are such widespread phenomena.

Adding overdeepenings back into the concept of valley allometry, I presume that when CSA ratio indicates a speed up, this is the time when overdeepenings are growing. As valley allometry tends towards a value of 1.0 the overdeepening process lessens, finally perhaps ceasing once 1.0 is reached. The data discussed earlier and table 24 are consistent with this, and are an actual demonstration of it occurring (see below).

Outcomes from hypothesis testing indicate that erosion is more effective due to weakness in the structural zone than elsewhere in the Labrador study region, producing greater valley height via increased overdeepening depths. I suggest that results show that confluence allometry in the structural zone is closer to a mature equilibrium steady-state than is achieved by confluences elsewhere (table 24, reproduced here from section 5.4.5.2). In such a scenario I propose that glacial erosion alters confluence allometry, seeking to minimise ice speed up. This results not only in increased overdeepening depths but also larger mean confluence area, larger mean down-trunk valley width (i.e. less noticeable pinch features within confluences), and a reduced mean speed up ratio of confluences. In such a scenario confluences are observed to have already (i.e. more effectively) initiated a greater number of overdeepenings than is found to be the case elsewhere. All of these expected observations occur within the structural zone (see table 24, and section 5.4.5.1).

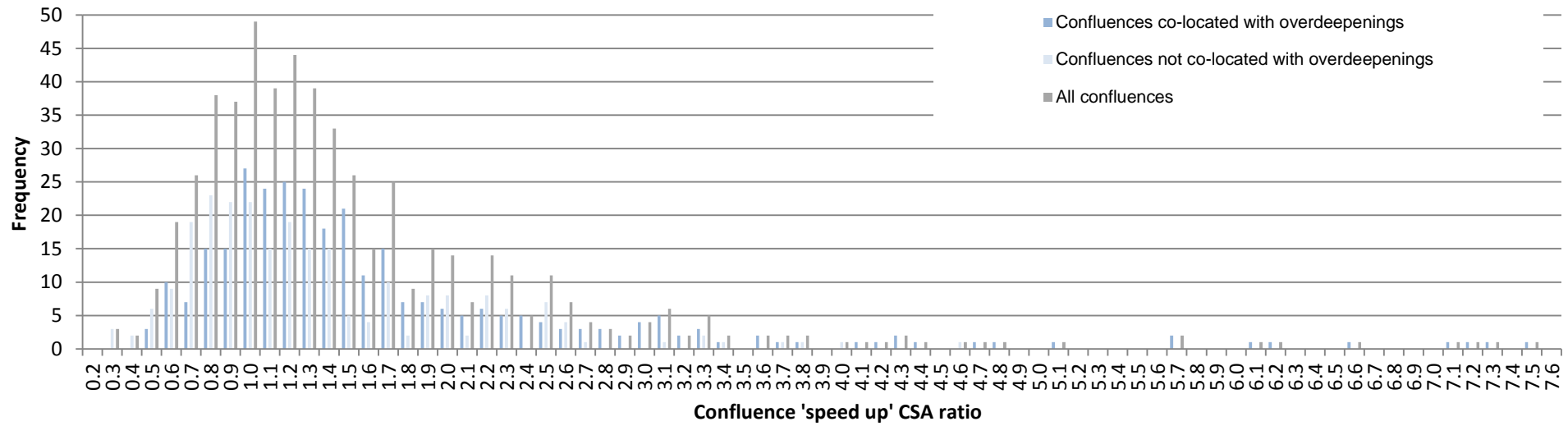


Figure 87. A summary graph of frequency distribution of confluence 'speed up' ratio.

A summary graph (a reproduction of figure 74), showing the frequency distribution of confluence 'speed up' ratio for confluences co-located with overdeepenings (blue), confluences not co-located with overdeepenings (light blue), and all confluences regardless of overdeepening co-location (grey) within the Labrador study region.

Confluence Location	Mean area of confluences (km <sup>2</sup> )	Mean trunk valley width at pinch (km)	Mean 'speed up' ratio of confluences
Within the study region	14.1	1.8	1.9
Within study region (co-located with overdeepenings)	19.1	2.1	2.3
Within the geological study region	13.9	1.9	1.9
Within geological study region (co-located with overdeepenings)	18.3	2.1	2.3
Within structural geology zone	17.3	2.2	1.5
Within structural geology zone (co-located with overdeepenings)	22.3	2.5	1.6
Outwith structural geology zone	10.2	1.5	2.4
Outwith structural geology zone (co-located with overdeepenings)	13.8	1.6	3.1

**Table 24. Statistics, for subsets of confluences within the Labrador study region (reproduction of table 22).**

**Statistics for within the study region presented un-highlighted; within the geological study region, grey; within the structural zone, yellow; outwith the structural zone, purple.**

Analysis suggests that the pinch feature (located at the downstream end of confluences, where the decrease in trunk valley CSA is at its maximum) is most apparent in confluences where allometry is furthest from an equilibrium steady-state. Quantitative analysis (table 24) suggests that confluences within the structural zone do not exhibit the pinch feature to the same extent as confluences outwith the structural zone. As discussed above, confluences in the structural zone have much wider mean down-trunk valley widths and are thought to be closer to a mature equilibrium steady-state. Consequently the clarity with which the pinch feature is evident in the landscape should be diagnostic of glacial erosion within valleys. An exciting possibility exists that numerical modelling of the concept of valley allometry (making particular use of the pinch feature, and overdeepenings) could be used to estimate erosion rates in confluences.

Confluence allometry is altered to a greater extent for confluences with overdeepening(s), than might occur for confluences without (table 24). This is because for confluences without overdeepenings (where glacial erosion is not sufficient to produce one) presumably glacial erosion is also not effective enough to significantly alter allometry over a similar timescale.

The change in confluence allometry along the continuum from non-equilibrated to progressively more equilibrated (although not reaching) steady-state is evident when confluence mean speed up ratio is considered for confluences with overdeepenings, and for confluences regardless of overdeepening co-location, within and outwith the structural zone (table 24). The ratios (of 1.6 and 1.5 respectively) within the structural zone are significantly closer in value than the respective ratios (of 3.1 and 2.4) for confluences outwith the structural zone. Further, the allometry of confluences is significantly altered within the structural zone, relative to allometry outwith the structural zone. This is especially the case for those confluences co-located with overdeepenings (mean area, 22.3 km<sup>2</sup>; mean down-trunk valley width 2.5 km), in a way that is not observed outwith the structural zone (mean area, 13.8 km<sup>2</sup>; mean down-trunk valley width 1.6 km) over the same timescale (table 24).

Further, I suggest that the principle of confluence allometry can be extended to simple valley narrowing, which is not obvious within the landscape of the study region. The more simple allometry of valley narrowings may allow the feature to move towards an equilibrium steady-state (where the narrowing is eroded away, and ice speed up no longer occurs) more readily (i.e. within glacial timescales) than is the case for glacial confluences.

### **6.3 The development of Labradorian topography: The influence of topographical and glacial controls upon geology**

The study region has complex geology with significant structural faulting, as discussed in section 2.8. In the northern part, structural faulting is largely east-west, and north-west to south-east trending (Wardle, et al., 1997). In the southern part, structural faulting is largely north-west to south-east, with some south-west to north-east trending (Wardle, et al., 1997). Visual analysis of the study region suggests the exploitation of structural fault zones by topographical processes to create valley networks (i.e. good co-location is apparent between fault zones and valley networks). This is supported by the strong (quantified) co-location relationships between structural fault zones and valley confluences (and associated overdeepenings). There is strong evidence for the topographic steering of ice through valley networks (Glasser, 1995; Herman & Braun, 2008; Kessler, et al., 2008; Alley, et al., 2003; Swift, et al., 2008). Towards the Labradorian east coast, ice movement was topographically controlled during the late glacial stages (Batterson, 1990). There is strong evidence for east flowing valley glaciers post-dating northeast-flowing ice on surrounding highlands (Batterson, 1990; Batterson & Liverman, 2011; Winsborrow, et al., 2004). It is therefore reasonable to suggest the exploitation of structural fault zones by glacial processes to further erode (i.e. widen and deepen) valley networks, as supported by outcomes from this investigation.

#### **6.4 Glacial buzz-saw: Accounting for the difference between valley overdeepening depth in the Labradorian compared to the Swiss structural zone**

It is reasonable to propose that greater overdeepening depth in Swiss valley overdeepenings, relative to overdeepening depth in locations of interest within Labrador, can be accounted for by the glacial buzz-saw process (discussed by Brozovic, et al., 1997; Meigs & Sauber, 2000; Small & Anderson, 1998). This is because within the western Alps glacial erosion has been significantly greater than in the Labrador Peninsula, whilst rock uplift has been greater in the western Alps than in the valley networks and fjords of Labrador (where confluence and structural fault co-located overdeepenings are most commonly observed). Further to this, rock uplift has been spatially and temporally significantly more consistent within the western Alps than has been the case within the Labrador Peninsula. For example, the Torngat mountain range and eastern coastal region of Labrador (where many overdeepenings are located) has undergone negligible uplift, whereas the inland plateau of Labrador has undergone substantial uplift. This section will account for these assertions. Both study regions have experienced extensive and repeated glaciations (Buoncristiani & Campy, 2011; Occhietti, et al., 2011). Bedrock mass strength will be similar in each area of interest, as both are extensively faulted structural zones with orogenic igneous and metamorphic bedrock (Swiss Federal Office of Topography (SwissTopo), 2010; Wardle, et al., 1997).

As discussed by Preusser et al. (2010), in mountain areas glacial erosion is considered either to enhance isostatic uplift (Molnar & England, 1990; Champagnac, et al., 2007) or to keep at least pace with rock uplift. Thus, glacial erosion represents a 'buzz-saw' effect, i.e. a climatically controlled limitation of elevation at large scale (Brozovic, et al., 1997; Meigs & Sauber, 2000), and increased relief at smaller scale because ranges are narrow relative to the flexural wavelength of the lithosphere (Small & Anderson, 1998). Overdeepening processes are a fundamental characteristic of glacial erosion, so the extra overdeepening depth observed in the Swiss study is effectively extra valley depth, or extra relief, generated by the buzz-saw process as a consequence of the greater glacial erosion and uplift. Structural faulting in both study regions is exploited by glacial erosion, no doubt further enhancing this process.

The Torngat mountain range constitutes ancient cratonic shield rock (St-Onge, et al., 2009), and has been extensively denudated, including by numerous (ice sheet scale) glaciations (Occhietti, et al., 2011; Staiger, et al., 2005). The lithosphere of the Labrador Peninsula has a thick (maximum thickness of 52 km (Funck, et al., 2000)) remnant Palaeo-Proterozoic crustal root of high flexural rigidity (Mengel, et al., 1991; Hall, et al., 2002; Staiger, et al., 2005; Montgomery, 2002), especially at the flexural wavelength of valleys. Periods of rock uplift

since the genesis of Labradorian terrains have been sporadic. Cooke (1929), McMillan (1973), Gradstein and Srivastava (1980), Chalmers (2000) and Japsen and Chalmers (2000) indicate that the Torngat Mountain topography was rejuvenated during Neogene time (Staiger, et al., 2005), but the reasons for this exhumation remain uncertain. Tectonic forces, plume activity and post-glacial isostatic rebound have been suggested (Japsen & Chalmers, 2000; Japsen, et al., 2005). West Greenland appears to have undergone a total of 2.5–3 km of uplift in Neogene times (Chalmers, 2000) by one estimate, or a total of approximately 1-2 km of uplift by another (Japsen, et al., 2005), which is similar to the Neogene uplift recognized as occurring around the North Atlantic. Such uplift extended at least as far as the margins of eastern Canada (Japsen & Chalmers, 2000), and it is reasonable to expect a similar amount of uplift to have occurred for Labrador as for West Greenland, in view of their proximity and similar geological history.

Geologically recent uplift (i.e. last 2 Ma) of the Labrador region is probably a response to glacial erosion, and to the post-glacial removal of ice (i.e. isostatic rebound) since the Last Glacial Maximum (Staiger, et al., 2005). The three-dimensional thermo-mechanically coupled ice-sheet model of Tarasov & Peltier (2004) demonstrates that eastern coastal areas of Labrador exhibit no uplift currently, but that uplift increases rapidly towards the Labrador Plateau (to the south-west), where uplift rate exceeds  $4000 \text{ m Ma}^{-1}$  (Batterson & Liverman, 2010; Tarasov & Peltier, 2004). It does therefore seem that exhumation (of Labrador) has continued in the Quaternary. Such recent uplift is feasible, when it is considered that: (1) the palaeo-equilibrium line altitude based on average cirque floor elevation (c. 800 m) in places is below the plateau; (2) the fracture density is locally high (decimetre fracture spacings are common); and (3) the entire region falls within the zone of continuous permafrost activity which may help contribute regolith and tools for efficient fluvial and glacial erosion (Staiger, et al., 2005). Post-glacial uplift of the plateau would explain the lack of confluences in the south-west of the study region as denudation compensates more uniformly for uplift across the plateau area, where there is no glacial (buzz-saw) erosion to (re)define valleys. Geologically recent uplift is negligible (or least significant) where confluence and structural fault co-located overdeepenings are most commonly observed (i.e. in valley networks and fjords at the eastern coast). The Glacial erosion rate for valleys in the Torngat mountain range has been measured empirically (via in situ terrestrial cosmogenic nuclide concentrations) as  $>2 \text{ m}$  during a single glacial–interglacial cycle. On summit plateaus the long-term (over several glacial–interglacial cycles) erosion rate has been calculated as  $<1.4 \text{ m Ma}^{-1}$  (Staiger, et al., 2005). Glacial erosion rate for valleys in the Torngat mountain range therefore equates to  $>20 \text{ m Ma}^{-1}$  if 100 Ka duration is assumed for a single glacial–interglacial cycle.

The Swiss study region forms part of the Alpine orogenic belt; which is very young in geological terms, having formed over the last 100 Ma (Froitzheim, et al., 1996) due to intense tectonic and isostatic uplift (the latter especially during geologically recent glaciations) (Champagnac, et al., 2007). The Alps have significantly greater relief than the Torngat mountain range, and have been similarly frequently glaciated (Buoncristiani & Campy, 2011; Occhietti, et al., 2011). Uplift is considerable across the Alpine belt, and is spatially and temporally consistent (Champagnac, et al., 2007). Confluence, and structural fault co-located valley overdeepenings are observed across the mountain belt. The Alps have a thick crustal root (maximum thickness of 58 km (Kahle, et al., 1976)). The combined studies of Hinderer (2001), Gudmundsson (1994), Barletta, et al. (2006) and Champagnac, et al. (2007) suggest that virtually all of present-day Alpine vertical motion results from climatic change manifested in part by melting ice and in part by enhanced erosion rates in Plio-Quaternary time, although other processes cannot be excluded such as those related to deep dynamics (slab breakoff, crustal delamination, etc.) (Champagnac, et al., 2007). The two-dimensional flexural lithospheric model of Champagnac, et al. (2007), demonstrates that a significant part (50%) of the current vertical motion of the western Alps can be attributed to an enhanced erosion rate during the last 1 Ma (Champagnac, et al., 2007). An average glacial erosion rate for the western Alps has been measured empirically (via volumes of sediment accumulation in regions surrounding the Alps) as  $150 \text{ m Ma}^{-1}$  before 5 Ma BP, rising to  $480 \text{ m Ma}^{-1}$  since 1 Ma BP (Kuhleemann, 2000). Before ca. 5 Ma BP, it can be assumed that Alpine peaks eroded at the same rate as Alpine valleys. However, for times of enhanced erosion, especially in Plio-Quaternary time in which glacial erosion dominated, it can be assumed that the rate of erosion in valleys exceeded that on peaks (Champagnac, et al., 2007) and that the highest rates of glacial erosion were concentrated in valleys. Most of the western Alpine area exhibits a current modelled rock uplift rate exceeding  $400 \text{ m Ma}^{-1}$  (Champagnac, et al., 2007).

## 7 Conclusions

*This chapter summarises the major outcomes and findings of the investigation. Avenues of future research are indicated, which may further the assessment of the significance of overdeepenings within glacial, landscape, and (ultimately) global climate systems.*

### 7.1 Outcomes of analyses

This investigation has used inferred ice velocity changes within glacial valley confluences proximal to/ within Labrador, Canada, to gain insight into controls upon overdeepening location and size. The investigation has examined glacial valley cross-sectional area (CSA) change within confluences (a topographical control), and bedrock mass strength change within confluences (a geological control). Examination of these controls has improved our understanding of the overdeepening processes at work. A summary of the most significant outcomes from the investigation follows:

1. Overdeepenings are preferentially located in glacial valley confluence because this is where ice velocity speed up (due to change in glacial valley CSA) occurs. This investigation is the first quantitative demonstration that overdeepenings exist in confluences.
2. It has been demonstrated that there is no relationship between overdeepening depth and ice velocity speed up within confluences, across the database.
3. Within structural geology zones, overdeepening depth is found to increase when there is an increase in speed up within confluences. Therefore ice velocity increase can enhance overdeepening depth given weak enough rock. Joint spacing in structurally weak (faulted) rock is therefore assumed to be key to overdeepening development.
4. This leads to a finding regarding the process in operation, that quarrying is most likely to be the main process by which overdeepenings develop. This is deduced because of the above described overdeepening enhancement in structurally weak rocks, where jointing favours quarrying over abrasion.
5. It is suggested that confluence allometry adjusts to achieve an equilibrium steady-state, as a consequence of glacial erosion.

6. Valley overdeepenings observed in the Swiss study region are deeper than corresponding overdeepenings in the Labrador study. This is interpreted as evidence of the glacial buzz-saw process enhancing valley relief by a different amount in each region due to differing rates of uplift and glacial erosion.
7. Maps produced to inform future research regarding the location of likely overdeepenings within the limit of the LGM, show that overdeepenings are a major feature of the global glacial landscape.

Outcomes of hypothesis testing support the hypothesis that overdeepenings are preferentially located at glacial valley confluence because this is where ice velocity speed up (due to change in glacial valley CSA) should occur. This is important for understanding glacial erosion because it is a strong (and rare) actual demonstration of the oft-assumed relationship that scales increased erosion with increased ice velocity. The findings reported here therefore provide support for glacial landscape evolution models that, in the absence of a fuller process treatment, scale erosion with ice velocity.

At the whole database level there is no evidence to support the hypothesis that overdeepenings are deeper in confluences where our proxy for ice velocity shows more speed up. This is curious as it is a reasonable expectation that this should occur following from the earlier finding of erosion scaling with velocity. No evidence exists to support the hypothesis that overdeepenings more frequently occur in confluences with weaker bedrock (e.g. sedimentary rocks vs. igneous). Again this is surprising. However, by examining in more detail the relationship between overdeepenings and, rather than bulk rock type, weaknesses as recorded by zones of structural weakness, such data are found to support the hypothesis that overdeepening depth is larger in confluences with weaker bedrock, specifically geological zones of structural weakness (i.e. faults, at valley glacier scale only). It thus seems that variations in bedrock mass strength (i.e. of an intact homogenous rock type) found in the study area do little to control overdeepening, but that variations in strength arising from structural weaknesses do. Given that glacial abrasion does not require bedrock jointing but that glacial plucking is thought to be highly dependent upon this, it leads to the interesting conclusion that within the Labrador region the process of overdeepening was mostly likely to have been accomplished by plucking rather than abrasion. This could be an important process insight gained from morphometric exploration.

Findings indicate that glacial valley confluence allometry may adjust to achieve an equilibrium steady-state as a consequence of glacial erosion; with confluences that are co-located with overdeepenings and weaker (faulted) bedrock exhibiting the most change towards larger areas and larger down-trunk valley widths. This results in lower ice velocity and subsequent lower glacial erosion in confluence.

Differing rates of uplift and glacial erosion (a consequence of the glacial buzz-saw process) are interpreted as being responsible for the greater depths of confluence and structural fault co-located overdeepenings observed in the Swiss study region, relative to depths observed for corresponding overdeepenings within Labrador.

This investigation concludes that confluence valley CSA change is a primary control upon overdeepening location within confluences, and that change in bedrock mass strength is a primary control upon the maximum depth of confluence co-located overdeepenings, within zones of structural weakness (at valley glacier scale only). This latter finding is corroborated by findings in an alternative (Swiss) study region.

At global scale, probable overdeepenings within the limits of the Last Glacial Maximum (LGM) have been identified, and maps produced, in order to inform future research. Overdeepenings are a major feature of the global glacial landscape. Most of the deepest (i.e. > 1000 m) overdeepenings occur in Antarctica, with others occurring predominantly in Patagonia and Norway.

Findings of this investigation have made it possible to draw conclusions as to some of the glacial, geomorphological and geological processes that control overdeepening location and size. This increases understanding of the glacial system and of landscape evolution, and lays foundations for future work on the topic. Future research will allow the significance of overdeepenings within glacial, landscape, and (ultimately) global climate systems to be assessed.

## 7.2 Future Research

Previous studies have shown, implied or speculated the existence of various types of overdeepening, as discussed within this thesis. Outcomes from this investigation indicate the existence of types of overdeepening other than the confluence type, occurring within and outwith glacial valleys, the latter occurring at a variety of (glacial valley to ice sheet) scales which should be further investigated. Within glacial valleys, overdeepenings associated with valley-floor perturbations such as steps or hanging valleys should be investigated. Overdeepenings associated with steps or hanging valleys are likely to have a control that is independent of any proximal confluence, for reasons expressed in section 2.7.2 (valley-floor perturbation, an external topographical control upon overdeepening location and size). During the course of this investigation, visual assessment of overdeepenings in the study region has suggested that steps are infrequently co-located with confluence. A separate study of this potential control is necessary.

Preliminary outcomes from this investigation suggest that the boundary between lithological zones (i.e. the change in rock mass strength across the divide between two different lithologies) may act as a separate control upon confluence, and upon the location and/or size of confluences with overdeepenings, in addition to the controls described elsewhere in this thesis. Such a control may occur within (i.e. a secondary control) or outwith (i.e. a primary control) confluences. Confluences and co-located overdeepenings situated on a lithological boundary have distinctive characteristics relative to those situated elsewhere. Such overdeepenings are significantly smaller in area than average, and are typically found 600-700 m downstream of the position of estimated peak ice velocity within the confluence. This is unusual, as in other geological zones most confluence co-located overdeepenings occur at (or much nearer to) the position of peak ice velocity. Further, for confluences co-located on a lithological boundary, confluence area and down-trunk valley widths are similar to that observed for confluences co-located in a structural zone (i.e. larger than is found elsewhere), emphasising the likelihood of a geological influence upon confluence and overdeepenings at lithological boundaries at local scale. This warrants further study.

It is surprising that no evidence has been found to support the hypothesis that overdeepening size is larger in glacial valley confluences where there is greater ice velocity speed up (due to change in glacial valley CSA), where ice erosion should be greatest. It is reasonable to expect that this relationship be found, as outcomes of hypothesis testing support the hypothesis that overdeepenings are preferentially located at confluence, where speed up occurs. It is therefore suggested that the relationship may simply be very well obscured as a result of another control or controls (most likely operating distally to the confluence) influencing confluence co-located

overdeepening location and size at local and/or regional scales. If the effects of the other control can be isolated (i.e. using subsets of data) then it may be possible to identify a relationship, and to discover the influence of the other control. This should be examined further in future work (in this and other study regions). Further to this, secondary controls upon overdeepening location and size within confluences should be investigated using the same technique.

Similarly, although there is no evidence to support the hypothesis that overdeepenings more frequently occur in confluences with weaker bedrock, where there should be greater potential for erosion and removal of material, it is possible that such a relationship is obscured because the range in strength of rock types in the area was not large enough to reveal differences. The change in allometry will have the effect of reducing the ice velocity speed up that is apparent for confluences within the structural zone, potentially masking a relationship when the frequency distribution of speed up for confluences is compared within and outwith the structural zone. Further investigation of this hypothesis should assess other study regions and bigger datasets. Most importantly, results should be considered in the light of outcomes of further hypothesis testing using more sophisticated datasets (see below).

As suggested by previous discussion, further investigation of the influence of bedrock mass strength upon overdeepening location and size should explore not simply ice velocity, but also meltwater abundance and the more complex process of glacial quarrying. These processes should be examined within whole geological zones (not just within confluences), especially within structural fault zones. The acquisition of data (with good coverage) regarding quarrying rates is therefore fundamental to further work in this area.

This investigation has implications for landscape evolution modelling. Results indicate that landscape evolution models should scale erosion with ice velocity. However it might be better to formulate better implementations of quarrying, noting that quarrying is thought to depend upon water abundance/pressure not just ice velocity. Also, in relation to landscape evolution modelling, when connecting output landscapes to reality, much data in this thesis could be used to test how realistically models create landscapes. For example, do speed up ratios in modelled landscapes show the same distribution as is found in nature?

The bimodal frequency distribution for confluences with overdeepenings within the structural zone may be diagnostic of a structural influence upon confluences, and especially overdeepenings within confluences. It is suggested that the bimodality perhaps indicates a preferred confluence speed up ratio value (of 1.5) where confluences control overdeepening initiation and where there is also a structural control. This characteristic is worthy of future examination, particularly for other study regions.

The concept of confluence allometry discussed in this thesis should be explored for other study regions to see whether it is apparent elsewhere. The concepts established regarding co-development of overdeepenings and confluence allometry could form the basis of some interesting modelling experiments regarding estimating erosion rates in confluences.

Further, for those overdeepenings within structural zones in other study regions, particularly those which have experienced significant uplift and occur in areas of greater relief, the magnitude of overdeepening depth values should be compared with further study regions to see whether there is further evidence for the glacial buzz-saw.

## References

- ALLEY, R. B., CUFFEY, K. M., EVENSON, E. B., STRASSER, J. C., LAWSON, D. E. and LARSON, G. J. (1997). How glaciers entrain and transport basal sediment: physical constraints, *Quaternary Science Reviews*, 16, pp. 1017-1038.
- ALLEY, R. B., LAWSON, D. E., LARSON, G. J., EVENSON, E. B. and BAKER, G. S. (2003). Stabilizing feedbacks in glacier-bed erosion, *Nature*, 424, pp. 758-760.
- AMUNDSON, J. M. and IVERSON, N. R. (2006). Testing a glacial erosion rule using hang heights of hanging valleys, Jasper National Park, Alberta, Canada, *Journal of Geophysical Research: Earth Surface*, 111 (F01020, doi: 10.1029/2005JF000359).
- ANDERSON, R. S., MOLNAR, P. and KESSLER, M. A. (2006). Features of glacial valley profiles simply explained, *Journal of Geophysical Research: Earth Surface*, 111 (F01004, doi: 10.1029/2005JF000344).
- ANIYA, M. and WELCH, R. (1981). Morphometric analyses of Antarctic cirques from photogrammetric measurements, *Geografiska Annaler. Series A, Physical Geography*, 63 (1-2), pp. 41-53.
- ANTÓN, L., RODÉS, A., DE VICENTE, G., PALLÀS, R., GARCIA-CASTELLANOS, D., STUART, F. M., BRAUCHER, R. and BOURLÈS, D. (2012). Quantification of fluvial incision in the Duero Basin (NW Iberia) from longitudinal profile analysis and terrestrial cosmogenic nuclide concentrations, *Geomorphology*, 165-166, pp. 50-61.
- ARGIALAS, D. P. (1995). Towards structured-knowledge models for landform representation, *Zeitschrift fur Geomorphologie. N.F. Supplementband*, 101, pp. 85-108.
- BAKKER, J. P. (1965). A forgotten factor in the interpretation of glacial stairways, *Zeitschrift fur Geomorphologie*, 9, pp. 18-34.
- BAMBER, J. L., EKHOLM, S. and KRABILL, W. B. (2001a). A new, high resolution digital elevation model of Greenland fully validated with airborne laser altimeter data, *Journal of Geophysical Research: Solid Earth*, 106 (B4, doi: 10.1029/2000JB900365), pp. 6733-6745.

- BAMBER, J. L., LAYBERRY, R. L. and GOGENINI, S. P. (2001b). A new ice thickness and bed data set for the Greenland ice sheet 1: Measurement, data reduction, and errors, *Journal of Geophysical Research: Atmospheres*, 106 (D24, doi: 10.1029/2001JD900054), pp. 33773-33780.
- BARLETTA, V. R., FERRARI, C., DIOLAIUTI, G., CARNIELLI, T., SABADAINI, R. and SMIRAGLIA, C. (2006). Glacier shrinkage and modeled uplift of the Alps, *Geophysical Research Letters*, 33 (doi: 10.1029/2006GL026490).
- BATTERSON, M. J. (1990). Quaternary geology and glacial history of Labrador: an overview. *Geology of Labrador*. St. John's. CERR/ Department of Earth Sciences, Memorial University of Newfoundland.
- BATTERSON, M. J. and LIVERMAN, D. G. E. (2010). *Past and Future Sea-Level Change in Newfoundland and Labrador: Guidelines for Policy and Planning*, in Pereira, C. P. G. and Walsh, D. G. (eds.) *Current Research*, (10-1), pp. 129-141. 392p. St. John's: Newfoundland and Labrador Department of Natural Resources, Geological Survey.
- BATTERSON, M. J. and LIVERMAN, D. G. E. (2011). Contrasting styles of glacial dispersal in Newfoundland and Labrador: methods and case studies, *Geological Society, London, Special Publications*, 185 (doi: 10.1144/GSL.SP.2001.185.01.12), pp. 267-285.
- BERTHIER, E., RAUP, B. and SCAMBOS, T. (2003). New velocity map and mass-balance estimate of Mertz Glacier, East Antarctica, derived from Landsat sequential imagery, *Journal of Glaciology*, 49 (167), pp. 503-511.
- BO, S., SIEGERT, M. J., MUDD, S. M., SUGDEN, D. E., FUJITA, S., XIANGBIN, C., YUNYUN, J., XUEYUAN, T. and YUANSHEG, L. (2009). The Gamburtsev mountains and the origin and early evolution of the Antarctic Ice Sheet, *Nature*, 459, pp. 690-693.
- BOGORODSKY, V. V., BENTLEY, C. R. and GUDMANDSEN, P. E. (1985). *Radioglaciology*. Dordrecht: D. Reidel Publishing Company. 265p.
- BOULTON, G. S. (1996). Theory of glacial erosion, transport and deposition as a consequence of subglacial sediment deformation, *Journal of Glaciology*, 42 (140), pp. 43-62.

- BRITISH ANTARCTIC SURVEY (BAS) (2000). Ice thickness and subglacial topographic model of the Antarctic. [Online]. Available at:  
[http://www.antarctica.ac.uk/bas\\_research/data/access/bedmap/](http://www.antarctica.ac.uk/bas_research/data/access/bedmap/) (Accessed: August 2012).
- BRONGE, C. (1996). The excavation of the Storglaciaren trough during the Quaternary, *Geografiska Annaler. Series A, Physical Geography*, 78A, pp. 163-169.
- BROOK, E. J., NESJE, A., LEHMAN, S. T., RAISBECK, G. M. and YIOU, F. (1996). Cosmogenic nuclide exposure ages along a vertical transect in western Norway: implications for the height of the Fennoscandian ice sheet, *Geology*, 24, pp. 207-210.
- BROWN, I. and WARD, R. (1996). The influence of topography on snowpatch distribution in southern Iceland: A new hypothesis for glacier formation, *Geografiska Annaler. Series A, Physical Geography*, 78 (4), pp. 197-207.
- BROZOVIC, N., BURBANK, D. W. and MEIGS, A. J. (1997). Climatic limits on landscape development in the north western Himalaya, *Science*, 276, pp. 571-574.
- BUONCRISTIANI, J. and CAMPY, M. (2011). Quaternary Glaciations in the French Alps and Jura, in Ehlers, J., Gibbard, P. L. and Hughes, P. D. (eds.) *Quaternary Glaciations - Extent and Chronology, A closer look*. Oxford: Elsevier, pp. 117-126.
- BYRD POLAR RESEARCH CENTER - REMOTE SENSING LABORATORY (2001a). Ice Velocity vectors for Lambert Glacier, Antarctica; RadarSAT, 2000 Antarctic Mapping Mission: public domain image. [Online]. Available at:  
[http://bprc.osu.edu/rsl/radarsat/Images/velocity\\_lambert.jpg](http://bprc.osu.edu/rsl/radarsat/Images/velocity_lambert.jpg) (Accessed: August 2012).
- BYRD POLAR RESEARCH CENTER - REMOTE SENSING LABORATORY (2001b). RADARSAT-1 Antarctic Mapping Project. [Online]. Available at:  
<http://bprc.osu.edu/rsl/radarsat/radarsat.html> (Accessed: August 2012).
- CHALMERS, J. A. (2000). Offshore evidence for Neogene uplift in central West Greenland, *Global and Planetary Change*, 24, pp. 311-318.
- CHAMPAGNAC, J. D., MOLNAR, P., ANDERSON, R. S., SUE, C. and DELACOU, B. (2007). Quaternary erosion-induced isostatic rebound in the western Alps, *Geology*, 35, pp. 195-198.

- CLARK, P. U. and POLLARD, D. (1998). Origin of the middle Pleistocene transition by ice sheet erosion of regolith, *Paleoceanography*, 13, pp. 1-9.
- COHEN, D., HOOYER, T. S., IVERSON, N. R., THOMASON, J. F. and JACKSON, M. (2006). Role of transient water pressure in quarrying: a subglacial experiment using acoustic emissions, *Journal of Geophysical Research: Earth Surface*, 111 (F03006, doi: 10.1029/2005JF000439).
- COOK, S. J. and SWIFT, D. A. (2012). Subglacial basins: their origin and importance in glacial systems and landscapes, *Earth-Science Reviews*, 115 (4), pp. 332-372.
- COOKE, H. C. (1929). Studies of the physiography of the Canadian Shield: 1, Mature valleys of the Labrador Peninsula, *Transactions of the Royal Society of Canada*, 23 (24), pp. 91-120.
- CORMIER, C. A., VERNON, J. H. and HOAG JR., R. B. (1998). Sunapee, New Hampshire bedrock well project saves nearly \$1,000,000, *Journal of the New England Water Works Association*, 112 (1), pp. 70-74.
- DAHL, S. O., BALLANTYNE, C. K., MCCARROLL, D. and NESJE, A. (1996). Maximum altitude of Devensian glaciation on the Isle of Skye, *Scottish Journal of Geology*, 32, pp. 107-115.
- DAVENPORT, P. H., NOLAN, L. W., WARDLE, R. W., STAPLETON, G. J. and KIFOIL, G. J. (1999). *Digital Geoscience Atlas of Labrador*, in Pereira, C. P. G. and Walsh, D. G. (eds.) *Current Research*, (99-1), pp. 1-16. 356p. St. John's: Newfoundland and Labrador Department of Mines and Energy, Geological Survey. [Online]. Available at: <http://www.nr.gov.nl.ca/mines&en/geosurvey/publications/cr1999/davenport.pdf> (Accessed: March 2012).
- DAVIS, P. T., BIERMAN, P. R., MARSELLA, K. A., CAFFEE, M. W. and SOUTHON, J. R. (1999). Cosmogenic analysis of glacial terrains in the eastern Canadian Arctic; a test for inherited nuclides and the effectiveness of glacial erosion, *Annals of Glaciology*, 28, pp. 181-188.
- DAVIS, W. M. (1954). *Geographical Essays*. New York: Dover Publishing. 777p.

- DUHNFORTH, M., ANDERSON, R. S., WARD, D. and STOCK, G. M. (2010).  
Bedrock fracture control of glacial erosion processes and rates, *Geology*, 38 (5),  
pp. 423-426.
- DURST STUCKI, M., REBER, R. and SCHLUNEGGER, F. (2010). Subglacial tunnel valleys  
in the Alpine foreland: An example from Bern, Switzerland,  
*Swiss Journal of Geosciences*, 103, pp. 363–374.
- DURST STUCKI, M., SCHLUNEGGER, F., CHRISTENER, F., OTTO, J.-C. and GOTZ, J.  
(2012). Deepening of inner gorges through subglacial meltwater - An example from the  
UNESCO Entlebuch area, Switzerland, *Geomorphology*, 139-140, pp. 506-517.
- EGHOLM, D. L., KNUDSEN, M. F., CLARK, C. D. and LESEMANN, J. E. (2011).  
Modeling the flow of glaciers in steep terrains: The integrated second-order shallow ice  
approximation (iSOSIA), *Journal of Geophysical Research: Earth Surface*, 116  
(F02012, doi: 10.1029/2010JF001900).
- EGHOLM, D. L., PEDERSEN, V. K., KNUDSEN, M. F. and LARSEN, N. K. (2012a).  
On the importance of higher order ice dynamics for glacial landscape evolution,  
*Geomorphology*, 141-142, pp. 67-80.
- EGHOLM, D. L., PEDERSEN, V. K., KNUDSEN, M. F. and LARSEN, N. K. (2012b).  
Coupling the flow of ice, water and sediment in a glacial landscape evolution model,  
*Geomorphology*, 141-142, pp. 47-66.
- EHLERS, J., GIBBARD, P. L. and HUGHES, P. D. (2011a). Quaternary Glaciations - Extent  
and Chronology, A closer look (map datasets). [Online]. Available at:  
<http://booksite.elsevier.com/9780444534477/> (Accessed: December 2011).
- EHLERS, J., GIBBARD, P. L. and HUGHES, P. D. (2011b). Preface & Introduction, in  
Ehlers, J., Gibbard, P. L. and Hughes, P. D. (eds.) *Quaternary Glaciations - Extent and  
Chronology, A closer look*. Oxford: Elsevier, pp. xvii-14.
- EHSANI, A. H. and QUIEL, F. (2008). Geomorphometric feature analysis using morphometric  
parameterization and artificial neural networks, *Geomorphology*, 99, pp. 1-12.

ELVERHOI, A., HOOKE, R. L. and SOLHEIM, A. (1998). Late Cenezoic erosion and sediment yield from the Svalbard Barents Sea region: implications for understanding erosion of glacierized basins, *Quaternary Science Reviews*, 17, pp. 209-241.

ERIKSSON, M. (1990). *The Bottom Topography of Storglaciären measured by radio echo sounding*, 29p. Stockholm: University of Stockholm.

ESRI INC. (2007a). ESRI Data & Maps 2006 - An ESRI White Paper 2007. [Online]. Available at: [http://downloads2.esri.com/support/whitepapers/ao\\_/J9509\\_ESRI\\_DataandMaps2006.pdf](http://downloads2.esri.com/support/whitepapers/ao_/J9509_ESRI_DataandMaps2006.pdf) (Accessed: February 2012).

ESRI INC. (2007b). ArcNews Online: Global Elevation Data Now Available in Esri Data & Maps. [Online]. Available at: <http://www.esri.com/news/arcnews/spring07/articles/global-elevation.html> (Accessed: February 2012).

ESRI INC. (2008a). ESRI ArcGIS Desktop 9.3 Help. Topic: Universal Transverse Mercator (Supported Map Projections). [Online]. Available at: [http://webhelp.esri.com/arcgisdesktop/9.3/index.cfm?TopicName=Universal\\_Transverse\\_Mercator](http://webhelp.esri.com/arcgisdesktop/9.3/index.cfm?TopicName=Universal_Transverse_Mercator) (Accessed: March 2012).

ESRI INC. (2008b). ESRI ArcGIS Desktop 9.3 Help. Topic: Fuller Map Projection (Supported Map Projections). [Online]. Available at: <http://webhelp.esri.com/arcgisdesktop/9.3/index.cfm?TopicName=Fuller> (Accessed: March 2012).

ESRI INC. (2008c). ESRI ArcGIS Desktop 9.2 Help. Topic: How Slope Works. [Online]. Available at: <http://webhelp.esri.com/arcgisdesktop/9.2/index.cfm?TopicName=How%20Slope%20works> (Accessed: March 2012).

ESRI INC. (2009). ESRI ArcGIS Desktop 9.3 Help. Topic: Cell size and resampling in analysis (Performing Analysis in Spatial Analyst). [Online]. Available at: [http://webhelp.esri.com/arcgisdesktop/9.3/index.cfm?TopicName=Cell\\_size\\_and\\_resampling\\_in\\_analysis](http://webhelp.esri.com/arcgisdesktop/9.3/index.cfm?TopicName=Cell_size_and_resampling_in_analysis) (Accessed: March 2012).

- ESRI INC. (2010). ESRI ArcGIS Desktop 9.3 Help. Topic: Project Raster (Data Management).  
[Online]. Available at:  
[http://webhelp.esri.com/arcgisDEsktop/9.3/index.cfm?TopicName=Project\\_Raster\\_\(Data\\_Management\)](http://webhelp.esri.com/arcgisDEsktop/9.3/index.cfm?TopicName=Project_Raster_(Data_Management))  
(Accessed: February 2012).
- ESRI INC./ US GEOLOGICAL SURVEY (2006). ESRI Data & Maps 2006 –  
GTOPO30 dataset (DVD-ROM).
- ESRI INC./ US NASA (2006). ESRI Data & Maps 2006 - SRTM dataset (DVD-ROM).
- EVANS, I. S. (1980). An integrated system of terrain analysis and slope mapping,  
*Zeitschrift fur Geomorphologie Supplementband*, 36, pp. 274-295.
- EVANS, I. S. (2006). Allometric development of glacial cirque form: geological, relief and  
regional effects on the cirques of Wales, *Geomorphology*, 80, pp. 245-266.
- EVANS, I. S. (2012). Geomorphometry and landform mapping: What is a landform,  
*Geomorphology*, 137, pp. 94-106.
- FABEL, D., FINK, D., FREDIN, O., HARBOR, J., LAND, M. and STROEVEN, A. P. (2006).  
Exposure age from relict lateral moraines overridden by the Fennoscandian ice sheet,  
*Quaternary Research*, 65, pp. 136-146.
- FARR, T. G., ROSEN, P. A., CARO, E., CRIPPEN, R., DUREN, R., HENSLEY, S.,  
KOBRIK, M., PALLER, M., RODRIGUEZ, E., ROTH, L., SEAL, D., SHAFFER, S.,  
SHIMADA, J. and UMLAND, J. (2007). *The Shuttle Radar Topography Mission*, 43p.  
California: US NASA Jet Propulsion Laboratory, California Institute of Technology.  
[Online]. Available at: [http://www2.jpl.nasa.gov/srtm/SRTM\\_paper.pdf](http://www2.jpl.nasa.gov/srtm/SRTM_paper.pdf)  
(Accessed: February 2012).
- FASTOOK, J. L. and HUGHES, T. J. (2013). New perspectives on paleoglaciology,  
*Quaternary Science Reviews*, 80, pp. 169-194.
- FISHER, P., WOOD, J. and CHENG, T. (2004). Where is Helvellyn? Fuzziness of multi-scale  
landscape morphometry, *Transactions of the Institute of British Geographers*, 29,  
pp. 106-128.

FREY, H., HAEBERLI, W., LINSBAUER, A. and HUGGEL, C. (2010). A multi-level strategy for anticipating future glacier lake formation and associated hazard potentials, *Natural Hazards and Earth System Science*, 10 (2), pp. 339-352.

FROITZHEIM, N., SCHMID, S. M. and FREY, M. (1996). Mesozoic paleogeography and the timing of eclogite-facies metamorphism in the Alps: a working hypothesis, *Eclogae Geologicae Helvetiae*, 89, pp. 81-110.

FUNCK, T., LOUDEN, K. E., WARDLE, R. J., HALL, J., HOBRO, J. W., SALISBURY, M. H. and MUZZATI, A. M. (2000). Three-dimensional structure of the Torngat Orogen (NE Canada) from active seismic tomography, *Journal of Geophysical Research: Solid Earth*, 105 (B10, doi: 10.1029/2000JB900228), pp. 23403–23420.

GANNETT, H. (1898). Lake Chelan, *National Geographic*, 9, pp. 417-428.

GEBCO (2003). Centenary Edition of the GEBCO Digital Atlas. User Guide to the GEBCO One Minute Grid. [Online]. Available at:  
[http://www.gebco.net/data\\_and\\_products/gridded\\_bathymetry\\_data/documents/gridhelp.pdf](http://www.gebco.net/data_and_products/gridded_bathymetry_data/documents/gridhelp.pdf)  
(Accessed: February 2012).

GEBCO (2009a). General Bathymetric Chart of the Oceans (GEBCO) 30 arc-second data. [Online]. Available at: [http://www.gebco.net/data\\_and\\_products/gridded\\_bathymetry\\_data/](http://www.gebco.net/data_and_products/gridded_bathymetry_data/)  
(Accessed: February 2012).

GEBCO (2009b). General Bathymetric Chart of the Oceans GEBCO\_08 Grid (30 arc-second) documentation. [Online]. Available at:  
[http://www.gebco.net/data\\_and\\_products/gridded\\_bathymetry\\_data/documents/gebco\\_08.pdf](http://www.gebco.net/data_and_products/gridded_bathymetry_data/documents/gebco_08.pdf)  
(Accessed: February 2012).

GEBCO, IHO and IOC (2014). *The IHO-IOC GEBCO Cookbook*. IHO Publication B-11, IOC Manuals & Guides 63. IHO, IOC, 331p. [Online]. Available at:  
[http://www.star.nesdis.noaa.gov/sod/lisa/GEBCO\\_Cookbook/documents/CookBook.9.3.14.pdf](http://www.star.nesdis.noaa.gov/sod/lisa/GEBCO_Cookbook/documents/CookBook.9.3.14.pdf)  
(Accessed: October 2014).

GILBERT, G. K. (1877). *The geology of the Henry Mountains, Geographical and Geological Survey of the Rocky Mountain Region (U.S.)*, 160p. Washington D.C: US Government Printing Office.

- GLASSER, N. F. (1995). Modelling the effect of topography on ice sheet erosion, Scotland, *Geografiska Annaler. Series A, Physical Geography*, 77 (1-2), pp. 67-82.
- GLASSER, N. F. and BENNETT, M. R. (2004). Glacial erosional landforms: origins and significance for palaeoglaciology, *Progress in Physical Geography*, 28, pp. 43-75.
- GLASSER, N. F. and GHIGLIONE, M. C. (2009). Structural, tectonic and glaciological controls on the evolution of fjord landscapes, *Geomorphology*, 105, pp. 291-302.
- GOWER, C. F. (1996). The evolution of the Grenville Province in eastern Labrador, Canada, *Geological Society, London, Special Publications*, 112 (doi: 10.1144/GSL.SP.1996.112.01.11), pp. 197-218.
- GRADSTEIN, F. M. and SRIVASTAVA, S. P. (1980). Aspects of Cenozoic stratigraphy and paleoceanography of the Labrador Sea and Baffin Bay, *Palaeogeography, Palaeoclimatology, Palaeoecology*, 30, pp. 261–295.
- GROHMANN, C. H., SMITH, M. J. and RICCOMINI, C. (2011). Multiscale Analysis of Topographic Surface Roughness in the Midland Valley, Scotland, *IEEE Transactions on Geoscience and Remote Sensing*, 49 (4), pp. 1200-1213.
- GUDMUNDSSON, G. H. (1994). An order-of-magnitude estimate of the current uplift rates in Switzerland by the Würm Alpine deglaciation, *Eclogae Geologicae Helvetiae*, 87, pp. 545–557.
- GUDMUNDSSON, G. H. (1999). A three-dimensional numerical model of the confluence area of Unteraargletscher, Bernese Alps, Switzerland, *Journal of Glaciology*, 45 (150), pp. 219-230.
- GUDMUNDSSON, G. H., IKEN, A. and FUNK, M. (1997). Measurements of ice deformation at the confluence area of Unteraargletscher, Bernese Alps, Switzerland, *Journal of Glaciology*, 43 (145), pp. 548-556.
- HAKLAY, M., BASIOUKA, S., ANTONIOU, V. and ATHER, A. (2010). How many volunteers does it take to map an area well? The validity of Linus' law to volunteered geographic information, *Cartographic Journal*, 47 (4), pp. 315-322.

- HALL, J., LOUDEN, K. E., FUNCK, T. and DEEMER, S. (2002). Geophysical characteristics of the continental crust along the Lithoprobe Eastern Canadian Shield Onshore-Offshore Transect (ECSOOT): a review, *Canadian Journal of Earth Sciences*, 39, pp. 569–587.
- HALLET, B. (1996). Glacial quarrying: a simple theoretical model, *Annals of Glaciology*, 22, pp. 1-8.
- HALLET, B., HUNTER, L. and BOGEN, J. (1996). Rates of erosion and sediment evacuation by glaciers: A review of field data and their implications, *Global and Planetary Change*, 12, pp. 213-235.
- HAYNES, V. M. (1968). The influence of glacial erosion and rock structure on corries in Scotland, *Geografiska Annaler. Series A, Physical Geography*, 50 (4), pp. 221-234.
- HERMAN, F., BEAUD, F., CHAMPAGNAC, J.-D., LEMIEUX, J.-M. and STERNAI, P. (2011). Glacial hydrology and erosion patterns: A mechanism for carving glacial valleys, *Earth and Planetary Science Letters*, 310, pp. 498-508.
- HERMAN, F. and BRAUN, J. (2008). Evolution of the glacial landscape of the Southern Alps of New Zealand: Insights from a glacial erosion model, *Journal of Geophysical Research: Earth Surface*, 113 (F02009, doi: 10.1029/2007JF000807).
- HINDERER, M. (2001). Late Quaternary denudation of the Alps, valley and lake fillings and modern river loads, *Geodinamica Acta*, 14 (doi: 10.1016/S0985-3111(01)01070-1), pp. 231–263.
- HOLTEDAHL, H. (1967). Notes on the formation of fjords and fjord valleys, *Geografiska Annaler. Series A, Physical Geography*, 49 (2-4), pp. 188-203.
- HOOKE, R. L. (1991). Positive feedbacks associated with erosion of glacial cirques and overdeepenings, *Geological Society of America Bulletin*, 103 (8), pp. 1104-1108.
- HOOKE, R. L. (2005). Chapter 11. Numerical Modeling, in *Principles of glacier mechanics*. 2nd edn. Cambridge: Cambridge University Press, pp. 288-314.

- HUTTER, K. (1983). *Mathematical approaches to geophysics: Theoretical glaciology; material science of ice and the mechanics of glaciers and ice sheets*. Dordrecht/ Boston/ Lancaster/ Tokyo: Springer (D. Reidel Publishing Co./ Terra Scientific Publishing Co.). 548p.
- JACKSON, L. E., PHILLIPS, F. M., SHIMAMURA, K. and LITTLE, E. C. (1997). Cosmogenic <sup>36</sup>Cl dating of the Foothills erratics train, Alberta, Canada, *Geology*, 25, pp. 195-198.
- JAMIESON, S. S., HULTON, N. R. and HAGDORN, M. (2008). Modelling landscape evolution under ice sheets, *Geomorphology*, 97, pp. 91-108.
- JAPSEN, P. and CHALMERS, J. A. (2000). Neogene uplift and tectonics around the North Atlantic: overview, *Global and Planetary Change*, 24, pp. 165–173.
- JAPSEN, P., GREEN, P. F. and CHALMERS, J. A. (2005). Separation of Palaeogene and Neogene uplift on Nuussuaq, West Greenland, *Journal of the Geological Society*, 162 (doi: 10.1144/0016-764904-038), pp. 299-314.
- KAHLE, H. G., KLINGELE, E., MUELLER, S. and EGLOFF, R. (1976). The variation of crustal thickness across the Swiss Alps based on gravity and explosion seismic data, *Pure and Applied Geophysics*, 114 (3), pp. 479-494.
- KESSLER, M. A., ANDERSON, R. S. and BRINER, J. P. (2008). Fjord insertion into continental margins driven by topographic steering of ice, *Nature Geoscience*, 1, pp. 365-369.
- KRABBENDAM, M. and BRADWELL, T. (2011). Lateral plucking as a mechanism for elongate erosional glacial bedforms: explaining megagrooves in Britain and Canada, *Earth Surface Processes and Landforms*, 36, pp. 1335-1349.
- KRABBENDAM, M. and GLASSER, N. F. (2011). Glacial erosion and bedrock properties in NW Scotland: Abrasion and plucking hardness and joint spacing, *Geomorphology*, 130, pp. 374-383.
- KRIZEK, M., VOCADLOVA, K. and ENGEL, Z. (2012). Cirque overdeepening and their relationship to morphometry, *Geomorphology*, 139-140, pp. 495-505.

- KUHLEMANN, J. (2000). Post-Collisional Sediment Budget of Circum-Alpine Basins (Central Europe), *Memorie Scienze Geologiche (Padova)*, 52, pp. 1-91.
- LAYBERRY, R. L. and BAMBER, J. L. (2001). A new ice thickness and bed data set for the Greenland ice sheet 2: Relationship between dynamics and basal topography, *Journal of Geophysical Research: Atmospheres*, 106 (D24, doi: 10.1029/2001JD900053), pp. 33781-33788.
- LEWIS, W. V. (1960). *Norwegian Cirque Glaciers*. RGS Research Series, 4. London: Royal Geographical Society. 104p.
- LINSBAUER, A., PAUL, F. and HAEBERLI, W. (2012). Modeling glacier thickness distribution and bed topography over entire mountain ranges with glabtop: Application of a fast and robust approach, *Journal of Geophysical Research: Earth Surface*, 117 (F03007, doi: 10.1029/2011JF002313).
- LINTON, D. L. (1963). The forms of glacial erosion, *Transactions of the Institute of British Geographers*, 33, pp. 1-28.
- LOWE, J. J. and WALKER, M. J. C. (1997). *Reconstructing Quaternary Environments*. London: Longman. 446p.
- LYTHE, M. B., VAUGHAN, D. G. and CONSORTIUM, T. B. (2001). BEDMAP- A new ice thickness and subglacial topographic model of Antarctica, *Journal of Geophysical Research: Solid Earth*, 106 (B6, doi: 10.1029/2000JB900449), pp. 11335-11351.
- MACGREGOR, K. R., ANDERSON, R. S., ANDERSON, S. P. and WADDINGTON, E. D. (2000). Numerical simulations of glacial-valley longitudinal profile evolution, *Geology*, 28 (11), pp. 1031-1034.
- MACGREGOR, K. R., ANDERSON, R. S. and WADDINGTON, E. D. (2009). Numerical modelling of glacial erosion and headwall processes in Alpine valleys, *Geomorphology*, 103 (1), pp. 189-204.
- MACKIN, J. H. (1948). Concept of the graded river, *Geological Society of America Bulletin*, 59 (5), pp. 463-511.

- MAKOS, M., NITYCHORUK, J. and ZREDA, M. (2013). Deglaciation chronology and paleoclimate of the Pieciu Stawów Polskich/Roztoki Valley, high Tatra Mountains, Western Carpathians, since the Last Glacial Maximum, inferred from  $^{36}\text{Cl}$  exposure dating and glacier-climate modelling, *Quaternary International*, 293 (doi: 10.1016/j.quaint.2012.01.016), pp. 63-78.
- MALYUTKIN, B. V. and MOLOKOV, L. A. (1985). Engineering-geological conditions of construction of the Shamkhor hydro development on the Kura River, *Hydrotechnical Construction*, 19 (3), pp. 118-124.
- MATTHES, F. E. (1930). *Geologic History of the Yosemite Valley, Professional Paper* (160), 137p. Reston, Virginia: US Geological Survey. [Online]. Available at: [http://www.nps.gov/history/history/online\\_books/geology/publications/pp/160/contents.htm](http://www.nps.gov/history/history/online_books/geology/publications/pp/160/contents.htm) (Accessed: February 2012).
- MCMILLAN, N. J. (1973). Shelves of Labrador Sea and Baffin Bay, Canada, in McCrossan, R. G. (ed.) *Future Petroleum Provinces of Canada – Their Geology and Potential: CSPG Special Publications - Memoir 1*. Calgary: Canadian Society of Petroleum Geologists, pp. 473–517.
- MEIGS, A. and SAUBER, J. (2000). Southern Alaska as an example of the long-term consequences of mountain building under the influence of glaciers, *Quaternary Science Reviews*, 19, pp. 1543–1562.
- MENGEL, F., RIVERS, T. and REYNOLDS, P. (1991). Lithotectonic elements and tectonic evolution of the Torngat Orogen, Saglek Fiord, northern Labrador, *Canadian Journal of Earth Sciences* 28, pp. 1407–1423.
- MEYER, R. F., ATTANASI, E. D. and FREEMAN, P. A. (2007). *Heavy oil and natural bitumen resources in geological basins of the world, Open File-Report* (2007-1084), 42p. Reston, Virginia: US Geological Survey. [Online]. Available at: <http://pubs.usgs.gov/of/2007/1084/> (Accessed: February 2012).
- MINAR, J. and EVANS, I. S. (2008). Elementary forms for land surface segmentation: The theoretical basis of terrain analysis and geomorphological mapping, *Geomorphology*, 95, pp. 236-259.

- MINDRESCU, M. and EVANS, I. S. (2014). Cirque form and development in Romania: Allometry and the buzzsaw hypothesis, *Geomorphology*, 208, pp. 117-136.
- MOLNAR, P. and ENGLAND, P. (1990). Late Cenozoic uplift of mountain ranges and global climate change: Chicken or egg, *Nature* 346, pp. 29–34.
- MONTGOMERY, D. R. (2002). Valley formation by fluvial and glacial erosion, *Geology*, 30 (11), pp. 1047–1050.
- OCCHIETTI, S., PARENT, M., LAJEUNESSE, P., ROBERT, F. and GOVARE, E. (2011). Late Pleistocene-Early Holocene Decay of the Laurentide Ice Sheet in Quebec-Labrador, in Ehlers, J., Gibbard, P. L. and Hughes, P. D. (eds.) *Quaternary Glaciations - Extent and Chronology, A closer look*. Oxford: Elsevier, pp. 601-630.
- OERLEMANS, J. (1984). Numerical experiments on large scale glacial erosion, *Zeitschrift fur Gletscherkunde und Glazial geologie*, 20, pp. 107-126.
- PENCK, A. (1900). Die Uebertiefung der Alpentaler, *12th International Geographical Congress*, 2, pp. 232-240.
- PEUCKER, T. K. and DOUGLAS, D. H. (1974). Detection of surface specific points by local parallel processing of discrete terrain elevation data, *Computer Graphics and Image Processing*, 4, pp. 375-387.
- PODWYSOCKI, M. H., MOIK, J. G. and SHOUP, W. C. (1975). Quantification of geologic lineaments by manual and machine processing techniques. *Proceedings of the NASA Earth Resources Survey Symposium*. Greenbelt, Maryland. US NASA.
- PORTER, S. C. (2001). Snowline depression in the tropics during the last glaciation, *Quaternary Science Reviews*, 20, pp. 1067-1091.
- PREUSSER, F., REITNER, J. M. and SCHLUCHTER, C. (2010). Distribution, geometry, age and origin of overdeepened valleys and basins in the Alps and their foreland, *Swiss Journal of Geosciences*, 103, pp. 407-426.
- RABUS, B. R., EINEDER, M., ROTH, A. and BAMLER, R. (2003). The shuttle radar topography mission - a new class of digital elevation models acquired by spaceborne radar, *ISPRS Journal of Photogrammetry & Remote Sensing*, 57, pp. 241-262.

- RODRÍGUEZ, E., MORRIS, C. S., BELZ, J. E., CHAPIN, E. C., MARTIN, J. M., DAFFER, W. and HENSLEY, S. (2005). *An assessment of the SRTM topographic products*. D-31639. US NASA Jet Propulsion Laboratory, California Institute of Technology, 143p. [Online]. Available at: [http://www2.jpl.nasa.gov/srtm/SRTM\\_D31639.pdf](http://www2.jpl.nasa.gov/srtm/SRTM_D31639.pdf) (Accessed: February 2012).
- ROSS, N., SIEGERT, M. J., WOODWARD, J., SMITH, A. M., CORR, H. F. J., BENTLEY, M. J., HINDMARSH, R. C. A., KING, E. C. and RIVERA, A. (2011). Holocene stability of the Amundsen-Weddell ice divide, West Antarctica, *Geology*, 39, pp. 935-938.
- RUDBERG, S. (1992). Multiple glaciation in Scandinavia - seen in gross morphology or not, *Geografiska Annaler. Series A, Physical Geography*, 74A, pp. 231-243.
- RUDBERG, S. (1994). Glacial cirques in Scandinavia, *Norsk Geografisk Tidsskrift*, 48, pp. 179-197.
- RUDBERG, S. (1997). Glacial and interglacial erosion in Scandinavian mountains in a W-E comparison including an approach to a quantitative calculation, *Zeitschrift fur Geomorphologie*, 41, pp. 183-204.
- SANDWELL, D. T. and SMITH, W. H. F. (1997). Marine gravity anomaly from Geosat and ERS 1 satellite altimetry, *Journal of Geophysical Research: Solid Earth*, 102 (B5, doi: 10.1029/96JB03223), pp. 10039-10054.
- SCHNEIDER, J. F. and RYBACH, L. (1999). The first deep Quaternary groundwater capture in Switzerland: Combined use and environmental benefits, *Environmental Geology*, 39 (2), pp. 144-148.
- SEAMAN, P. G. (1998). *Ikaite formation in a fjord environment with special reference to Ikka fjord (unpublished phd thesis)*. University of London. Imperial College of Science, Technology, and Medicine. [Online]. Available at: <http://www.reocities.com/RainForest/Vines/1486/ikkap.htm> (Accessed: February 2012).

- SEGUINOT, J. (2008). *Glacial quarrying and development of overdeepenings in glacial valleys; Modelling experiments and case studies at Erdalen, Western Norway (MSc dissertation)*. Geological Survey of Norway, Trondheim; and Ecole normale superieure, Paris. Department of Earth, Atmosphere, and Ocean. [Online]. Available at: <http://people.su.se/~jsegu/files/julien-m1.pdf> (Accessed: February 2012).
- SEIJMONSBERGEN, A. C., HENGL, T. and ANDERS, N. S. (2011). Semi-Automated Identification and Extraction of Geomorphological Features Using Digital Elevation Data, in Smith, M. J., Paron, P. and Griffiths, J. (eds.) *Geomorphological Mapping: A Handbook of Techniques and Applications*. Amsterdam: Elsevier, pp. 297-335.
- SHORTRIDGE, A. M. and GOODCHILD, M. F. (1999). Communicating uncertainty for global data sets. *International Symposium on Spatial Data Quality*. Hong Kong. The International Society for Photogrammetry and Remote Sensing, pp. 59-65. [Online]. Available at: [https://www.msu.edu/~ashton/research/pubs/global\\_uncert.pdf](https://www.msu.edu/~ashton/research/pubs/global_uncert.pdf) (Accessed: March 2012).
- SIEGAL, B. S. (1977). Significance of operator variation and the angle of illumination in lineament analysis of synoptic images, *Modern Geology*, 6, pp. 75-85.
- SMALL, E. E. and ANDERSON, R. S. (1998). Pleistocene relief production in Laramide mountain ranges, western United States, *Geology*, 26, pp. 123-126.
- SMITH, W. H. F. and SANDWELL, D. T. (1997). Global seafloor topography from satellite altimetry and ship depth soundings, *Science*, 277, pp. 1957-1962.
- SPEEDING, N. and EVANS, D. J. (2002). Sediments and landforms at Kviarjokull, southeast Iceland: a reappraisal of the glaciated valley landsystem, *Sedimentary Geology*, 149, pp. 21-42.
- SPENCELEY, A. P. (2001). Grooves and striations on the Stanthorpe Adamellite: evidence for a possible late Middle-Late Triassic age glaciation, *Australian Journal of Earth Sciences*, 48, pp. 777-784.
- STAIGER, J. K., GOSSE, J. C., JOHNSON, J. V., FASTOOK, J., GRAY, J. T., STOCKLI, D. F., STOCKLI, L. and FINKEL, R. (2005). Quaternary relief generation by polythermal glacier ice, *Earth Surface Processes and Landforms*, 30, pp. 1145-1159.

- STANGE, K. M., BALEN, R., VANDENBERGHE, J., PEÑA, J. L. and SANCHO, C. (2013). External controls on Quaternary fluvial incision and terrace formation at the Segre River, Southern Pyrenees, *Tectonophysics*, 602 (doi: org/10.1016/j.tecto.2012.10.033), pp. 316-331.
- ST-ONGE, M. R., VAN GOOL, J. A. M., GARDE, A. A. and SCOTT, D. J. (2009). Correlation of Archaean and Palaeoproterozoic units between northeastern Canada and western Greenland: constraining the pre-collisional upper plate accretionary history of the Trans-Hudson orogen, *Geological Society, London, Special Publications*, 318 (doi: 10.1144/SP318.7), pp. 193-235.
- STROEVEN, A. P. and SWIFT, D. A. (2008). Glacial landscape evolution - Implications for glacial processes, patterns and reconstructions, *Geomorphology*, 97, pp. 1-4.
- SUGDEN, D. E. (1977). Reconstruction of the morphology, dynamics and thermal characteristics of the Laurentide ice sheet at its maximum, *Arctic and Alpine Research*, 9, pp. 21-47.
- SUGDEN, D. E. (1978). Glacial erosion by the Laurentide ice sheet, *Journal of Glaciology*, 20 (83), pp. 367-391.
- SUGDEN, D. E. and JOHN, B. S. (1976). *Glaciers and Landscape. A Geomorphological Approach*. London: Arnold. 376p.
- SWIFT, D. A., NIENOW, P. W. and HOEY, T. B. (2005). Basal sediment evacuation by subglacial meltwater: suspended sediment transport from Haut Glacier d'Arolla, Switzerland, *Earth Surface Processes and Landforms*, 30, pp. 867-883.
- SWIFT, D. A., PERSANO, C., STUART, F. M., GALLAGHER, K. and WHITHAM, A. (2008). A reassessment of the role of ice sheet glaciations in the long-term evolution of the East Greenland fjord region, *Geomorphology*, 97, pp. 109-125.
- SWISS FEDERAL OFFICE OF TOPOGRAPHY (SWISSTOPO) (2010). Geological Map of Switzerland; 1:500,000 scale, v.1.2. [Online]. Available at: <http://www.swisstopo.admin.ch/internet/swisstopo/en/home/products/maps/geology/geomaps/gm500.html> (Accessed: September 2011).

SWISS FEDERAL OFFICE OF TOPOGRAPHY (SWISSTOPO) (2011). FAQ - Geological vector datasets. [Online]. Available at:

[http://www.swisstopo.admin.ch/internet/swisstopo/en/home/products/maps/geology/geocover/FAQ\\_vectordata.html](http://www.swisstopo.admin.ch/internet/swisstopo/en/home/products/maps/geology/geocover/FAQ_vectordata.html)  
(Accessed: March 2012).

SWISS FEDERAL OFFICE OF TOPOGRAPHY (SWISSTOPO) (2012). List of base maps for the compilation of GeoCover records. [Online]. Available at:

<http://www.swisstopo.admin.ch/internet/swisstopo/en/home/products/maps/geology/geocover.parsys.75101.downloadList.88948.DownloadFile.tmp/listecompiletionweben.pdf> (Accessed: March 2012).

SYKES, J. F., NORMANI, S. D., YIN, Y., SYKES, E. A. and JENSEN, M. R. (2009).

Hydrogeologic modelling in support of a proposed deep geologic repository in Canada for low and intermediate level radioactive waste. *Proceedings of the 12th International Conference on Radioactive Waste Management and Environmental Remediation*. Liverpool. ASME, ICEM.

TALBOT, C. J. (1999). Ice ages and nuclear waste isolation, *Engineering Geology*, 52, pp. 177-192.

TARASOV, L. and PELTIER, W. R. (2004). A geophysically constrained large ensemble analysis of the deglacial history of the North American ice-sheet complex, *Quaternary Science Reviews*, 23, pp. 359-388.

TAYLOR, W. P. and WILSON, C. D. V. (1997). Tectonically influenced glacial erosion, and ensuing valley infill: A geophysical survey, *Quarterly Journal of Engineering Geology*, 30 (2), pp. 97-113.

TOMKIN, J. H. (2009). Numerically simulating alpine landscapes: The geomorphologic consequences of incorporating glacial erosion in surface process models, *Geomorphology*, 103 (2), pp. 180-188.

TOMKIN, J. H. and BRAUN, J. (2002). The influence of alpine glaciation on the relief of tectonically active mountain belts, *American Journal of Science*, 302, pp. 169-190.

TURNBULL, J. M. and DAVIES, T. R. H. (2006). A mass movement origin for cirques, *Earth Surface Processes and Landforms*, 31, pp. 1129-1148.

US DEFENSE MAPPING AGENCY (1992). Military specification Digital Chart of the World (DCW) *MIL-D-89009*. [Online]. Available at:  
[http://earth-info.nga.mil/publications/specs/printed/89009/89009\\_DCW.pdf](http://earth-info.nga.mil/publications/specs/printed/89009/89009_DCW.pdf)  
(Accessed: February 2012).

US DEFENSE MAPPING AGENCY (1995a). Performance Specification. Vector Smart Map (VMAP) Level 0 *MIL-PRF-89039*. [Online]. Available at:  
[http://earth-info.nga.mil/publications/specs/printed/89039/PRF\\_8903.PDF](http://earth-info.nga.mil/publications/specs/printed/89039/PRF_8903.PDF) (Accessed: March 2012).

US DEFENSE MAPPING AGENCY (1995b). Performance Specification. Vector Smart Map (VMAP) Level 1 *MIL-PRF-89033*. [Online]. Available at:  
[http://earth-info.nga.mil/publications/specs/printed/89033/VMAP\\_89033.pdf](http://earth-info.nga.mil/publications/specs/printed/89033/VMAP_89033.pdf)  
(Accessed: March 2012).

US DEFENSE MAPPING AGENCY (1995c). Performance Specification. Operational Navigational Charts (ONC) *MIL-O-89102*. [Online]. Available at:  
<http://earth-info.nga.mil/publications/specs/printed/89102/89102.pdf> (Accessed: May 2012).

US DEFENSE MAPPING AGENCY (1996). Performance Specification. Digital Terrain Elevation Data (DTED) *MIL-PRF-89020A*. [Online]. Available at:  
[http://earth-info.nga.mil/publications/specs/printed/89020A/89020A\\_DTED.pdf](http://earth-info.nga.mil/publications/specs/printed/89020A/89020A_DTED.pdf)  
(Accessed: February 2012).

US GEOLOGICAL SURVEY (1997). GTOPO30 Data Readme. [Online]. Available at:  
<http://www1.gsi.go.jp/geowww/globalmap-gsi/gtopo30/gtopo30.html> (Accessed: February 2012).

US NATIONAL AERONAUTICS AND SPACE ADMINISTRATION (NASA) (2012). SRTM data coverage (image). [Online]. Available at: <http://www2.jpl.nasa.gov/srtm/datacoverage.html>  
(Accessed: February 2012).

US NATIONAL GEOSPATIAL-INTELLIGENCE AGENCY (2003). SRTM Water Body Data Product Specific Guidance (v.2.0, March 12, 2003). [Online]. Available at:  
[http://dds.cr.usgs.gov/srtm/version2\\_1/SWBD/SWBD\\_Documentation/SWDB\\_Product\\_Specific\\_Guidance.pdf](http://dds.cr.usgs.gov/srtm/version2_1/SWBD/SWBD_Documentation/SWDB_Product_Specific_Guidance.pdf)  
(Accessed: March 2012).

US NATIONAL GEOSPATIAL-INTELLIGENCE AGENCY (2005). Documentation for the Shuttle Radar Topography Mission (SRTM) Water Body Data Files. [Online].

Available at:

[http://dds.cr.usgs.gov/srtm/version2\\_1/SWBD/SWBD\\_Documentation/Readme\\_SRTM\\_Water\\_Body\\_Data.pdf](http://dds.cr.usgs.gov/srtm/version2_1/SWBD/SWBD_Documentation/Readme_SRTM_Water_Body_Data.pdf)

(Accessed: March 2012).

US NATIONAL SNOW & ICE DATA CENTER (NSIDC) (2005). Greenland 5 km DEM, Ice Thickness, and Bedrock Elevation Grids. [Online]. Available at:

[http://nsidc.org/data/docs/daac/nsidc0092\\_greenland\\_ice\\_thickness.gd.html](http://nsidc.org/data/docs/daac/nsidc0092_greenland_ice_thickness.gd.html) (Accessed: August 2012).

VAN COILLIE, F. M. B., GARDIN, S., ANSEEL, F., DUYNCK, W., VERBEKE, L. P. C. and DE WULF, R. R. (2014). Variability of operator performance in remote-sensing image interpretation: the importance of human and external factors, *International Journal of Remote Sensing*, 35 (2), pp. 754-778.

WARBURTON, J. and BEECROFT, I. (1993). Use of meltwater stream material loads in the estimation of glacial erosion rates, *Zeitschrift fur Geomorphologie*, 37, pp. 19-28.

WARDLE, R. J., GOWER, C. F., RYAN, B., NUNN, G. A., JAMES, D. T. and A, K. (1997). *Geological map of Labrador; 1:1,000,000 scale. Map 97-07. GS# LAB/1226*. St. John's: Newfoundland and Labrador Department of Mines and Energy, Geological Survey.

WARDLE, R. J. and VAN KRANENDONK, M. J. (1996). The Palaeoproterozoic Southeastern Churchill Province of Labrador-Quebec, Canada: orogenic development as a consequence of oblique collision and indentation, *Geological Society, London, Special Publications*, 112 (doi: 10.1144/GSL.SP.1996.112.01.08), pp. 137-153.

WHIPPLE, K. X., KIRBY, E. and BROCKLEHURST, S. H. (1999). Geomorphic limits to climate-induced increases in topographic relief, *Nature*, 401, pp. 39-43.

WINSBORROW, M. C., CLARK, C. D. and STOKES, C. R. (2004). Ice streams of the Laurentide ice sheet, *Geographie physique et Quaternaire*, 58 (2-3), pp. 269-280.

WOOD, J. (1996). *The geomorphological characterisation of digital elevation models (unpublished phd thesis)*. University of Leicester. Department of Geography. [Online]. Available at: <http://www soi.city.ac.uk/~jwo/phd> (Accessed: February 2010).

WOOD, J. (2002). Landserf: Visualisation and analysis of terrain models. [Online].

Available at: <http://www.landserf.org> (Accessed: February 2010).

## Appendix

### 8 The internal geometry of confluences: Discussion

The boundary line that denotes the transition between the tributary and trunk valley within a confluence is termed the down-tributary termination (DTT). DTTs have been defined (in part), by the use of a tributary valley-side divergence angle threshold of  $45^\circ$ , at selected confluence extent (i.e. confluence perimeter). As discussed previously, the  $45^\circ$  threshold has been chosen partly because of its visual simplicity when manually measuring and assessing many hundreds of potential confluences. Further, the  $45^\circ$  threshold has been chosen because it is large enough that DTTs are placed sufficiently down-tributary so as to avoid measuring unrepresentative valley-width and CSA measurements which might be observed in the up-tributary extent of confluences. The  $45^\circ$  divergence threshold is also large enough that it commonly visually pre-empts (i.e. occurs immediately up-tributary of) where a tributary joins (visibly, at selected confluence extent) with an adjacent tributary and the trunk valley, within a confluence. The position of the DTT is consequently well suited to indicate the transition from the tributary valley into the trunk valley. The  $45^\circ$  angle is smaller than the minimum angle possible when calculating the true geometrical boundary between a tributary and trunk valley. This minimum angle might best be termed the minimum *absolute* valley-side divergence angle. The following elucidation is offered regarding these concepts.

#### 8.1 Defining the absolute tributary-trunk valley boundary (ADTT)

The method used to define a DTT has been selected to simplify what is essentially a difficult task. The internal geometry of a confluence is often complex and so ascertaining exactly where a tributary ends and the trunk begins is frequently tricky to interpret. The DTT method is simply one way of representatively, reliably, and repeatedly defining the transition between the tributary and trunk valley within a confluence, according to the series of rules set out in section 4.3.3. The true geometrical boundary between tributary and trunk, within a confluence, might best be termed the *absolute* down-tributary termination (ADTT; see figure A1, top). The concept assumes that the ADTTs meet to form two sides of a triangle, with the third side (termed the 'trunk line' here) as a notional line across the trunk. The triangle is the smallest (by area) that will fit within the confluence perimeter, between the ADTTs and the notional trunk line, whilst maintaining respective valley axes at  $90^\circ$  to ADTTs and trunk line, at selected confluence extent. The trunk line is used simply to obtain the smallest triangle in order that ADTTs may be defined effectively. The trunk line should not be confused with the down-trunk termination, which defines the down-trunk end of a confluence.

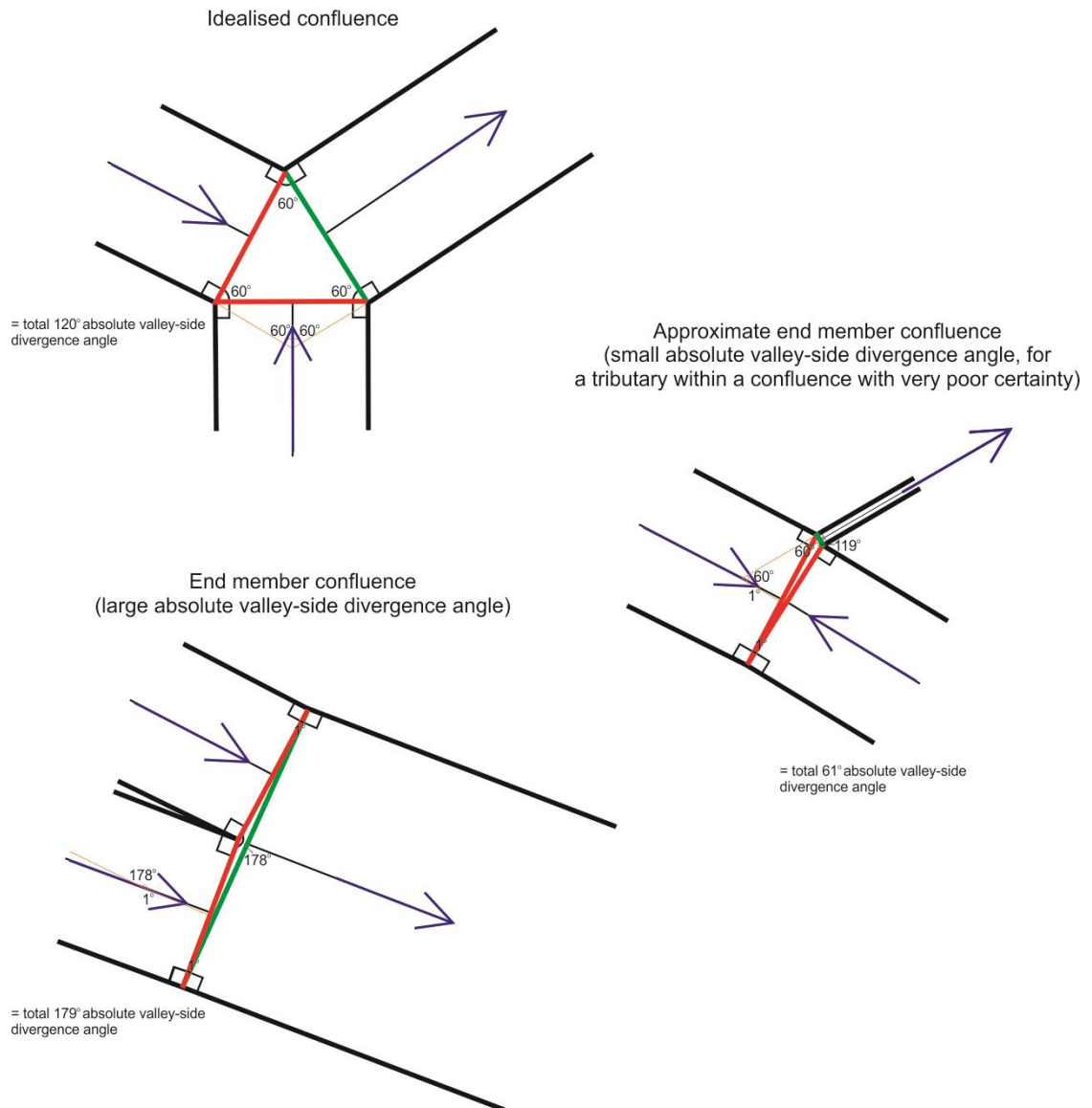


Figure A1. Defining the absolute tributary-trunk valley boundary (ADTT)

(Top) Schematic of an idealised confluence. The true geometrical boundary between tributary and trunk, within a confluence, is here termed the *absolute* down-tributary termination (ADTT, red lines). ADTTs meet to form two sides of a triangle, with the third side (the ‘trunk line’, green line) as a notional line across the trunk (see text). The absolute valley-side divergence angle is different for each tributary within every confluence. In this example, the idealised confluence has ADTTs and trunk line form an equilateral triangle with internal angles of 60°. Consequently, the absolute divergence angle for this example is 120° (i.e. the sum of angles denoted in orange). Valley axes are denoted by thin black lines. Ice flow direction is denoted by blue arrows. (Middle, Bottom) Schematics of confluence ‘end member’ geometries. The absolute divergence (end member) angles that are possible in a confluence will range between approximately 60° and <180°, for geometrical reasons. The smallest absolute divergence angle that might be valid depends upon perceived visual appearance of the confluence. The approximate end member confluence shown here (middle) has very poor certainty and is quite unlikely to occur in nature.

ADTTs are positioned where tributary valley-side contour lines diverge (absolutely) downstream relative to each other. The internal geometry of every confluence is unique. Consequently, the absolute valley-side divergence angle is different for each tributary within every confluence. This results in 'end member' confluence geometries (figure A1, middle and bottom). The absolute divergence (end member) angles that are possible in a confluence will range between approximately  $60^\circ$  and  $<180^\circ$ , for geometrical reasons. The smallest absolute divergence angle that might be valid depends upon the perceived visual appearance of the confluence (i.e. tributary-trunk angle, is confluence natural and continuous?). Confluences that contain a tributary with a particularly small absolute divergence angle will have very poor certainty and are quite unlikely to occur in nature.

## 8.2 Applying the ADTT method: Problems

In real confluences, tributary valley axes will usually change direction significantly, immediately upstream of ADTTs. The change in direction can be very much more acute than is found upstream of DTTs, and occurs for geometrical reasons (figure A2). The complexities of confluence geometry, where tributary and trunk valleys meet (absolutely), makes applying the ADTT concept (i.e. evaluating internal confluence geometry, determining the absolute valley-side divergence angle of each tributary, and positioning ADTTs within each confluence) difficult and overly time consuming. Further to this, down-tributary valley-width and CSA cannot often be properly assessed at the ADTT, as valley-width and CSA at this location is often unrepresentative of tributary width a short distance up-tributary (figure A2). Valley-width at the ADTT becomes least representative of down-tributary width, in confluences where the geometry is such that ADTT position is most removed from DTT position.

### 8.2.1 The DTT method: A solution

The DTT method removes the need for complicated geometrical calculations to establish the absolute divergence angle, for each tributary within every confluence, by the use of a *constant* valley-side divergence angle of  $45^\circ$ . The angle has been selected based upon initial study of the Labrador DEM and the geometries of associated confluences, and for the reasons already discussed in this thesis. Further to these reasons, the DTT divergence angle is smaller than the minimum (geometrically possible) absolute divergence angle, and thus usually positions the DTT further upstream than the ADTT. Valley axis direction is more consistent at such positions, thus reducing the complexity of applying the method. Further, because the DTT is positioned slightly up-tributary, a transverse profile line taken at the DTT can be employed as a

representative measure of down-tributary valley-width and CSA within confluences. This allows accurate assessment of CSA change through confluences in subsequent analysis.

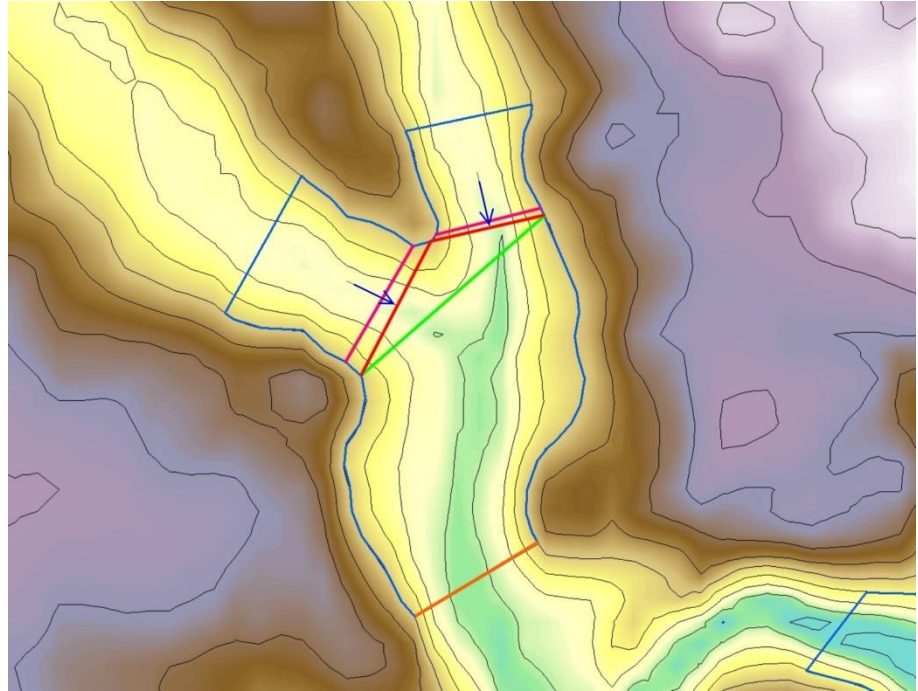


**Figure A2. Applying the ADTT method, problems.**

For any given confluence (blue perimeter), tributary valley axes (thick black lines) are at 90°, at the location of ADTTs (red lines). This is for geometrical reasons. When the ADTT concept is applied to real confluences it is observable that there is usually a significant change in the direction of valley axes, immediately up-tributary of the ADTT. This makes determining ADTT position complex; and means that the ADTT is not a suitable position to accurately assess down-tributary valley-width and CSA, as this location is often unrepresentative of tributary width a short distance up-tributary. The notional trunk line is denoted by a green line. The down-trunk termination is denoted by an orange line. Tributary ice flow direction (at ADTTs) is denoted by blue arrows. DTTs are denoted by pink lines. SRTM3 land topography data are shown in ESRI ArcGIS 'elevation' colour scale (ll coord 57.1, -63.4 DD). SRTM contours are placed at 20 m intervals (black lines).